Modeling of Circular-Grating Surface-Emitting Lasers

by

Ali M. Shams-Zadeh-Amiri

A thesis
presented to the University of Waterloo
in fulfillment of the
thesis requirement for the degree of
Doctor of Philosophy
in
Electrical Engineering

Waterloo, Ontario, Canada, 1997

The University of Waterloo requires the signatures of all persons using or photocopying this thesis. Please sign below, and give address and date.

Abstract

Grating-coupled surface-emitting lasers became an area of growing interest due to their salient features. Emission from a broad area normal to the wafer surface, makes them very well suited in high power applications and two-dimensional laser arrays. These new possibilities have caused an interest in different geometries to fully develop their potential. Among them, circular-grating lasers have the additional advantage of producing a narrow beam with a circular cross section. This special feature makes them ideal for coupling to optical fibers. All existing theoretical models dealing with circular-grating lasers only consider first-order gratings, or second-order gratings, neglecting surface emission.

In this thesis, the emphasis is to develop accurate models describing the laser performance by considering the radiation field. Toward this aim, and due to the importance of the radiation modes in surface-emitting structures, a theoretical study of these modes in multilayer planar structures has been done in a rigorous and systematic fashion. Problems like orthogonality of the radiation modes have been treated very accurately. We have considered the inner product of radiation modes using the distribution theory. Orthogonality of degenerate radiation modes is an important issue. We have examined its validity using the transfer matrix method. It has been shown that orthogonality of degenerate radiation modes in a very special case leads to the Brewster theorem. In addition, simple analytical formulas for the normalization of radiation modes have been derived. We have shown that radiation modes can be handled in a much easier way than has been thought before.

A closed-form spectral dyadic Green's function formulation of multilayer planar structures has been developed. In this formulation, both rectangular and cylindrical structures can be treated within the same mathematical framework. The Hankel

transform of some auxiliary functions defined on a circular aperture has been used to obtain the far-field pattern of the aperture. It has been shown that the far-field patterns of all circular apertures except those with the first harmonic azimuthal variation have a dark spot at their centers.

Threshold analysis of circular-grating lasers has been performed by considering surface emission. In this study, we have assumed that the laser beam is circularly symmetric. Based on the large argument approximation of the Hankel functions, we have shown that the interaction between the amplitudes of the guided modes can be described by coupled-mode equations containing coupling factors to the radiation field. These factors have been obtained by using the Green's function approach. The transfer matrix method is essential in obtaining the Green's function.

The relationship between the input current and the output power of circular-grating lasers producing circularly symmetric beams has been derived by developing suitable rate equations for the total number of photons and the phase of the optical amplitude in the laser cavity. We have solved the rate equations above the threshold under steady state conditions. Formulas for radiating power and far-field patterns have also been presented.

The theoretical treatment of the radiation modes developed earlier makes it possible to include radiation modes in coupled-mode equations in cylindrical structures. We have done so to pave the way for treating laser fields that are not circularly symmetric. Among them, the laser fields that have the first harmonic azimuthal variation are highly desirable due to the nonzero value of the radiation field on the axis of the laser.

Acknowledgements

I would like to extend my sincere thanks to my supervisor, Professor Wei-Ping Huang, for his encouragement, continuous support, guidance and constant inspiration throughout the entire course of this research work. I am very impressed by his great personality and supportive character. Besides introducing me to the area of photonics and DFB lasers, he taught me how to unravel complex physical pictures by using some intuitive ideas. Working under his supervision during the period of my Ph.D. research work has a great impact on my life and future career.

Special thanks also go to Dr. Xun Li who spent many patient hours teaching me DFB lasers. Much of this work would not have been possible without his assistance. It was a great opportunity for me to have many counseling sessions with him. I found him so knowledgeable in many aspects of DFB lasers that during each discussion we have had, I realized that I do not know much about DFB lasers. What I owe him is beyond the evaluation. I would also like to express my gratitude to him for tailoring the DFB mode solver extensively used in this thesis.

I wish especially to thank Dr. Toshiko Makino, manager of semiconductor laser design at Nortel, for his encouragement in pursuing this project.

It is my great pleasure to thank Professor Sujeet K. Chaudhuri, one of the members of my examination committee, for giving me constructive criticism of the manuscript and for allowing me to audit his course in Fourier optics. From that course, the idea of using distribution theory in the proof of orthogonality of radiation modes crossed my mind. I would also like to extend my gratitude to Professor Robert H. MacPhie and Professor Marek S. Wartak, the other members of my examination committee, for their useful suggestions. My gratitude is also due to the external examiner of this thesis, Professor Romain Maciejko from École

Polytechnique de Montrèal, for his interest in this work and his helpful insight.

I will forever be in debt to Professor Safieddin Safavi-Naeini, my advisor during master program at the University of Tehran. His superb knowledge in electromagnetics and distinguished teaching skill was a great motivation for continuing my studies in this area. I appreciate his help in various aspects of my life.

I am also indebted to Mr. Fred Ma and Dr. Masoud Yousefi for helping me in the numerical simulation at the early stages of this work. I also thank Dr. Andrew M. Sarangan for his technical advice. I would also acknowledge Dr. Ramin Sabry, Dr. Brent Little, Dr. Chenglin Xu, Dr. Sylvain Lessard, Dr. Gordon Strachan, Mr. Rob Singh, Mr. Wei Li, Mr. Vien Van, and Mr. Essam Tony, the other members of the Waterloo Photonics Group, for their social interaction.

I acknowledge the Ministry of Culture and Higher Education of Iran for the financial support.

Finally, I would like to extend my love and gratitude to my wife, Fatereh, for her patience, encouragement and moral support, to my daughter, Roya, for the fun she brought to me. The last, but not the least, I am grateful to my parents for their love, support and constant blessing, to my brother and sisters for their love, to my parents-in-law for their encouragement and support.

To my parents, who devoted their lives to the prosperity of their children.

To my wife for sacrificing the best times of her life and enduring the hardship of this work more than me.

To my brother and sisters for their love.

To the memory of my uncle, Hashem Shams-Zadeh-Amiri, my first teacher in mathematics.

Contents

List of Tables

List of Figures

List of Abbreviations

CGSEL	Circular-Grating Surface-Emitting Laser
DBR	Distributed Bragg Reflector
DFB	Distributed Feedback
FD	Finite Difference
GCSEL	Grating-Coupled Surface-Emitting Laser
HIP	Hermitian Inner Product
LSE	Longitudinal-Section Electric
LSEM	Longitudinal-Section Electric and Magnetic
LSM	Longitudinal-Section Magnetic
MPS	Multilayer Planar Structure
PMM	Power Matrix Method
SEL	Surface-Emitting Laser
SIP	Symmetric Inner Product
TE	Transverse Electric
TLM	Transmission Line Method
TM	Transverse Magnetic
TMM	Transfer Matrix Method
VCM	Volume Current Method
VCSEL	Vertical Cavity Surface-Emitting Laser

Chapter 1

Introduction

1.1 Background

The advent of photonic technology constitutes a very important chapter in the history of telecommunications. The arrival of low loss silica fibers in the early 1970s emphasized the need for compact, low-cost, high-performance, and reliable optical sources. As a result of improved material technology and extensive activities in the past fifteen years, semiconductor laser technology has undergone rapid advances such that today it is one of the principal constituents of optical communications. In fact, the information age heavily relies upon two technological achievements: (1) the production of low-loss optical fibers and (2) the practical realization of semiconductor lasers operating at room temperature.

The laser technology has also attractive applications in areas other than communications such as manufacturing, medicine, and biology. Compact optical disks and optical interconnects between computers are very popular applications.

Undoubtedly the development of lasers and integrated optic technology will

continue over the next century. They promise novel applications and far-reaching impact in the near future. The rapid pace of these technological advances shows that one can expect the replacement of electrons by photons in many stages of data processing.

1.2 Surface-Emitting Lasers

In edge-emitting laser structures, shown in Fig. 1.1, the emission of the lasing radiation is parallel to the plane of the active layer. Surface-emitting lasers (SELs) are distinguished from edge-emitting ones by emission of light normal to the substrate plane. This salient feature causes the laser output to be easily accessed without cleaving and dicing. Therefore, it is possible to integrate a SEL into an optoelectronic integrated circuit without separating it from the rest of the chip.

SELs, depending on the mechanism of surface emission, are divided into three basic types which are briefly described in the following sections.

1.2.1 Vertical Cavity SEL

A generic vertical cavity SEL (VCSEL) structure utilizes the feedback mechanism in the direction normal to the surface of the wafer in the laser cavity. A Fabry-Perot version of these types of lasers is shown in Fig 1.2 (a). Two mirrors parallel to the wafer surface provide the feedback and cause the light to be emitted from the broad surface area. In a distributed Bragg reflector version, the active region is sandwiched between alternating low-index and high-index layers forming the Bragg mirror.

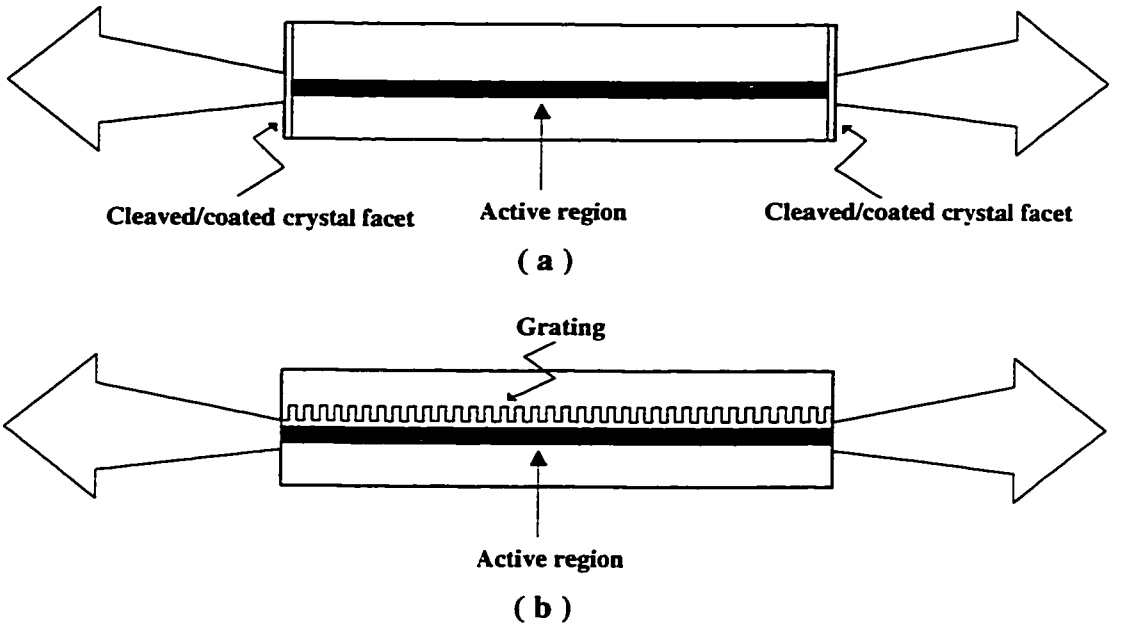

Figure 1.1: Conventional edge-emitting lasers. (a) Fabry-Perot cavity type. (b) Distributed feedback type.

The first VCSEL in 1977 [1] attracted little attention among the research community, due to its poor performance, e.g., high threshold current and no CW operation at room temperature. The research activity in this area was limited to a single group led by Kenichi Iga at the Tokyo Institute of Technology [2]. However, as a result of the contributions of many research groups in the past few years, today's state-of the-art VCSELs operate at threshold currents below 1mA [3]. Their small sizes make it possible that a large number of them can be packed in a small area. In high power applications an array of VCSELs also has been reported [4].

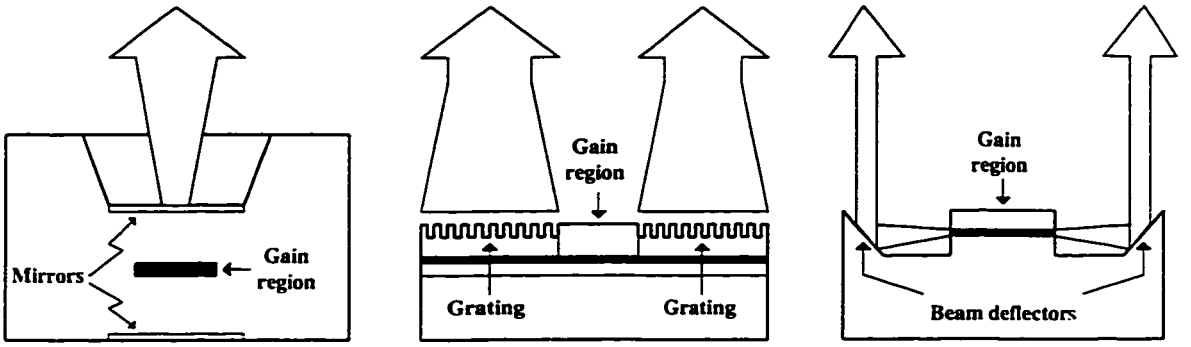

Figure 1.2: Three basic types of surface-emitting lasers. (a) Vertical cavity SEL. (b) Grating-coupled SEL. (c) Folded cavity SEL.

1.2.2 Grating-Coupled SEL

These kinds of lasers use grating to provide both feedback for laser oscillation and a converting mechanism to the surface emission. The schematic diagram of these devices is illustrated in Fig. 1.2 (b). Historically, the invention of DFB dye lasers by Kogelnik and Shank [5], [6] led many researchers to use Bragg scattering properties of periodic corrugation as a feedback mechanism in semiconductor DFB lasers [7].

At wavelengths around 0.85 μm, fabrication difficulties required the use of distributed Bragg reflectors of second- and higher- orders rather than first-order. As a result, constructive interference of the low-order diffraction of counter-running waves led to radiation of the power from the surface of the grating. Therefore, the demonstration of grating SELs took place simultaneously with the realization of conventional edge-emitting DFB lasers [8]-[11]. However, the radiative output coupling was referred to as radiation loss [12] and considered as a mode discrimination mechanism for edge-emitting lasers.

In recent years, many research activities have been concentrated in the area of grating-coupled SELs (GCSELs). This is mainly due to their potential advantages, emission from a broad surface area and ease of being integrated monolithically in an array or other planar photonic devices.

In comparison with VCSELs which offer small size and extremely large-scale integration possibilities, GCSELs are desirable for high power applications, due to their large emission area. They can also be fabricated on less demanding layer structures [13]. In particular, by the diffraction mechanism, it is potentially possible to control the direction and the shape of the output beam by designing more complex gratings.

1.2.3 Folded Cavity SEL

The performance of the third kind of SELs like GCSELs is based upon the characteristics of conventional edge-emitting lasers. That is, a grating provides feedback mechanism for laser oscillation. However, another approach is used for converting the edge emission to the surface emission. As shown schematically in Fig. 1.2 (c), in a common version of this architecture, a deflecting integrated mirror is located internal or external to the laser cavity for redirection of the laser beam. This technique for fabrication of SELs is more recent than the other two and has been developed extensively during the past few years [14].

These structures in comparison with GCSELs allow denser packing in a two-dimensional laser array. Moreover, the feedback and redirection mechanism in these structures, unlike GCSELs, are independent. This means that they can potentially be used in two-dimensional arrays resulting in an overall performance equivalent to conventional edge-emitting lasers. The design and fabrication of integrated deflec-

tors is an important issue in these structures and faces technological challenges.

1.3 Applications and Future Prospects of Surface-Emitting Lasers

Light emission from the broad surface area of surface-emitting lasers opens up new applications which can exploit this unique property. In addition, SELs lend themselves to be tested at the wafer level. This yields improved performance and reliability and tremendous reduction in costs. More importantly, they can be easily integrated with other photonic devices. The surface-emission property of SELs has opened new possibilities of integrating them into two-dimensional arrays which have wide range of potential applications. These exciting new devices have also potential applications in high power operations with controlled output beams for space communication, data storage, laser printing, medicine, neural networks and optical computing. Individual SELs may represent an alternative to existing cleaved-facet lasers.

As a result of the growing interest in this area, surface-emitting lasers are in a stage of dynamic development. The threshold current in these devices has been decreased and further progress is possible by using current confining structures. An important issue in high power applications is the development of thermal packaging of laser arrays. This is under investigation. The rapid pace of this progress shows that in the near future coherent two-dimensional surface-emitting laser arrays with good beam quality and with high output power will enter into major industrial and commercial use.

1.4 Research Progress in the Area of Circular-Grating Surface-Emitting Lasers

By circular grating, we mean a perturbation in the electrical properties of a structure which appears as a periodic function of the distance ρ from the origin. We only consider shallow radial corrugations at the dielectric interfaces of a multilayer planar structure. Such perturbations couple the inward propagating cylindrical mode with the outward one. The result of such a performance is the establishment of a standing wave. This is the characteristic behavior of a resonator.

The idea of using curved-line grating as reflectors and resonators in integrated optics was first proposed by Tien [15]. Kerner *et al.* [16] were the first to investigate the coupling between the guided waves in a circular grating. The quality factor of circular grating resonators was discussed by Zheng and Lacroix [17] through development of coupled-mode equations. Following Kogelnik's approach [18], Wu *et al.* [19] ,[20] developed a self-consistent coupled-wave theory for circular gratings and discussed the cross coupling between TE and TM waves.

The two-dimensional nature of such resonators allows their use in a number of practical applications which cannot apply straight gratings. Some applications of these resonators are shown in Fig. 1.3 where the coupling mechanism between the input and output is provided by implanting a taper-like structure into the resonator [17]. In addition to the resonance property, these architectures can be used to focus and collect a light beam into an optical detector [21]. Similar to their one-dimensional straight grating counterparts, circular gratings can couple two propagating modes with the radiation field by means of the diffraction mechanism.

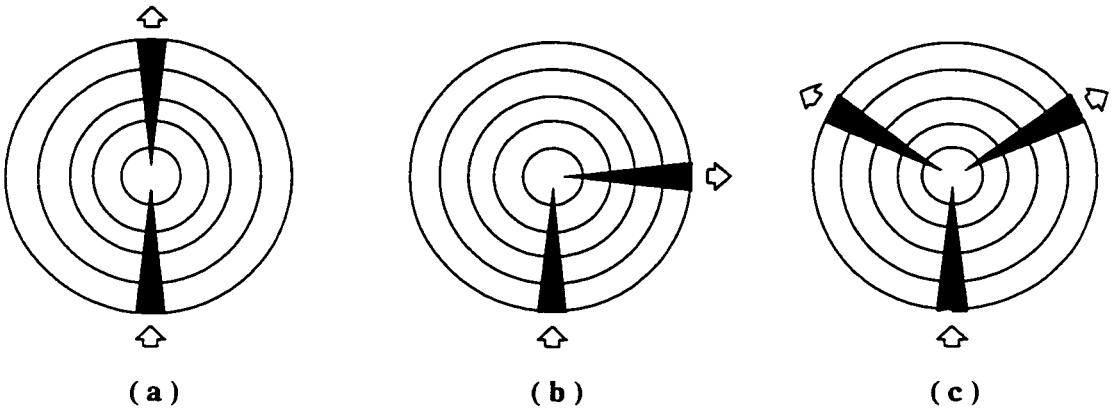

Figure 1.3: Schematic of circular-grating resonators. (a) Filter with aligned input and output. (b) Filter with perpendicular input and output. (c) Optical star coupler (After [17]).

Demonstration of the resonant behavior of circular gratings led Schimpe [22] to patent the idea of using circular gratings in DFB lasers. Although the circular-grating structure is an unusual scheme for edge-emitting lasers, it has potential advantages for the realization of SELs. The output beam emitting from a large *circular aperture* is an important feature which is not present in conventional straight-grating surface-emitting lasers. This feature can be used effectively in two-dimensional planar arrays. The output beam with a circular cross section also allows efficient coupling to the fiber. However, the one dimensional nature of straight gratings with output beams of unequal divergence angles in two different directions causes the reduction of coupling efficiency.

The issued patent of Schimpe and the analytical approach of Toda [23] for potential disk-shaped DFB lasers were brought to the attention of two research groups in the United States and Canada. Their research activities were triggered to challenge the realization of circular-grating surface-emitting lasers (CGSELs) and place their analysis in a proper structural form. Erdogan and Hall [24] were

the first to analyze the near-threshold behavior of a circularly symmetric first-order DFB laser. They developed coupled-mode theory for all azimuthal modes of a scalar field. This theoretical work further stimulated the interest in these structures. The first practical demonstration of an optically-pumped CGSEL was presented by Wu *et al.* [25]. The 1.283 μm double heterostructure GaInAsP/InP laser was tested under pulsed conditions at room temperature. Only a short time later, Erdogan *et al.* [26], [27] reported the observation of a 0.8175 μm low divergence circularly symmetric surface emission from a AlGaAs/GaAs quantum well semiconductor laser. The laser was tested under pulsed conditions while mounted on a heat sink held at $\sim$ 77 K.

Wu *et al.* [28], [29] succeeded in presenting the lasing characteristics of the first 1.3 μm electrically-pumped circular-grating surface-emitting DBR laser. The GaInAs/InP heterostructure operated at room temperature under pulsed conditions. The reported threshold current and the output power were 170 mA and 10 mW, respectively.

In addition to these experimental demonstrations, more accurate analytical formulations have also been reported. Erdogan and Hall [30] derived coupled-mode equations for radially outward and inward-going cylindrical modes in a first-order circular grating. They carefully treated the vector orientation of the transverse electric (TE) fields. The effect of ignoring the vector nature of the fields in the coupled-mode equations can best be seen by comparing the asymptotic behavior of these equations for large values of ρ with those obtained from their scalar approach. The fundamental difference between these two approaches is the interchange of the even and odd azimuthal modes in a DFB laser cavity. Makino and Wu [31] analyzed threshold current for DFB and DBR lasers with circular symmetry. This was followed by the threshold gain and threshold current analysis of the first-order

circular-grating DFB and DBR laser [32].

One can predict from the periodic nature of the azimuthal direction in a CGSEL that the lateral modes are in competition. This means that the laser field, in general, is a linear combination of these modes. This multimode operation is an obvious drawback in single-mode applications like satellite communications and nonlinear optics. Gong *et al.* [33], [34] by the coupled-mode approach, treated effective reflectivity and the threshold gain of all lateral modes in an electrically-pumped surface-emitting DBR laser. They analyzed second-order gratings surrounding the pumped region at the center. Their model predicts the suppression of unwanted lateral modes of odd symmetry by introducing a small perturbation into the complex dielectric constant of the active region. However, they ignored the coupling to the radiation fields in their coupled-mode formalism.

As a closer step toward gaining high power and low threshold current, Fallahi *et al.* [35] reported the fabrication of electrically-pumped circular-grating surface-emitting DBR laser. The InGaAS/GaAs strained single-quantum-well laser was tested under pulsed conditions with a threshold current below 85 mA, output power more than 20 mW, and a divergence of less than 1° FWHM. In their recent experimental work [36], as a result of advances in the material technology and especially of improved electron-beam lithography techniques for producing circular gratings, they have reported a low threshold CW operation circular-grating DBR laser . The threshold current was reported as low as 26 mA at the operating wavelength 0.98 μm. All of the works on first-order circular gratings that have been reported until the end of 1996 were restricted to the threshold analysis. Recently, Kasunic and Fallahi [37] reported the above-threshold analysis of first-order circular gratings by considering the gain and index saturation.

In addition to conventional structures, some novel ideas have also been reported

in the fabrication of CGSELs. Wu *et al.* [38] reported a novel CGSEL with an emission from the center. In this structure, a second-order circular grating is located right at the center of the laser and the optical gain is obtained by injecting current through the annular active region that surrounds the second-order grating at the center. Optical feedback is provided by the first-order grating that encloses both the annular region and the central region. Unlike the previous designs, since the second-order circular grating is located at the center of the structure, the emission surface is circular. This is the most obvious advantage of this device. Moreover, each of these three regions has an independent effect on the laser performance. This is ideal for the purpose of optimization. An additional advantage of this new design is that the bonding wire is no longer in the way of the emitted light. Using the same idea, recently another type of circular-grating laser has been fabricated [39]. In this design, the conventional first-order circular-grating DBR laser with the active region at the center is surrounded by a second-order grating to defocus the light.

Radiation from circular gratings etched on the planar waveguides has been considered in non resonant cases [40],[41], and [42]. All of these considerations are based on the azimuthally invariant field assumption.

To the best of our knowledge, the above review reflects the present status of the reported research activities in the field of CGSELs. Although the pace of advances in this area has been very rapid, the problem of considering the radiation field in these structures is still an open problem and must be overcome. The main body of this thesis is based on this challenge. The more details of this matter are addressed in the next section.

1.5 Thesis Outline

As mentioned in the previous section, one of the challenging issues in the study of CGSELs is the inclusion of the radiation effect in their analysis. Our primary goal is to consider this effect. Specifically, obtaining the relationship between the output power emitted from the surface of the laser and its excitation is highly desirable. From this relationship, it is also possible to optimize the laser performance which can be used in the design of the laser. In this dissertation, we are aiming at developing some general frameworks based on the well-established models to analyze circular-grating lasers. Moreover, tailoring some of these well-established models to fit some particular situations is of paramount importance.

In surface-emitting structures the importance of the radiation modes of a multilayer planar structure comes into perspective. On the other hand, dealing with the radiation modes in the open-boundary structures is not a straightforward matter. Especially, in cylindrical structures, this situation is more complicated. Therefore, developing a systematic approach to treat the radiation modes with mathematical rigor is highly desirable. In this thesis, for the first time, we have achieved this important step. We have developed a general model to consider guided and radiation modes on the same footing.

By introducing suitable scalar potential functions and the factorization method, we have shown that the complicated electromagnetic problem in a multilayer planar structure reduces to two independent scalar one-dimensional problems. The elements of this functional space are called *form functions*. Based on the assumption that the waveguide structure is lossless, we have shown that theses *form functions* are the solutions of a self-adjoint differential operator. Moreover , it has been shown that the functional space of the *form functions* of the guided modes is real-valued.

Whereas, that of the the radiation modes is complex-valued. We have also considered the possibility of constructing real functional space of the *form functions* of the radiation modes.

Since the *form functions* are the solutions of a self-adjoint operator, it is possible to define suitable inner products. In fact, we have considered two different inner products in these functional spaces. In general, we have shown that the *form functions* are orthogonal in the sense of these inner products. The orthogonality of the *form functions* of the guided modes seems a trivial matter. However, due to the oscillatory nature of the *form functions* of the radiation modes in the substrate and the cover regions, their orthogonality needs more deliberation.

The unique feature in our study is using the distribution theory in the proof of the orthogonality of the radiation modes. This idea can also be used to prove the orthogonality of the kernel of the Fourier transform. More importantly, we have shown that the *form functions* of the radiation modes can be used as the generalized kernel of the Fourier transform. In addition, we have demonstrated that the suitable *form functions* defined for the radiation modes are orthogonal for two degenerate modes. Using the orthogonality relation of degenerate radiation modes, we have introduced and proved the Brewster theorem. Of particular interest is the problem of the normalization of the *form functions* of the radiation modes. Based on the idea of power conservation, we have derived and proved very simple formulas for constructing normalized basis functions. Finally, we have considered the problem of orthogonality and normalization of the vector fields by using their simpler scalar counterparts.

Since these subject matters are completely general and are treated in a self-contained mathematically rigorous fashion, we have covered the complete details of this particular study in Appendices A and B. However, this by no way means that

the importance of these materials are less than the other parts of this thesis. The systematic approach and its mathematical rigor are two of the main contributions of this thesis.

Chapter 2 focuses on the spectral dyadic Green's functions of multilayer planar structures and the circular aperture theory. It can be considered as a natural extension of the materials covered in Appendix A. The purpose of this chapter is to provide the same mathematical framework for treating rectangular and cylindrical coordinate systems. This has been done by defining suitable auxiliary functions based on two recursive identities of the Bessel functions. The transfer matrix method (TMM) is fundamental in our formulation.

The TMM makes it possible to obtain the closed-form dyadic Green's function. Besides, some theoretical conclusions can also be explicitly drawn which are very important in the numerical calculations. Among them is the nature of the poles of the Green's functions which are naturally the zeros of the characteristic equation of the guided modes. Moreover, it can also be shown that the Green's functions are independent of the branch cut of the dispersion parameter in each layer of finite thickness.

The main reason for introducing the Green's functions is twofold. First, we have used the Green's functions in the spectral domain to obtain the general expression for the far-field pattern of a circular aperture. From these expression, it has been shown that only aperture fields with the first harmonic of azimuthal variation produces a nonzero far field pattern on the axis of the aperture. In fact, there will be a dark spot at the center of the far-field pattern of circular-grating lasers, if the azimuthal modes other than the first harmonic are excited. Second, we have used the Green's function approach in a perturbational manner to derive the far-field pattern of circular-grating lasers.

Threshold analysis of CGSELs is the subject of Chapter 3. The effect of the radiation field on the amplitudes of the guided modes has been properly included. This special feature, distinguishes Chapter 3 from previous works in the literature. For the sake of mathematical simplicity, we have assumed that the laser beam is circularly symmetric. The modal analysis based on this assumption provides the fundamental background material for treating circular-grating lasers above the threshold. In addition, we have shown that within the limits of the validity of large argument approximation of the Hankel functions, the coupled-mode equations describing the behavior of the guided modes reduce to those conventional equations governing second-order DFB lasers with straight gratings.

We have used the Green's function method to obtain the coupling factor to the radiation field. Again, the TMM is the basic tool in the derivation of a suitable Green's function in a multilayer planar structure. It has been shown that this factor as a function of the grating's duty cycle in a rectangular grating is almost symmetric about the 50% point. Moreover, in almost all practical cases the real part of it is less than 10 cm^{-1}. We have also shown that to increase the amount of the radiation field, some feedback in the laser cavity must be sacrificed.

Chapter 4 covers the main body of this thesis. In this chapter we have formulated the rate equations of second-order DFB lasers using the time domain standing wave approach. Above-threshold analysis of second-order DFB lasers reported so far is based on the traveling wave approach in the time domain or using the power matrix method (PMM). Therefore, this formulation provides an alternative approach in treating second-order DFB lasers above the threshold. This method is the modified version of the original formulation developed in the Optics Group at the University of Waterloo. Based on this approach, we have derived rate equations for the number of photons and the phase of the optical amplitude inside the laser

cavity.

The formulation of the rate equations is two dimensional in nature, i.e, it is assumed that the optical field is invariant with respect to one of the coordinate variables. Therefore, it is very well suited in treating circularly symmetric beams in circular-grating lasers. The formulation is such that nonlinear and spatial hole burning effects can be treated properly. Moreover, it lends itself in small signal and large signal analysis. However, for the purpose of this thesis and since circular-grating lasers are in the early stages of experiments, we have only considered the above-threshold static analysis. In Chapter 4 the relation between the excitation and the output power has been obtained. Moreover, the far field-patterns of the radiation field at different bias currents have also been derived.

The major part of this thesis is based on the assumption of a circularly symmetric laser beam. On the other hand, a circularly symmetric beam is not the most desirable laser output. At least, the far-field pattern has a dark spot at its center. However, the laser field with the azimuthal variation as $cos\phi$ and $sin\phi$ is the only field which is nonzero on the laser's axis in the far zone. Therefore, the next step is to include the azimuthal variations in the study of circular-grating lasers. To this end, in Chapter 5, we have developed generalized coupled-mode equations governing cylindrical waveguides with circular grating in the presence of the radiation modes. This work is a generalization of Erdogan' method [30] in dealing with circular-grating structures. Inclusion of the radiation modes in the coupled-mode equations is the unique feature of this generalized method. Moreover, the theoretical concepts covered in Appendix A are the fundamental basis of this formulation. Therefore, we claim that, this generalization is the original work that includes the radiation fields in the governing coupled-mode equations of circular-gratings.

We have essentially used two different approaches. In the first approach, the

so-called scalar approach, we ignore variations of the dielectric perturbation in the radial direction. Whereas, in the vector formulation this effect is properly included. We do not claim that this formulation is the only way to consider arbitrary azimuthal variation in the laser's performance. Therefore, we intend to find some easier and more efficient ways to treat these cases. This may be reflected in our future work. Finally, in Chapter 6 we give some guidelines for the future work in the area of circular-grating lasers.

Throughout this thesis an attempt has been made to present the materials in a continuous and inductive manner. In particular, many formulas have been derived carefully. In order not to disrupt the continuity of the treatment, the derivation of all formulas are relegated in the appendices.

Chapter 2

Spectral Dyadic Green's Function of Multilayer Planar Structures and Theory of Circular Apertures

2.1 Introduction

This chapter is the natural extension of the subject matters treated in Appendix A. In that appendix, we have exclusively considered the source-free electromagnetic field in a multilayer planar structure (MPS). That investigation led to the intrinsic features of a MPS. In this chapter, we focus on a MPS in the presence of a source. This in turn calls for the Green's functions in these structures. The main goal here is to develop a mathematical tool that allows us to accurately predict the related radiation field of a source in the presence of a MPS.

From a mathematical point of view, the solution of an inhomogeneous linear differential equation can be obtained from the solution of the corresponding homo-

geneous equation. Therefore, one might expect that many characteristic features of the Green's function can be related to the intrinsic properties of a MPS. Our formulation is based on the potential approach. However, instead of obtaining a nonhomogeneous differential equation satisfied by the potential functions, we consider the source as a discontinuity condition imposed on the some field components. These conditions in turn can be transformed to appropriate conditions on the potential functions.

To use many results developed in Appendix A, we use integral transform techniques, the so-called spectral domain method in the solution of our problem. As will be illustrated, we discover why the method of separation of variables lies at the heart of the integral transform technique. The complexity of the space domain Green's function is another reason behind using the spectral domain approach. More importantly, by using the transfer matrix method, we will show that the spectral domain Green's function is mathematically more tractable.

In this chapter two formulation technique are described. First, the Green's function transformed in the Fourier domain will be considered. This is followed by the Hankel transform method in the cylindrical coordinate system. However, before stating the Green's function formulation, in the next section we describe how an integrated optic problem can be considered as an excitation of a MPS by a current source. This is another motivation for using Green's function approach.

2.2 Volume Current Method

Essentially, the volume current method (VCM) is based upon the scattering theorem in the electromagnetic theory. This technique was originally formulated by Snyder [43] to investigate the radiation loss due to unexpected variations of the radius

along the length of a fiber. White [44] used a general form of the method to treat the scattered field as the radiation field in bent structures. The applicability of this method in the treatment of practical radiation loss dielectric structures was also investigated by Kuznetsov and Haus [45]. Jordan and Hall [41] used this approach to find the radiation field from a concentric-circle grating located at the film-cover interface of a three layer planar optical waveguide.

Although the volume current method can be applied for an arbitrary structure, for the purposes of this thesis, we illustrate this method by considering two multilayer geometries as illustrated in Fig. 2.1. By *unperturbed structure*, we mean that the electrical properties of the structure is piecewise homogeneous in the direction normal to the planar interfaces and there is no variation along the planes transverse to the z axis. Let us assume that $\mathbf{E}^i$ and $\mathbf{H}^i$ (called *incident waves* in scattering terminology) satisfy Maxwell's equations in the unperturbed geometry shown in Fig. 2.1 (a)

$$\begin{aligned} \nabla \times \mathbf{E}^i &= -j\omega\mu_o\,\mu_r(z)\,\mathbf{H}^i \\ \nabla \times \mathbf{H}^i &= j\omega\epsilon_o\,\epsilon_r(z)\,\mathbf{E}^i \end{aligned} \tag{2.1}$$

where a time dependence $e^{j\omega t}$ has been assumed. Introducing inhomogeneity in the unperturbed structure in the otherwise piecewise homogeneous structure, as illustrated in Fig. 2.1 (b), modifies the incident fields by the amount of inhomogeneity-induced scattered fields $\mathbf{E}^s$ and $\mathbf{H}^s$ such that

$$\begin{aligned} \nabla \times (\mathbf{E}^i + \mathbf{E}^s) &= -j\omega\mu_o\,\mu_r(x,y,z)\,(\mathbf{H}^i + \mathbf{H}^s) \\ \nabla \times (\mathbf{H}^i + \mathbf{H}^s) &= j\omega\epsilon_o\,\epsilon_r(x,y,z)\,(\mathbf{E}^i + \mathbf{E}^s) \end{aligned} \tag{2.2}$$

Expanding (2.2) and using (2.1) leads to the following equations for $\mathbf{E}^s$ and $\mathbf{H}^s$:

$$\begin{aligned} \nabla \times \mathbf{E}^s &= -j\omega\mu_o\,\mu_r(z)\,\mathbf{H}^s - \mathbf{M} \\ \nabla \times \mathbf{H}^s &= j\omega\epsilon_o\,\epsilon_r(z)\,\mathbf{E}^s + \mathbf{J} \end{aligned} \tag{2.3}$$

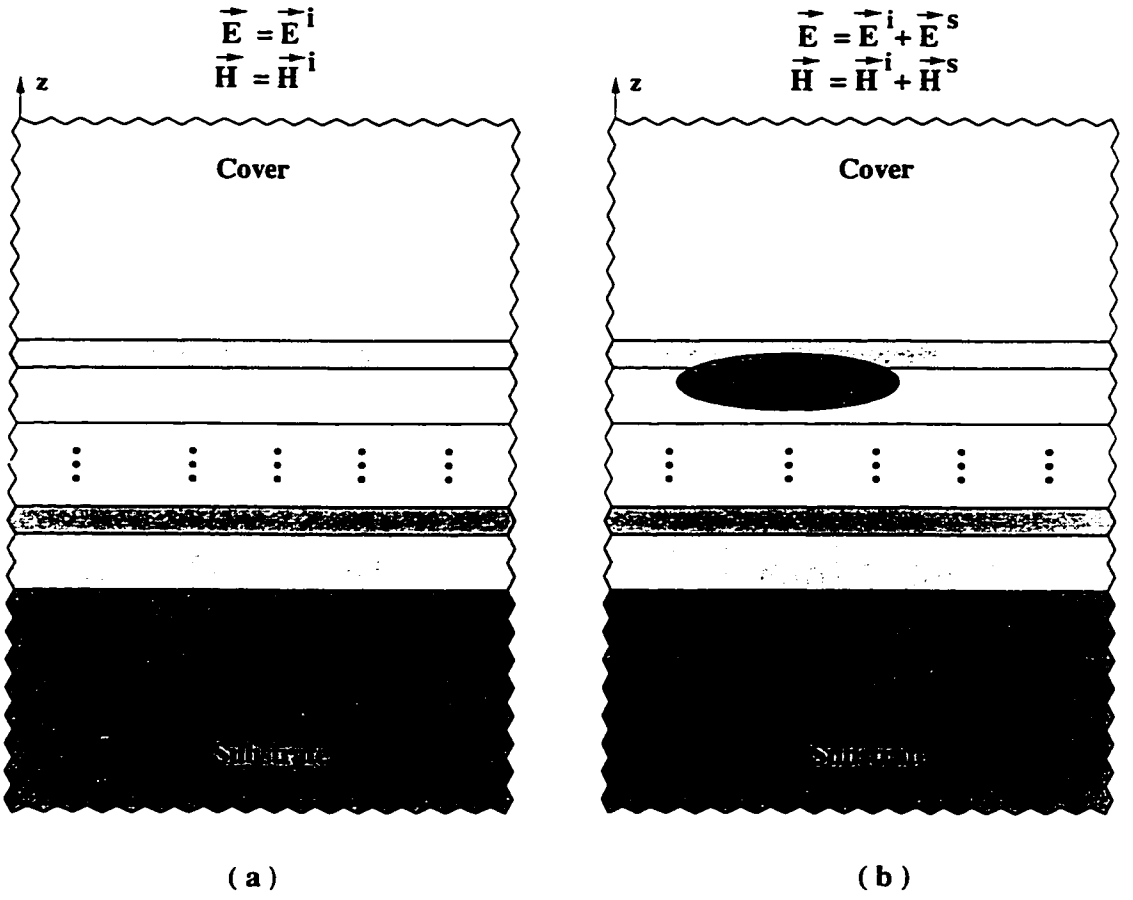

Figure 2.1: Schematic illustration of the volume current method. (a) Unperturbed geometry. (b) Perturbed geometry.

where

$$\mathbf{M}(x,y,z) = j\omega\mu_o\,[\,\mu_r(x,y,z) - \mu_r(z)\,]\,(\mathbf{H}^i + \mathbf{H}^s) \tag{2.4a}$$

$$\mathbf{J}(x,y,z) = j\omega\epsilon_o\,[\,\epsilon_r(x,y,z) - \epsilon_r(z)\,]\,(\mathbf{E}^i + \mathbf{E}^s) \tag{2.4b}$$

M is the equivalent magnetic current source which accounts for inhomogeneity in the magnetic properties. Similarly, **J** is the equivalent electric current source. This current source excites the scattered fields due to the inhomogeneity in the electrical properties.

The volume current method is based on the equations in (2.3). According to (2.3), solutions for the unknown scattered fields, $\mathbf{E}^s$ and $\mathbf{H}^s$, leads to the solution of the unperturbed planar structure excited by $\mathbf{J}$ and $\mathbf{M}$. However, these current sources are field dependent. Especially, they depend on the unknown scattered fields. Despite the fact that the equations in (2.3) are exact, however, the presence of the dependent current sources in these equations makes the volume current method an approximate approach in nature.

The approximation involved in this method depends on two factors: (1) estimation of the equivalent current sources and (2) derivation of the scattered fields from these sources. Therefore, the accuracy of this method can be improved by (1) improving the estimation for the current sources, and (2) improving the methods for solving (2.3). In the literature, an estimation about the current sources are made by ignoring the scattered fields inside the structure. This approximation is reasonable for perturbational problems. Moreover, by taking advantage of the small differences between the electrical properties of each layer in the unperturbed geometry, the exact dyadic Green's function is approximated by the Green's function in the uniform space, e.g., [41]. As a step toward more accurate results, we have developed an exact Green's function formulation in this chapter.

After considering integrated optic problems as a current excitation of a MPS, in the next section we turn to the formulation of the spectral domain dyadic Green's function in the rectangular coordinate system.

2.3 Green's Function in the Rectangular Coordinate System: Fourier Transform

Spectral method has been used extensively in the study of the characteristics of either single or multilayer planar structures. The so-called *immittance* approach [46], [47] enables one to obtain the Green's function by decomposing the fields into LSE and LSM parts and using transmission line concepts. This method has also been used to obtain the dyadic Green's function under three-dimensional source excitation inside a single-layer microstrip line [48]. Although the immittance approach is very sophisticated and insightful, the large number of layers makes the formulation complicated. In this section an attempt has been made to formulate the problem with the transfer matrix method which makes it very well suited for arbitrary number of layers. Moreover, some field-theoretic concepts can be derived from this formulation.

To illustrate the formulation process, let us consider a multilayer stack excited by a volume current density inside as depicted in Fig. 2.2. Note that the current excitation may be either in the substrate or in the cover. Therefore, we aim at solving

$$\begin{aligned} \nabla \times \mathbf{E} &= -j\omega\mu_o\mu_r(z)\mathbf{H} \\ \nabla \times \mathbf{H} &= j\omega\epsilon_o\epsilon_r(z)\mathbf{E} + \mathbf{J} \end{aligned} \tag{2.5}$$

for $\mathbf{E}(\mathbf{r})$ and $\mathbf{H}(\mathbf{r})$ in a MPS based on the $e^{j\omega t}$ time variation. For the purposes of this thesis and the sake of mathematical formulation, we only consider a volume current density with components transverse to the z axis. That is,

$$\mathbf{J}(x,y,z) = J_x(x,y,z)\hat{\mathbf{x}} + J_y(x,y,z)\hat{\mathbf{y}} \tag{2.6}$$

In order to obtain the complete response to the volume excitation, one may apply the principle of superposition and divide the volume current into planar slices.

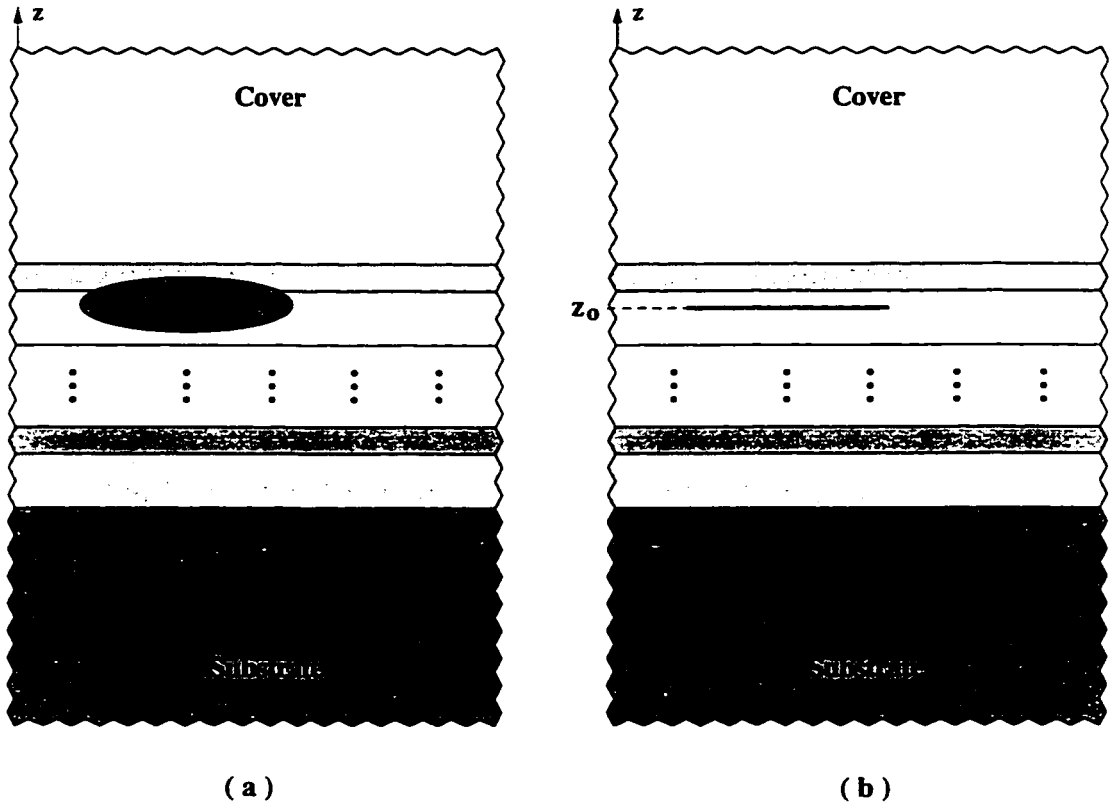

Figure 2.2: Excitation of a multilayer planar structure by electric current source. (a) Excitation by a volume current. (b) Excitation by a planar slice current.

Therefore, it is only necessary to consider the partial responses due to these planar excitations as illustrated in Fig. 2.2-(b). The planar excitation of MPS makes it possible to consider the whole stack as two semi-infinite piecewise homogeneous regions without any sources. Therefore, the fields in each source free region can be derived from the superposition of two types of the Hertzian scalar potential functions as described in Appendix A. The unknown amplitudes of the potential functions can be obtained by applying suitable boundary conditions at the source position.

Let us illustrate the basic idea by considering a MPS shown in Fig. 2.2-(b). It

is excited by a planar slice of the electric current located at $z = z_o$ inside. The current excitation can be expressed by the following relation:

$$\mathbf{J}(x,y,z) = [J_x(x,y,z_o)\hat{\mathbf{x}} + J_y(x,y,z_o)\hat{\mathbf{y}}]\,\delta(z-z_o) \qquad \frac{\mathrm{A}}{\mathrm{m}^2} \tag{2.7}$$

where $\delta(\cdot)$ stands for the Dirac delta function. The electromagnetic field in each homogeneous layer above and below $z = z_a$ can be derived from the two vector potential functions

$$\mathbf{\Pi}_i^{(e,h)}(x,y,z) = \hat{\mathbf{z}}\Psi^{(e,h)}(x,y,z) \tag{2.8}$$

where $\Psi^{(e,h)}$ is the solution of the homogeneous scalar Helmholtz equation given by (A.16). In Appendix A, it has been shown that the simplest form of the potential functions in a source free MPS are factorable into the *form functions* and the amplitude functions. This is possible only in the absence of a source. However, in the presence of the source there is no such a possibility. Despite this fact, one may take advantage of the linear property of the Helmholtz equation and express $\Psi^{(e,h)}$ as a superposition of these elemental solutions. This in turn leads to the idea of using the integral transform techniques with the *form function* or the amplitude function as its kernel.

For the electromagnetic problem in Fig. 2.2-(b) it is more appropriate to consider an integral transform with amplitude functions as its kernel. More precisely, $\Psi^{(e,h)}(x,y,z)$ in (2.8) can be considered as a superposition of the elemental potential functions

$$\psi^{(e,h)}(x,y,z) = F^{(e,h)}(z;k_x,k_y)e^{-j(k_x x+k_y y)} \tag{2.9}$$

Therefore, one may write

$$\Psi^{(e,h)}(x,y,z) = \int_{-\infty}^{\infty}\int_{-\infty}^{\infty} F^{(e,h)}(z;k_x,k_y)e^{-j(k_x x+k_y y)}dk_x\,dk_y \tag{2.10}$$

where $F^{(e,h)}(z;k_x,k_y)$ satisfies (A.28) with $\beta^2 = k_x^2 + k_y^2$ and the same boundary conditions for LSE and LSM modes in each source-free region. For the radiation spectrum, however, the presence of the source at $z = z_a$ eliminates the need for the incoming amplitude in the expression of $F^{(e,h)}(z;k_x,k_y)$ in the cover or the substrate region. That is, there is no difference between the mathematical representation of the *form functions* of substrate and cover modes. In fact, since the source of the wave is located inside, the coefficients in the substrate and cover are of the scattered type. Moreover, as will be illustrated later, the *form functions* in (2.10) depend on the spectral variables k_x and k_y. Whereas, in a source-free MPS, except for the type, the *form functions* depend on $k_x^2 + k_y^2$.

Equation (2.10) can be rewritten in a more appropriate form. To this end, if we define the two dimensional Fourier transform of $\Psi^{(e,h)}(x,y,z)$ as

$$\tilde{\Psi}^{(e,h)}(k_x,k_y,z) = \frac{1}{4\pi^2}\int_{-\infty}^{\infty}\int_{-\infty}^{\infty}\Psi^{(e,h)}(x,y,z)e^{j(k_x x+k_y y)}dx\,dy \tag{2.11}$$

we obtain

$$\Psi^{(e,h)}(x,y,z) = \int_{-\infty}^{\infty}\int_{-\infty}^{\infty}\tilde{\Psi}^{(e,h)}(k_x,k_y,z)e^{-j(k_x x+k_y y)}dk_x\,dk_y \tag{2.12}$$

Comparing (2.12) with (2.10), we come up with

$$\tilde{\Psi}^{(e,h)}(k_x,k_y,z) = F^{(e,h)}(z;k_x,k_y) \tag{2.13}$$

That is, the two dimensional Fourier transform of the Hertzian scalar potential functions play the same role as the *form functions*. Furthermore, in each source-free region $\Psi^{(e,h)}$ are the solutions of the scalar Helmholtz equation. Therefore, in each source-free region, substituting (2.12) into (A.16) leads to

$$\frac{\partial^2\tilde{\Psi}^{(e,h)}}{\partial z^2} - [\beta^2 - \mu_r(z)\epsilon_r(z)\,k_o^2]\tilde{\Psi}^{(e,h)} = 0 \tag{2.14}$$

Now it remains to to find the relation between the Fourier transforms of the potential functions and the excitation. This in turn requires one to obtain the field components in each homogeneous region by substituting (2.8) into (A.12) and (A.13). To this end, we may proceed in two ways. We can either choose the coordinate transformation that is usually used in the immittance approach or proceed directly. However, as will be seen later, using the transfer matrix formulation eliminates the need of coordinate transformation. Therefore, we choose the second approach and proceed directly. If $\Psi^{(e,h)}(x,y,z)$ is replaced by its spectral representation in (2.12), the electric field components an be obtained as

$$\begin{bmatrix} E_x(x,y,z) \\ E_y(x,y,z) \\ E_z(x,y,z) \end{bmatrix} = \int_{-\infty}^{\infty}\int_{-\infty}^{\infty} \vec{\vec{\mathbf{A}}}\,(k_x,k_y,z) \begin{bmatrix} \tilde{\Psi}^e(k_x,k_y,z) \\ \tilde{\Psi}^h(k_x,k_y,z) \end{bmatrix} e^{-j(k_x x+k_y y)}\,dk_x\,dk_y \tag{2.15}$$

where $\vec{\vec{\mathbf{A}}}\,(k_x,k_y,z)$ is the dyadic operator given by

$$\vec{\vec{\mathbf{A}}}_i\,(k_x,k_y,z) = \begin{bmatrix} -\frac{jk_x}{\epsilon_r(z)}\frac{\partial}{\partial z} & -\omega\mu_o k_y \\ -\frac{jk_y}{\epsilon_r(z)}\frac{\partial}{\partial z} & \omega\mu_o k_x \\ \frac{k_x^2+k_y^2}{\epsilon_r(z)} & 0 \end{bmatrix} \tag{2.16}$$

Using (2.16) in (2.15), the Fourier transform of the electric field components may be written as

$$\begin{bmatrix} \tilde{E}_x(k_x,k_y,z) \\ \tilde{E}_y(k_x,k_y,z) \\ \tilde{E}_z(k_x,k_y,z) \end{bmatrix} = \begin{bmatrix} -\frac{jk_x}{\epsilon_r(z)}\frac{\partial}{\partial z} & -\omega\mu_o k_y \\ -\frac{jk_y}{\epsilon_r(z)}\frac{\partial}{\partial z} & \omega\mu_o k_x \\ \frac{k_x^2+k_y^2}{\epsilon_r(z)} & 0 \end{bmatrix} \begin{bmatrix} \tilde{\Psi}^e(k_x,k_y,z) \\ \tilde{\Psi}^h(k_x,k_y,z) \end{bmatrix} \tag{2.17}$$

For the electric current excitation without any z component, the electric field components transverse to the z axis are continuous for all values of z. Therefore, the Fourier transform of these components must also be continuous. The above

statement means that for each value of z the following matrix equation is valid.

$$\begin{bmatrix} -jk_x & -\omega\mu_o k_y \\ -jk_y & \omega\mu_o k_x \end{bmatrix} \begin{bmatrix} \frac{1}{\epsilon_r(z^+)}\frac{\partial\tilde{\Psi}^e(k_x,k_y,z^+)}{\partial z} - \frac{1}{\epsilon_r(z^-)}\frac{\partial\tilde{\Psi}^e(k_x,k_y,z^-)}{\partial z} \\ \tilde{\Psi}^h(k_x,k_y,z^+) - \tilde{\Psi}^h(k_x,k_y,z^-) \end{bmatrix} = \begin{bmatrix} 0 \\ 0 \end{bmatrix} \tag{2.18}$$

Since the determinant of the coefficient matrix of the above equation is nonzero, the only solutions are zero. That is, for each value of z, we have

$$\frac{1}{\epsilon_r(z^+)}\frac{\partial\tilde{\Psi}^e(k_x,k_y,z^+)}{\partial z} = \frac{1}{\epsilon_r(z^-)}\frac{\partial\tilde{\Psi}^e(k_x,k_y,z^-)}{\partial z} \tag{2.19a}$$

$$\tilde{\Psi}^h(k_x,k_y,z^+) = \tilde{\Psi}^h(k_x,k_y,z^-) \tag{2.19b}$$

In a similar fashion, one may write the Fourier transform of the components of the magnetic field as

$$\begin{bmatrix} \widetilde{H}_x(k_x,k_y,z) \\ \widetilde{H}_y(k_x,k_y,z) \\ \widetilde{H}_z(k_x,k_y,z) \end{bmatrix} = \begin{bmatrix} \omega\epsilon_o k_y & -\frac{jk_x}{\mu_r(z)}\frac{\partial}{\partial z} \\ -\omega\epsilon_o k_x & -\frac{jk_y}{\mu_r(z)}\frac{\partial}{\partial z} \\ 0 & \frac{k_x^2+k_y^2}{\mu_r(z)} \end{bmatrix} \begin{bmatrix} \tilde{\Psi}^e(k_x,k_y,z) \\ \tilde{\Psi}^h(k_x,k_y,z) \end{bmatrix} \tag{2.20}$$

Since the electric current excitation has only x and y components, the magnetic field components transverse to the z axis are only discontinuous at $z = z_o$. That is,

$$\hat{\mathbf{z}} \times [\mathbf{H}(x,y,z_o^+) - \mathbf{H}(x,y,z_o^-)] = J_x(x,y,z_o)\hat{\mathbf{x}} + J_y(x,y,z_o)\hat{\mathbf{y}} \tag{2.21}$$

The above condition in the spectral domain can be written as

$$\hat{\mathbf{z}} \times [\widetilde{\mathbf{H}}(k_x,k_y,z_o^+) - \widetilde{\mathbf{H}}(k_x,k_y,z_o^-)] = \tilde{J}_x(k_x,k_y,z_o)\hat{\mathbf{x}} + \tilde{J}_y(k_x,k_y,z_o)\hat{\mathbf{y}} \tag{2.22}$$

Substituting (2.20) into (2.22), one may obtain the boundary conditions for the potential functions as follows

$$\begin{bmatrix} \omega\epsilon_o k_y & -jk_x \\ -\omega\epsilon_o k_x & -jk_y \end{bmatrix} \begin{bmatrix} \tilde{\Psi}^e(k_x,k_y,z_o^+) - \tilde{\Psi}^e(k_x,k_y,z_o^-) \\ \frac{1}{\mu_r(z_o^+)}\frac{\partial\tilde{\Psi}^h(k_x,k_y,z_o^+)}{\partial z} - \frac{1}{\mu_r(z_o^-)}\frac{\partial\tilde{\Psi}^h(k_x,k_y,z_o^-)}{\partial z} \end{bmatrix} = \begin{bmatrix} \tilde{J}_y(k_x,k_y,z_o) \\ -\tilde{J}_x(k_x,k_y,z_o) \end{bmatrix} \tag{2.23}$$

Therefore, at $z = z_o$, we have

$$\begin{bmatrix} \tilde{\Psi}^e(k_x, k_y, z_o^+) - \tilde{\Psi}^e(k_x, k_y, z_o^-) \\ \frac{1}{\mu_r(z_o^+)} \frac{\partial \tilde{\Psi}^h(k_x, k_y, z_o^+)}{\partial z} - \frac{1}{\mu_r(z_o^-)} \frac{\partial \tilde{\Psi}^h(k_x, k_y, z_o^-)}{\partial z} \end{bmatrix} = \begin{bmatrix} \omega\epsilon_o k_y & -jk_x \\ \omega\epsilon_o k_x & jk_y \end{bmatrix}^{-1} \begin{bmatrix} \tilde{J}_y(k_x, k_y, z_o) \\ \tilde{J}_x(k_x, k_y, z_o) \end{bmatrix} \tag{2.24}$$

Of course for $z \neq z_o$, we have

$$\tilde{\Psi}^e(k_x, k_y, z^+) = \tilde{\Psi}^e(k_x, k_y, z^-) \tag{2.25a}$$

$$\frac{1}{\mu_r(z^+)} \frac{\partial \tilde{\Psi}^h(k_x, k_y, z^+)}{\partial z} = \frac{1}{\mu_r(z^-)} \frac{\partial \tilde{\Psi}^h(k_x, k_y, z^-)}{\partial z} \tag{2.25b}$$

Equations (2.19), (2.24) and (2.25) can be used in a meaningful comparison of the behavior of the *form functions* $F^{(e,h)}(z; s)$ in Appendix A and of $\tilde{\Psi}^{(e,h)}(k_x, k_y, z)$. These two groups of functions with the same superscripts satisfy the same differential equation and the same boundary conditions, except at $z = z_o$. The most important feature of $\tilde{\Psi}^{(e,h)}(k_x, k_y, z)$ is that they can also be treated independently at all interfaces especially at the source location. This special feature is a consequence of choosing the direction of the vector potentials normal to the interfaces. The coupling between the LSE and LSM fields only enter into the formulation after applying the boundary conditions at $z = z_o$. More importantly, the boundary conditions at $z = z_o$, as reflected in (2.24), are decoupled. From (2.24), it can be easily seen that each spectral component

$$\frac{-jk_y \tilde{J}_x(k_x, k_y, z_o) + jk_x \tilde{J}_y(k_x, k_y, z_o)}{k_x^2 + k_y^2}$$

excites the LSE field and the LSM field is excited by each spectral component

$$\frac{k_x \tilde{J}_x(k_x, k_y, z_o) + k_y \tilde{J}_y(k_x, k_y, z_o)}{\omega\epsilon_o(k_x^2 + k_y^2)}.$$

The same result is obtained from immittance approach with suitable coordinate transformation in the x-y plane. This is due to the common feature between our

approach and the immittance approach; that is, decomposition of the total field as LSE and LSM fields. In the space domain approach, it has been shown that the coupling between the LSE and LSM fields is imposed by the edge conditions [49]. Let us rewrite Eqs. (2.19),(2.24), and (2.25) as follows

$$\begin{cases} \tilde{\Psi}^e(k_x,k_y,z^+) - \tilde{\Psi}^e(k_x,k_y,z^-) = \begin{cases} \frac{k_x\tilde{J}_x(k_x,k_y,z_o)+k_y\tilde{J}_y(k_x,k_y,z_o)}{\omega\epsilon_o(k_x^2+k_y^2)} & z=z_o \\ 0 & z\neq z_o \end{cases} \\ \frac{1}{\epsilon_r(z^+)}\frac{\partial\tilde{\Psi}^e(k_x,k_y,z^+)}{\partial z} - \frac{1}{\epsilon_r(z^-)}\frac{\partial\tilde{\Psi}^e(k_x,k_y,z^-)}{\partial z} = 0 \end{cases} \tag{2.26}$$

$$\begin{cases} \tilde{\Psi}^h(k_x,k_y,z^+) - \tilde{\Psi}^h(k_x,k_y,z^-) = 0 \\ \frac{1}{\mu_r(z^+)}\frac{\partial\tilde{\Psi}^h(k_x,k_y,z^+)}{\partial z} - \frac{1}{\mu_r(z^-)}\frac{\partial\tilde{\Psi}^h(k_x,k_y,z^-)}{\partial z} = \begin{cases} -j\frac{k_y\tilde{J}_x(k_x,k_y,z_o)-k_x\tilde{J}_y(k_x,k_y,z_o)}{k_x^2+k_y^2} & z=z_o \\ 0 & z\neq z_o \end{cases} \end{cases} \tag{2.27}$$

Then, one may expect that the transfer matrix formulation with some modifications can be used to find the dyadic Green's function. In fact, we consider three cases separately:

$$\begin{aligned} &\underline{\text{Case A:}} && z_o \geq d_N \\ &\underline{\text{Case B:}} && d_{k-1} \leq z_o < d_k \qquad (k=1,\ldots,N) \\ &\underline{\text{Case C:}} && z_o < 0 \end{aligned} \tag{2.28}$$

where the various layers of the multilayer structure are indicated in Fig. A.1. The details of the derivation of $\tilde{\Psi}^{(e,h)}(k_x,k_y,z)$ in each of the above cases are given in Appendices C.1, C.2, and C.3, respectively.

After obtaining $\tilde{\Psi}^{(e,h)}(k_x,k_y,z)$, the components of the electric and magnetic fields can be obtained from (2.17) and (2.20), respectively. This information can be used directly, as will be explained later, or can be transformed into the space domain by applying inverse transform. As mentioned before, some field-theoretic

concepts can be derived directly using the transfer matrix method which are not clear from other methods. The following statements reflects these concepts.
(I) The poles of the Green's functions are zeros of the characteristic equations of LSE and LSM modes. That is, the Greens functions of MPS have the so-called surface wave pole.
(II) It can be seen that the Green's functions of a MPS are functions of $\gamma_i = \sqrt{k_x^2 + k_y^2 - \mu_{r_i}\epsilon_{r_i}, k_o^2} = \sqrt{\beta^2 - \mu_{r_i}\epsilon_{r_i} k_o^2}$ $(i = 1, \ldots, N)$. From the transfer matrix method it can be seen that the Green's function of a MPS is independent of the branch cut of γ_i $(i = 1, \ldots, N)$.

It is interesting to note that the magnetic current excitation can be dealt with in a similar fashion, if one uses the concepts of duality. In the next section, we focus on the spectral domain Green's function in the cylindrical coordinate system. In the process of formulation we use the Hankel transform technique.

2.4 Green's Function in the Cylindrical Coordinate System: Hankel Transform

In this section, the full-wave analysis of the field excitation of a MPS by electric current in cylindrical coordinate system will be presented. We follow the same idea that has been used in the preceding section and use the integral transform technique on the scalar potential functions. The kernel of this transform is the amplitude function in the cylindrical coordinate system. Therefore, it is natural to see how the Hankel transform come into play. The premises of the approach we adopt are based on the method first used for predicting the characteristics of a circular patch conductor printed on a grounded dielectric slab [50]. This method

was originally applied to a surface current excitation of a single-layer structure. We have extended it to a MPS excited by a volume current [52].

To illustrate the basic ideas, let the cylindrical coordinate system be oriented as (ρ, ϕ, z). We place the same constraint on the excitation as before. That is, we assume a volume current source without any z component. Moreover, we divide the volume current into planar slices and consider the response to the planar excitation at $z = z_o$. That is,

$$\mathrm{J}(\rho, \phi, z) = \left[J_\rho(\rho, \phi, z_o)\hat{\rho} + J_\phi(\rho, \phi, z_o)\hat{\phi}\right] \delta(z - z_o) \qquad [\frac{\mathrm{A}}{\mathrm{m}^2}] \tag{2.29}$$

The electromagnetic field in each homogeneous source-free region above and below $z = z_o$ can be derived from two vector potential functions

$$\Pi^{(e,h)}(\rho, \phi, z) = \hat{\mathbf{z}}\Psi^{(e,h)}(\rho, \phi, z) \tag{2.30}$$

where the Hertzian scalar potential functions $\Psi^{(e,h)}(\rho, \phi, z)$ are the solution of the scalar Helmholtz equation in cylindrical coordinate system; i.e.,

$$\left[\frac{\partial^2}{\partial\rho^2} + \frac{1}{\rho}\frac{\partial}{\partial\rho} + \frac{1}{\rho^2}\frac{\partial^2}{\partial\phi^2} + \frac{\partial^2}{\partial z^2} + \epsilon_r(z)\mu_r(z)k_o^2\right] \Psi^{(e,h)} = 0 \tag{2.31}$$

Since $\Psi_i^{(e,h)}(\rho, \phi, z)$ must be periodic functions of ϕ with period 2π, they can be expressed in terms of the Fourier series

$$\Psi^{(e,h)}(\rho, \phi, z) = \sum_{n=-\infty}^{\infty} \Psi_n^{(e,h)}(\rho, z)e^{jn\phi} \tag{2.32}$$

Let us use the notation

$$\mathcal{H}_n[f(\rho); \alpha]$$

to denote the nth order Hankel transform of $f(\rho)$. By definition we have

$$\mathcal{H}_n[f(\rho); \alpha] \stackrel{\text{def}}{=} \hat{f}(\alpha) = \int_0^\infty f(\rho)J_n(\alpha\rho)\rho d\rho \tag{2.33}$$

where $J_n(\alpha\rho)$ is the nth order Bessel function of the first kind. The inversion theorem of the Hankel transform states that $\mathcal{H}_n^{-1} = \mathcal{H}_n$ [51]. This means that

$$f(\rho) = \int_0^\infty \widehat{f}(\alpha) J_n(\alpha\rho)\alpha d\alpha. \tag{2.34}$$

If the same order Hankel transform with respect to ρ is applied to the Fourier coefficients in (2.32), $\Psi_n^{(e,h)}(\rho, z)$ may be related to their Hankel transforms by the following relation

$$\widehat{\Psi}_n^{(e,h)}(\alpha, z) = \int_0^\infty \Psi_n^{(e,h)}(\rho, z) J_n(\alpha\rho)\rho d\rho. \tag{2.35}$$

According to the inversion theorem, we may write

$$\Psi_n^{(e,h)}(\rho, z) = \int_0^\infty \widehat{\Psi}_n^{(e,h)}(\alpha, z) J_n(\alpha\rho)\alpha d\alpha. \tag{2.36}$$

Spectral representation of $\Psi^{(e,h)}(\rho, \phi, z)$ can be obtained by substituting (2.36) into (2.32). Hence,

$$\Psi^{(e,h)}(\rho, \phi, z) = \sum_{n=-\infty}^{\infty} e^{jn\phi} \int_0^\infty \widehat{\Psi}_n^{(e,h)}(\alpha, z) J_n(\alpha\rho)\alpha d\alpha. \tag{2.37}$$

Eq. (2.37) can be rewritten as

$$\Psi^{(e,h)}(\rho, \phi, z) = \sum_{n=-\infty}^{\infty} \int_0^\infty \widehat{\Psi}_n^{(e,h)}(\alpha, z) e^{jn\phi} J_n(\alpha\rho)\alpha \, d\alpha \tag{2.38}$$

As can be seen from the above relation, we have constructed the solution for the potential functions by the Fourier-Bessel integrals. The kernel of this transform is simply the amplitude function. In view of (2.38), the potential functions can be considered as the superposition of the elemental solutions of a source free MPS. This is due to the linear property of the differential operator in (2.31). Moreover, $\widehat{\Psi}_n^{(e,h)}(\alpha, z)$ can be interpreted as the *form functions* of these elemental solutions. Since $\widehat{\Psi}_n^{(e,h)}(\alpha, z)$ convey all spectral information of the field components, we try to

find them. In Appendix C.4, we show that $\widehat{\Psi}_n^{(e,h)}(\alpha, z)$ satisfies the second-order homogeneous differential equation

$$\left(\frac{\partial^2}{\partial z^2} - [\alpha^2 - \epsilon_r(z)\mu_r(z)k_o^2]\right)\widehat{\Psi}_n^{(e,h)}(\alpha, z) = 0 \tag{2.39}$$

The above result is completely expected. This is because the method of the separation of variables is the heart of the integral transform techniques.

To obtain the boundary conditions satisfied by $\widehat{\Psi}_n^{(e,h)}(\alpha, z)$, one may invoke the expression for the field components in terms of the potential functions. As expected, like *form functions*, $\widehat{\Psi}_n^{(e,h)}(\alpha, z)$ satisfy the same boundary conditions at the source-free interfaces. Now let us see how these boundary conditions must be modified at the source location. To this end, we try to find the field components in the spectral domain in terms of $\widehat{\Psi}_n^{(e,h)}(\alpha, z)$. This can be done by substituting spectral representation of the potential function in each homogeneous source-free region into (A.12) and (A.13).

In the cylindrical coordinate system the derivative of the kernel of the integral transform with respect to ρ is not proportional to itself. Therefore, the spectral domain formulation in the cylindrical coordinate system is not as straightforward as the formulation in the rectangular coordinate system. To remove this difficulty, as suggested in [50], we use the following identities which are valid for any Bessel functions $B_n(\alpha\rho)$.

$$\frac{dB_n(\alpha\rho)}{d(\alpha\rho)} = \frac{1}{2}\left[B_{n-1}(\alpha\rho) - B_{n+1}(\alpha\rho)\right] \tag{2.40a}$$

$$\frac{n}{\alpha\rho}B_n(\alpha\rho) = \frac{1}{2}\left[B_{n-1}(\alpha\rho) + B_{n+1}(\alpha\rho)\right] \tag{2.40b}$$

Using the above identities and substituting the spectral representation of the potential function into (A.12) the nonaxial electric field components can be obtained

from $\widehat{\Psi}_n^{(e,h)}(\alpha, z)$ as follows:

$$\begin{bmatrix} E_\rho(\rho,\phi,z) \\ E_\phi(\rho,\phi,z) \end{bmatrix} = \sum_{n=-\infty}^{\infty} e^{jn\phi} \int_0^\infty \overleftrightarrow{\mathbf{L}}(\alpha,\rho) \begin{bmatrix} \widehat{\Psi}_n^e(\alpha,z) \\ \widehat{\Psi}_n^h(\alpha,z) \end{bmatrix} \alpha d\alpha \tag{2.41}$$

The dyadic operator $\overleftrightarrow{\mathbf{L}}(\alpha,\rho)$ is given by

$$\overleftrightarrow{\mathbf{L}}(\alpha,\rho) = \frac{\alpha}{2} \begin{bmatrix} [J_{n-1}(\alpha\rho) - J_{n+1}(\alpha\rho)]\frac{1}{\epsilon_r(z)}\frac{\partial}{\partial z} & \omega\mu_o[J_{n-1}(\alpha\rho) + J_{n+1}(\alpha\rho)] \\ j[J_{n-1}(\alpha\rho) + J_{n+1}(\alpha\rho)]\frac{1}{\epsilon_r(z)}\frac{\partial}{\partial z} & j\omega\mu_o[J_{n-1}(\alpha\rho) - J_{n+1}(\alpha\rho)] \end{bmatrix} \tag{2.42}$$

In a dual manner, the components transverse to the z axis of the magnetic field can be obtained from by the following relation

$$\begin{bmatrix} H_\rho(\rho,\phi,z) \\ H_\phi(\rho,\phi,z) \end{bmatrix} = \sum_{n=-\infty}^{\infty} e^{jn\phi} \int_0^\infty \overleftrightarrow{\mathbf{P}}(\alpha,\rho) \begin{bmatrix} \widehat{\Psi}_n^e(\alpha,z) \\ \widehat{\Psi}_n^h(\alpha,z) \end{bmatrix} \alpha d\alpha \tag{2.43}$$

where the dyadic operator $\overleftrightarrow{\mathbf{P}}(\alpha,\rho)$ is given by

$$\overleftrightarrow{\mathbf{P}}(\alpha,\rho) = \frac{\alpha}{2} \begin{bmatrix} -\omega\epsilon_o[J_{n-1}(\alpha\rho) + J_{n+1}(\alpha\rho)] & [J_{n-1}(\alpha\rho) - J_{n+1}(\alpha\rho)]\frac{1}{\mu_r(z)}\frac{\partial}{\partial z} \\ -j\omega\epsilon_o[J_{n-1}(\alpha\rho) - J_{n+1}(\alpha\rho)] & j[J_{n-1}(\alpha\rho) + J_{n+1}(\alpha\rho)]\frac{1}{\mu_r(z)}\frac{\partial}{\partial z} \end{bmatrix} \tag{2.44}$$

The expressions (2.41)–(2.44) clearly show that the Bessel functions of different orders appear for the description of the nonaxial components of the electromagnetic field. For the purpose of spectral representation it is highly desirable to have only one type of the Bessel function. Hopefully, the form of equations in (2.41)–(2.44) suggests that a linear combination of the nonaxial field may be represented by only one type of the Bessel function. In fact, this idea is the basis of this outlined method. To illustrate the basic idea, let us define the auxiliary functions, $E^+(\rho,\phi,z)$, $E^-(\rho,\phi,z)$, $H^+(\rho,\phi,z)$, and $H^-(\rho,\phi,z)$ by the following relations

$$E^\pm(\rho,\phi,z) = E_\rho(\rho,\phi,z) \pm jE_\phi(\rho,\phi,z) \tag{2.45a}$$

$$H^\pm(\rho,\phi,z) = H_\rho(\rho,\phi,z) \pm jH_\phi(\rho,\phi,z) \tag{2.45b}$$

Using (2.41) and (2.42), we have

$$E^{\pm}(\rho,\phi,z) = \sum_{n=-\infty}^{\infty} e^{jn\phi} \int_0^{\infty} \widehat{E}^{\pm}_{n\pm1}(\alpha,z) J_{n\pm1}(\alpha\rho)\alpha d\alpha \tag{2.46}$$

where

$$\widehat{E}^{\pm}_{n\pm1}(\alpha,z) = \alpha\left[\mp\frac{1}{\epsilon_r(z)}\frac{\partial}{\partial z}\widehat{\Psi}^{e}_{n}(\alpha,z) + \omega\mu_o\widehat{\Psi}^{h}_{n}(\alpha,z)\right] \tag{2.47}$$

Note that (2.46) clearly shows that $E^{\pm}(\rho,\phi,z)$ do not satisfy the Helmholtz equation. This result is expected, due to the fact that neither $E_\rho(\rho,\phi,z)$ nor $E_\phi(\rho,\phi,z)$ satisfy the scalar Helmholtz equation. In a similar fashion, from (2.43) and (2.44), we have

$$H^{\pm}(\rho,\phi,z) = \sum_{n=-\infty}^{\infty} e^{jn\phi} \int_0^{\infty} \widehat{H}^{\pm}_{n\pm1}(\alpha,z) J_{n\pm1}(\alpha\rho)\alpha d\alpha \tag{2.48}$$

where

$$\widehat{H}^{\pm}_{n\pm1}(\alpha,z) = \alpha\left[-\omega\epsilon_o\widehat{\Psi}^{e}_{n}(\alpha,z) \mp \frac{1}{\mu_r(z)}\frac{\partial}{\partial z}\widehat{\Psi}^{h}_{n}(\alpha,z)\right] \tag{2.49}$$

We have defined the auxiliary functions as a linear combination of the nonaxial components of the electric and the magnetic fields. Moreover, it has been assumed that the MPS is excited by a planar slice of electric current with only transverse components to the z axis. Therefore, it is natural to use the same idea and define the auxiliary functions $J^{\pm}(\rho,\phi,z_o)$ as follows

$$J^{\pm}(\rho,\phi,z_o) = J_\rho(\rho,\phi,z_a) \pm jJ_\phi(\rho,\phi,z_a) \tag{2.50}$$

In order to obtain $\widehat{\Psi}^{(e,h)}(\alpha,z)$ the exact behavior of these functions and their normal derivatives at all interfaces especially at the source location must be determined. On the other hand, from (2.47) and (2.49) it is obvious that $\widehat{E}^{\pm}_{n\pm1}(\alpha,z)$ and $\widehat{H}^{\pm}_{n\pm1}(\alpha,z)$ can be expressed in terms of these potential functions and their derivatives with respect to z. Therefore, the required information can be extracted from the behavior of these auxiliary functions at those specific values of z.

To obtain the boundary conditions for $E^{\pm}$ we take advantage of the continuity of E_ρ and E_ϕ for all values of z. Since $E^{\pm}$ are obtained as two independent linear combinations of E_ρ and E_ϕ, continuity of E_ρ and E_ϕ leads to the continuity of $E^{\pm}$ and vice versa. Using (2.46) continuity of $E^{\pm}$ leads to the continuity of $\widehat{E}^{\pm}_{n\pm1}(\alpha, z)$. This last statement requires that for each value of z, we have

$$\frac{1}{\epsilon_r(z^+)}\frac{\partial\widehat{\Psi}^e(\alpha,z^+)}{\partial z} - \frac{1}{\epsilon_r(z^-)}\frac{\partial\widehat{\Psi}^e(\alpha,z^-)}{\partial z} = 0 \tag{2.51a}$$

$$\widehat{\Psi}^h(\alpha,z_o^+) - \widehat{\Psi}^h(\alpha,z_o^-) = 0 \tag{2.51b}$$

This is due to the fact that from (2.47), we have

$$\begin{bmatrix} \frac{1}{\epsilon_r(z^+)}\frac{\partial\widehat{\Psi}^e_n(\alpha,z^+)}{\partial z} - \frac{1}{\epsilon_r(z^-)}\frac{\partial\widehat{\Psi}^e_n(\alpha,z^-)}{\partial z} \\ \widehat{\Psi}^h_n(\alpha,z^+) - \widehat{\Psi}^h_n(\alpha,z^-) \end{bmatrix} = \mathbf{D}\begin{bmatrix} \widehat{E}^+_{n+1}(\alpha,z^+) - \widehat{E}^+_{n+1}(\alpha,z^-) \\ \widehat{E}^-_{n-1}(\alpha,z^+) - \widehat{E}^-_{n-1}(\alpha,z^-) \end{bmatrix} \tag{2.52}$$

where

$$\mathbf{D} = \frac{1}{\alpha}\begin{bmatrix} -1 & \omega\mu_o \\ 1 & \omega\mu_o \end{bmatrix}^{-1}$$

Similarly, at those interfaces where H_ρ and H_ϕ are continuous, $\widehat{H}^{\pm}_{n\pm1}(\alpha, z)$ are also continuous. At $z = z_o$, the nonaxial magnetic field components are discontinuous by the amount of the electric current. That is,

$$J_\rho(\rho,\phi,z_o)\hat{\boldsymbol{\rho}} + J_\phi(\rho,\phi,z_o)\hat{\boldsymbol{\phi}} = \hat{\mathbf{z}} \times \left[\mathbf{H}(\rho,\phi,z_o^+) - \mathbf{H}(\rho,\phi,z_o^-)\right]$$

The above boundary condition can be easily transformed in terms of the auxiliary functions $J^{\pm}$ and $H^{\pm}$ as follows

$$J^{\pm}(\rho,\phi,z_a) = \pm j\left[H^{\pm}(\rho,\phi,z_o^+) - H^{\pm}(\rho,\phi,z_o^-)\right] \tag{2.53}$$

Substituting (2.48) into (2.53), we obtain

$$J^{\pm}(\rho,\phi,z_o) = \sum_{n=-\infty}^{\infty} J^{\pm}_n(\rho,z_o)e^{jn\phi} \tag{2.54}$$

where

$$J_n^{\pm}(\rho, z_o) = \int_0^{\infty} \widehat{J}_{n\pm1}^{\pm}(\alpha, z_o) J_{n\pm1}(\alpha\rho)\, \alpha d\alpha \tag{2.55}$$

and

$$\widehat{J}_{n\pm1}^{\pm}(\alpha, z_o) = \pm j \left[\widehat{H}_{n\pm1}^{\pm}(\rho, \phi, z_o^+) - \widehat{H}_{n\pm1}^{\pm}(\rho, \phi, z_o^-)\right] \tag{2.56}$$

Eq. (2.55) means that

$$\widehat{J}_{n\pm1}^{\pm}(\alpha, z_o) = \int_0^{\infty} J_n^{\pm}(\rho, z_o) J_{n\pm1}(\alpha\rho)\, \rho d\rho \tag{2.57}$$

Using (2.49), the above conditions can be stated in terms of the potential functions in the transformed domain. More precisely,

$$\begin{bmatrix} \widehat{\Psi}_n^e(\alpha, z_o^+) - \widehat{\Psi}_n^e(\alpha, z_o^-) \\ \frac{1}{\mu_r(z_o^+)} \frac{\partial \widehat{\Psi}_n^h(\alpha, z_o^+)}{\partial z} - \frac{1}{\mu_r(z_o^-)} \frac{\partial \widehat{\Psi}_n^h(\alpha, z_o^-)}{\partial z} \end{bmatrix} = \frac{1}{\alpha} \begin{bmatrix} -\omega\epsilon_o & -1 \\ -\omega\epsilon_o & 1 \end{bmatrix}^{-1} \begin{bmatrix} -j\widehat{J}_{n+1}^{+}(\alpha, z_o) \\ j\widehat{J}_{n-1}^{-}(\alpha, z_o) \end{bmatrix} \tag{2.58}$$

Of course for $z \neq z_o$, we have

$$\begin{bmatrix} \widehat{\Psi}_n^e(\alpha, z^+) - \widehat{\Psi}_n^e(\alpha, z^-) \\ \frac{1}{\mu_r(z^+)} \frac{\partial \widehat{\Psi}_n^h(\alpha, z^+)}{\partial z} - \frac{1}{\mu_r(z^-)} \frac{\partial \widehat{\Psi}_n^h(\alpha, z^-)}{\partial z} \end{bmatrix} = \begin{bmatrix} 0 \\ 0 \end{bmatrix} \tag{2.59}$$

Now the boundary conditions (2.51), (2.58) and (2.59) can be rewritten as follows

$$\begin{cases} \widehat{\Psi}_n^e(\alpha, z^+) - \widehat{\Psi}_n^e(\alpha, z^-) = \begin{cases} \frac{j}{2a\omega\epsilon_o}[\widehat{J}_{n+1}^{+}(\alpha, z_o) - \widehat{J}_{n-1}^{-}(\alpha, z_o)] & z = z_o \\ 0 & z \neq z_o \end{cases} \\ \frac{1}{\epsilon_r(z^+)} \frac{\partial \widehat{\Psi}_n^e(\alpha, z^+)}{\partial z} - \frac{1}{\epsilon_r(z^-)} \frac{\partial \widehat{\Psi}_n^e(\alpha, z^-)}{\partial z} = 0 \end{cases} \tag{2.60}$$

$$\begin{cases} \widehat{\Psi}_n^h(\alpha, z^+) - \widehat{\Psi}_n^h(\alpha, z^-) = 0 \\ \frac{1}{\mu_r(z^+)} \frac{\partial \widehat{\Psi}_n^h(\alpha, z^+)}{\partial z} - \frac{1}{\mu_r(z^-)} \frac{\partial \widehat{\Psi}_n^h(\alpha, z^-)}{\partial z} = \begin{cases} \frac{j}{2\alpha}[\widehat{J}_{n+1}^{+}(\alpha, z_o) + \widehat{J}_{n-1}^{-}(\alpha, z_o)] & z = z_o \\ 0 & z \neq z_o \end{cases} \end{cases} \tag{2.61}$$

The boundary conditions in (2.60) and (2.61) reveal that $\widehat{\Psi}_n^{(e,h)}(\alpha, z)$ can be treated independently at all interfaces especially at the source located at $z = z_o$.

Again this special feature is a direct consequence of choosing the direction of the vector potentials normal to the interfaces. The spectral component

$$\frac{j}{2\alpha}[\hat{J}^{+}_{n+1}(\alpha, z_o) + \hat{J}^{-}_{n-1}(\alpha, z_o)]$$

excites the LSE field and the LSM field is excited by

$$\frac{j}{2\alpha\omega\epsilon_o}[\hat{J}^{+}_{n+1}(\alpha, z_o) - \hat{J}^{-}_{n-1}(\alpha, z_o)]$$

For a circularly symmetric ρ-directed excitation, we have

$$J^{+}(\rho, \phi, z) = J^{-}(\rho, \phi, z)$$

Consequently,

$$\hat{J}^{+}_{1}(\alpha, z) = -\hat{J}^{-}_{-1}(\alpha, z)$$

where we have used

$$J_{-1}(\alpha\rho) = -J_{1}(\alpha\rho) \tag{2.62}$$

Therefore, this type of current can excite only a LSM field. Using the same argument one can easily see that a circularly symmetric ϕ-directed current excitation produces only LSE field. From the above consideration it can be seen that for a circularly symmetric excitation, the ρ component of the current is responsible for LSM field and LSE part of the field is excited by the ϕ component. The above results are direct consequences of spectral domain approach.

The boundary conditions stated in (2.60) and (2.61) make it possible to take advantage of the transfer matrix formulation. Specifically, the formulation that we have done for three different cases A, B, and C in the rectangular coordinate system can be used directly for the cylindrical coordinate system with minor modifications. First, the unknown coefficients describing $\hat{\Psi}^{(e,h)}_{n}$ in each region must be considered

as a function of (n, α) rather than (k_x, k_y). The spectral source excitation

$$\begin{bmatrix} \tilde{J}_x(k_x, k_y, z_o) \\ \tilde{J}_y(k_x, k_y, z_o) \end{bmatrix}$$

must be changed to

$$\begin{bmatrix} \hat{J}^+_{n+1}(\alpha, z_o) \\ \hat{J}^-_{n-1}(\alpha, z_o) \end{bmatrix}$$

Moreover, as can be obtained from (2.60) and (2.61), in the cylindrical coordinate system the matrices $\mathbf{A}^e(k_x, k_y)$ and $\mathbf{A}^h(k_x, k_y)$ are replaced by

$$\mathbf{A}^e(\alpha) = \begin{bmatrix} \frac{j}{2\alpha\omega\epsilon_o} & -\frac{j}{2\alpha\omega\epsilon_o} \\ 0 & 0 \end{bmatrix}$$

and

$$\mathbf{A}^h(\alpha) = \begin{bmatrix} 0 & 0 \\ \frac{j}{2\alpha} & \frac{j}{2\alpha} \end{bmatrix},$$

respectively. Note that $\mathbf{A}^{(e,h)}(\alpha)$ are independent of the the order of the Hankel transformation.

For the future references it is desirable to define a 2×2 dyadic Green's function $\overleftrightarrow{\mathbf{Z}}(\alpha)$ as an impedance matrix. It shows that $\hat{E}^{\pm}_{n\pm1}(\alpha, d_N \text{ or } 0)$ can be related to $\hat{J}^{\pm}_{n\pm1}(\alpha, z_a)$ by the matrix equation

$$\begin{bmatrix} \hat{E}^+_{n+1}(\alpha, d_N \text{ or } 0) \\ \hat{E}^-_{n-1}(\alpha, d_N \text{ or } 0) \end{bmatrix} = \overleftrightarrow{\mathbf{Z}}(\alpha, d_N \text{ or } 0 \mid z_o) \begin{bmatrix} \hat{J}^+_{n+1}(\alpha, z_o) \\ \hat{J}^-_{n-1}(\alpha, z_o) \end{bmatrix}. \tag{2.63}$$

where

$$\overleftrightarrow{\mathbf{Z}}(\alpha, d_N \text{ or } 0 \mid z_o) = \begin{bmatrix} Z^{++}(\alpha, d_N \text{ or } 0 \mid z_o) & Z^{+-}(\alpha, d_N \text{ or } 0 \mid z_o) \\ Z^{-+}(\alpha, d_N \text{ or } 0 \mid z_o) & Z^{--}(\alpha, d_N \text{ or } 0 \mid z_o) \end{bmatrix} \tag{2.64}$$

The most important feature of the impedance matrix is that its elements are independent of the angular index n. This is the direct consequence of stating these

equations in the Hankel transform domain [50]. Furthermore, using the transfer matrix formulation, it can be shown that the diagonal elements are equal to each other and the same is true for the off diagonal elements. In fact, from (2.47), one may show that

$$Z^{(\pm)^a(\pm)^b}(\alpha, d_N \mid z_o) = (\pm)^a \gamma_c \begin{bmatrix} R_c^e(\alpha, z_o) & S_c^e(\alpha, z_o) \end{bmatrix} \begin{bmatrix} (\pm)^b \times 1 \\ 0 \end{bmatrix} + \begin{bmatrix} R_c^h(\alpha, z_o) & S_c^h(\alpha, z_o) \end{bmatrix} \begin{bmatrix} 0 \\ 1 \end{bmatrix} \tag{2.65}$$

where

$$\gamma_c = \sqrt{\alpha^2 - \mu_{r_c} \epsilon r_c k_o^2}$$

From (2.65), one may easily deduce that

$$Z^{++}(\alpha, d_N \mid z_o) = Z^{--}(\alpha, d_N \mid z_o)$$

$$Z^{+-}(\alpha, d_N \mid z_o) = Z^{-+}(\alpha, d_N \mid z_o)$$

Similarly,

$$Z^{(\pm)^a(\pm)^b}(\alpha, 0 \mid z_o) = (\mp)^a \gamma_s \begin{bmatrix} R_s^e(\alpha, z_o) & S_s^e(\alpha, z_o) \end{bmatrix} \begin{bmatrix} (\pm)^b \times 1 \\ 0 \end{bmatrix} + \begin{bmatrix} R_s^h(\alpha, z_o) & S_s^h(\alpha, z_o) \end{bmatrix} \begin{bmatrix} 0 \\ 1 \end{bmatrix} \tag{2.66}$$

where

$$\gamma_s = \sqrt{\alpha^2 - \mu_{r_s} \epsilon r_s k_o^2}$$

Thus,

$$Z^{++}(\alpha, 0 \mid z_o) = Z^{--}(\alpha, 0 \mid z_o)$$

$$Z^{+-}(\alpha, 0 \mid z_o) = Z^{-+}(\alpha, 0 \mid z_o)$$

In the next section, we apply the formulation developed so far in this chapter to obtain the electric field in the far zone. Especially, in the cylindrical coordinate system, we will show that the far field pattern of the electric field can be obtained directly from the Hankel transform of the the auxiliary functions defined earlier. Therefore, it is not necessary to carry out time consuming inverse Hankel transform by numerical methods.

2.5 Application to the Radiation Problem

In this section we investigate the radiation electric field in the cladding and the substrate regions. To this end, we start with a general formula from which the far field pattern due to an aperture can be obtained. Let us consider an aperture parallel to the x-y plane. It is well-known that the far field pattern is the Fourier transform of the tangential aperture field. More precisely, it is shown that [54], [55]

$$\begin{aligned} \mathrm{E}(r,\theta,\phi) &= jk\frac{e^{-jkr}}{2\pi r}\Big(\hat{\theta}\left[\tilde{E}_x(k_x,k_y,z_a)\,cos\phi+\tilde{E}_y(k_x,k_y,z_a)\,sin\phi\right]+ \\ &\quad \hat{\phi}\left[\tilde{E}_y(k_x,k_y,z_a)\,cos\phi-\tilde{E}_x(k_x,k_y,z_a)\,sin\phi\right]cos\theta\Big) \end{aligned} \tag{2.67}$$

where r, θ, and ϕ are the spherical coordinate variables and θ is the polar angle measured from the z axis. k is the wave number of the half space seen from the aperture. Moreover, $\tilde{E}_x(k_x,k_y,z_a)$ and $\tilde{E}_y(k_x,k_y,z_a)$ are the two-dimensional Fourier transform of E_x and E_y on the aperture at $z=z_a$, respectively. That is,

$$\begin{bmatrix} \tilde{E}_x(k_x,k_y,z_a) \\ \tilde{E}_y(k_x,k_y,z_a) \end{bmatrix} = \int_{-\infty}^{\infty}\int_{-\infty}^{\infty}\begin{bmatrix} E_x(x,y,z_a) \\ E_y(x,y,z_a) \end{bmatrix} e^{j(k_x x+k_y y)}dxdy$$

where

$$k_x = k\,sin\theta\,cos\phi \tag{2.68a}$$

$$k_y = k\,sin\theta\,sin\phi \tag{2.68b}$$

In the rectangular coordinate system, the Fourier transforms of the tangential aperture field can be easily obtained from (2.17). In the cylindrical coordinate system, the radiation field can be expressed in terms of the Hankel transform of the aperture field. This is due to the relation which exists between the two-dimensional Fourier transform and the Hankel transform. To establish the formula for the radiation field in the cylindrical coordinate system, first we consider the following transformation between the cylindrical and rectangular coordinate systems

$$\begin{bmatrix} E_x(x,y,z) \\ E_y(x,y,z) \end{bmatrix} = \begin{bmatrix} cos\phi & -sin\phi \\ sin\phi & cos\phi \end{bmatrix} \begin{bmatrix} E_\rho(\rho,\phi,z) \\ E_\phi(\rho,\phi,z) \end{bmatrix}$$

where

$$\begin{cases} x = \rho\, cos\phi \\ y = \rho\, sin\phi \end{cases}$$

Now if one uses (2.45a) to express $E_\rho(\rho,\phi,z)$ and $E_\phi(\rho,\phi,z)$ in terms of $E^\pm(\rho,\phi,z)$, one obtains

$$E_x(x,y,z) = \frac{E^+(\rho,\phi,z)e^{j\phi} + E^-(\rho,\phi,z)e^{-j\phi}}{2} \tag{2.69a}$$

$$E_y(x,y,z) = \frac{E^+(\rho,\phi,z)e^{j\phi} - E^-(\rho,\phi,z)e^{-j\phi}}{j2} \tag{2.69b}$$

Using (2.46), one may write

$$E_x(x,y,z) = \frac{\sum_{n=-\infty}^{\infty} E^+_{n+1}(\rho,z)e^{j(n+1)\phi} + \sum_{n=-\infty}^{\infty} E^-_{n-1}(\rho,z)e^{j(n-1)\phi}}{2} \tag{2.70a}$$

$$E_y(x,y,z) = \frac{\sum_{n=-\infty}^{\infty} E^+_{n+1}(\rho,z)e^{j(n+1)\phi} - \sum_{n=-\infty}^{\infty} E^-_{n-1}(\rho,z)e^{j(n-1)\phi}}{j2} \tag{2.70b}$$

where

$$E^\pm_{n\pm1}(\rho,z) = \int_0^\infty \widehat{E}^\pm_{n\pm1}(\alpha,z)J_{n\pm1}(\alpha\rho)\alpha d\alpha \tag{2.71}$$

Since $E_x(x,y,z)$ and $E_y(x,y,z)$ satisfy the Helmholtz equation, (2.70) and (2.71) are completely expected. In Appendix C.5, the relation between the two dimensional Fourier transform and the Hankel transform has been derived. According to

this relation, if

$$f(x,y,z) = \sum_{n=-\infty}^{\infty} f_n(\rho,z)e^{jn\phi} \tag{2.72}$$

then we have

$$\tilde{f}(k_x,k_y,z_a) = \sum_{n=-\infty}^{\infty} 2\pi j^n \hat{f}_n(\alpha)e^{jn\nu} \tag{2.73}$$

where $\hat{f}_n(\alpha)$ is the nth order Hankel transform of $f_n(\rho)$ and the pair (α,ν) is dual of (ρ,ϕ) in the spectral domain. That is,

$$\begin{cases} k_x = \alpha\, cos\nu \\ k_y = \alpha\, sin\nu \end{cases} \tag{2.74}$$

The expressions for $E_x(x,y,z)$ and $E_y(x,y,z)$ in (2.70) are similar to (2.72). Therefore, according to (2.73), by changing the role of n to $n \pm 1$, we may write

$$\begin{aligned} \tilde{E}_x(k_x,k_y,z_a) &= \sum_{n=-\infty}^{\infty} \pi j^{n+1} \hat{E}^+_{n+1}(\alpha,z_a)e^{j(n+1)\nu} + \\ &\quad \sum_{n=-\infty}^{\infty} \pi j^{n-1} \hat{E}^-_{n-1}(\alpha,z_a)e^{j(n-1)\nu} \qquad (2.75a) \\ \tilde{E}_y(k_x,k_y,z_a) &= -j \sum_{n=-\infty}^{\infty} \pi j^{n+1} \hat{E}^+_{n+1}(\alpha,z_a)e^{j(n+1)\nu} + \\ &\quad j \sum_{n=-\infty}^{\infty} \pi j^{n-1} \hat{E}^-_{n-1}(\alpha,z_a)e^{j(n-1)\nu} \qquad (2.75b) \end{aligned}$$

where from (2.71), we have used

$$\int_0^{\infty} E_{n\pm1}(\rho,z_a)J_{n\pm1}(\alpha\rho)\,\rho d\rho = \hat{E}^{\pm}_{n\pm1}(\alpha,z_a) \tag{2.76}$$

On the other hand, comparing (2.74) with (2.68) leads to the following expressions for α and ν

$$\alpha = k\, sin\theta \tag{2.77a}$$

$$\nu = \phi \tag{2.77b}$$

The above relations means that $(k\,sin\theta, \phi)$ is the dual of (ρ, ϕ) in the spectral domain. Let us rewrite (2.67) as

$$\begin{aligned} \mathbf{E}(r,\theta,\phi) &= jk\frac{e^{-jkr}}{2\pi r}\Big(\hat{\theta}\left[\tilde{E}^{-}(k_x,k_y,z_a)e^{j\phi}+\tilde{E}^{+}(k_x,k_y,z_a)e^{-j\phi}\right]+ \\ &\quad \hat{\phi}\left[j\tilde{E}^{-}(k_x,k_y,z_a)e^{j\phi}-j\tilde{E}^{+}(k_x,k_y,z_a)e^{-j\phi}\right]cos\theta\Big) \end{aligned} \tag{2.78}$$

where

$$\begin{aligned} \tilde{E}^{\pm}(k_x,k_y,z_a) &= \frac{\tilde{E}_x(k_x,k_y,z_a)\pm j\tilde{E}_y(k_x,k_y,z_a)}{2} \\ &= \sum_{n=-\infty}^{\infty}\pi j^{n\pm1}\hat{E}_{n\pm1}(\alpha,z_a)e^{j(n\pm1)\nu} \end{aligned} \tag{2.79}$$

In deriving (2.79) we have used (2.75) for substitution of $\tilde{E}_x$ and $\tilde{E}_y$. Substituting (2.79) into (2.78) and noting that α and ν are expressed by (2.77), the electric field in the far-zone can be obtained according to the following relation

$$\mathbf{E}(r,\theta,\phi)=jk\frac{e^{-jkr}}{r}\sum_{n=-\infty}^{\infty}j^n\left[\hat{\theta}\hat{E}_n^o(k\,sin\theta,z_a)+\hat{\phi}\,cos\theta\hat{E}_n^e(k\,sin\theta,z_a)\right]e^{jn\phi} \tag{2.80}$$

where

$$\hat{E}_n^e(\alpha,z_a)=\frac{\hat{E}_{n-1}^{-}(\alpha,z_a)+\hat{E}_{n+1}^{+}(\alpha,z_a)}{2} \tag{2.81a}$$

$$\hat{E}_n^o(\alpha,z_a)=\frac{\hat{E}_{n-1}^{-}(\alpha,z_a)-\hat{E}_{n+1}^{+}(\alpha,z_a)}{j2} \tag{2.81b}$$

As might be expected the radiation field has the same azimuthal variation as the aperture field. Eq. (2.80) is the fundamental relation which gives the far-field pattern in the cylindrical coordinate system due to an aperture in the x-y plane. As explained before, the electric field in the far-zone can be expressed in terms of the Hankel transform of the aperture field. More importantly, these expressions are directly related to the Hankel transform of the auxiliary functions defined in the preceding section. By the transfer matrix method, we have developed a systematic

algebraic procedure to obtain $\widehat{E}^{\pm}_{n\pm1}(\alpha, z_a)$ in terms of $\widehat{J}^{\pm}_{n\pm1}(\alpha, z_a)$. Thus, the far field pattern algebraically related to $\widehat{J}^{\pm}_{n\pm1}(\alpha, z_a)$. This is one of the important consequences of the spectral domain (Hankel transform) method. In fact, the electric field in the far-zone can be obtained from suitable integrals of the current sources. In this process there is no need to enter into the space domain. Therefore, carrying out the time consuming inverse Hankel transform is eliminated.

In many applications of integrated optics, normal emission from a planar stack is highly desirable. For example, surface emitting lasers are designed to behave in this manner. In these cases the radiation efficiency and the far field pattern strongly depends on the aperture field distribution. Fortunately, (2.67) and (2.80) provide the necessary background from which the characteristic dependence of the radiation field on the aperture field can be derived. We address this important issue in the next section.

2.5.1 Various Aperture Fields and Normal Emission

As mentioned earlier, many applications in integrated optics demand to have emission normal to the planar interfaces of a stack. Especially, in the highly directional beam applications the behavior of the radiation field on the z axis is very important. In this section, we investigate this matter by considering various types of the aperture fields. To this end, first we define some concepts by the following definitions.

DEFINITION 2.1 *The field of a circular or an annular shaped aperture centered at the origin in the x-y plane is called* **circularly symmetric** *if the field expressions in the cylindrical coordinate system are independent of the azimuthal angle ϕ.*

DEFINITION 2.2 *Consider an aperture in the x-y plane. The aperture vector field is called* **uniform** *if it is constant throughout the aperture. That is,*

$$\mathbf{E}_a(x,y) = \hat{\mathbf{u}} E_o \tag{2.82}$$

where $\hat{\mathbf{u}}$ *is a constant unit vector.*

DEFINITION 2.3 *By* **antisymmetric** *aperture field, we mean a field of a symmetric aperture in the x-y plane such that*

$$\mathbf{E}_a(-x,-y) = -\mathbf{E}_a(x,y) \tag{2.83}$$

Note that an antisymmetric aperture field can exist on those apertures which themselves are symmetric about the origin. Circularly symmetric aperture fields can be obtained from the Hertzian scalar potential functions in (2.32) by considering only the term with $n = 0$. For this special case, the electric field on the aperture of a LSE mode has only a ϕ component and that of LSM mode has only a ρ component.

Let us consider the behavior of the radiation field on the z axis. All points along the z axis correspond to $\theta = 0$. On the other hand, we have

$$\hat{\boldsymbol{\theta}} = \hat{\mathbf{x}}\, cos\theta\, cos\phi + \hat{\mathbf{y}}\, cos\theta\, sin\phi - \hat{\mathbf{z}} sin\theta \tag{2.84a}$$

$$\hat{\boldsymbol{\phi}} = -\hat{\mathbf{x}}\, sin\phi + \hat{\mathbf{y}}\, cos\phi \tag{2.84b}$$

Therefore, at all points along z axis, we have

$$\hat{\boldsymbol{\theta}} = \hat{\mathbf{x}}\, cos\phi + \hat{\mathbf{y}}\, sin\phi \tag{2.85}$$

Substituting (2.84b) and (2.85) into (2.67), the radiation field along the z axis can be obtained from the following relation

$$\mathbf{E}(r,0,\phi) = jk\frac{e^{-jkr}}{2\pi r}\left[\hat{\mathbf{x}}\tilde{E}_x(0,0,z_a) + \hat{\mathbf{y}}\tilde{E}_y(0,0,z_a)\right] \tag{2.86}$$

where by noting that $\theta = 0$, we have used

$$k_x = k_y = 0.$$

Despite the fact that, the azimuthal angle on the z axis is ambiguous, (2.86) clearly shows that the radiation field is independent of ϕ. This result is completely expected due to the fact that along each direction we approach to the z axis, the same result for the electric field must be obtained. Note that (2.86) can be obtained if we put $\phi = 0$ in (2.67). Moreover, as can be seen from (2.86) the radiation field along the z axis due to the aperture in the x-y does not have a component along the z direction. This result is also completely expected. In fact, due to the solenoidal character of the radiation field, the field in the far-zone does not have any component in the direction of observation [55] .

From (2.86) and the theory of the Fourier transform, it can be seen that the radiation field on the z axis is is directly related to the average values of E_x and E_y on the aperture. That is,

$$\begin{aligned} \mathbf{E}(r,0,\phi) &= jk\frac{e^{-jkr}}{2\pi r}A_a\left[\hat{\mathbf{x}}\bar{E}_x(z_a)+\hat{\mathbf{y}}\bar{E}_y(z_a)\right] \\ &= jk\frac{e^{-jkr}}{2\pi r}A_a\bar{\mathbf{E}}_t(z_a) \end{aligned} \tag{2.87}$$

where

$$\bar{\mathbf{E}}_t(z_a) = \frac{1}{A_a}\int_{-\infty}^{\infty}\int_{-\infty}^{\infty}\left[\hat{\mathbf{x}}E_x(x,y,z_a)+\hat{\mathbf{y}}E_y(x,y,z_a)\right]\,dxdy \tag{2.88}$$

and A_a is the area of the aperture. Therefore, nonzero average values of the electric field on the aperture is a necessary and sufficient condition for nonvanishing of the radiation field on the z axis. This important result can also be translated in the cylindrical coordinate system. To this end, let us assume that in the cylindrical coordinate system the aperture field is of the nth order azimuthal mode. That is,

$$E_\rho(\rho,\phi,z_a) = A_n(\rho,z_a)e^{jn\phi} \tag{2.89a}$$

$$E_\phi(\rho,\phi,z_a) = B_n(\rho,z_a)e^{jn\phi} \tag{2.89b}$$

Now from (2.69) and (2.45a), we have

$$E_x = \frac{[A_n(\rho,z_a)+jB_n(\rho,z_a)]e^{j(n+1)\phi} + [A_n(\rho,z_a)-jB_n(\rho,z_a)]e^{j(n-1)\phi}}{2} \tag{2.90a}$$

$$E_y = \frac{[A_n(\rho,z_a)+jB_n(\rho,z_a)]e^{j(n+1)\phi} - [A_n(\rho,z_a)-jB_n(\rho,z_a)]e^{j(n-1)\phi}}{j2} \tag{2.90b}$$

Substituting (2.90) into (2.88) and carrying out the resulting integral in the cylindrical coordinate system, it can be seen that for all values of $n \neq \pm 1$, we have $\bar{\mathbf{E}}_t(z_a) = 0$. This result implies that, for a circular aperture centered at the origin in the x-y plane all azimuthal order except $n \neq \pm 1$ produce a null on the z axis in the far-zone. For $n = 1$, we have

$$\bar{\mathbf{E}}_t(z_a) = \pi(\hat{\mathbf{x}} + j\,\hat{\mathbf{y}})\int_0^\infty [A_1(\rho,z_a) - jB_1(\rho,z_a)]\,\rho d\rho \tag{2.91}$$

Whereas, for $n = -1$

$$\bar{\mathbf{E}}_t(z_a) = \pi(\hat{\mathbf{x}} - j\,\hat{\mathbf{y}})\int_0^\infty [A_{-1}(\rho,z_a) + jB_{-1}(\rho,z_a)]\,\rho d\rho \tag{2.92}$$

From (2.91) and (2.92), we see that in order to have a nonzero far field pattern on the z axis, at least one of the integrals in (2.91) or (2.92) must be nonzero. The above result can also be obtained directly from (2.80). In fact, along the z axis $\alpha = 0$ and we have

$$\mathbf{E}(r,\theta=0,\phi) = jk\frac{e^{-jkr}}{r}\sum_{n=-1,1} j^n\left[\hat{\boldsymbol{\theta}}\widehat{E}_n^o(0,z_a) + \hat{\boldsymbol{\phi}}\widehat{E}_n^e(0,z_a)\right]e^{jn\phi} \tag{2.93}$$

For all points along the z axis, from (2.84b) and (2.85), one may write

$$\hat{\boldsymbol{\theta}} = \frac{(\hat{\mathbf{x}}-j\hat{\mathbf{y}})}{2}e^{j\phi} + \frac{(\hat{\mathbf{x}}+j\hat{\mathbf{y}})}{2}e^{-j\phi} \tag{2.94a}$$

$$\hat{\boldsymbol{\phi}} = j\frac{(\hat{\mathbf{x}}-j\hat{\mathbf{y}})}{2}e^{j\phi} - j\frac{(\hat{\mathbf{x}}+j\hat{\mathbf{y}})}{2}e^{-j\phi} \tag{2.94b}$$

Substituting (2.94) into (2.93), using (2.81) and collecting nonvanishing terms, we obtain

$$\mathbf{E}(r,\theta=0,\phi)=jk\frac{e^{-jkr}}{2r}\left[(\hat{\mathbf{x}}-j\,\hat{\mathbf{y}})\widehat{E}_0^+(0,z_a)+(\hat{\mathbf{x}}+j\,\hat{\mathbf{y}})\widehat{E}_0^-(0,z_a)\right] \tag{2.95}$$

where

$$\begin{aligned}\widehat{E}_0^{\pm}(0,z_a) &= \int_0^{\infty} E_0^{\pm}(\rho,z_a)J_0(\alpha\rho)\,\rho d\rho\Big|_{\alpha=0}\\ &= \int_0^{\infty} E_0^{\pm}(\rho,z_a)\,\rho d\rho\end{aligned} \tag{2.96}$$

In deriving (2.95) we have used

$$J_{n\pm1}(0)=0 \qquad n\neq\pm1,$$

$$\widehat{E}^{\pm}_{n\pm1}(0,z_a)=0 \qquad n\neq\pm1.$$

Therefore, nonvanishing field on the z axis in the far-zone requires that at least one of the above integrals be nonzero. This result is exactly the same as that we have obtained before, if one notes that

$$E_0^+(\rho,z_a)=E_{n+1}^+(\rho,z_a)\Big|_{n=-1}=A_{-1}(\rho,z_a)+jB_{-1}(\rho,z_a) \tag{2.97a}$$

$$E_0^-(\rho,z_a)=E_{n-1}^-(\rho,z_a)\Big|_{n=1}=A_1(\rho,z_a)-jB_1(\rho,z_a) \tag{2.97b}$$

It should be emphasized that due to the ambiguity of designating azimuthal angle along the z axis, the far field pattern must be independent of ϕ. Actually, (2.95) is in the form as it should be.

From the above considerations, a nonzero radiation field on the z axis requires a nonvanishing average value of the electric field on the aperture in the x-y plane. Therefore, the far field pattern on the z axis due to a uniform aperture field in the x-y plane is bright. For example, the intensity distribution of the Fraunhofer

diffraction pattern of a circular aperture illuminated by a normally incident plane wave follows the Airy pattern [57]. In fact, for a circular uniform aperture field $\mathbf{E} = E_x\,\hat{\mathbf{x}} + E_y\,\hat{\mathbf{y}}$, we have

$$E_\rho(\rho,\phi) = \frac{E_x - jE_y}{2}e^{j\phi} + \frac{E_x + jE_y}{2}e^{-j\phi} \tag{2.98a}$$

$$E_\phi(\rho,\phi) = j\frac{E_x - jE_y}{2}e^{j\phi} - j\frac{E_x + jE_y}{2}e^{-j\phi} \tag{2.98b}$$

As can be seen, a uniform aperture field is of the type of first-order azimuthal mode which has a nonzero far field on the z axis.

From the above considerations, an antisymmetric aperture field produces a null on the far field pattern along the z axis. Circularly symmetric aperture field is a special case of antisymmetric aperture fields. Therefore, one might expect a vanishing far field pattern on the z axis. In fact,
circularly symmetric beam can not have a nonzero far field pattern on its axis.
This behavior is unwanted in practical applications. For example, surface-emitting lasers using circular aperture and producing circularly symmetric beam have a dark spot at the center of the far-field pattern. We will turn to this point later.

In the next section as an example we consider a novel circular grating laser and we obtain its far field pattern by using the volume current method.

2.6 Radiation Pattern of a Novel Circular Grating Laser

In this section we obtain some insight on the far field intensity pattern of a novel circular-grating DFB laser at threshold by using volume current method. The laser

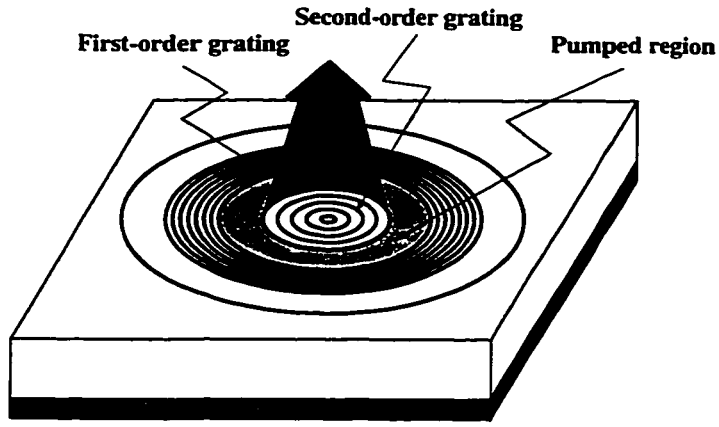

Figure 2.3: Schematic view of a novel circular-grating surface-emitting DBR laser

structure to be analyzed is depicted in Fig. 2.3. This structure has been reported by Wu *et al.* [38].

As illustrated in Fig. 2.3, the second-order circular-grating is located right at the center of the laser, optical gain is obtained by injecting current through the annular active region surrounding the second-order grating at the center. The optical feedback is provided by the first-order grating that encloses both the annular region and the central region. By ignoring the radiation field and using coupled-mode theory [30], [32], we have analyzed a bulk DBR laser. Then, the central second-order grating is considered as an equivalent electric current source which excites the unperturbed waveguide. The physical parameters of this structure are shown in Fig. 2.4. The reference wavelength λ is assumed to be 1.55 μm.

First, we assume that the laser beam is circularly symmetric. The grating periods Λ_1 and Λ_2 are chosen such that the corresponding gratings be of first-order and second-order resonant gratings, respectively. For this special geometry we have $\Lambda_2 = .477$ μm. The material loss is assumed to be 10 cm^{-1} and we consider only zero reflection coefficient at the outer edge of the laser. The radius of the central

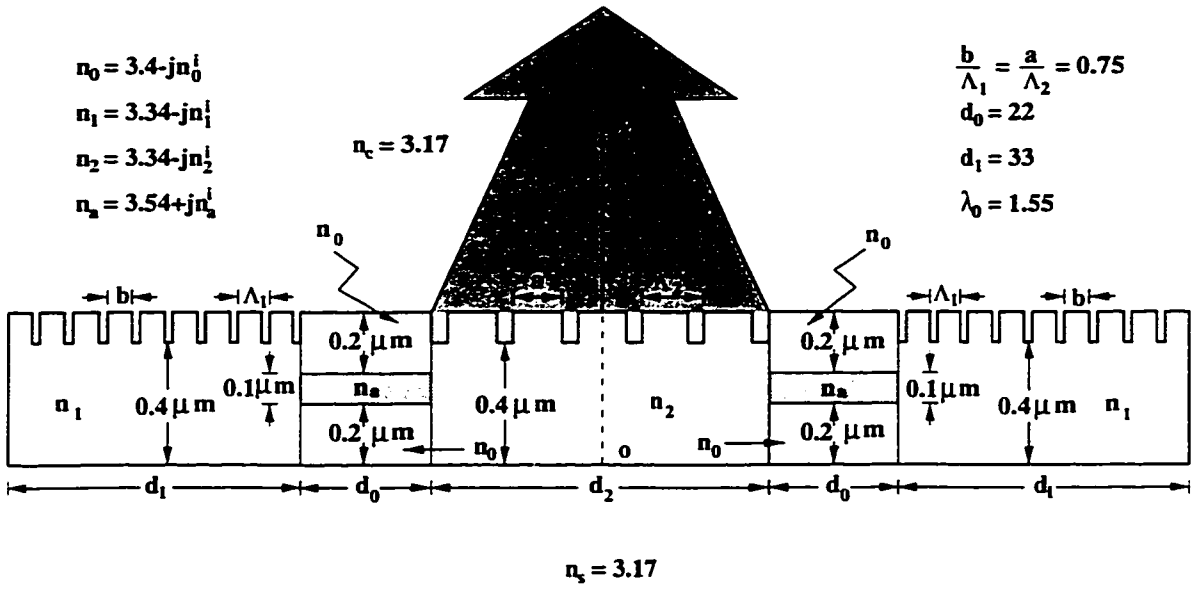

Figure 2.4: Cross-sectional view of a novel circular-grating surface-emitting DBR laser

region is the only parameter that we play with. We express this parameter in terms of the number of gratings N_g in the radial direction. For $N_g = 80$, the normalized far field intensity pattern of the laser is shown in Fig. 2.5. As expected, there is a dark spot at the center of the laser beam. Except for this dark spot, most of the laser power is concentrated in the angular region $0.2° - 0.5°$ off the laser axis. Obviously the laser is highly directional. For the purpose of comparison, the far field intensity patterns of the laser beam in the cover and substrate are shown in Fig. 2.6. The intensity pattern in the substrate is normalized to the maximum value of the intensity in the cover. As illustrated, the intensity pattern in the substrate is almost identical to that in the cover. This is due to the fact that the layers are very low-contrast and thin.

To show the dependence of laser beam to the aperture area, the normalized far field intensity patterns for three different values of N_g is depicted in Fig. 2.7. Each

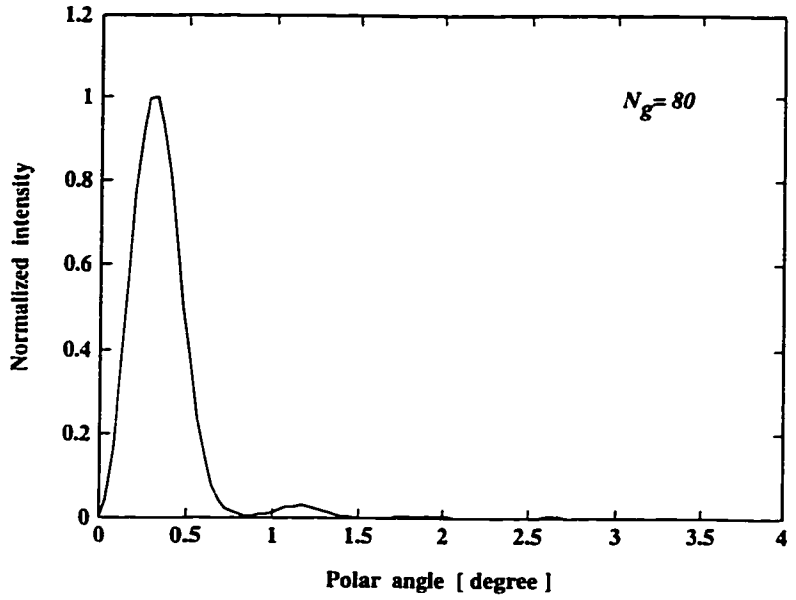

Figure 2.5: Normalized intensity pattern of a circularly symmetric laser beam in the cover region for $N_g = 80$

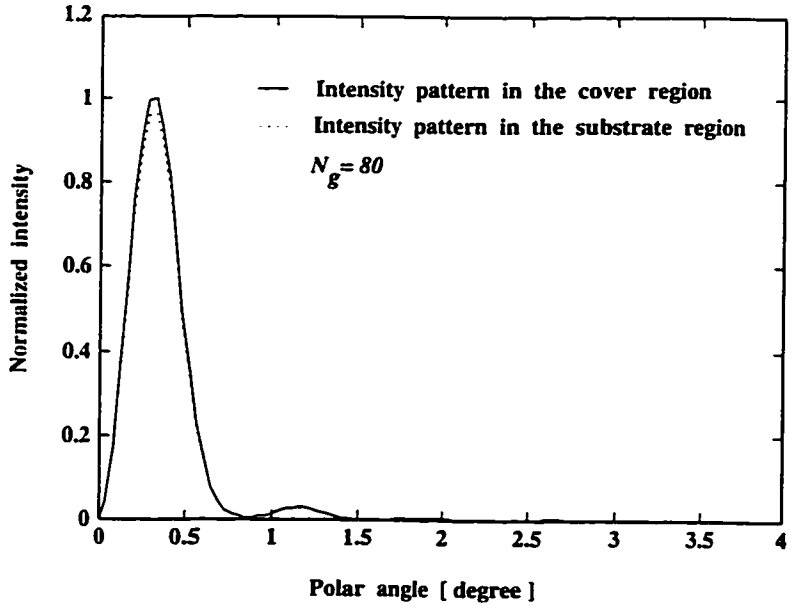

Figure 2.6: Normalized intensity patterns of a circularly symmetric laser beam in the cover and substrate regions for $N_g = 80$.

pattern is normalized to its own maximum value. As can be seen the larger the aperture area the narrower the laser beam. In Fig. 2.8, it is assumed that the laser field at the center of the second-order grating is the same for three different values of N_g. The far field intensity patterns for $N_g = 60, 80$ are normalized to the maximum value of the field intensity for $N_g = 100$. As expected, if we increase the aperture radius more power will be emitted from the laser. Finally, in Fig. 2.9, the intensity pattern of non-resonant grating is compared with that of resonant one. It can be seen that the main lobe is shifted toward higher polar angles. Moreover, the emitted power is much less than in the resonant case. This is due to the fact that the spectral components of the equivalent current source responsible for the radiation field are very weak compared to the resonant grating.

In the second part of this section, we investigate the far-field intensity pattern of the laser field with azimuthal variation $e^{\pm j\phi}$. The laser structure is the same as that depicted in Figs. 2.3 and 2.4. In this case as one might expect the far field intensity pattern is a function of the azimuthal angle. The intensity pattern of the laser structure with $N_g = 80$ observed at $\phi = 0°$ is shown in Fig. 2.10. As anticipated before, for this type of azimuthal variation a bright spot is observable at the center of the laser beam. Moreover, the laser beamwidth is very narrow and is less than 0.5°. Since the contrast between the different layers is very low and the layers are very thin, one might expect approximately the same far field intensity pattern in the substrate. This fact is clearly illustrated in Fig. 2.11. The dependence of the laser beamwidth on the aperture radius is shown in Fig. 2.12. The plots correspond to $\phi = 0°$. The far-field intensity patterns due to different apertures are normalized to their own maximum values. As illustrated, the narrower beams are due to the larger emitting areas.

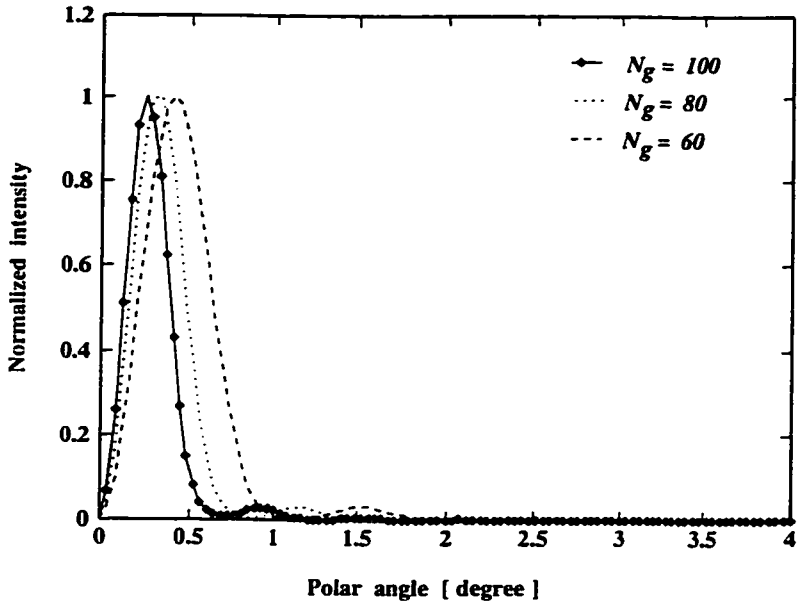

Figure 2.7: Normalized intensity patterns of a circularly symmetric laser beam in the cover region for three different values of N_g.

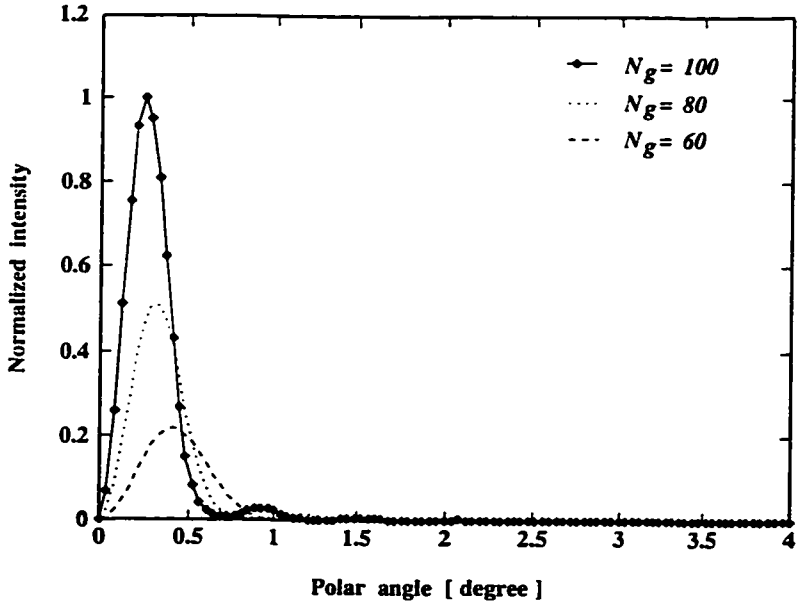

Figure 2.8: Normalized intensity patterns of a circularly symmetric laser beam in the cover region for three different values of N_g.

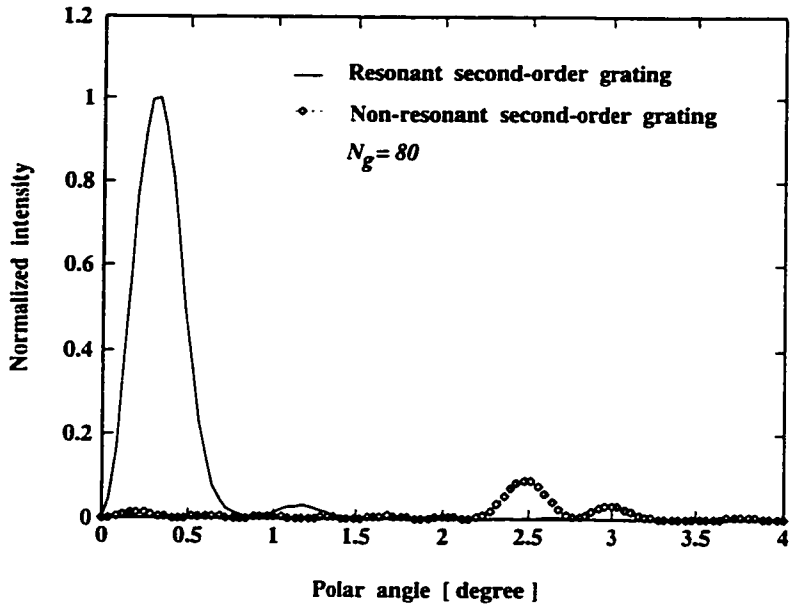

Figure 2.9: Normalized intensity patterns of a circularly symmetric laser beam for resonant and non-resonant second-order gratings

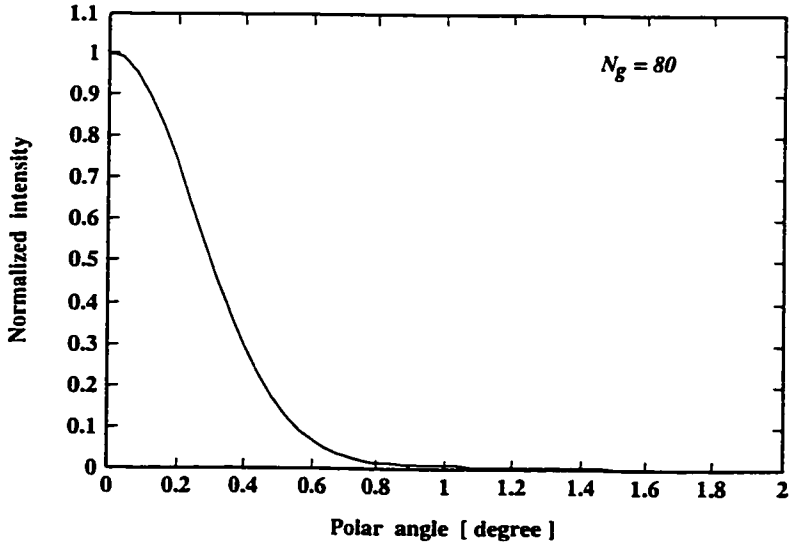

Figure 2.10: Normalized intensity patterns of the first azimuthal harmonic laser beam in the cover for $N_g = 80$.

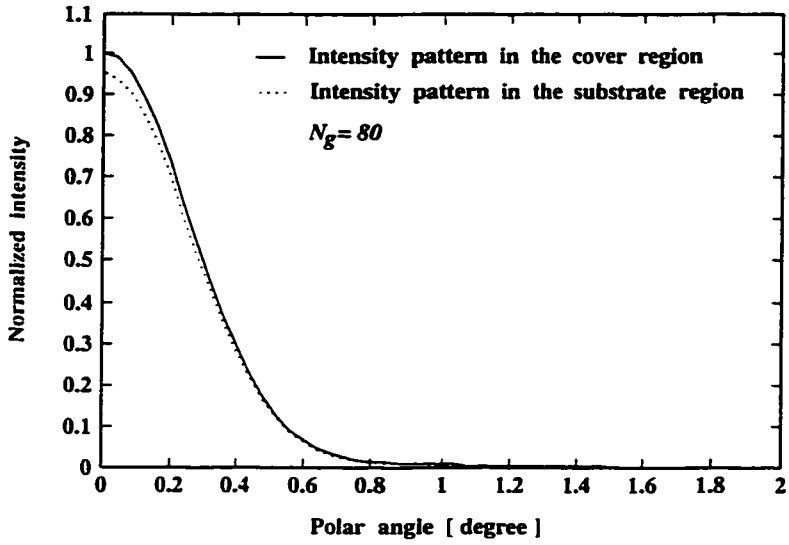

Figure 2.11: Normalized intensity patterns of the first azimuthal harmonic of the laser beam in the cover and substrate regions for $N_g = 80$.

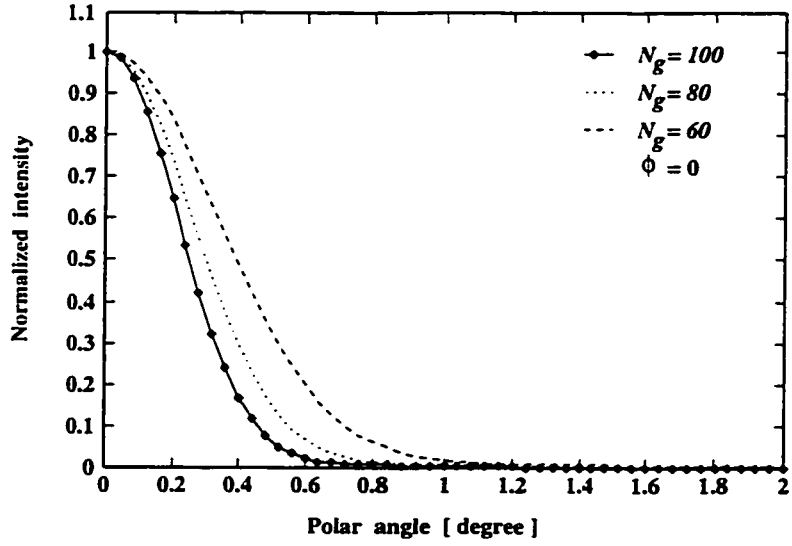

Figure 2.12: Normalized intensity patterns of the first azimuthal harmonic of the laser beam in the cover region for three different values of N_g.

Similar to the circularly symmetric beam, in Fig. 2.13 it is assumed that the laser field at the center of the laser is the same for three different central radii. The far field intensity pattern for $N_g = 60, 80$ are normalized to the maximum value of the field intensity for $N_g = 100$. All the plots correspond to $\phi = 0°$. The behavior shown in Fig. 2.13 is completely expectable. More power in a narrower beam is emitted from larger apertures. In Fig. 2.14 the functional dependence of the laser beam on the azimuthal angle is shown. The intensity pattern follows the same behavior in every quadrant of ϕ. Obviously, as shown before, the laser intensity on the laser axis is independent of the azimuthal angle. In Fig. 2.15 three dimensional far field intensity pattern in the cover is plotted for $N_g = 80$.

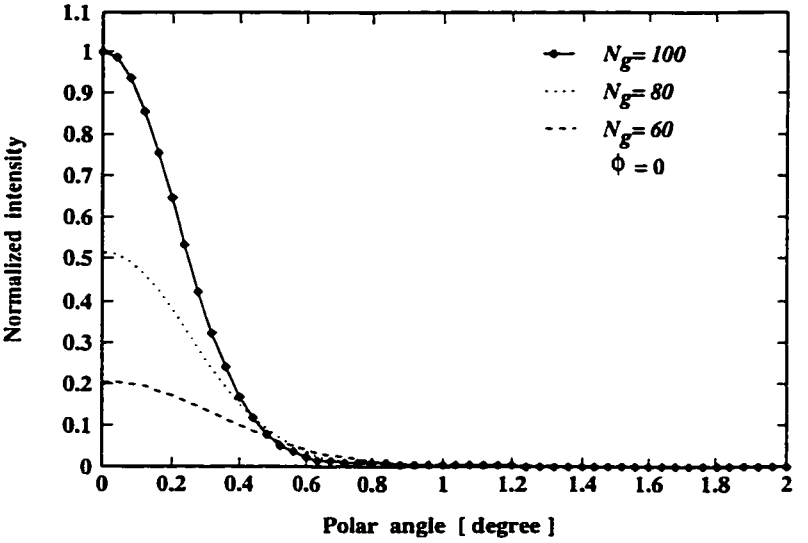

Figure 2.13: Normalized intensity patterns of the first azimuthal harmonic of the laser beam in the cover region for three different values of N_g.

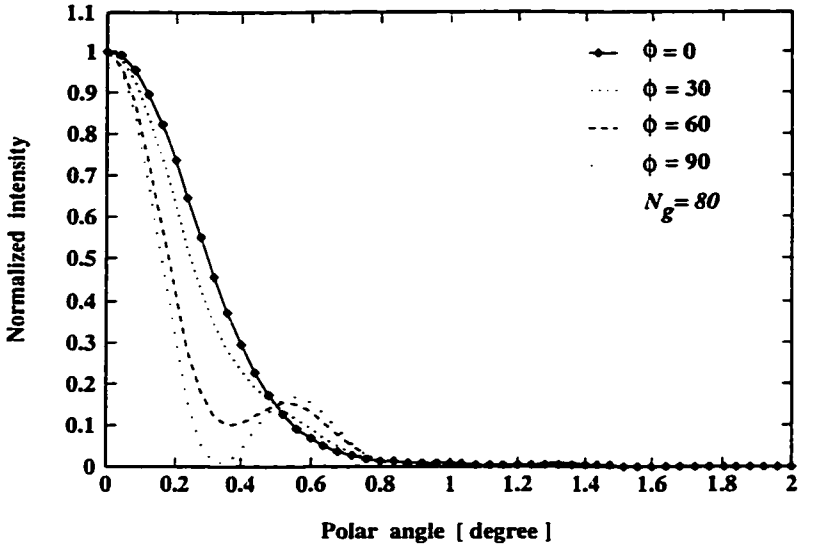

Figure 2.14: Normalized intensity patterns of the first azimuthal harmonic of the laser beam in the cover for four different azimuthal angles.

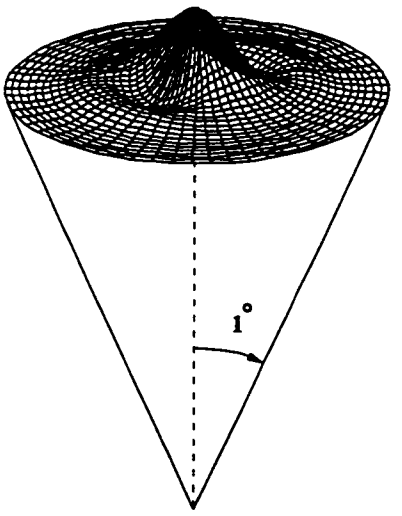

Figure 2.15: Three dimensional intensity pattern of the laser beam in the cover for $N_g = 80$.

2.7 Summary

In this chapter the volume current method (VCM) for multilayer planar structures has been derived based on the induction theorem in the electromagnetic theory. This has been followed by the closed-form Green's function formulation of multilayer planar structures both in the rectangular and cylindrical coordinate systems. The salient feature of the TMM has been demonstrated in the process of the formulation. In the derivation of the Green's function, we have assumed that the current excitation does not have any components transverse to the planar interfaces. Then volume current method and Green's functions have been directly connected to the radiation problem. It has been shown that circular apertures have a dark spot at the center of their far-field patterns in the absence of the first azimuthal harmonic in the aperture field. Finally, the far-field intensity pattern of a novel circular-grating surface-emitting DBR laser for circularly symmetric beam and the beam with the first harmonic of azimuthal variation have been illustrated.

Chapter 3

Two-Dimensional Threshold Analysis of Circular-Grating Surface-Emitting Lasers

3.1 Introduction

As is well-known, the operating principle of DFB lasers is based on the propagation of the guided waves in active multilayer planar structures with periodic modulation of the dielectric properties. The periodic modulation of the dielectric properties can be realized either as straight or circular gratings. In DFB and DBR lasers, the gratings are of the resonant type, i.e, the grating period Λ satisfies the Bragg condition,

$$\beta_o = N\frac{\pi}{\Lambda} \tag{3.1}$$

where β_o is the propagation constant of light in the guide and N is called the order of grating. The laser operation strongly depends on the value of N. This

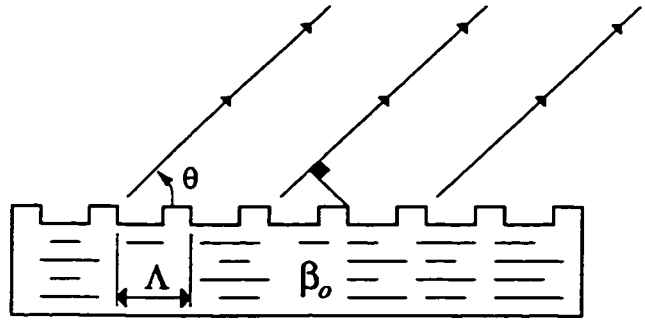

Figure 3.1: A typical resonant grating

dependence can be seen from the condition for the constructive interference at resonance. Referring to Fig. 3.1 and by using the geometrical optic concepts, constructive interference requires that the path difference between the rays be equal to an integer multiple of the guide wavelength. More precisely,

$$\Lambda(1 - cos\theta) = n\frac{2\pi}{\beta_o} \tag{3.2}$$

Substitution of (3.1) into (3.2) leads to

$$cos\theta = 1 - \frac{2n}{N} \tag{3.3}$$

Real values of θ can be obtained by choosing $n = 0, 1, \ldots, N$. Regardless of the value of N, there are always two extreme values of n; that is, $n = 1$ and $n = N$. These values of n correspond to $\theta = 0$ and $\theta = \pi$, respectively. This means that at resonance two coherent contra-directional waves jointly interact with the grating. These two partial waves provide the feedback mechanism for the laser oscillation. More importantly, partial waves related to $\theta = 0$ and $\theta = \pi$ are trapped in the laser cavity. In fact, these two waves are guided modes and of energy type. These two modes are responsible for the stimulated emission in the laser cavity. In DFB laser, which are self-oscillating devices, the fields are generated inside due to the

spontaneous emission coupled to these coherent waves. The fields are built up as a result of the exchange of energy between these two coherent oppositely-going waves.

Other possible values of n result in the radiation field. This radiation field is due to the joint interaction of the guided modes with the grating. In fact, the grating produces a mechanism that the two coherent waves radiate power. Therefore, with radiation field, the laser characteristic operation changes. One important effect of the radiation loss is the presence of asymmetrical longitudinal mode structure even for symmetrical boundary conditions [12],[58], and [60].

Of particular importance is the second-order grating, where the only possible values of n are 0, 1, and 2. In this case, the partial scattered wave arising from $n = 1$ is the radiation field. This scattered wave is emitted normal or near-normal to the surface of the grating.

From the above considerations, one can conclude that in resonance cases, surface emission requires grating order of two or higher. This is the key idea for the realization of grating coupled surface-emitting lasers.

In second- and higher-order gratings radiation fields provide another mechanism for exchange of the energy between the two coherent oppositely-going waves. Consequently, in an accurate treatment of this type of grating, the coupled-mode equations describing the behavior of the amplitudes of the coherent waves must be modified. For straight grating DFB lasers this modification has been reported in three excellent papers [58],[59], and [60]. Streifer *et al.* [58] started from the Floquet mode expansion of the electromagnetic field in the laser cavity to include the effects of the radiation and other partial nonradiating fields in the coupled-mode equations. Although this method is accurate, however, it is restricted to the straight gratings. In [59] the improved coupled-mode theory is based on a set of

coupled-mode equations for the guided and radiation modes. This approach is more general than that of [58]. The only difficulty is the presence of the radiation modes for expressing the radiation field. Kazarinov and Henry [60] derived explicit expressions for the radiation coupling factor by using Green's function method. More importantly, for shallow rectangular gratings they have obtained simple analytical formulas for the radiation coupling coefficient.

Radiation from a circular grating etched on the planar waveguides has been considered in non-resonant cases [40], [41], and [42]. In [40] and [42] the azimuthally polarized radiation field emitted from the surface of a shallow, circular grating has been described by using the field expansion method. This approach uses a boundary perturbation method to obtain an integral expression correct to first-order for the radiation field. In [41] the volume current method has been used to find the circularly symmetric field radiated by a circular grating.

Radiation from a circular grating at resonance has not been considered so far. For the first time, we have investigated azimuthally invariant radiation field from a circular grating at resonance [61]. In this chapter, we consider the general formulation of second-order circular gratings at threshold. As will be shown later, this formulation gives general modal analysis of a circular grating which produces circularly symmetric beam which can be exploited in the above threshold analysis. Before presenting the general formulation, however, in the next section we present a general comment on the type of the fundamental mode that can be supported by cylindrical structures.

3.2 Fundamental Mode in Cylindrical Structures and Photon's Ground State in Circular Apertures

The purpose of this section is to consider general evidences to predict the shape of the fundamental mode supported by a circular aperture. To this end, we use the *minimum energy principle*. According to this principle, any physical system tries to attain its minimum available energy state in any given set of circumstances. This means that the wave function associated with the minimum state of energy has smallest spatial variation. This property can be seen for a constraint particle. In fact, according to the accepted principle of quantum mechanics, the energy of a particle is the eigenvalue of the Hamiltonian operator. Since the Hamiltonian operator is related to the spatial variation of the wave function, it is obvious that the minimum energy corresponds to a wave function with minimum spatial variation. The wave function of an electron in a potential well of either finite or infinite barrier is a good evidence for this fact.

The same idea may be used when we consider the wave function associated with a photon. In electromagnetic theory the fundamental mode of different structures has very smooth spatial variation. For example, the electric field of the fundamental mode in a rectangular waveguide with perfect conducting boundaries varies smoothly in the transverse plane. The same is true in a dielectric slab waveguide. More importantly, ignoring the variation in one dimension directly leads to the fundamental modes in rectangular structures.

Unfortunately, this is not the case in cylindrical structures. Despite the fact that the mathematical description of azimuthally invariant electromagnetic field in

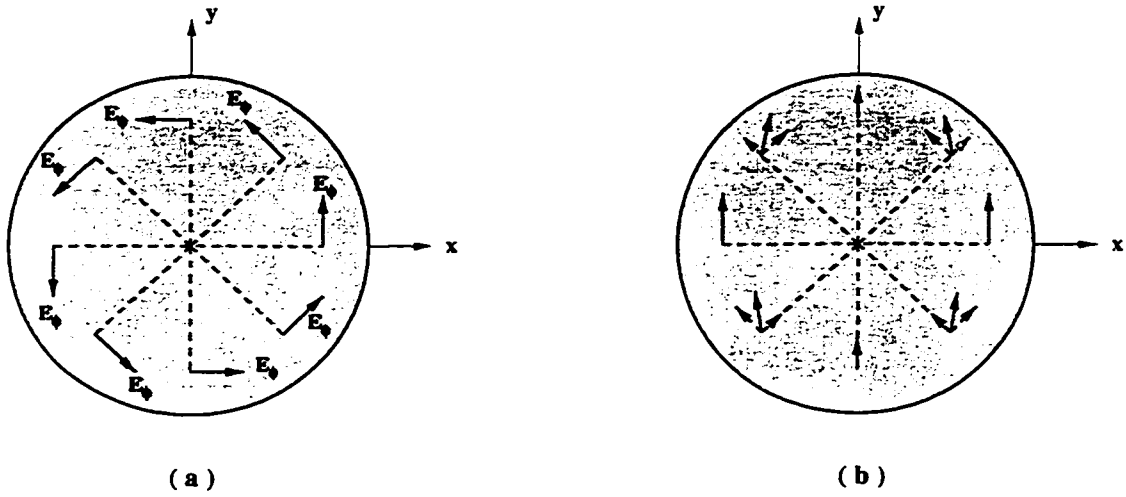

Figure 3.2: Near field pattern of the electric field. (a) Azimuthally invariant mode. (b) The mode with first-order azimuthal variation.

a cylindrical structure is very simple, however, the electric field vector does not have necessarily very mild variation. This fact can be seen in Fig 3.2 (a). For azimuthally invariant field the electric field has only ϕ component. Moreover, as can be seen from Fig. 3.2 (a) the field is highly asymmetric whereas its intensity is circularly symmetric.

On the other hand, consider the near field pattern of the first azimuthal order in Fig. 3.2 (b). By first azimuthal order we mean the field components vary as $cos\,\phi$ and $sin\,\phi$ with ϕ. For this case, it can be seen that the field pattern is more uniform than that of azimuthally invariant field. As illustrated, the field pattern is almost linearly polarized in the y direction.

In the preceding chapter we have shown that the far field pattern on the z axis due to an aperture field in the x-y plane is a measure of uniformity of the field on the aperture. Since only aperture field of first azimuthal order produces nonzero far field pattern on the aperture axis, one may consider this type of aperture

field as the photon's *ground state.* There are two electromagnetic examples which confirm the above assertion. The fundamental mode of a circular waveguide with perfect conducting boundary is TE_{11} which varies as first azimuthal order. The fundamental HE_{11} mode in an optical fiber is another evidence that verifies the first order azimuthal mode is the ground state for the photon in the circular apertures.

In the case of circular-grating lasers, it seems that by adjusting the grating phase, the threshold gain of the fundamental circular mode does not have necessarily the lowest value. That is, the fundamental circular mode is not necessarily the fundamental mode of the laser. This fact is the result of the numerical simulations of first-order circular-grating lasers in the limit of the validity of large argument approximation of the Hankel functions [24], [30], and [32]. Similarly, Gong *et al.* [34] have shown the same situation in treating second-order circular-grating DBR lasers by ignoring the radiation fields.

From the above considerations, we strongly believe that the circularly symmetric aperture field and the aperture field that varies as $cos\,\phi$ and $sin\,\phi$ with ϕ are the fundamental modes of the laser among all other azimuthal orders. Despite the fact that a circularly symmetric beam may not be the mostly desirable field pattern due to presence of a dark spot on the far-field pattern, however, for the the sake of mathematical simplicity, we assume that the laser field is azimuthally invariant.

3.3 Basic Formulation

In this section, we present a general approach in treating circular-grating DFB and DBR lasers producing azimuthally invariant field. Let us consider the DFB and DBR lasers shown in Fig. 3.3. We aim at deriving modified coupled-mode equations such that the radiation coupling factor are properly included. To this end, starting

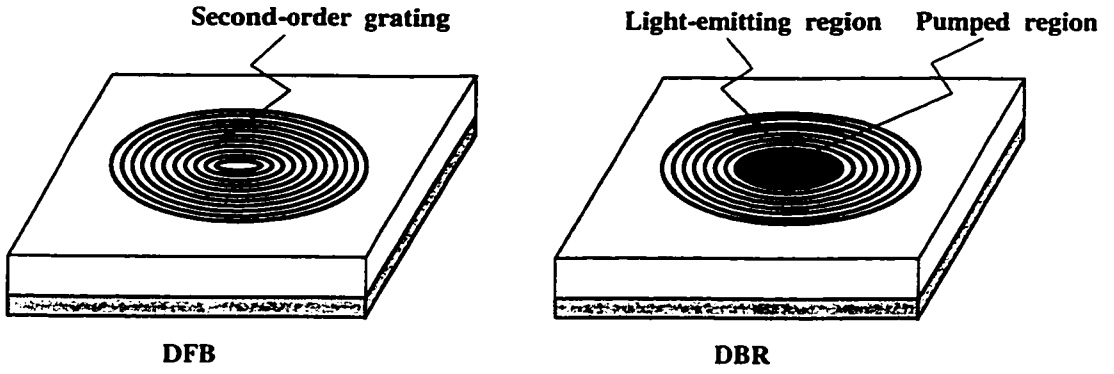

Figure 3.3: Circular-grating surface-emitting lasers.

from Maxwell's equations, we have

$$\nabla \times \nabla \times \mathbf{E} - k_o^2 \epsilon_r(\mathbf{r})\mathbf{E} = 0 \tag{3.4}$$

where k_o is the wave number of free space. $\mathbf{E}$ is of TE_z or LSE type field. It should be noted that for azimuthally invariant LSE field the electric field has only ϕ component.

In DFB lasers using second-order gratings the electric field has three basic part. Two of them are the guided waves which are responsible for feedback mechanism and the stimulated emission. The third part is the radiation field which leaves the laser cavity in the nearly normal direction. Let $\mathbf{E}^a$ and $\mathbf{E}^b$ be the guided fields which travel radially outward and inward, respectively. Moreover, assume that $\mathbf{E}^{rad}$ is the radiation part. The mutual interaction of these fields can be best described by the volume current method (see Sec. 2.2). In fact, as will be shown later, Eq. (3.4) can be considered as three coupled equations

$$\nabla \times \nabla \times \mathbf{E}^a - k_o^2[\epsilon_{r_i}(z) + j\epsilon_r'(z) - j\epsilon_r''(z)]\mathbf{E}^a = -j\omega\mu_o\mathbf{J}^a \tag{3.5a}$$

$$\nabla \times \nabla \times \mathbf{E}^b - k_o^2[\epsilon_{r_i}(z) + j\epsilon_r'(z) - j\epsilon_r''(z)]\mathbf{E}^b = -j\omega\mu_o\mathbf{J}^b \tag{3.5b}$$

$$\nabla \times \nabla \times \mathbf{E}^{rad} - k_o^2[\epsilon_{r_i}(z) + j\epsilon_r'(z) - j\epsilon_r''(z)]\mathbf{E}^{rad} = -j\omega\mu_o\mathbf{J}^{rad} \tag{3.5c}$$

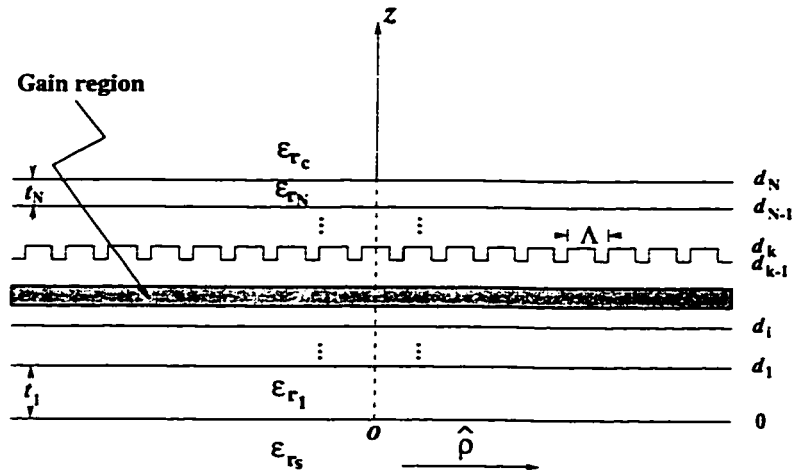

Figure 3.4: The cross section of a circular-grating index-guided DFB laser

The meaning of each term in the above equations will be clear later. For example $\mathbf{J}^a$ is an equivalent current which accounts for the interaction of $\mathbf{E}^b$ and $\mathbf{E}^{rad}$ with the grating to produce $\mathbf{E}^a$.

Let us apply the general method described above in a special case of interest. We construct the cylindrical coordinate system (ρ, ϕ, z) such that the z axis passes through the center of the laser cavity. We assume that the origin of the z axis is fixed at the interface between the substrate and the first layer as shown in Fig. 3.4. The field components of an arbitrary azimuthally invariant TE_z mode are E_ϕ, H_ρ, and H_z. Assuming that $\frac{\partial}{\partial \phi} \equiv 0$, rfeq-4.4) leads to

$$\frac{\partial^2 E_\phi}{\partial \rho^2} + \frac{1}{\rho}\frac{\partial E_\phi}{\partial \rho} - \frac{1}{\rho^2}E_\phi + \frac{\partial^2 E_\phi}{\partial z^2} + \epsilon_r(\rho, z)\, k_o^2 E_\phi = 0 \tag{3.6}$$

where

$$\epsilon_r(\rho, z) = \epsilon_r(z) + j\epsilon_r'(z) - j\epsilon_r''(z) + \delta\epsilon_r(\rho, z) \tag{3.7}$$

k_0 is the wave number of the free space at a reference frequency and $\epsilon_r(z)$ is the dielectric constant of the unperturbed lossless multilayer structure. $\epsilon_r'(z)$ and $\epsilon_r''(z)$ are the gain and loss profiles, respectively. Based on the assumption of $e^{j\omega t}$ time

variation, both gain and loss profiles must be positive in (3.7). $\delta\epsilon_r(\rho, z)$ is a periodic function of ρ with zero average accounting for the grating and it is only nonzero within grating layer; that is, $d_{k-1} \leq z \leq d_k$.

Let $\delta\epsilon_r(\rho, z)$ be expressed by its Fourier series expansion as

$$\delta\epsilon_r(\rho, z) = \sum_{m \neq 0} \eta_m(z) e^{-jm\frac{2\pi}{\Lambda}(\rho-\rho_o)} \tag{3.8}$$

where Λ is the grating period and $e^{jm\frac{2\pi}{\Lambda}\rho_o}$ is a phase shifting factor making $\eta_m(z)$ real. It should be noted that based on the above assumptions we only consider index-guided lasers. Furthermore, let us assume that the grating be of second-order; that is,

$$\beta_o = \frac{2\pi}{\Lambda} \tag{3.9}$$

where β_o is the propagation constant of light in the guide. Therefore, the two coherent guided-waves couple to each other in second-order Bragg diffraction and they jointly interact with the nearly normal radiating field $E^{rad}(\rho, z)$ in first-order Bragg diffraction. More precisely, (3.6) allows us to write $E_\phi(\rho, z)$ as

$$\begin{aligned} E_\phi(\rho, z) &= A(\rho) e^{j\beta_o\rho_o} H_1^{(2)}(\beta_o\rho)\widehat{F}(z) - jB(\rho) e^{-j\beta_o\rho_o} H_1^{(1)}(\beta_o\rho)\widehat{F}(z) + \\ &\quad E^{rad}(\rho, z) \end{aligned} \tag{3.10}$$

where $H_1^{(1)}(\beta_o\rho)$ and $H_1^{(2)}(\beta_o\rho)$ are the first-order Hankel functions of the first and the second kind, respectively. $A(\rho)$ and $B(\rho)$ are slowly varying amplitudes of outward- and inward-going guided modes, respectively. $\widehat{F}(z)$ is the normalized transverse profile of the guided modes satisfying the eigenvalue equation

$$\left[\frac{d^2}{dz^2} + \epsilon_{r_o}(z)\, k_o^2\right] \widehat{F}(z) = \beta^2 \widehat{F}(z) \tag{3.11}$$

subject to the continuity of $\widehat{F}(z)$ and its normal derivative at the interfaces of the

unperturbed multilayer waveguide. By normalized, we mean that

$$\int_{-\infty}^{\infty} \widehat{F}^2(z)dz = 1 \tag{3.12}$$

In fact, $\widehat{F}(z)$ is the normalized *form function* of the fundamental TE_z guided mode. The choice of the coefficients in (3.10), especially introducing the j factor in front of $B(\rho)$ will be clear later. The characteristic feature of our formulation is the inclusion of the radiation component resulting from first-order Bragg diffraction in the electric field expression.

Substituting (3.10) into (3.6) and using (3.7), (3.8), and (3.11), the *almost phase matching* condition requires that

$$\begin{bmatrix} f_1^{(2)}(\rho,z) & 0 \\ 0 & f_1^{(1)}(\rho,z) \end{bmatrix} \begin{bmatrix} \frac{dA}{d\rho} \\ \frac{dB}{d\rho} \end{bmatrix} = \begin{bmatrix} p_1^{(2)}(\rho,z) & q_2^{(1)}(\rho,z) \\ q_{-2}^{(2)}(\rho,z) & p_1^{(1)}(\rho,z) \end{bmatrix} \begin{bmatrix} A(\rho) \\ B(\rho) \end{bmatrix} + \begin{bmatrix} r_1(\rho,z) \\ r_{-1}(\rho,z) \end{bmatrix} E^{rad}(\rho,z) \tag{3.13}$$

$$\left[\frac{\partial^2}{\partial\rho^2} + \frac{1}{\rho}\frac{\partial}{\partial\rho} - \frac{1}{\rho^2} + \frac{\partial^2}{\partial z^2}\right] E^{rad}(\rho,z) = -k_o^2\eta_{-1}(z)\widehat{F}(z)e^{j\beta_o\rho}H_1^{(2)}(\beta_o\rho)A(\rho) + jk_o^2\eta_1(z)\widehat{F}(z)e^{-j\beta_o\rho}H_1^{(1)}(\beta_o\rho)B(\rho) \tag{3.14}$$

Since the Hankel functions behave as a traveling wave for large arguments; i.e.,

$$\lim_{x\to\infty} H_n^{(1)}(x) = \sqrt{\frac{2}{j\pi x}}j^{-n}e^{jx} \tag{3.15a}$$

$$\lim_{x\to\infty} H_n^{(2)}(x) = \sqrt{\frac{j2}{\pi x}}j^{n}e^{-jx} \tag{3.15b}$$

the phase matching condition is not exact in deriving (3.13) and (3.14). Hence we use the term *almost* phase matching condition. We will discuss the validity of the

above approximation later. In fact, the guided modes around the center of the laser cavity are not exactly coherent. However, as far as the laser operation is concerned, (3.13) and (3.14) can be considered as the starting point in the threshold analysis. Different terms appearing in (3.13) are defined as follows

$$r_{\pm 1}(\rho, z) = -k_o^2\, \eta_{\pm 1}(z)\, e^{\mp j\beta_o \rho} \tag{3.16a}$$

$$q_{\pm 2}^{(1,2)}(\rho, z) = j^{1,2}\, k_o^2\, \eta_{\pm 2}(z)\, e^{\mp j2\beta_o \rho} H_1^{(1,2)}(\beta_o \rho)\widehat{F}(z) \tag{3.16b}$$

$$\begin{aligned} f_1^{(1,2)}(\rho, z) &= -j^{1,2}\,(2\frac{d}{d\rho} + \frac{1}{\rho})H_1^{(1,2)}(\beta_o \rho)\widehat{F}(z) \\ &= -j^{1,2}\,[\frac{3\beta_o}{2} H_o^{(1,2)}(\beta_o \rho) - \frac{\beta_o}{2} H_2^{(1,2)}(\beta_o \rho)]\widehat{F}(z) \end{aligned} \tag{3.16c}$$

$$p_1^{(1,2)}(\rho, z) = j^{1,2}\,[\beta^2 - \beta_o^2 + jk_o^2\epsilon_r'(z) - jk_o^2\epsilon_r''(z)]H_1^{(1,2)}(\beta_o \rho)\widehat{F}(z) \tag{3.16d}$$

In deriving (3.13), (3.14), and (3.16) we have used slowly varying amplitude approximation by neglecting $\frac{d^2A}{d\rho^2}$ and $\frac{d^2B}{d\rho^2}$. In addition, we have noted that for any Bessel function B_n of nth order, we have

$$\frac{dB_n(\beta_o \rho)}{d\rho} = \frac{\beta_o}{2}[B_{n-1}(\beta_o \rho) - B_{n+1}(\beta_o \rho)] \tag{3.17a}$$

$$\frac{n}{\rho} B_n(\beta_o \rho) = \frac{\beta_o}{2}[B_{n-1}(\beta_o \rho) + B_{n+1}(\beta_o \rho)] \tag{3.17b}$$

$$(\frac{d^2}{d\rho^2} + \frac{1}{\rho}\frac{d}{d\rho} - \frac{n}{\rho^2})B_n(\beta_o \rho) = -\beta_o^2\, B_n(\beta_o \rho) \tag{3.17c}$$

Moreover, in deriving (3.14) ϵ_r' and ϵ_r'' have been ignored in comparison with $\epsilon_r(z)$.

In order to derive the coupled-mode equations governing the amplitudes of the guided modes, $E^{rad}(\rho, z)$ in (3.14) must be expressed in terms of $A(\rho)$ and $B(\rho)$. Before doing that, it should be emphasized that (3.14) is not valid around the center of the laser cavity, especially at $\rho = 0$. Since the total field must be finite at the center of the laser cavity, the singularity of the Hankel functions must be removed. This can be done by choosing

$$A(0)e^{j\beta_o \rho_o} = -jB(0)e^{-j\beta_o \rho_o} \tag{3.18}$$

Thus, for any $\rho_o \neq 0$, the right hand side of (3.14) is singular at the origin. Consequently, (3.14) must be considered for sufficiently large values of ρ. However, if $\rho_o = 0$, one may consider the validity of (3.14) for all values of ρ. To solve (3.14) we use two different approaches described as follows

First approach

In this approach we take advantage of the fact that $E^{rad}(\rho, z)$ is a nearly normal radiation field. By nearly normal, we mean that the *form functions* $F_{c,s}(z)$ of the spectrum of the radiation field satisfy the following equation

$$\frac{d^2 F_{c,s}}{dz^2} + \epsilon_r(z)\, k_o^2\, F_{c,s} \approx 0 \tag{3.19}$$

Using (3.19) in (3.14), it is reasonable to assume that

$$(\frac{\partial^2}{\partial\rho^2} + \frac{1}{\rho}\frac{\partial}{\partial\rho} - \frac{1}{\rho^2})E^{rad}(\rho, z) \approx 0$$

Consequently, (3.14) reduces to

$$\begin{aligned}\frac{\partial^2 E^{rad}(\rho, z)}{\partial z^2} + \epsilon_r(z)k_o^2 E^{rad}(\rho, z) \;=\; & -k_o^2\eta_{-1}(z)\widehat{F}(z)e^{j\beta_o\rho}H_1^{(2)}(\beta_o\rho)A(\rho) + \\ & jk_o^2\eta_1(z)\widehat{F}(z)e^{-j\beta_o\rho}H_1^{(1)}(\beta_o\rho)B(\rho)\end{aligned} \tag{3.20}$$

To solve (3.20), we use the Green's function approach. Therefore, it is necessary to find the Green's function $G(z; z')$ satisfying

$$\frac{\partial^2 G(z; z')}{\partial z^2} + \epsilon_r(z)k_o^2\, G(z; z') = \delta(z - z') \tag{3.21}$$

in the unperturbed multilayer stack described by $\epsilon_r(z)$. The above equation also has been used by Kazarinov and Henry in treating second-order DFB lasers with straight gratings [60]. However, they solved it in a uniform space. We obtain the

exact Green's function using the transfer matrix method. The detailed derivation is given in Appendix D.1. Thus, solving (3.20) leads to

$$E^{rad}(\rho,z) = h_{-1}(z)e^{j\beta_o\rho}H_1^{(2)}(\beta_o\rho) - jh_1(z)e^{-j\beta_o\rho}H_1^{(1)}(\beta_o\rho) \tag{3.22}$$

where

$$h_{\pm 1}(z) = -k_o^2\int_{-\infty}^{\infty} G(z;z')\,\eta_{\pm 1}(z')\widehat{F}(z')\,dz' \tag{3.23}$$

If one substitutes for $E^{rad}(\rho,z)$ in (3.13), one obtains

$$\begin{bmatrix} f_1^{(2)}(\rho,z) & 0 \\ & f_1^{(1)}(\rho,z) \end{bmatrix}\begin{bmatrix} \frac{dA}{d\rho} \\ \frac{dB}{d\rho} \end{bmatrix} = \begin{bmatrix} t_1^{(2)}(\rho,z) & g_1^{(1)}(\rho,z) \\ g_{-1}^{(2)}(\rho,z) & t_{-1}^{(1)}(\rho,z) \end{bmatrix}\begin{bmatrix} A(\rho) \\ B(\rho) \end{bmatrix} \tag{3.24}$$

where

$$t_{\pm 1}^{(2,1)}(\rho,z) = p_1^{(2,1)}(\rho,z) - j^{2,1}r_{\pm 1}(\rho,z)h_{\mp 1}(z)\,e^{\pm j\beta_o\rho}H_1^{(2,1)}(\beta_o\rho) \tag{3.25a}$$

$$g_{\pm 1}^{(1,2)}(\rho,z) = q_{\pm 2}^{(1,2)}(\rho,z) - j^{1,2}r_{\pm 1}(\rho,z)h_{\pm 1}(z)e^{\mp j\beta_o\rho}H_1^{(1,2)}(\beta_o\rho) \tag{3.25b}$$

The coupled-mode equations in (3.24) are obtained based on the *almost phase matching* condition between slowly varying terms. They are exact in the limit of the validity of large argument approximation for the Hankel functions. The z-dependent part can be eliminated by multiplying both sides of the above system of equations by $\widehat{F}(z)$ and integrating from $-\infty$ to ∞. This procedure reduces the equations in (3.24) to a system of differential equations with variable coefficients. Thus, they can not be solved analytically. However, they can be more tractable if we substitute for the Hankel functions in (3.24) by their asymptotic functions given in (3.15).

To see the range of ρ such that the asymptotic behavior is valid, it is necessary to consider the Hankel functions in more detail. We have

$$H_1^{(1)}(\beta_o\rho)(x) = J_1(x) + jN_1(x) \tag{3.26a}$$

$$H_1^{(2)}(\beta_o\rho)(x) = J_1(x) - jN_1(x) \tag{3.26b}$$

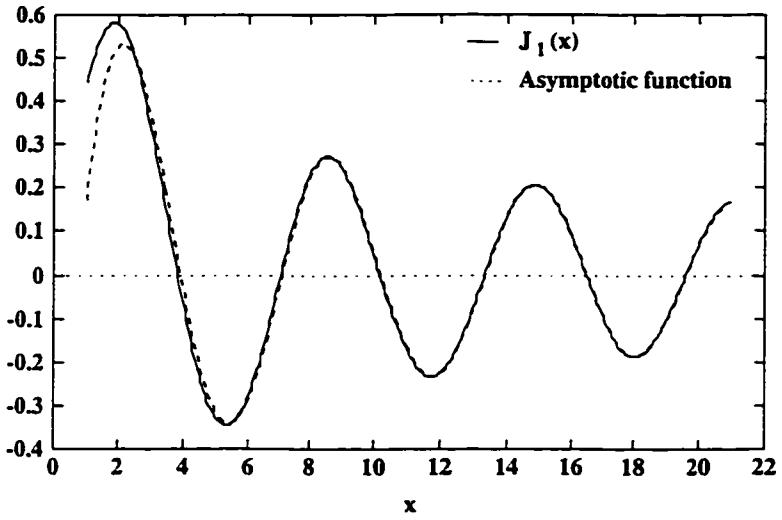

Figure 3.5: $J_1(x)$ and its asymptotic function

where $J_1(x)$ and $N_1(x)$ are the first-order Bessel function of the first and second kind, respectively. $N_1(x)$ is the so called Neumann function. For large values of x, if one uses the asymptotic series expansion of $J_1(x)$ and $N_1(x)$, from the leading terms one obtains [108] (p. 462)

$$\lim_{x\to\infty} J_1(x) = \sqrt{\frac{2}{\pi x}} sin(x - \frac{\pi}{2}) \tag{3.27a}$$

$$\lim_{x\to\infty} N_1(x) = -\sqrt{\frac{2}{\pi x}} cos(x - \frac{\pi}{2}) \tag{3.27b}$$

In Figs. 3.5 and 3.6, the exact values of the first-order Bessel functions is compared with their asymptotic values. As illustrated, for those arguments larger than 6, the first-order Hankel functions can be replaced by their asymptotic values without loosing the accuracy. This means that in practical cases this replacement is valid for $\rho > 0.5$ μm, i.e., only one grating period. Especially, this approximation is valid for DBR lasers.

For circularly symmetric beam, the near field radiation field around the center of the laser is negligible. This is so, because for circularly symmetric beam the field

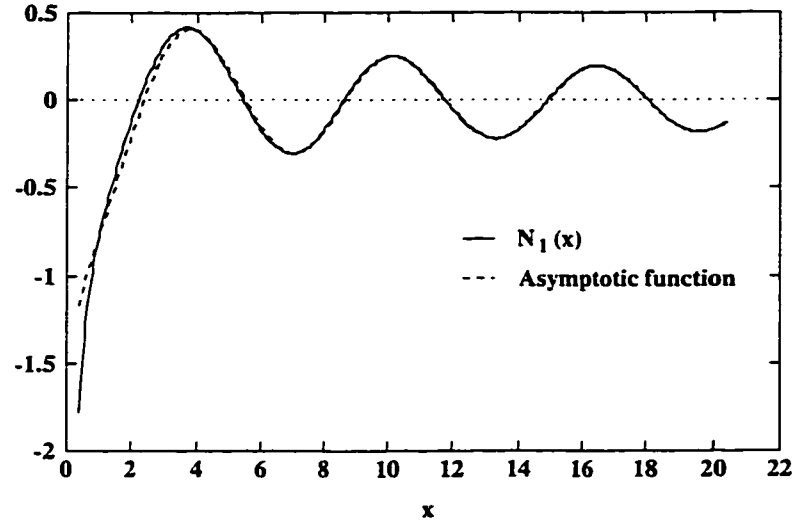

Figure 3.6: $N_1(x)$ and its asymptotic function

at the center of the laser vanishes due to the asymmetry of the field. In addition, the guided modes can not interact properly with the grating to produce radiation field. Therefore, as far as the laser operation and the radiation field are concerned, one may substitute the Hankel functions in (3.24) by their asymptotic functions.

This substitution reduces the coupled-mode equations in (3.24) to a system of differential equations with constant coefficients. The details of the derivation is very straightforward. The ρ-dependent terms from both sides of each equation are canceled, then the equations are multiplied by $\widehat{F}(z)$ and integrated from $-\infty$ to ∞. In addition, if one defines the detuning factor δ by

$$\delta = \beta - \beta_o \tag{3.28}$$

and substitutes $2\beta_o\delta$ for $\beta^2 - \beta_o^2$, one obtains the final form of the coupled-mode equations as follows

$$\begin{bmatrix} \frac{dA}{d\rho} \\ \frac{dB}{d\rho} \end{bmatrix} = \begin{bmatrix} g - \alpha - j\delta + \kappa^r_{(1,-1)} & \kappa^r_{(1,1)} + \kappa_2 \\ -\kappa^r_{(-1,-1)} - \kappa_{-2} & -g + \alpha + j\delta - \kappa^r_{(-1,1)} \end{bmatrix} \begin{bmatrix} A(\rho) \\ B(\rho) \end{bmatrix} \tag{3.29}$$

where

$$\alpha = \frac{k_o^2}{2\beta_o}\int_{-\infty}^{\infty} \epsilon_r''(z)\widehat{F}^2(z)dz \tag{3.30a}$$

$$g = \frac{k_o^2}{2\beta_o}\int_{-\infty}^{\infty} \epsilon_r'(z)\widehat{F}^2(z)dz \tag{3.30b}$$

$$\kappa_{\pm 2} = -j\frac{k_o^2}{2\beta_o}\int_{-\infty}^{\infty} \eta_{\pm 2}(z)\widehat{F}^2(z)dz \tag{3.30c}$$

$$\kappa^r_{(\pm 1,\pm 1)} = -j\frac{k_o^2}{2\beta_o}\int_{-\infty}^{\infty} \eta_{\pm 1}(z)h_{\pm 1}(z)\widehat{F}(z)dz \tag{3.30d}$$

The coupled-mode equations in (3.29) with the coefficients defined in (3.30) are exactly those equations which appear in treating the conventional second-order DFB lasers. This is the direct consequence of the asymptotic behavior of the Hankel functions and special form of the coefficients chosen in (3.10). An interesting feature of the coupled-mode equations in (3.29) is the modification of the coupling factors by introducing first-order Bragg diffraction effects $\kappa_{(\pm 1,\pm 1)}$. These factors account for coupling to the radiation field.

Symmetrical and asymmetrical grating structures are defined such that $\eta_{-m}(z) = \eta_m(z)$ and $\eta_{-m}(z) = -\eta_m(z)$, respectively. For either symmetrical and asymmetrical gratings the diagonal elements of the first-order coupling factors are equal. This can be easily seen from (3.23) and (3.30d). In fact, irrespective of the shape of the symmetrical or asymmetrical grating, we always have

$$\kappa^r_{(1,-1)} = \kappa^r_{(-1,1)} \tag{3.31a}$$

$$\kappa^r_{(1,1)} = \kappa^r_{(-1,-1)} \tag{3.31b}$$

Eq. (3.31a) guarantees that for symmetrical and asymmetrical gratings the eigenvalues of the coefficient matrix in (3.29) are negative of each other; that is,

$$\gamma_{1,2} = \pm\gamma = \pm\sqrt{(g - \alpha - j\delta + \kappa_{(1,-1)})^2 - (\kappa_{(1,1)} + \kappa_2)(\kappa_{(1,1)} + \kappa_{-2})} \tag{3.32}$$

Therefore, according to the theory of the system of linear differential equations [62], the solution of (3.29) can be written as

$$\begin{bmatrix} A(\rho) \\ B(\rho) \end{bmatrix} = \begin{bmatrix} K_+(\rho-\rho_a) & L_+(\rho-\rho_a) \\ L_-(\rho-\rho_a) & K_-(\rho-\rho_a) \end{bmatrix} \begin{bmatrix} A(\rho_a) \\ B(\rho_a) \end{bmatrix} \tag{3.33}$$

where ρ_a is an arbitrary reference radius and

$$L_\pm(\rho-\rho_a) = \pm(\kappa_{(1,1)} + \kappa_{\pm 2})\frac{sh\gamma(\rho-\rho_a)}{\gamma} \tag{3.34a}$$

$$K_\pm(\rho-\rho_a) = ch\gamma(\rho-\rho_a) \pm (g - \alpha - j\delta + \kappa_{(1,-1)})\frac{sh\gamma(\rho-\rho_a)}{\gamma} \tag{3.34b}$$

Solution in the form of (3.33) and (3.34) have two advantages: first, they are not sensitive to the sign of γ. The sign ambiguity in the exponential form of the solutions must be solved. Second, the characteristic equation for laser cavity can be easily found by applying suitable boundary conditions on the mode amplitudes. In particular, it is very well suited in dealing with DBR lasers.

Second approach

In this approach, in order to solve (3.14) for $E^{rad}(\rho,z)$, we write $E^{rad}(\rho,z)$ as a superposition of radiation modes. That is,

$$E^{rad}(\rho,z) = \sum_{i=s,c}\int_0^\infty R_i(\rho;s')\,\check{F}_i(z;s')\,ds' \tag{3.35}$$

where $i = s, c$ stand for the substrate and cover modes, respectively. $\check{F}_i(z;s)$ is the normalized *form function* of the radiation mode in the unperturbed waveguide and satisfies the following differential equation (see Appendix A.6)

$$\frac{d^2\check{F}_i(z;s)}{dz^2} + [\epsilon_r(z)k_o^2 - \beta_i^2(s)]\check{F}_i(z;s) = 0 \quad i = s,c \tag{3.36}$$

where

$$\beta_i = \sqrt{\epsilon_{r_i}k_o^2 - s^2} \qquad i = s,c \tag{3.37}$$

Moreover,

$$\int_{-\infty}^{\infty} \check{F}_s(z;s)\check{F}_c^*(z;s')\,dz = 0 \tag{3.38a}$$

$$\int_{-\infty}^{\infty} \check{F}_i(z;s)\check{F}_i^*(z;s')\,dz = \delta(s-s') \tag{3.38b}$$

Substituting (3.35) into (3.14), multiplying both sides of the resulting equation by $\check{F}_i^*(z;s)$ and integrating from $z=-\infty$ to ∞ result in the following equation for $R_i(\rho;s)$

$$\left[\frac{\partial^2}{\partial\rho^2}+\frac{1}{\rho}\frac{\partial}{\partial\rho}-\frac{1}{\rho^2}+\beta^2(s)\right]R_i(\rho;s) = h_{-1}^{(i)}(s)h_1^{(2)}(\beta_o\rho)A(\rho) - jh_1^{(i)}(s)h_1^{(1)}(\beta_o\rho)B(\rho) \qquad i=s,c \tag{3.39}$$

where

$$h_{\pm1}^{(i)}(s) = -k_o^2\int_{d_{k-1}}^{d_k}\eta_{\pm1}(z)\hat{F}(z)\check{F}_i^*(z;s)\,dz \tag{3.40}$$

$$h_1^{(2)}(\beta_o\rho) = e^{j\beta_o\rho}H_1^{(2)}(\beta_o\rho) \tag{3.41a}$$

$$h_1^{(1)}(\beta_o\rho) = e^{-j\beta_o\rho}H_1^{(1)}(\beta_o\rho) \tag{3.41b}$$

Equation (3.39) can be solved by the Green's function approach. The Green's function $G(r,\rho';s)$ satisfies the following differential equation

$$\left[\frac{\partial^2}{\partial\rho^2}+\frac{1}{\rho}\frac{\partial}{\partial\rho}-\frac{1}{\rho^2}+\beta^2(s)\right]G(\rho,\rho';s) = \frac{1}{\rho}\delta(\rho-\rho') \tag{3.42}$$

In Chapter 5, we will explain about more general Green's function in the radial direction. From this general expression, it can be seen that the Green's function satisfying (3.42) can be represented by the following expressions

(a) For $\beta^2(s)\neq 0$

$$G(\rho,\rho';s)j\frac{\pi}{2}J_1(-j\sqrt{-\beta^2(s)}\rho^<)H_1^{(2)}(-j\sqrt{-\beta^2(s)}\rho^>) \tag{3.43}$$

where $\rho^<$ and $\rho^>$ denote the smaller and the larger values of ρ and ρ', respectively.
(b) For $\beta^2(s) = 0$

$$G(\rho, \rho'; s) = -\frac{1}{2}\frac{\rho^<}{\rho^>} \tag{3.44}$$

Therefore,

$$R_i(\rho; s) = h_{-1}^{(i)}(s) \int_a^L G(\rho, \rho'; s) h_1^{(2)}(\beta_o \rho') A(\rho') \rho' d\rho' - j h_1^{(i)}(s) \int_a^L h_1^{(1)}(\beta_o \rho') B(\rho') \rho' d\rho' \tag{3.45}$$

where a is chosen such that for $\rho > a$ the *almost phase matching* condition is valid. L is the length of the laser cavity.

Eq. (3.45) states that $R_i(\rho; s)$ can be obtained in terms of $A(\rho)$ and $B(\rho)$. Consequently, using (3.35), $E^{rad}(\rho, z)$ can be expressed in terms of $A(\rho)$ and $B(\rho)$. Now, one may use the perturbation approach used by Yamamoto *et al.* [59] to obtain the coupled-mode equations between the amplitudes of the guided modes. That is, by ignoring the coupling between the guided and the radiation modes the amplitudes of the guided modes can be obtained first. Then these amplitude functions can be used to calculate the radiation field. From the calculated radiation field, the coupled-mode equation for the amplitudes of the guided modes can be modified. In order to improve the accuracy, the improved coupled-mode equations can be solved to obtain a better estimation of the radiation field. Continuing this procedure a self-consistent solution can be obtained.

Before concluding this section, we mention that there is still an other possibility in dealing with the circular-grating lasers. To this end, it is more convenient to write (3.6) in the following form

$$\frac{\partial^2 E_\phi}{\partial \rho^2} + \frac{1}{\rho}\frac{\partial E_\phi}{\partial \rho} - \frac{1}{\rho^2} E_\phi + \frac{\partial^2 E_\phi}{\partial z^2} + \epsilon_r(z)\, k_o^2 E_\phi = -\Delta\epsilon_r(\rho, z) k_o^2 E_\phi \tag{3.46}$$

The solution for $E_\phi(\rho, z)$ can be written as

$$E_\phi(\rho, z) = U(\rho)\widehat{F}(z) + \sum_{i=s,c} \int_0^\infty R_i(\rho; s)\check{F}_i(z; s)\, ds \tag{3.47}$$

where $\widehat{F}(z)$ is the normalized *form function* of the fundamental guided modes satisfying the eigenvalue problem (3.11). Moreover, $\check{F}_i(z; s)$ is the normalized *form function* of the cover and substrate radiation modes which is the solution of (3.36). The differential operator on the left hand side of (3.46) is of the type of Laplacian operator. Since this operator is separable, the solutions for $U(\rho)$ and $R_i(\rho; s)$ can be obtained by Green's function method. This in turn leads to the infinite set of the coupled-mode equations between the amplitudes of the guided and radiation modes. Since (3.46) is a special type of the more general equations treated in Chapter 5, more detailed discussion about this method is given in that chapter.

3.4 Threshold Analysis of Circular-Grating DBR Lasers

In this section, we apply the formulation developed in the preceding section in the investigation of the threshold gain and threshold current of circular-grating surface-emitting DBR lasers. The cross sectional view of this structure is illustrated in Fig. 3.7. The central uniform active region of radius ρ_1 is surrounded by the grating region, $\rho_1 < \rho < \rho_2$. In the central region we assume that

$$E_\phi(\rho, z) = A_1(\rho)H_1^{(2)}(\beta_1\rho)\widehat{F}_1(z) - jB_1(\rho)H_1^{(1)}(\beta_1\rho)\widehat{F}_1(z) \tag{3.48}$$

where $\widehat{F}_1(z)$ is the *form function* of the guided modes in the central unperturbed waveguide with eigenvalue β_1. Moreover, in this region we have $\kappa_{(\pm1,\pm1)} = \kappa_{\pm2} =$

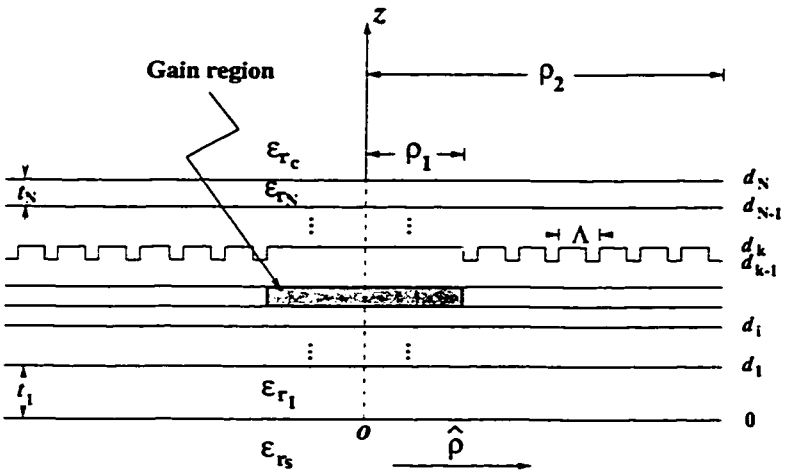

Figure 3.7: The cross section of a circular-grating DBR laser

$\delta = 0$. Therefore, from (3.33) and (3.34), it can be easily seen that

$$\begin{bmatrix} A_1(\rho) \\ B_1(\rho) \end{bmatrix} = \begin{bmatrix} e^{(g_1-\alpha_1)(\rho-\rho_a)} & 0 \\ 0 & e^{-(g_1-\alpha_1)(\rho-\rho_a)} \end{bmatrix} \begin{bmatrix} A_1(\rho_a) \\ B_1(\rho_a) \end{bmatrix} \qquad 0 < \rho, \rho_a < \rho_1 \tag{3.49}$$

with $A_1(0) = -jB_1(0)$. In the region $\rho_1 < \rho < \rho_2$, $E_\phi(\rho, z)$ can be written as

$$\begin{aligned} E_\phi(\rho, z) &= [e^{j\beta_o\rho_o}\widehat{F}(z) + e^{j\beta_o\rho}h_{-1}(z)]A(\rho)H_1^{(2)}(\beta_o\rho) - \\ &\quad j[e^{-j\beta_o\rho_o}\widehat{F}(z) + e^{-j\beta_o\rho}h_1(z)]B(\rho)H_1^{(1)}(\beta_o\rho) \end{aligned} \tag{3.50}$$

where all the parameters have been defined in Section 3.3. Moreover, $A(\rho)$ and $B(\rho)$ can be obtained from (3.33) and (3.34) with $g = 0$.

To obtain the characteristic equation of the laser, it is necessary to describe the interface between the active and the passive region at $\rho = \rho_1$. This can be done by matching the boundary conditions at $\rho = \rho_1$. More precisely, continuity of the tangential components of the electric and the magnetic field requires that both E_ϕ and $\frac{\partial E_\phi}{\partial \rho}$ be continuous at $\rho = \rho_1$. In the course of matching the boundary conditions,

however, we ignore the radiation the radiation field in the grating section. Therefore, the boundary conditions are matched based on the assumption of existence of the guided modes in each region only. This assumption allows us to introduce the coupling factor between the guided modes in each region [32]. The presence of the radiation field causes a negligible reduction of the coupling factor. Moreover, the radiation field in the grating section is produced by the guided modes in that region and it is not independent of those modes. This fact makes our assumption quite reasonable. Therefore, by introducing the power coupling factor efficiency C between the central active region and the grating section as [32]

$$C = \frac{4\beta_o\beta_1}{(\beta_o+\beta_1)^2}\left(\int_{-\infty}^{\infty}\hat{F}_1(z)\hat{F}(z)\,dz\right)^2 \tag{3.51}$$

we have

$$\begin{bmatrix} A(\rho_1) \\ B(\rho_1) \end{bmatrix} = \begin{bmatrix} \sqrt{C}e^{-j(\beta_1-\beta_o+\frac{\beta_o\rho_o}{\rho_1})\rho_1} & 0 \\ 0 & \frac{1}{\sqrt{C}}e^{j(\beta_1-\beta_o+\frac{\beta_o\rho_o}{\rho_1})\rho_1} \end{bmatrix} \begin{bmatrix} A_1(\rho_1) \\ B_1(\rho_1) \end{bmatrix} \tag{3.52}$$

Note that for real values of β_o and β_1, we have

$$(\beta_o+\beta_1)^2 > 4\beta_o\beta_1 \tag{3.53}$$

Moreover, according to the Schwarz' inequality for real functions [63], we have

$$\left(\int_{-\infty}^{\infty}\hat{F}_1(z)\hat{F}(z)\,dz\right)^2 \le \int_{-\infty}^{\infty}\hat{F}_1^2(z)\,dz\int_{-\infty}^{\infty}\hat{F}^2(z)\,dz = 1 \tag{3.54}$$

Consequently, (3.53) and (3.54) guarantee that $C < 1$.

Finally, let the facet at $\rho = \rho_2$ be described by the reflection coefficient factor Γ such that

$$-je^{-j\beta_o\rho_o}B(\rho_2)H_1^{(1)}(\beta_o\rho_2) = \Gamma e^{j\beta_o\rho_o}A(\rho_2)H_1^{(2)}(\beta_o\rho) \tag{3.55}$$

On substituting of large argument formulas for Hankel functions, (3.55) can be rewritten as

$$\begin{bmatrix} \Gamma e^{-j2\beta_o(\rho_2-\rho_o)} & -1 \end{bmatrix} \begin{bmatrix} A(\rho_2) \\ B(\rho_2) \end{bmatrix} = 0 \tag{3.56}$$

Now by successive application of the defined transfer matrices and the boundary condition at the center of the active region, we obtain

$$\begin{bmatrix} \Gamma e^{-j2\beta_o(\rho_2-\rho_o)} & -1 \end{bmatrix} \mathbf{T}\,\mathbf{K}\,\mathbf{T}_1 \begin{bmatrix} 1 \\ j \end{bmatrix} A_1(0) = 0 \tag{3.57}$$

where $\mathbf{T}$ is the 2×2 matrix defined in (3.34) and (3.35) with $\rho = \rho_2$ and $\rho_a = \rho_1$. $\mathbf{K}$ and $\mathbf{T}_1$ are also 2×2 matrices defined in (3.52) and (3.49), respectively. It should be noted that $\mathbf{T}_1$ can be obtained from (3.49) by substituting $\rho - \rho_a = \rho_1$. The nontrivial solution of (3.57) requires that the coefficient of $A_1(0)$ be zero. In fact, the coefficient of $A_1(0)$ is the characteristic equation of the circular-grating DBR laser. The unknowns g_1 and δ are the solutions of the characteristic equation. Each (g_1, δ) corresponds to a laser mode.

To obtain the threshold current density, it is necessary to consider the dynamics of the carrier density. In the absence of carrier diffusion and transport effects, the carrier rate equation is as follows [78] (pp. 35-36)

$$\frac{\partial N(\mathbf{r},t)}{\partial t} = \frac{J(t)}{ed} - [AN(\mathbf{r},t) + B_{eff}N^2(\mathbf{r},t) + C_{eff}N^3(\mathbf{r},t)] - R_s S(\mathbf{r},t) \tag{3.58}$$

where $J(t)$ is the injection current density, d is the active layer thickness, and e is the magnitude of the electron charge. A, B_{eff}, and C_{eff} are the non-radiative, effective bimolecular and effective Auger recombination coefficients, respectively The last term in (3.58) is due to stimulated recombination of carriers with intra-cavity photon density $S(\mathbf{r},t)$ and stimulated emission rate R_s. Under steady state conditions, the left hand side of (3.58) is zero. Moreover, at near-threshold, light is

mainly due to the spontaneous emission and the term $B_{eff}N^2(\mathbf{r},t)$ has a dominant effect in carrier recombination. Therefore, at threshold we have

$$J_{th} = edB_{eff}N_{th}^2 \tag{3.59}$$

where N_{th} is the carrier density at threshold.

In view of (3.59), we need N_{th} to obtain J_{th}. To this end, we assume that the peak gain varies linearly with carrier density N. That is,

$$g(N) = \Gamma_g\, a\,(N - N_{tr}) \tag{3.60}$$

where $g(N)$ is the field gain, a is the differential gain coefficient and N_{tr} is the injected carrier density required to make the gain medium transparent. Γ_g is the confinement factor accounting for spreading of optical field beyond the active region. Now from (3.59) and (3.60), we have

$$J_{th} = e\,d\,B_{eff}\,(\frac{g_{th}}{\Gamma_g\, a} + N_{tr})^2 \tag{3.61}$$

where $g_{th} = g(N_{th})$. Finally, using $I_{th} = \pi\rho_1^2 J_{th}$ yields

$$I_{th} = \pi\rho_1^2 e\,d\,B_{eff}\,(\frac{g_{th}}{\Gamma_g\, a} + N_{tr})^2 \tag{3.62}$$

After obtaining the relation for the threshold current for the laser, in the next section, we investigate an illustrative example.

3.4.1 Numerical results

As an example, we study a particular circular-grating DBR bulk laser shown in Fig. 3.8. As illustrated the grating shape is rectangular. It should be noted that a rectangular-shaped grating is a symmetrical grating. Therefore, we have $\kappa^r =$

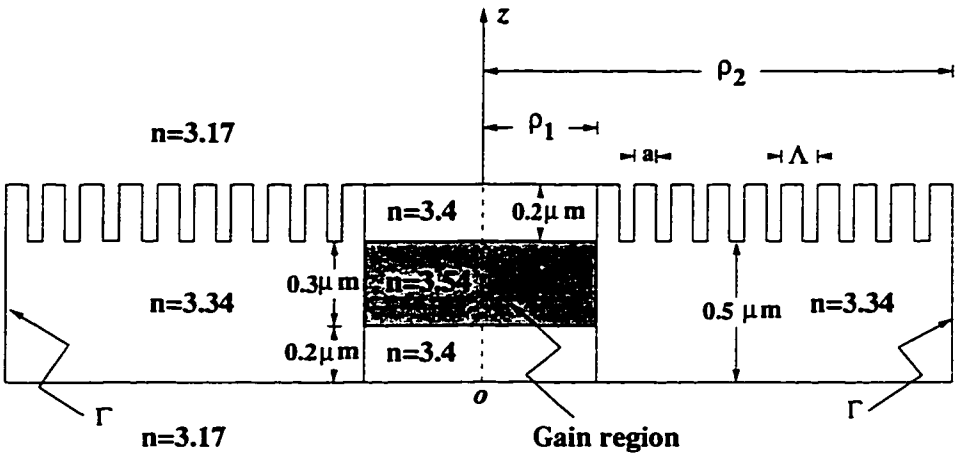

Figure 3.8: A circular-grating DBR bulk laser

$\kappa^r_{(\pm 1,\pm 1)}$. For this particular geometry, the dependence of the real and imaginary parts of κ^r on grating the grating duty cycle $\frac{a}{\Lambda}$ are shown in Fig. 3.9. The reference wavelength is assumed to be $\lambda = 1.55$ μm. As illustrated, the real part of κ^r is negative for all values of $\frac{a}{\Lambda}$. This result is completely expected due to the radiation loss. For the purpose of the comparison, the dependence of the radiation coupling factor κ^r and the imaginary part of the second-order Bragg diffraction coefficient $\kappa_{\pm 2}$ on the grating duty cycle are depicted in Fig. 3.10. To increase the radiation power, the first-order Bragg coupling coefficient must be increased. This coefficient reaches its maximum value around $\frac{a}{\Lambda} = 0.5$. For this value of $\frac{a}{\Lambda}$, however, the second-order Bragg diffraction coefficient $\kappa_{\pm 2}$ is very small. This in turn leads to higher values for the threshold gain. Therefore, optimization is a matter of compromise between the radiation field and the threshold gain.

The threshold gain and threshold current of the laser geometry shown in Fig. 3.8 are studied as a function of the reflection coefficient Γ of the facet at ρ_2. The results are obtained for two values of the grating duty cycle. The parameters used for the numerical calculations are listed in Table 3.1.

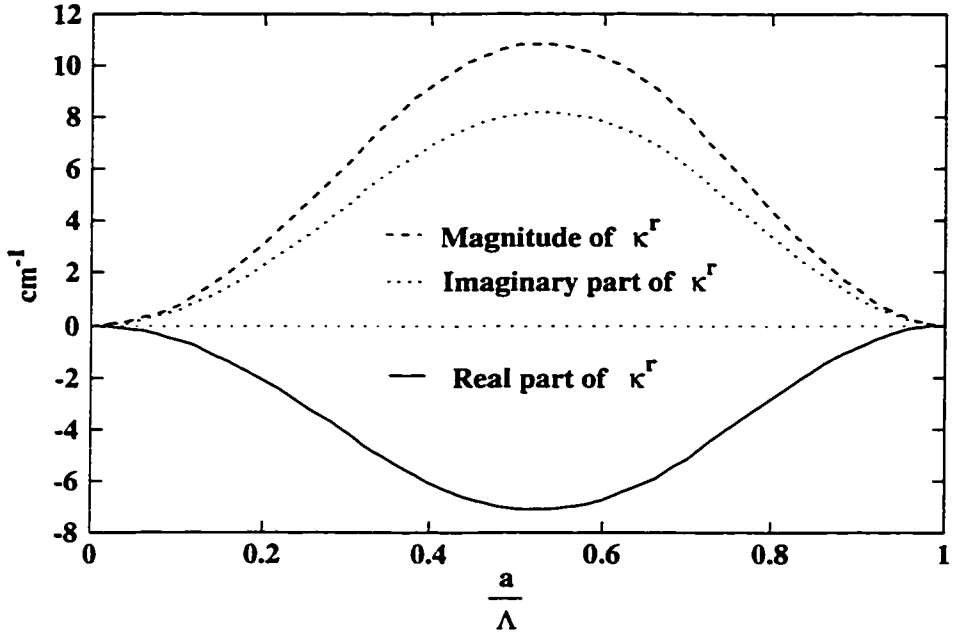

Figure 3.9: Radiation coupling factor

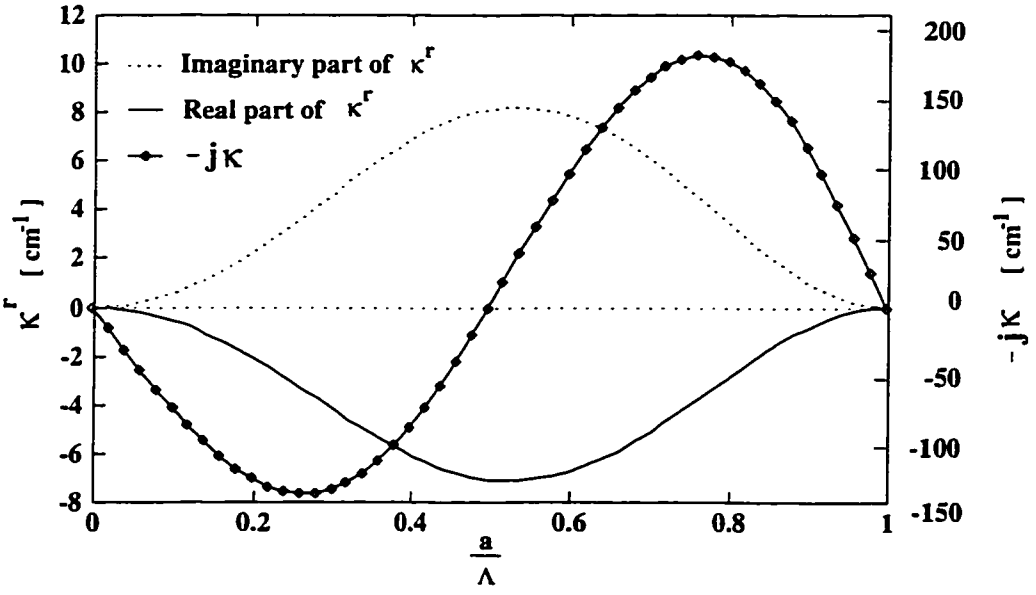

Figure 3.10: Radiation coupling factor and second-order Bragg diffraction coefficient

PARAMETERS	VALUES
Effective bimolecular Carrier recombination coefficient (B_{eff})	1.0×10^{-10} cm^3 s^{-1}
Gain coefficient (a)	2.5×10^{-16} cm^2
Transparency carrier density (N_{tr})	1.5×10^{18} cm^{-3}
Absorption and scattering loss of the central region (α_1)	10 cm^{-1}
Absorption and scattering loss of the Bragg reflector (α)	5 cm^{-1}

Table 3.1: Parameters used in the analysis of the circular-grating DBR laser

The threshold gain and threshold current as a function of the reflection coefficient for $\frac{a}{\Lambda} = 0.7$ are plotted in Figs. 3.11 and 3.12, respectively. The dotted lines correspond to the threshold gain and threshold current of the laser if one ignores the first-order Bragg coupling coefficients. As is expected, coupling to the radiation field causes additional loss and increases the threshold gain and threshold current. Furthermore, the above threshold parameters decrease as the reflection coefficient Γ of the facet increases. Although in some cases it is not a general trend, however, in this case since the DBR section is passive, the larger values of Γ result in less power coupling to the outside of the laser cavity through the facet, hence less threshold gain and threshold current. Note that, in general, this trend is not true. The same curves are plotted for $\frac{a}{\Lambda} = 0.4$ in Figs. 3.13 and 3.14, respectively. As illustrated, for this case, the corresponding threshold parameters are higher than those for $\frac{a}{\Lambda} = 0.7$. Referring to Fig. 3.10, in this case the radiation coupling factor is larger than that for $\frac{a}{\Lambda} = 0.7$. However, increasing of the threshold parameters is mostly due the change of the sign of the second-order Bragg diffraction coefficient.

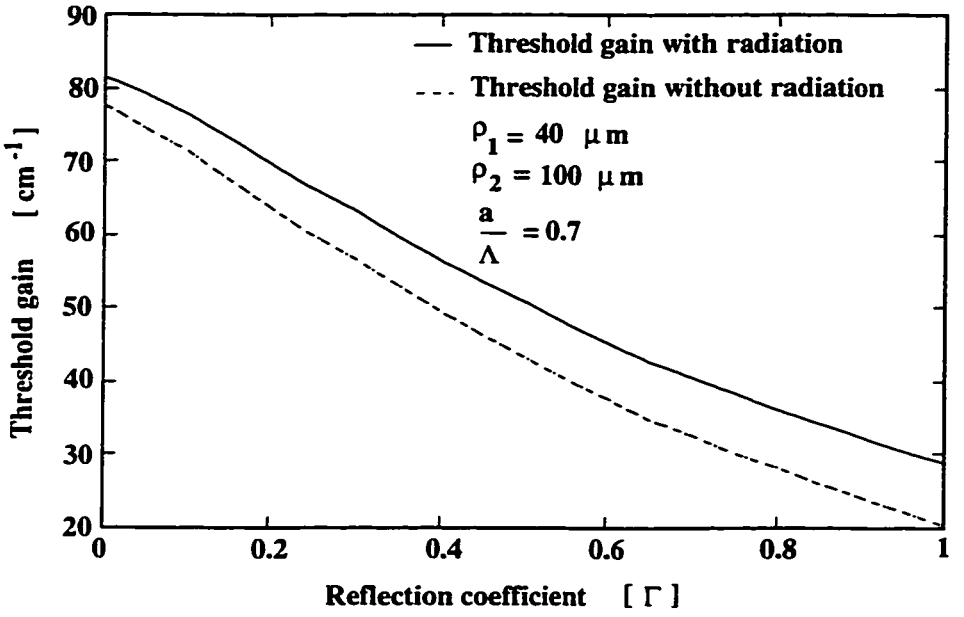

Figure 3.11: Threshold gain of the laser as a function of Γ

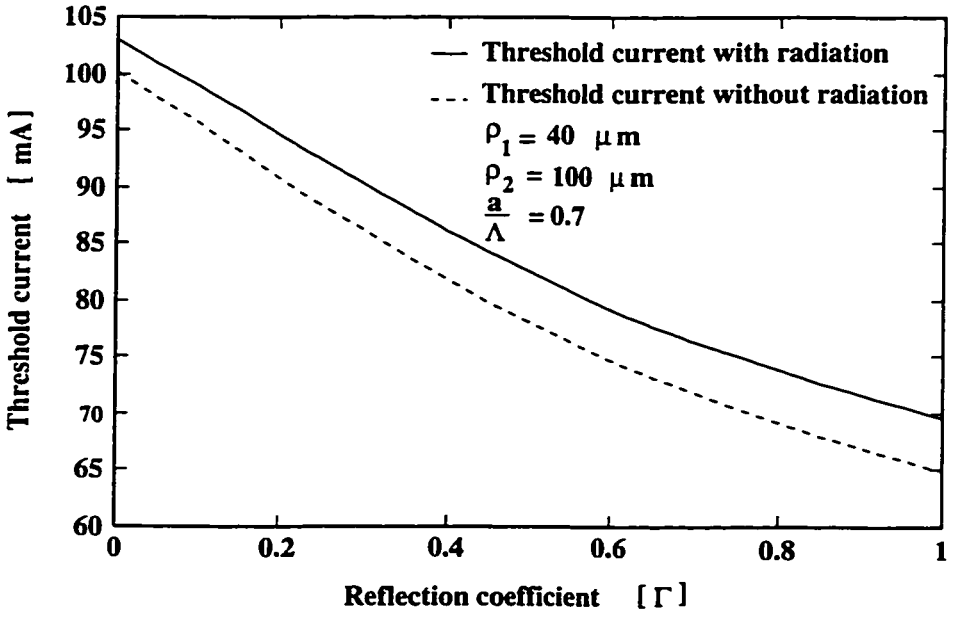

Figure 3.12: Threshold current of the laser as a function of Γ

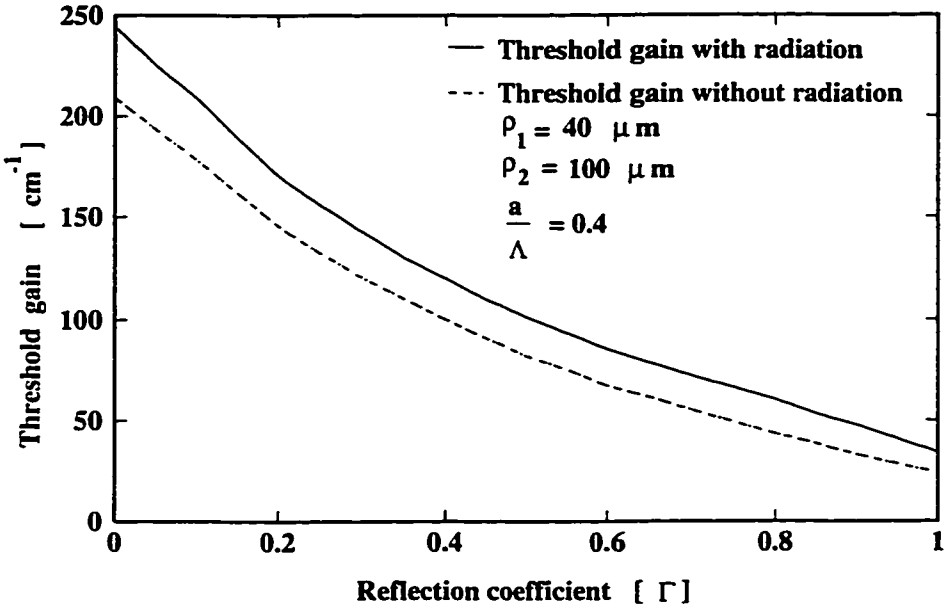

Figure 3.13: Threshold gain of the laser as a function of Γ

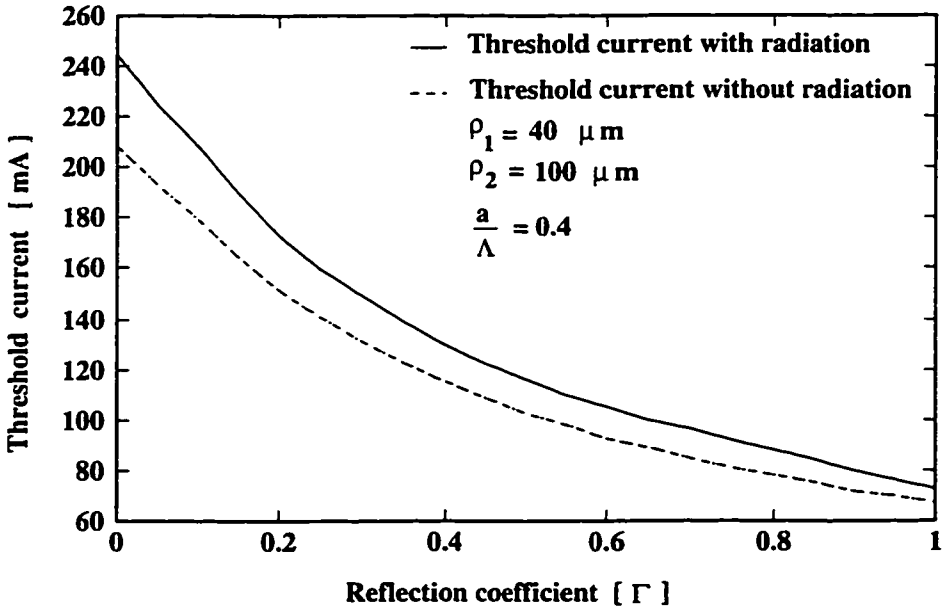

Figure 3.14: Threshold current of the laser as a function of Γ

3.5 Summary

In this chapter, for the first time, we have developed a general formalism to consider the effect of the radiation field in the performance of circular-grating surface-emitting lasers. For the sake of mathematical simplicity, we have assumed that the laser field is azimuthally invariant. Therefore, this formalism is two dimensional in nature.

Based on the large argument approximation for the Hankel functions, we have derived the coupled-mode equations governing the behavior of the amplitudes of the guided modes. Especially, the first-order Bragg diffraction coefficient which is the result of the joint interaction of the guided modes with the grating has been derived using the Green's function formulation. The Green's function has been derived by the transfer matrix method. In general, the radiation coupling coefficient depends on the depth and the duty cycle of the grating. It has been shown that there is a trade off between the radiation power and the laser feedback. Moreover, in almost all cases, the real and imaginary parts of the radiation coupling are not larger than 10 cm^{-1}. We have used this new formalism to obtain the threshold gain and threshold current of a circular-grating DBR laser.

Chapter 4

Rate Equations of Second-Order Distributed Feedback Lasers

4.1 Introduction

In the previous chapter the modal analysis of circular-grating lasers has been treated. This type of analysis is based on a linear model. In fact, we have obtained the eigenvalues and eigenvectors of a linear operator. This linear analysis is valid only in the threshold region. Essentially, lasers like any other oscillators are nonlinear in nature. Especially, this behavior manifest itself in the above-threshold region. Moreover, in the modeling of the DFB lasers several unique distinctive features must be taken into account. Among them are: (1) the spatial dependence of the photon density causes nonuniform carrier density and gain; (2) the coupling of the spontaneous emission into the lasing modes is affected significantly by the distributed feedback. Furthermore, as in other types of semiconductor lasers the carriers undergo complex diffusion and transport processes, which also lead to spa-

tially nonuniform carrier density and thus inhomogeneous complex index profile. All these factors need to be taken into account in the modeling and analysis of the semiconductor lasers.

To model the static behavior, almost all existing DFB laser models use either the coupled-wave theory (CWT) [65], [66] or the transfer matrix method (TMM) [67], [68], which are practically equivalent. For the dynamic analyses, there are essentially two approaches: *the traveling wave* approach and *the standing-wave* approach. The former treats interaction between the contra-directional propagating waves along the laser cavity in time and frequency domain. Vankwikelberge *et al.* [69] develop a coupled-wave formulation in time domain. The governing equations for the optical fields are partial differential equations for the forward and the backward propagating wave as function of z and t. Static, small signal dynamic, and noise characteristics of diode lasers with distributed feedback are analyzed.

A similar method is presented by Zhang and Carrol [70] and Zhang *et al.* [71] who solve the coupled-wave equations by the power matrix method (PMM) which is a mixed time/frequency domain model and the finite-difference (FD) method, respectively. A good comparison between these two methods is made by Tsang *et al.* [72]. Static and small/large signal dynamic behavior is simulated by these methods. Another method of this category is the transmission-line model (TLM) developed by Lowery *et al.* [73]. The TLM divides a DFB laser into a series of sections and then describes the interactions between the contra-directional propagating optical fields and the carriers within each section by using an equivalent circuit. Comparison among the different approaches appear to be in fairly good agreement [72], [74], and [75].

Standing-wave approach, on the other hand, utilizes the fact that the optical fields in a DFB laser manifest themselves as cavity modes with distinct resonance

frequencies. In this model, the conventional rate equations are a set of coupled ordinary differential equations that describe the optical field, carriers (both electrons and holes) and their interactions [76]-[80]. These rate equations are, however, derived based on the assumption that the optical field may be represented by a linear combination of the normal modes in a *closed* and *passive* cavity.

In the case of semiconductor DFB lasers, this assumption is not valid. This is because the laser cavity is open, especially for the DFB lasers with low loss κL. Moreover, the field within the cavity changes dramatically as a function of injection current due to spatial and spectral hole burning. Therefore, improved rate equations based on more realistic models are needed to reflect the characteristics of the DFB semiconductor lasers. Furthermore, an underlying assumption in the conventional rate equations is that both the carrier and the photon densities are uniform over the entire laser cavity and therefore they are functions of time only. This approximation is acceptable for many practical semiconductor lasers, but becomes questionable for DFB semiconductor lasers.

To treat nonuniformities in the carrier and photon distributions that occur in a wide range of semiconductor lasers, a variety of modifications of the conventional rate equations have been made [81], [82]. Many of these modifications are phenomenological and lack solid theoretical basis. Tromborg and co-workers developed a rigorous rate equation formulation by using the Green's function method in frequency domain [83], [84], an approach originally introduced by Henry [85].

Recently, an alternative approach to the optical rate equations by using a standing-wave in time domain, similar to that employed in the laser theory [77]-[80], has been presented [86]-[89]. Different from the conventional theory for the semiconductor lasers in which the optical fields are expressed in terms of the normal modes of a closed and passive cavity, the fields are represented by the normal modes

of an open and active cavity, which are adiabatic functions of the injection current. In comparison with the Green's function approach which starts in the frequency domain, the modal approach appears to be more straightforward and physically more intuitive.

In all the modified standing-wave time domain approaches reported so far [86]-[89], only DFB lasers with first-order gratings have been considered. In this chapter we apply this method on DFB lasers with second-order gratings. Two dimensional DFB lasers with straight and circular-gratings are treated on the same framework.

4.2 Time Domain Standing-Wave Approach

We start from the fundamental governing equation for the envelope of the laser field in its most general form (see Appendix E.1)

$$\nabla \times \nabla \times \mathbf{E} - k_o^2(\epsilon_{r_\tau} + \chi)\mathbf{E} + \frac{j2\omega_\tau}{v_o^2}\epsilon_g \frac{\partial \mathbf{E}}{\partial t} = \mu_o \omega_\tau^2 \mathbf{P}^s \tag{4.1}$$

where $\mathbf{E}$ and $\mathbf{P}^s$ are the slowly-varying envelopes of the electric field and the polarization associated with the spontaneous emission source, respectively. That is,

$$\mathcal{E}(\mathbf{r},t) = \mathrm{Re}\left\{\mathbf{E}(\mathbf{r},t)\, e^{j\omega_\tau t}\right\} \tag{4.2}$$

$$\mathcal{P}^s = \mathrm{Re}\left\{\mathbf{P}^s(\mathbf{r},t)\, e^{j\omega_\tau t}\right\} \tag{4.3}$$

ω_τ is a reference frequency, $v_o = \frac{1}{\sqrt{\mu_o \epsilon_o}}$, ϵ_{r_τ} is the Fourier transform of the dielectric constant at $\omega = \omega_\tau$, χ is the susceptibility of the lasing medium, and ϵ_g is the group dielectric constant given by

$$\epsilon_g = \epsilon_{r_\tau} + \frac{1}{2}\left[\frac{\partial \epsilon_r}{\partial \omega}\right]_{\omega_\tau} \omega_\tau$$

As can be seen the spontaneous emission is the main source for initiating the laser oscillation. Therefore, as one might expect, the envelope of the electric field is a random process. The statistics of $\mathbf{E}(\mathbf{r},t)$ heavily rely on that of $\mathbf{P}^s(\mathbf{r},t)$. The solution of the above equation in its most general form is a challenging issue. However, for the two dimensional problems in which either $\frac{\partial}{\partial y} \equiv 0$ or $\frac{\partial}{\partial \phi} \equiv 0$, it can be solved by using either the traveling wave or the standing wave approach.

The essence of the standing wave approach in solving (4.1) is based on the assumption that essentially two processes happen during the lasing oscillation. First, the cavity modes form as the adiabatic functions of the injection current. Then the amplitudes of the cavity modes fluctuate as a result of variation of the injection current. Based on this assumption it is natural to assume that

$$\mathbf{E}(\mathbf{r},t) = \sum_{i=1}^{N} C_i A_i(t) \mathbf{E}_i^m(\mathbf{r}) \tag{4.4}$$

Eq. (4.4) implies that the random function $\mathbf{E}(\mathbf{r},t)$ is expressed by a complete set of deterministic basis functions of the the spatial variables only. The amplitudes of these basis functions are complex-valued function of time which are not deterministic. The constants C_i's are chosen such that the total number of the photons inside the laser cavity, $S(t)$, can be expressed by

$$S(t) = \sum_{i=1}^{N} |A(t)|^2 \tag{4.5}$$

The spatial-dependent basis functions are the solutions of the following set of equations

$$\nabla \times \mathbf{E}_i^m = -j\omega\mu_o \mathbf{H}_i^m \tag{4.6}$$

$$\nabla \times \mathbf{H}_i^m = j\omega\epsilon_o(\epsilon_{r_r} + \bar{\chi} - \xi_i)\mathbf{E}_i^m \tag{4.7}$$

where $\bar{\chi}$ is the susceptibility of the lasing medium under the constant bias and is defined by the following relation

$$\chi(\mathbf{r},t) = \bar{\chi}(\mathbf{r}) + \Delta\chi(\mathbf{r},t) \tag{4.8}$$

ξ_i is a *constant* resulting from the separation of the temporal and spatial variables. Physically, this parameter is related to the steady-state net gain and frequency shift of the lasing mode. From (4.7) and (4.8), it can be seen that $\mathbf{E}_i^m$ is the solution of the following eigenvalue problem

$$\nabla \times \nabla \times \mathbf{E}_i^m - k_o^2(\epsilon_{r_r} + \bar{\chi})\mathbf{E}_i^m = -k_o^2\,\xi_i\,\mathbf{E}_i^m \tag{4.9}$$

Substituting (4.4) into (4.1) and using (4.9), we obtain

$$k_o^2 \sum_{i=1}^{N} C_i A_i(t)(\epsilon_{r_r}+\bar{\chi}+\Delta\chi-\xi_i)\mathbf{E}_i^m(\mathbf{r})+\frac{j2\omega_r}{v_o^2}\epsilon_g(\mathbf{r})\sum_{i=1}^{N} C_i\frac{\partial A}{\partial t}\mathbf{E}_i^m(\mathbf{r}) = \mu_o\omega_r^2\mathbf{P}^s \tag{4.10}$$

In order to obtain the equations for the amplitudes $A_i(t)$, one may define suitable inner product and obtain adjoint eigenmodes of $\mathbf{E}_i^m(\mathbf{r})$ and $\mathbf{H}_i^m(\mathbf{r})$. Then, taking inner product of the adjoint eigenmodes with (4.10), we may obtain a set of coupled first-order ordinary differential equations for the amplitude functions. This approach is very similar to the moment method in the electromagnetic theory [90]. These are the basic premises of the time domain standing-wave approach in dealing with the multimode lasers. However, we do not go further in treating multimode lasers. Instead, we follow the above approach to develop suitable rate equations in the investigation of second-order DFB lasers under single-mode operation.

4.3 Derivation of the Rate Equations

4.3.1 Field rate equations

In general, a normal mode of a DFB laser is a combination of the modes of the unperturbed cold cavity of the laser. By unperturbed we mean that no corrugation in the boundary, gain, or loss present in the cavity. Any mode of semiconductor lasers either of Fabry-Perot or DFB type consists of the fundamental guided modes traveling in the opposite longitudinal directions. These guided modes are of energy type. They are responsible for the total number of photons inside the laser cavity due to the stimulated emission and the spontaneous emission coupled to the laser mode. Different mechanisms of the loss, gain, and perturbation from the ideal geometry manifest their effects on the mutual interaction between the amplitudes of the guided modes. In fact, the exact behavior of these amplitudes strongly depends on the nature of the laser mode.

In a second- and higher-order DFB laser, the mutual interaction of the guided modes with the grating excites the radiation modes of the unperturbed waveguides. The inclusion of these modes in the description of the laser mode is necessary. However, these modes are of the power type fields and are party responsible for the escape of the photons from the laser cavity. Therefore, this loss mechanism changes the interaction between the fundamental guided modes.

Let us assume that a second-order DFB laser is single-mode and lases in the fundamental LSE or TE mode. For a two dimensional problem, the electric field has only one component. In the rectangular coordinate system, Eq. (4.1) reduces to

$$\nabla_{xz}^2 E_y + k_o^2(\epsilon_{r_r} + \chi)E_y - \frac{j2\omega_r}{v_o^2}\epsilon_g \frac{\partial E_y}{\partial t} = -\mu_o \omega_r^2 P_y^s \tag{4.11}$$

where

$$\nabla_{xz} = \frac{\partial^2}{\partial x^2} + \frac{\partial^2}{\partial z^2}$$

In the rectangular coordinate system, we assume that the transverse direction is along the x axis. In the cylindrical coordinate system with the z axis normal to the laser junction, we have

$$\mathcal{B}E_\phi + k_o^2(\epsilon_{r_r} + \chi)E_\phi - \frac{j2\omega_r}{v_o^2}\epsilon_g \frac{\partial E_\phi}{\partial t} = -\mu_o \omega_r^2 P_\phi^s \tag{4.12}$$

where

$$\mathcal{B} \equiv \frac{\partial}{\partial \rho^2} + \frac{1}{\rho}\frac{\partial}{\partial \rho} - \frac{1}{\rho^2} + \frac{\partial^2}{\partial z^2}$$

To illustrate the basic ideas, we assume a second-order DFB laser with straight grating. The circular grating can be treated in a similar manner. To obtain the laser field satisfying (4.11), we assume that the slowly-varying amplitude of the electric field can be written as

$$E_y(x, z, t, I) = C_n A(t)\Psi(x, z, N) \tag{4.13}$$

where we have considered $E_y(x, z, t, I)$ as a function of the injected current. $\Psi(x, z, N)$ is the carrier dependent mode function of the pumped laser cavity. C_n is a normalization constant to be determined such that $A(t)$ can be related to the total number of photons inside the cavity. It should be emphasized that the photon number is used only as a convenient measure of the optical energy and power inside the cavity. Later we will show that how the radiating power from the facets and the grating can be related to the photon number.

In this section, we obtain the rate equation for $A(t)$. To this end, we substitute (4.13) into (4.11). Thus

$$A(t)\left(\frac{\partial^2 \Psi}{\partial x^2} + \frac{\partial^2 \Psi}{\partial z^2}\right) + k_o^2(\epsilon_{r_r} + \chi)A(t)\Psi - \frac{j2\omega_c}{v_o^2}\epsilon_g \Psi \frac{dA}{dt} = \frac{-\mu_o \omega_c^2}{C_n} P^s \tag{4.14}$$

Let us assume that $\Psi(x, z, N)$ be the eigenvector of the following eigenvalue problem

$$\frac{\partial^2 \Psi}{\partial x^2} + \frac{\partial^2 \Psi}{\partial z^2} + k_o^2(\epsilon_{r_r} + \chi_o)\Psi = k_o^2 \xi(N)\Psi \tag{4.15}$$

where $\xi(N)$ is a carrier dependent constant resulting from the separation of the temporal and spatial variables. Recall that this parameter is related to the steady state net gain and frequency shift of the lasing mode. $\chi_o(x, z)$ is the static part of the susceptibility of the lasing medium. That is, we assume that

$$\chi(x, z; t) = \chi_o(x, z) + \Delta\chi(x, z; t) \tag{4.16}$$

Substituting (4.15) and (4.16) into (4.14), we have

$$\frac{j2\omega_c}{v_o^2}\epsilon_g(x, z)\Psi(x, z)\frac{dA}{dt} = k_o^2(\xi + \Delta\chi)\Psi(x, z)A(t) + \frac{\mu_o \omega_c^2}{C_n}P^s \tag{4.17}$$

Eq. (4.17) is the fundamental equation for the slowly-varying complex amplitude function of the laser based on the two-dimensional model. So far, no assumption has been made regarding the type of the laser. It can be used for Fabry-Perot, DFB, and DBR laser. The laser type comes into the picture through the eigenvalue problem in (4.15) and the slowly-varying of the spatial amplitudes in the longitudinal direction. Eq. (4.15) is very similar to the eigenvalue problem that we have used in the threshold analysis of the semiconductor laser. However, the main difference between (4.15) and that one used in the threshold analysis is that the eigenvector of the former is carrier dependent. That is, stimulated emission has the central role in the formation of the cavity mode. This in turn necessitates consideration of a nonlinear gain model. Moreover, due to the stimulated recombination, the nonuniform intensity distribution gives rise to the nonuniform carrier distribution. Therefore, nonuniform gain profile resulting from spatial hole burning must be taken into account.

Let us use (4.17) to obtain the equation for the amplitude of the mode of a second-order DFB laser. The starting point is to assume a general form for the eigenvector of the associated eigenvalue problem in (4.15). To this end, first we assume that the grating period is Λ and

$$\epsilon_{r_r} = \epsilon'_{ru}(x) - j\epsilon''_r(x) + \delta\epsilon(x,z) \tag{4.18}$$

$\epsilon'_{ru}(x)$ is the dielectric constant of the unperturbed geometry, i.e., the multilayer structure in the absence of the grating. $\epsilon''(x)$ accounts for the dielectric losses. $\delta\epsilon(x,z)$ is deviation of the dielectric profile from the unperturbed structure due to the presence of the grating. It can be expressed by the following Fourier series

$$\delta\epsilon(x,z) = \sum_{m\neq 0} \eta_m(x) e^{-jm\beta_o(z-z_o)} \tag{4.19}$$

where z_o is a fixed point accounting for the phase shift of the grating and

$$\beta_o = \frac{2\pi}{\Lambda} \tag{4.20}$$

Having defined the above parameters, we write the eigenvector $\Psi(x,z,N)$ as

$$\Psi(x,z,N) = \Psi^g(x,z) + \Psi^{rad}(x,z) \tag{4.21}$$

Ψ^g is the combination of fundamental coherent guided modes traveling in the opposite directions. These two coherent modes are produced by the stimulated recombination. In addition, each guided mode interacts with the grating in first-order diffraction. This joint interaction provides a mechanism that causes photons to escape from the laser cavity. This loss mechanism can be considered by including the radiation field, $\Psi^{rad}(x,z)$, in the laser eigenvector. Following the conventional method in treating second-order DFB lasers [60], we write

$$\Psi^g(x,z) = A_f(z)\, e^{-j\beta_o(z-z_o)}\widehat{F}(x) + A_b(z)\, e^{j\beta_o(z-z_o)}\widehat{F}(x) \tag{4.22}$$

where $\widehat{F}(x)$ is the normalized *form function* (transverse profile) of the guided modes satisfying the eigenvalue equation

$$\left[\frac{d^2}{dx^2} + \epsilon'_{ru}(x)\, k_o^2\right] \widehat{F}(x) = \beta^2 \widehat{F}(x) \tag{4.23}$$

subject to the continuity of $\widehat{F}$ and its normal derivative at the interfaces of the unperturbed multilayer waveguide. By normalized we mean that

$$\int_{-\infty}^{\infty} \widehat{F}^2(x)dx = 1 \tag{4.24}$$

The interaction between the laser field and the laser medium can be considered by mutual interaction between the slowly-varying amplitudes of the guided waves. This interaction is partly due to the presence of the radiation field. The ultimate goal is to obtain this interaction in the presence of the radiation field. To this end, we substitute (4.21) and (4.22) into (4.15) and make use of the slowly-varying amplitude approximation. By collecting slowly-varying terms with respect to z it can be shown that

$$\frac{\partial^2 \Psi^{rad}}{\partial x^2} + \epsilon_{ru} k_o^2 \Psi^{rad} = -k_o^2[A_f(z)\eta_{-1}(x)\hat{F}(x) + A_b(z)\eta_1(x)\hat{F}(x)] \tag{4.25}$$

where we have considered that ϵ''_r, χ_o, and ξ are negligible in comparison with ϵ_{ru}. Eq. (4.25) clearly shows that the the guided modes are the source for the radiation field. That is, radiation field is not independent of the guided modes. That is why we have used the same time varying amplitude for the radiation field. Eq. (4.25) can be solved by obtaining the Green's function satisfying

$$\frac{\partial^2 G(x;x')}{\partial x^2} + \epsilon'_{ru}(x) k_o^2 G(x;x') = \delta(x - x') \tag{4.26}$$

The Green's function satisfying the above equation can be obtained easily by using the transfer matrix method as described in Appendix D.1. Thus solving Eq. (4.25) for E^{rad} leads to

$$E^{rad}(x,z) = A_f(z)h_{-1}(x) + A_b(z)h_1(x) \tag{4.27}$$

where

$$h_{\pm 1}(x) = -k_o^2 \int_{-\infty}^{\infty} G(x;x')\,\eta_{\pm 1}(x')\widehat{F}(x')dx' \tag{4.28}$$

Radiation field expressed by (4.27) in turn interacts with guided modes via the first-order diffraction. Considering these mutual interactions leads to the following modified coupled-mode equations for the slowly-varying amplitudes of the guided modes.

$$\begin{bmatrix} \frac{dA_f}{dz} \\ \frac{dA_b}{dz} \end{bmatrix} = \begin{bmatrix} -\alpha - j\delta + (1+j\alpha_H)g + \xi' + \kappa_{ff}^r & \kappa_{fb}^r + \kappa_2 \\ \kappa_{bf}^r + \kappa_{-2} & \alpha + j\delta - (1+j\alpha_H)g - \xi' - \kappa_{bb}^r \end{bmatrix} \times \begin{bmatrix} A_f \\ A_b \end{bmatrix} \tag{4.29}$$

where we have assumed that

$$\chi_o = (-\alpha_H + j)\chi_i \tag{4.30}$$

α_H is the so-called linewidth enhancement factor which is also known as the Henry factor. The carrier-induced refractive index changes of the active medium is considered by the α_H factor. Furthermore,

$$\delta = \beta - \beta_o \tag{4.31a}$$

$$\xi' = \frac{jk_o^2}{2\beta_o}\xi \tag{4.31b}$$

$$\alpha = \frac{k_o^2}{2\beta_o}\int_{-\infty}^{\infty} \epsilon''(x)\widehat{F}^2(x)dx \tag{4.31c}$$

$$g = \frac{k_o^2}{2\beta_o}\int_{-\infty}^{\infty} \chi_i\widehat{F}^2(x)dx \tag{4.31d}$$

$$\kappa_{\pm 2} = \frac{-jk_o^2}{2\beta_o}\int_{-\infty}^{\infty} \eta_{\pm 2}(x)\widehat{F}^2(x)dx \tag{4.31e}$$

$$\kappa_{ff}^r = \frac{-jk_o^2}{2\beta_o}\int_{-\infty}^{\infty} \eta_1(x)h_{-1}(x)\widehat{F}(x)dx \tag{4.31f}$$

$$\kappa^r_{fb} = \frac{-jk_o^2}{2\beta_o}\int_{-\infty}^{\infty}\eta_1(x)h_1(x)\widehat{F}(x)dx \tag{4.31g}$$

$$\kappa^r_{bf} = \frac{-jk_o^2}{2\beta_o}\int_{-\infty}^{\infty}\eta_{-1}(x)h_{-1}(x)\widehat{F}(x)dx \tag{4.31h}$$

$$\kappa^r_{bb} = \frac{-jk_o^2}{2\beta_o}\int_{-\infty}^{\infty}\eta_{-1}(x)h_1(x)\widehat{F}(x)dx \tag{4.31i}$$

After describing the general characteristics of the laser modes in a second-order DFB laser, we return to (4.17). We will shortly show that it can be reduced to a more tractable form. If we substitute for $\Psi(x,z)$ into (4.17), we obtain

$$\frac{j2\omega_c}{v_o^2}\epsilon_g(x,z)[\Psi^g(x,z)+\Psi^{rad}(x,z)]\frac{dA}{dt} = k_o^2(\xi+\Delta\chi)[\Psi^g(x,z)+\Psi^{rad}]A(t)+\frac{\mu_o\omega_c^2}{C_n}P^s \tag{4.32}$$

The above equation should be valid for all spatial variables. However, due to the different behavior in the transverse direction, the guided mode must be separated from the radiation field. More precisely, one may write

$$\frac{j2\omega_c}{v_o^2}\epsilon_g(x,z)\Psi^g(x,z)\frac{dA}{dt} = k_o^2(\xi+\Delta\chi)\Psi^g(x,z)A(t)+\frac{\mu_o\omega_c^2}{C_n}P^s \tag{4.33}$$

It is interesting to note that (4.33) can be considered as the fundamental governing equation for the amplitude of the laser mode. At first glance, it might be thought that the radiation field has been ignored in deriving (4.33). However, it should be emphasized that the effect of the radiation field has been considered in a self consistent fashion in the eigenvalue of the laser. Moreover, the radiation field is not independent of the guided modes. It is the direct consequence of the lasing action. Therefore, it does not provide additional information for predicting the amplitude function.

As mentioned earlier, the laser operation heavily relies on the behavior of the guided modes which are of energy type fields. Photon density inside the laser cavity can be obtained from these fields. The coupled-mode equations in (4.29) completely

reflect such a behavior. In fact, the effect of the radiation field is included in a self consistent manner in the laser operation by considering it as a loss mechanism. This means that as far as the laser operation is concerned, one may ignore the radiation field in the analysis of second-order DFB laser provided that one includes the coupling factor to the radiation field in the coupled-mode equations. Furthermore, the spontaneous emission directly coupled to the radiation field couples to the guided mode through first-order diffraction. This part of the indirect mechanism of noise coupling is reflected through the modified longitudinal eigenmodes as will be described later. More importantly, the use of standing wave approach is based on the evolution of the laser mode which means that the cavity mode is considered in the presence of the radiation field. Following the same reasoning, it can be shown that (4.33) is not valid only for first- and second-order gratings. It is also valid for DFB laser with higher-order grating.

It is more convenient to write (4.33) in terms of the refractive indices. Therefore, let

$$\epsilon_{r_r}(x,z) = n^2(x,z) \tag{4.34}$$

Then, (4.33) can be rewritten as

$$\frac{j2\omega_r}{v_o^2} n(x,z)\, n_g(x,z) \Psi^g(x,z) \frac{dA}{dt} = k_o^2(\xi + \Delta\chi)\Psi^g(x,z)A(t) + \frac{\mu_o \omega_r^2}{C_n} P^s \tag{4.35}$$

where

$$n_g(x,z) = n(x,z) + \left[\frac{\partial n}{\partial \omega}\right]_{\omega_r} \omega_r \tag{4.36}$$

In order to obtain the equation for the amplitude function, the spatial-dependent part must be eliminated. To this end, we use a procedure which is very similar to that used in the electromagnetic theory, the so-called *moment method.* However, before that we define some terms. From now on by a laser eigenmode we mean the longitudinal dependence part of the laser mode which is described by the guided

mode. These eigenmodes are the eigenvectors of an open resonator operator which is non-Hermitian or non-self-adjoint operator. Therefore, they are not energy orthogonal (with complex conjugation) [91]. However, the laser eigenmodes are *biorthogonal* (without complex conjugation) to a set of adjoint eigenmodes. The adjoint eigenmodes correspond physically to the modes traveling in the reverse direction in the same resonators [91], [92]. We will return to this point later. However, for the time being, we use the concept of the adjoint modes to reduce (4.35) to a function of time only.

First, it is natural to multiply both sides of (4.35) by the normalized transverse profile $\widehat{F}(x)$ and integrate from $-\infty$ to ∞. After that we integrate the resulting equation in the lateral direction. Thus,

$$\frac{j2\omega_r}{v_o^2}\mathrm{w}\bar{n}(z)\,\bar{n}_g(z)\Psi_t(z)\frac{dA}{dt} = k_o^2\mathrm{w}[\xi + \Gamma_g(z)\Delta\chi(z)]\Psi_t(z)A(t) + \frac{\mu_o\omega_r^2}{C_n}f^s(z,t) \quad (4.37)$$

where w is the width of the laser in the lateral direction. We have also assumed that $\Delta\chi(x,z)$ is constant along the transverse direction and replace the overlap integral of $\Delta\chi(x,z)$ with the optical field by $\Gamma_g(z)\Delta\chi(z)$. Note that, for gain-guided lasers, Γ_g changes along the longitudinal direction. However, for second-order gratings we consider it fixed along this direction. $\Psi_t(z)$ is the longitudinal eigenmode. $\bar{n}(z)$ and $\bar{n}_g(z)$ are defined such that

$$\int_{-\infty}^{\infty} n(x,z)\,n_g(x,z)\widehat{F}^2(x)dx = \bar{n}(z)\bar{n}_g(z) \quad (4.38)$$

It is natural to choose $\bar{n}(z)$ and $\bar{n}_g(z)$ as the average values of $n(x,z)$ and $n_g(x,z)$, respectively. Moreover,

$$f^s(z,t) = \int_0^{\mathrm{W}}\int_{-\infty}^{\infty} P^s\widehat{F}(x)dxdy \quad (4.39)$$

Multiplying both sides of (4.37) by $\Psi_t^{\dagger}(z)$, the adjoint eigenmode of $\Psi_t(z)$, and

integrating along the laser cavity leads to

$$\frac{dA}{dt} = -j\frac{\omega_r}{2}\left[\frac{\int_0^L[\xi + \Gamma_g(z)\Delta\chi(z)]\Psi_t(z)\Psi_t^\dagger(z)dz}{\int_0^L \bar{n}(z)\bar{n}_g(z)\Psi_t(z)\Psi_t^\dagger(z)dz}\right]A(t) - j\frac{\omega_r}{2\epsilon_o C_n w}\frac{\int_0^L \Psi_t^\dagger(z)f^s(z,t)dz}{\int_0^L \bar{n}(z)\bar{n}_g(z)\Psi_t(z)\Psi_t^\dagger(z)dz} \tag{4.40}$$

where we have used

$$v_o^2 = \frac{1}{\mu_o\epsilon_o}$$

Eq. (4.40) is the final governing rate equation for the amplitude function. This equation and the coupled-mode equations in (4.29) along with the boundary conditions at the laser facets are the fundamental equations predicting the dynamics of the second-order DFB lasers. It should be, however, noted that the eigenvalue ξ and the normalization constant C_n are yet to be determined. At first glance, it seems that the only unknown in (4.29) is the complex number ξ' which is related to the eigenvalue ξ through (4.31b). In fact, this is not the case. As mentioned earlier, due to the spatial hole burning effect, the carrier density is affected by the optical field and the photon density inside the cavity which are not uniform along the cavity. Therefore, the spatial dependence of the laser gain must be considered in the coupled-mode equations. To this end, we write (4.40) in a more convenient form. We address this issue in the next section.

4.3.2 Rate Equations for the Photon Numbers and Phases

In the preceding section we have pointed out that the gain of the laser medium depends on the photon density. Therefore, in treating the laser above the threshold, it is usually more convenient to express the laser field in terms of the intensity and the phase of the optical field. The stored energy in the laser cavity is proportional to

the number of photons inside the cavity and is also proportional to the square of the modulus of the field amplitude. Therefore, it is possible to choose the normalization constant such that the complex amplitude $A(t)$ can be related to the total number of photons inside the cavity through the following relation

$$A(t) = \sqrt{S(t)}e^{j\phi(t)} \tag{4.41}$$

where S(t) is the total number of photons of the laser mode inside the cavity.

From (4.41), one may write

$$\frac{dA}{dt} = \frac{1}{2A^*(t)}\frac{dS}{dt} + j\frac{d\phi}{dt}A(t) \tag{4.42}$$

Now

$$\frac{dA}{dt}A^*(t) = \frac{1}{2}\frac{dS}{dt} + j\frac{d\phi}{dt}S(t) \tag{4.43}$$

where we have used

$$S(t) = A(t)A^*(t)$$

From (4.43) one may easily find that

$$\frac{dS}{dt} = 2\mathrm{Re}\left\{\frac{dA}{dt}A^*(t)\right\} \tag{4.44}$$

$$\frac{d\phi}{dt} = \frac{1}{S(t)}\mathrm{Im}\left\{\frac{dA}{dt}A^*(t)\right\} \tag{4.45}$$

If we multiply both sides of Eq. (4.40) by $A^*(t)$ and use (4.44) and (4.45), we obtain

$$\frac{dS}{dt} = \omega_r \mathrm{Im}\left\{\frac{\int_0^L [\xi + \Gamma_g(z)\Delta\chi(z)]\Psi_l(z)\Psi_l^\dagger(z)dz}{\int_0^L \bar{n}(z)\bar{n}_g(z)\Psi_l(z)\Psi_l^\dagger(z)dz}\right\} S(t) + \mathrm{Re}\{p(t)A^*(t)\} \tag{4.46}$$

$$\frac{d\phi}{dt} = -\frac{\omega_r}{2}\mathrm{Re}\left\{\frac{\int_0^L [\xi + \Gamma_g(z)\Delta\chi(z)]\Psi_l(z)\Psi_l^\dagger(z)dz}{\int_0^L \bar{n}(z)\bar{n}_g(z)\Psi_l(z)\Psi_l^\dagger(z)dz}\right\} + \frac{1}{S(t)}\mathrm{Im}\{p(t)A^*(t)\} \tag{4.47}$$

where

$$p(t) = -j\frac{\omega_r}{2\epsilon_o C_n \mathrm{w}}\frac{\int_0^L \Psi_l^\dagger(z)f^s(z,t)dz}{\int_0^L \bar{n}(z)\bar{n}_g(z)\Psi_l(z)\Psi_l^\dagger(z)dz} \tag{4.48}$$

On the other hand, it can be shown [77] (pp. 306-307) that

$$< p(t)A^*(t) >= \frac{1}{2}R_{sp} \tag{4.49}$$

where $< \ldots >$ denotes the ensemble average. R_{sp} is the ensemble average of the rate of the spontaneously emitted photons into the lasing mode and will be determined later. Since $p(t)A^*(t)$ is a complex random process, from (4.49), one may write

$$p(t)A^*(t) = \frac{R_{sp}}{2} + \frac{F_s(t)}{2} + jF_\phi(t)S(t) \tag{4.50}$$

with

$$< F_s(t) >=< F_\phi(t) >= 0 \tag{4.51}$$

Carrying (4.50) into (4.46) and (4.47), we get

$$\frac{dS}{dt} = \omega_\tau \mathrm{Im}\left\{\frac{\int_0^L [\xi + \Gamma_g(z)\Delta\chi(z)]\Psi_t(z)\Psi_t^\dagger(z)dz}{\int_0^L \bar{n}(z)\bar{n}_g(z)\Psi_t(z)\Psi_t^\dagger(z)dz}\right\} S(t) + R_{sp} + F_s(t) \tag{4.52}$$

$$\frac{d\phi}{dt} = -\frac{\omega_\tau}{2}\mathrm{Re}\left\{\frac{\int_0^L [\xi + \Gamma_g(z)\Delta\chi(z)]\Psi_t(z)\Psi_t^\dagger(z)dz}{\int_0^L \bar{n}(z)\bar{n}_g(z)\Psi_t(z)\Psi_t^\dagger(z)dz}\right\} + F_\phi(t) \tag{4.53}$$

Eqs. (4.52) and (4.53) are of the form of Langevin rate equations in the fluctuation theory [93]. $F_s(t)$ and $F_\phi(t)$ are the Langevin intensity and the phase noise sources due to the spontaneous emission which cause fluctuation in the optical intensities (or photon numbers) and phases of the lasing modes. It should be noted that, in the presence of Langevin noises, $S(t)$ and $\phi(t)$ become stochastic processes. Fluctuation in the phase of the laser field is the main source of the broadening of the laser line. On the other hand, the change in the intensity also leads to the change of the phase of the laser field [94]. Therefore, to calculate the line broadening due to the spontaneous emission, the combined effect of the fluctuations in the intensity and the phase of the optical field must be considered. This in turn calls for the statistics of $S(t)$ and $\phi(t)$. Since the Langevin forces are the random sources of the

field intensity and phase, the statistics of $S(t)$ and $\phi(t)$ can be obtained in terms of the statistics of the Langevin forces. In choosing $F_s(t)$ and $F_\phi(t)$, it is commonly assumed that the system is *markoffian* with zero mean. This assumption can be completely justified in the semiconductor laser for which the spontaneous emission is the major source of the fluctuations. In fact, the spontaneous emission is only a correlated process for a carrier scattering time of order 10^{-13} s, which is negligibly short time [95].

In addition to (4.51), the Langevin forces satisfy the following general relation [94]

$$< F_a(t)F_b(t') >= 2D_{ab}\delta(t-t') \qquad a,b = S \text{ or } \phi \tag{4.54}$$

where the so called diffusion coefficients D_{ab} satisfy

$$2D_{SS} = 2R_{sp}S \tag{4.55}$$

$$2D_{S\phi} = 0 \tag{4.56}$$

$$2D_{\phi\phi} = \frac{1}{2}\frac{R_sp}{S} \tag{4.57}$$

From the diffusion coefficients only the mean square fluctuation can be calculated. To calculate the spectral linewidth it is assumed that the Langevin forces have Gaussian amplitude distributions [95]. Since in this thesis we do not plan to do noise analysis of the laser, we do not go into the details in treating the Langevin forces. However, the ensemble average of the spontaneous emission, R_{sp}, coupled to the laser mode is very important in the laser operation.

To obtain R_{sp}, we invoke the cross-correlation product of the noise polarization $P^s(\mathbf{r},t)$ [96]

$$< P^s(\mathbf{r},t)\, P^{s^*}(\mathbf{r}',t') >= \frac{8\,\hbar n_{sp}(\mathbf{r})\, n_a(\mathbf{r})\, G(\mathbf{r})\, v_o\, \epsilon_o}{\omega_r}\,\delta(\mathbf{r}-\mathbf{r}')\,\delta(t-t') \tag{4.58}$$

where n_a is the refractive index of the active medium. n_{sp} is the inversion factor describing the degree of inversion [97]. This parameter is a measure of the incomplete population inversion associated with the unoccupied levels of the lasing transition. It is always larger than 1 and decreases with an increase of the pumping level. For complete inversion n_{sp} approaches unity. Under typical lasing conditions, it is in the range of 1.5, ..., 2.5. $G(x,z)$ is the intensity gain coefficient and $\hbar$ is the reduced Planck constant. v_o is the velocity of light in vacuum. Using (4.39) and (4.58), one may write

$$< f(z,t)\, f(z',t') >= \frac{8\mathrm{w}\hbar\Gamma_g(z) n_{sp}(z)\, n_a(z)\, G(z)\, v_o \epsilon_o}{\omega_\tau}\delta(z-z')\delta(t-t') \qquad (4.59)$$

where $n_{sp}(x,z)$, $n(x,z)$, and $G(x,z)$ are considered constant along the transverse direction. Thus the overlap of the product of these three terms with the optical field is replaced by $\Gamma_g(z) n_{sp}(z)\, n(z)\, G(z)$. Now from (4.48) and (4.59), we obtain

$$< p(t)\, p^*(t) >= \frac{2\hbar\omega_\tau v_o}{\epsilon_o C_n^2 \mathrm{w}} \frac{\int_0^L \Gamma(z) n_{sp}(z) n_a(z) G(z) |\Psi_t^\dagger(z)|^2 dz}{|\int_0^L \bar{n}(z)\bar{n}_g(z)\Psi_t(z)\Psi_t^\dagger(z)dz|^2}\delta(t-t') \qquad (4.60)$$

On the other hand, R_{sp} is equal to the diffusion coefficient of the Langevin force responsible for the fluctuation of $A(t)$ [97]. That is,

$$< p(t)\, p^*(t) >= R_{sp}\delta(t-t') \qquad (4.61)$$

On comparison of (4.60) and (4.61), it can be easily seen that

$$R_{sp} = \frac{2\hbar\omega_\tau v_o}{\epsilon_o C_n^2 \mathrm{w}} \frac{\int_0^L \Gamma_g(z) n_{sp}(z) n_a(z) G(z) |\Psi_t^\dagger(z)|^2 dz}{|\int_0^L \bar{n}(z)\bar{n}_g(z)\Psi_t(z)\Psi_t^\dagger(z)dz|^2} \qquad (4.62)$$

To complete the expression for R_{sp}, we need to calculate normalization constant C_n. As mentioned earlier, we choose C_n such that the total number of photons inside the laser cavity is equal to $A(t)A^*(t)$. To this end, we need to obtain the stored

energy inside the cavity. Using the energy density function in dispersive media [98], the average stored energy inside the cavity can be obtained as

$$\begin{aligned} W(t) &= \frac{1}{2}\epsilon_o \int_0^{\mathrm{W}} dy \int_0^L dz \int_{-\infty}^{\infty} n(x,z) n_g(x,z) C_n^2 < A(t)\, A^*(t) > \widehat{F}^2(x) |\Psi_t(z)|^2 dx \\ &= \frac{1}{2}\epsilon_o C_n^2 \mathrm{W} < A(t)\, A^*(t) > \int_0^L \bar{n}(z)\bar{n}_g(z) |\Psi_t(z)|^2 dz \end{aligned} \tag{4.63}$$

where we have used (4.38). On the other hand, the stored energy must be proportional to the number of photons inside the cavity. That is,

$$W(t) =< A(t)\, A^*(t) > \hbar\omega_r \tag{4.64}$$

Comparing (4.63) and (4.64) leads to the following expression for C_n

$$C_n^2 = \frac{2\hbar\omega_r}{\epsilon_o \mathrm{W}} \left(\int_0^L \bar{n}(z)\bar{n}_g(z) |\Psi_t(z)|^2 dz \right)^{-1} \tag{4.65}$$

Substituting for C_n^2 in (4.62), we obtain

$$R_{sp} = v_o \frac{\int_0^L \bar{n}(z)\bar{n}_g(z) |\Psi_t(z)|^2 dz \int_0^L \Gamma_g(z) n_{sp}(z) n_a(z) G(z) |\Psi_t^{\dagger}(z)|^2 dz}{|\int_0^L \bar{n}(z)\bar{n}_g(z) \Psi_t(x) \Psi_t^{\dagger}(z) dz|^2} \tag{4.66}$$

Let R_{spon} be the spontaneous emission rate coupled to the lasing mode obtained according to the usual Einstein relation [99]. According to this relation, the rate of spontaneous emission per laser mode is equal to the stimulated emission rate per laser photon number. Using $r_{spon}(\mathbf{r})$ as the local rate of spontaneous emission according to Einstein relation, we have

$$R_{spon} = \frac{\int_{\mathrm{V}} r_{spon}(\mathbf{r}) n_a(\mathbf{r}) n_g(\mathbf{r}) |\Psi(\mathbf{r})|^2 dv}{\int_{\mathrm{V}} n(\mathbf{r}) n_g(\mathbf{r}) |\Psi(\mathbf{r})|^2 dv} \tag{4.67}$$

where V is the volume of the laser cavity. $r_{spon}(\mathbf{r})$ for a semiconductor laser is given by [99]

$$r_{spon}(\mathbf{r}) = v_g(\mathbf{r}) n_{sp}(\mathbf{r}) G(\mathbf{r}) \tag{4.68}$$

For a two dimensional case, based on the conditions we have set forth on n_{sp}, n_a, and G, we obtain

$$R_{spon} = \frac{\int_0^L \Gamma_g(z)\, v_g(z)\, n_{sp}(z)\, n_a(z)\, n_g(z)\, G(z)\, |\Psi_t(z)|^2 dz}{\int_0^L \bar{n}(z)\bar{n}_g(z)|\Psi_t(z)|^2 dz} \tag{4.69}$$

Comparing (4.66) with (4.69) and noting that $v_g(z) = \frac{v_o}{n_g(z)}$ and $|\Psi_t^\dagger|^2 = |\Psi_t|^2$, we have

$$R_{sp} = K_P R_{spon} \tag{4.70}$$

where

$$K_P = \left[\frac{\int_0^L \bar{n}(z)\bar{n}_g(z)|\Psi_t(z)|^2 dz}{|\int_0^L \bar{n}(z)\bar{n}_g(z)\Psi_t(z)\Psi_t^\dagger(z)dz|}\right]^2 \tag{4.71}$$

If one examines (4.71) and notes that

$$\Psi_t(z)\Psi_t^\dagger(z) = \Psi_t^2(z) \tag{4.72}$$

one finds that

$$K_P > 1 \tag{4.73}$$

According to the accepted principle of the quantum-noise theory, the rate of the spontaneous emission into any resonant mode of a cavity must be exactly equal to the stimulated emission rate that would be produced by one extra photon in the same electromagnetic mode [100]. In other words, the spontaneous emission per laser mode is equal to the stimulated emission rate per laser photon. However, (4.70), (4.71) and (4.73) state that a second-order DFB laser is subject to an *excess-spontaneous-emission.* This behavior is a direct consequence of the non-self-adjoint nature of the longitudinal eigenmodes. In fact, due to non energy orthogonal property of longitudinal eigenmodes the spontaneous emission coupled to the different modes are correlated and one might expect larger amount of the spontaneous emission coupled to a laser mode. Therefore, DFB lasers like all open-sided optical resonator are subject to the *excess-spontaneous-emission.*

Since the spontaneous emission is completely uncorrelated with the coherent stimulated emission, it plays an important role in determining the static, dynamic, and the spectral characteristic of the semiconductor laser. As an example, we consider the adverse behavior of the spontaneous emission on the laser linewidth. Following Henry [94], the linewidth of a single-mode semiconductor laser is given by

$$\Delta\nu = \frac{R_{sp}(1+\alpha_H^2)}{4\pi S} = K_p \frac{R_{spon}(1+\alpha_H^2)}{4\pi S} \tag{4.74}$$

where S is the number of photons in the laser cavity. Therefore, the linewidth of the laser is enhanced by the factor K_p.

For the first time, Petermann calculated the excess-spontaneous-emission in stripe gain-guided lasers [101]. Thus, the K_p factor is usually referred as Petermann's factor or Petermann's excess noise factor in the literature. Eqs. (4.70) with (4.69) and (4.71) are completely general. If the longitudinal variations of $n(z)$ and $n_g(z)$ are slow, the K_p factor reduces to the expressions by Petermann [77] (pp. 41-44).

So far, we have obtained the rate equations for the total number of photons and the phase of the optical amplitude inside the laser cavity. These rate equations and the eigenvalue problem in (4.29) must be solved simultaneously. However, to complete the formulation, we need the dynamics of the carriers upon which the interaction between the carriers and the optical field is described. This matter will be investigated in the next section.

4.3.3 Carrier Rate Equation

In this section, we complete the rate equations of second-order DFB lasers by including the carrier dynamics. However, before that, let us see what we have done

so far. We have started from the guided mode of a second-order DFB laser which is of the form

$$\Psi^g(x,z) = \Psi_t(z)\widehat{F}(x) \tag{4.75}$$

where $\widehat{F}(x)$ is defined via (4.23) and (4.24). $\Psi_t(z)$ is the longitudinal eigenmode given by

$$\Psi_t(z) = A_f(z)e^{-j\beta_o(z-z_o)} + A_b(z)e^{j\beta_o(z-z_o)} \tag{4.76}$$

It satisfies the following eigenvalue problem

$$\begin{bmatrix} \frac{dA_f}{dz} \\ \frac{dA_b}{dz} \end{bmatrix} = \begin{bmatrix} -\alpha - j\delta + (1+j\alpha_H)g + \xi' + \kappa^r_{ff} & \kappa^r_{fb} + \kappa_2 \\ \kappa^r_{bf} + \kappa_{-2} & \alpha + j\delta - (1+j\alpha_H)g - \xi' - \kappa^r_{bb} \end{bmatrix} \times \begin{bmatrix} A_f \\ A_b \end{bmatrix} \tag{4.77}$$

subject to the boundary conditions at the laser facets. The total number of photons inside the cavity and the phase of the optical amplitude are the solutions of the following rate equations

$$\frac{dS}{dt} = \omega_r \mathrm{Im}\left\{ \frac{\int_0^L [\xi + \Gamma_g(z)\Delta\chi(z)]\Psi_t(z)\Psi_t^\dagger(z)dz}{\int_0^L \bar{n}(z)\bar{n}_g(z)\Psi_t(z)\Psi_t^\dagger(z)dz} \right\} S(t) + R_{sp} + F_s(t) \tag{4.78}$$

$$\frac{d\phi}{dt} = -\frac{\omega_r}{2}\mathrm{Re}\left\{ \frac{\int_0^L [\xi + \Gamma_g(z)\Delta\chi(z)]\Psi_t(z)\Psi_t^\dagger(z)dz}{\int_0^L \bar{n}(z)\bar{n}_g(z)\Psi_t(z)\Psi_t^\dagger(z)dz} \right\} + F_\phi(t) \tag{4.79}$$

where all parameters have been defined in the previous sections. ξ' is related to the eigenvalue ξ via (4.31b). For those cases where $n(z)$ and $n_g(z)$ can be considered constant along the longitudinal direction, from (4.78) and (4.79), it can be seen that the imaginary part of ξ is related to the steady-state net gain shift and its real part is a measure of the frequency shift. Eqs. (4.78) and (4.79) indicate that the longitudinal eigenmode of the laser and the corresponding eigenvalue are necessary in the investigation of the dynamics of the laser.

To solve the eigenvalue problem in (4.77), additional information must be provided. That is, one must consider the relation between the input current and the gain and also the interaction between the carriers and the optical field. This can be done by including the carrier rate equation in the set of equations listed in this section. We use the conventional rate equations for the carrier density [70]

$$\frac{dN}{dt} = \frac{J}{ed} - \frac{N}{\tau_e} - \frac{a(N - N_{tr})}{(1 + \epsilon p)} v_g p \tag{4.80}$$

The first term on the right represent the injection of the electrons. J is the current density of the driving current, e is the electron charge, and d is the thickness of the active layer. τ_e is the carrier lifetime and is a function of N such that

$$\frac{1}{\tau_e} = A + BN + CN^2 \tag{4.81}$$

where A, B, and C are the non-radiative, radiative and Auger recombination coefficients, respectively. a is the differential gain coefficient, N_{tr} is the carrier density at transparency, ϵ is the nonlinear gain suppression factor, v_g is the group velocity and p is the photon density. We assume that the carrier density is uniform over the transverse cross section of the active region. For simplicity, the carrier diffusion and transport effects have been neglected. From the field amplitude, we have

$$\begin{aligned} p &= \frac{\epsilon_o}{2\hbar\omega_r d_{eff}} C_n^2 |A(t)|^2 \int_{-\infty}^{\infty} n(x,z) n_g(x,z) |\Psi_t(z)|^2 \widehat{F}^2(x) dx \\ &= S(t) \frac{\bar{n}(z)\bar{n}_g(z)|\Psi_t(z)|^2}{\mathrm{w} d_{eff} \int_0^L \bar{n}(z)\bar{n}_g(z)|\Psi_t(z)|^2 dz} \end{aligned} \tag{4.82}$$

where $d_{eff} = \frac{d}{\Gamma_g}$ is the the effective length of the transversal photon distribution and d is the thickness of the active layer. Finally, the material gain which includes the saturation effect at large photon density, is given by

$$G = \frac{a(N - N_{tr})}{(1 + \epsilon p)} \tag{4.83}$$

Eq. (4.80) along with (4.77) and (4.78) are the complete system of equations describing the dynamics of second-order DFB lasers. These equations can be used in the investigation of the above-threshold static, dynamic small signal, and dynamic large signal analysis. For the purpose of this thesis, we only consider the above-threshold static analysis. However, before dealing with this issue, we obtain expressions for the output radiating power from the facets and the grating section. The details of the derivations are given in the next section.

4.3.4 Output Power

To calculate the output power from the facets and the grating, we use the concept of the photon flux density traveling in the longitudinal direction. This idea makes use of considering the standing wave pattern of the longitudinal eigenmode as the superposition of two contra-directional traveling waves. The power density of each wave passing through a plane transverse to the longitudinal direction is simply equal to the energy flux density times the group velocity of the photons at that plane. Thus, the power passing through the plane $z = z_1$ can be obtained according to the following relation

$$\begin{aligned} P_{f,b} &= v_g(z_1)\frac{\epsilon_o}{2}C_n^2|A(t)|^2\int_0^W dy\int_{-\infty}^{\infty} n(x,z_1)n_g(x,z_1)|A_{f,b}(z_1)|^2\,\widehat{F}^2(x)dx \\ &= v_o\hbar\omega_r S(t)\frac{\bar{n}(z_1)|A_{f,b}(z_1)|^2}{\int_0^L \bar{n}(z)\bar{n}_g(z)|\Psi_1(z)|^2dz} \end{aligned} \tag{4.84}$$

where f and b refers to forward and backward traveling waves. Moreover, we have used $n_g(z_1)v_g(z_1) = v_o^2$. Eq. (4.84) is the fundamental equation from which the output radiating power from the facets and the grating can be obtained. The power radiating from the facet at $z = L$ is equal to the difference between the

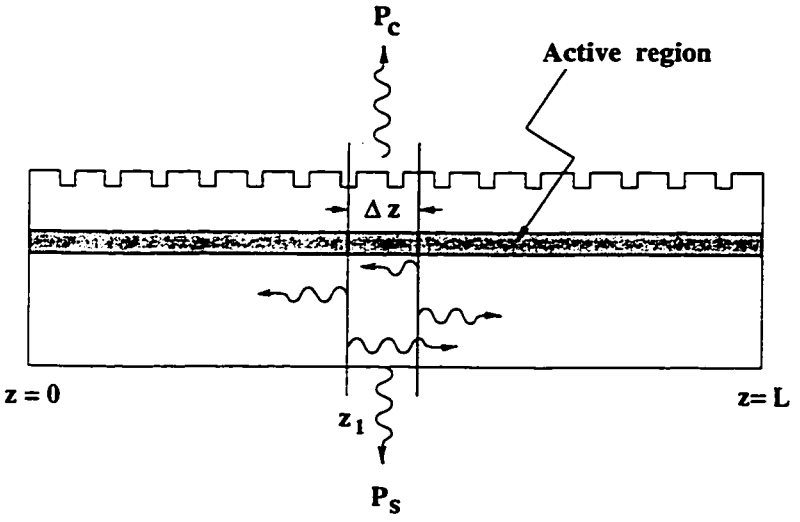

Figure 4.1: Cross sectional view of a second-order DFB laser

power carried by each traveling wave at $z = L$. More precisely, we have

$$\begin{aligned} P_L &= \frac{v_o \hbar \omega_r S(t) \bar{n}(z=L)}{\int_0^L \bar{n}(z)\bar{n}_g(z)|\Psi_t(z)|^2 dz}(|A_f(L)|^2 - |A_b(L)|^2) \\ &= \frac{v_o \hbar \omega_r S(t) \bar{n}(z=L)}{\int_0^L \bar{n}(z)\bar{n}_g(z)|\Psi_t(z)|^2 dz}|A_f(L)|^2(1 - R_L^2) \end{aligned} \tag{4.85}$$

where R_L is the amplitude reflectivity of the facet at $z = L$. Note how the output power is related to the total number of photons inside the laser cavity. Using the same reasoning, one may find the radiating power from the facet at $z = 0$.

The situation for calculating radiating power from the grating is more complicated than the previous case. In this case, it is more convenient to calculate the power density going into the cover and the substrate per unit length in the longitudinal direction. Referring to Fig. 4.1 the amount of the power due to the forward traveling wave which enters the region of the length Δz in the longitudinal direction is

$$p_{in}^f = v_g(z_1)\frac{\epsilon_o}{2}C_n^2 w|A(t)|^2\bar{n}(z_1)\bar{n}_g(z_1)|A_f(z_1)|^2 -$$

$$v_g(z_1+\Delta z)\frac{\epsilon_o}{2}C_n^2 \mathrm{w}|A(t)|^2\bar{n}(z_1+\Delta z)\bar{n}_g(z_1+\Delta z)|A_f(z_1+\Delta z)|^2 \tag{4.86}$$

The power due to the backward traveling wave which enters this region is

$$\begin{aligned} p_{in}^b &= v_g(z_1+\Delta z)\frac{\epsilon_o}{2}C_n^2 \mathrm{w}|A(t)|^2 v_g(z_1+\Delta z)\bar{n}(z_1+\Delta z)\bar{n}_g(z_1+\Delta z)|A_b(z_1+\Delta z)|^2 \\ &\quad -v_g(z_1)\frac{\epsilon_o}{2}C_n^2 \mathrm{w}|A(t)|^2 v_g(z_1)\bar{n}(z_1)\bar{n}_g(z_1)|A_b(,z_1)|^2 \end{aligned} \tag{4.87}$$

In addition to the power budget in (4.86) and (4.87), in this region we must also consider the stimulated power, the radiating power from the gratings and the power absorption due to the material loss. Let us assume that p_s, p_g and p_{ab} are the powers per unit length in the longitudinal direction of the stimulated emission, radiation from the grating and absorption, respectively. Then optical power conservation requires that

$$p_s\Delta z + p_{in}^f + p_{in}^b = p_g\Delta z + p_{ab}\Delta z \tag{4.88}$$

where we have assumed that Δz is vanishingly small. Before proceeding further, we assume that the variations of the refractive index and the group index is much smaller than that of $|A_f|^2$ and $|A_b|^2$. Considering this assumption and substituting (4.86) and (4.87) into (4.88), and after dividing by Δz, we get

$$p_s - p_g - p_{ab} = v_g(z_1)\frac{\epsilon_o}{2}C_n^2 \mathrm{w}|A(t)|^2\bar{n}(z)\bar{n}_g(z)\frac{d}{dz}\left(|A_f|^2 - |A_b|^2\right) \tag{4.89}$$

where the derivative is calculated at $z = z_1$.

In order to obtain the derivatives in (4.89), we invoke the coupled-mode equations in (4.77). Without lose of generality, we consider two types of gratings; i.e, symmetric and asymmetric gratings. By symmetric grating we mean those types of gratings such that

$$\eta_{-m}(x) = \eta_m(x) \tag{4.90}$$

where $\eta_m(x)$ are the coefficients of the Fourier expansion of the grating perturbation. Asymmetric gratings are such that the coefficients of the Fourier expansion have odd symmetry. That is,

$$\eta_{-m}(x) = -\eta_m(x) \tag{4.91}$$

For a symmetric grating we have

$$\kappa_2 = \kappa_{-2} \tag{4.92a}$$

$$\kappa^r_{ff} = \kappa^r_{fb} = \kappa^r_{bf} = \kappa^r_{bb} \tag{4.92b}$$

Applying the coupled-mode equations in (4.77) for symmetric gratings, we have

$$\begin{aligned}\frac{d}{dz}\left(|A_f|^2 - |A_b|^2\right) &= [-2\alpha + 2g + 2\mathrm{Re}\{\xi'\} - 2\mathrm{Re}\{\kappa_s\}]\left(|A_f(z)|^2 + |A_b(z)|^2\right) + \\ &\quad 2\mathrm{Re}\{\kappa^r_s\}|A_f(z) + A_b(z)|^2 + 2\mathrm{Re}\{\kappa_s\}|A_f(z) + A_b(z)|^2\end{aligned} \tag{4.93}$$

where

$$\kappa_s = \kappa_2 = \kappa_{-2} \tag{4.94a}$$

$$\kappa^r_s = \kappa^r_{ff} = \kappa^r_{fb} = \kappa^r_{bf} = \kappa^r_{bb} \tag{4.94b}$$

Using (4.93) in (4.89) and substitution for C_n^2 and $|A(t)|^2$, we obtain

$$p_s = v_o\hbar\omega_r S(t)\frac{(2g + 2\mathrm{Re}\{\xi'\})\bar{n}(z)\left(|A_f(z)|^2 + |A_b(z)|^2\right)}{\int_o^L \bar{n}(z)\bar{n}_g(z)|\Psi_t(z)|^2 dz} \tag{4.95}$$

$$p_g = -v_o\hbar\omega_r S(t)\frac{2\mathrm{Re}\{\kappa^r_s\}\bar{n}(z)|A_f(z) + A_b(z)|^2}{\int_o^L \bar{n}(z)\bar{n}_g(z)|\Psi_t(z)|^2 dz} \tag{4.96}$$

$$p_{ab} = v_o\hbar\omega_r S(t)\frac{2\alpha\left(|A_f(z)|^2 + |A_b(z)|^2\right)}{\int_o^L \bar{n}(z)\bar{n}_g(z)|\Psi_t(z)|^2 dz} \tag{4.97}$$

It should be noted that for index-guided lasers k_s is purely imaginary. Using (4.96), one may obtain the total power radiating via grating as

$$P_g = -v_o\hbar\omega_r S(t)2\mathrm{Re}\{\kappa^r_s\}\frac{\int_o^L \bar{n}(z)|A_f(z) + A_b(z)|^2 dz}{\int_o^L \bar{n}(z)\bar{n}_g(z)|\Psi_t(z)|^2 dz} \tag{4.98}$$

The above result is completely expected. More precisely, for symmetric gratings (4.28) leads to

$$h_1(x) = h_{-1}(x) \tag{4.99}$$

Thus, using (4.27), we have

$$E^{rad}(x,z) = [A_f(z) + A_b(z)]\, h_{-1}(x) \tag{4.100}$$

For asymmetric grating, we have

$$\begin{aligned}\frac{d}{dz}\left(|A_f|^2 - |A_b|^2\right) &= [-2\alpha + 2g + 2\mathrm{Re}\{\xi'\} - 2\mathrm{Im}\{\kappa_a\}]\left(|A_f(z)|^2 + |A_b(z)|^2\right) + \\ &\quad 2\mathrm{Re}\{\kappa_a^r\}|A_f(z) - A_b(z)|^2 + 2\mathrm{Im}\{\kappa_a\}|A_f(z) + jA_b(z)|^2\end{aligned} \tag{4.101}$$

where

$$\kappa_a = \kappa_2 = -\kappa_{-2} \tag{4.102a}$$

$$\kappa_a^r = \kappa_{ff}^r = -\kappa_{fb}^r = -\kappa_{bf}^r = \kappa_{bb}^r \tag{4.102b}$$

For the index-guided DFB lasers, κ_a is purely real. More importantly, following the same line as we have used in the case of symmetric gratings, for asymmetric gratings the total radiation power from the grating can be obtained from the following relation

$$P_g = -v_o \hbar \omega_r S(t) 2\mathrm{Re}\{\kappa_s^r\} \frac{\int_o^L \bar{n}(z)|A_f(z) - A_b(z)|^2 dz}{\int_o^L \bar{n}(z)\bar{n}_g(z)|\Psi_1(z)|^2 dz} \tag{4.103}$$

Again, the validity of the above result can be verified by noting that for asymmetric gratings (4.28) yields

$$h_1(x) = -h_{-1}(x) \tag{4.104}$$

Consequently, from (4.27), we have

$$E^{rad}(x,z) = [A_f(z) - A_b(z)]\, h_{-1}(x) \tag{4.105}$$

It should be emphasized that (4.98) and (4.103) refer to the total power radiating from the grating into the cover and the substrate. Needless to say, the minus sign in (4.98) and (4.103) is necessary due to the fact that κ_a and κ_s^r have negative real parts. As mentioned earlier, we can see how the total power radiating from the grating is proportional to the total number of photons inside the laser cavity. This is the direct consequence of the fact that the total number of photons inside the laser cavity is directly proportional to the optical energy.

Having completed the analysis of second-order DFB lasers with straight grating, in the next section we turn to the circular gratings. As will be shown, only minor modifications are needed and based on the large argument approximation of the Hankel functions the formulation is essentially the same.

4.4 Circular-Grating DFB Lasers

In this section we show that essentially the same equations that we have obtained for ordinary second-order DFB lasers can be used in the case of circular-grating DFB lasers. To this end, first we set up the cylindrical coordinate system as we adopted in Chapter 3. We choose the z axis to coincide with the axis of the laser. Let us assume that

$$\Delta\epsilon_r(\rho, z) = \sum_{m\neq 0} \eta_m(z) e^{-jm\beta_o(\rho-\rho_o)} \tag{4.106}$$

where β_o is given by (4.20). According to (4.106), we use the following expression for the fundamental guided mode of the laser

$$\Psi^g(\rho, z) = \Psi_t(\rho)\widehat{F}(z) \tag{4.107}$$

where $\widehat{F}(z)$ is defined through (4.23) and (4.24) by changing the role of x to z. $\Psi_t(\rho)$ is the *radial* eigenmode which is of the form

$$\Psi_t(\rho) = A_f(\rho)e^{j\beta_o\rho_o}H_1^{(2)}(\beta_o\rho) - jA_b(\rho)e^{-j\beta_o\rho_o}H_1^{(1)}(\beta_o\rho) \tag{4.108}$$

Based on the large argument approximation of the Hankel functions, the radial eigenmode $\Psi_t(\rho)$ satisfies the same eigenvalue problem in (4.78). For the sake of simplicity, we use the same coupling factor defined in (4.32) in the coupled-mode equations. The boundary condition at the center; that is,

$$A_f(0)e^{j\beta_o\rho_o} = -jA_b(0)e^{-j\beta_o\rho_o} \tag{4.109}$$

and appropriate facet reflection must be considered in solving the eigenvalue problem. Eq. (4.35) remains the same with changing (x, z) to (ρ, z). If we multiply the new version of (4.35) by $\widehat{F}(z)$ and integrate from $-\infty$ to ∞ and then we integrate the resulting equation in the azimuthal direction, we obtain (4.37) where z and w are replaced by ρ and 2π, respectively. In order to obtain the final equation, we replace the spatial delta function in the cross-correlation product of the noise polarization by

$$\delta(\mathbf{r} - \mathbf{r}') = \frac{1}{\rho}\delta(\rho - \rho')\,\delta(\phi - \phi')\,\delta(z - z')$$

Multiplying by the radial eigenmode and integrating in the radial direction must be weighted by ρ. Therefore, (4.52) and (4.53) reduce to

$$\frac{dS}{dt} = \omega_\tau \mathrm{Im}\left\{\frac{\int_0^L[\xi + \Gamma_g(\rho)\Delta\chi(\rho)]\Psi_t(\rho)\Psi_t^\dagger(\rho)\rho d\rho}{\int_0^L \bar{n}(\rho)\bar{n}_g(\rho)\Psi_t(\rho)\Psi_t^\dagger(\rho)\rho d\rho}\right\} S(t) + R_{sp} + F_s(t) \tag{4.110}$$

$$\frac{d\phi}{dt} = -\frac{\omega_\tau}{2}\mathrm{Re}\left\{\frac{\int_0^L[\xi + \Gamma_g(\rho)\Delta\chi(\rho)]\Psi_t(\rho)\Psi_t^\dagger(\rho)\rho d\rho}{\int_0^L \bar{n}(\rho)\bar{n}_g(\rho)\Psi_t(\rho)\Psi_t^\dagger(\rho)\rho d\rho}\right\} + F_\phi(t) \tag{4.111}$$

where

$$R_{sp} = \frac{2\hbar\omega_\tau v_o}{2\pi\epsilon_o C_n^2}\frac{\int_0^L \Gamma_g(\rho)n_{sp}(\rho)n_a(\rho)G(\rho)|\Psi_t^\dagger(\rho)|^2\rho d\rho}{|\int_0^L \bar{n}(\rho)\bar{n}_g(\rho)\Psi_t(\rho)\Psi_t^\dagger(\rho)\rho d\rho|^2} \tag{4.112}$$

and

$$C_n^2 = \frac{2\hbar\omega_r}{2\pi\epsilon_o \int_0^L \bar{n}(\rho)\bar{n}_g(\rho)|\Psi_t(\rho)|^2\rho d\rho} \tag{4.113}$$

The photon density in (4.82) is replaced by

$$p = S(t)\frac{\bar{n}(\rho)\bar{n}_g(\rho)|\Psi_t(\rho)|^2}{2\pi d_{eff} \int_0^L \bar{n}(\rho)\bar{n}_g(\rho)|\Psi_t(\rho)|^2\rho d\rho} \tag{4.114}$$

Finally, by using the asymptotic values for the Hankel functions, the radiation power from the symmetric grating can be obtained by the following relation

$$P_g = -2v_o\hbar\omega_r S(t)\mathrm{Re}\{\kappa_s^r\}\frac{\int_o^L \bar{n}(\rho)\bar{n}_g(\rho)|A_f(\rho) + A_b(\rho)|^2 d\rho}{\int_o^L \bar{n}(\rho)\bar{n}_g(\rho)(|A_f(\rho)|^2 + |A_b(\rho)|^2)d\rho} \tag{4.115}$$

In the next section we consider the static behavior of the two dimensional second-order DFB lasers above the threshold.

4.5 Static Analysis and Steady State Characteristics

In this section, we only consider the static behavior of second-order DFB lasers. If the injection current is constant, the photons and the carriers reach steady state and are invariant with time. In this case, $\Delta\chi = 0$ and the rate equations in (4.78), (4.79) and (4.80) reduce to

$$\begin{aligned} S(t) = S_o &= -\left[\omega_r \mathrm{Im}\left\{\frac{\xi \int_0^L \Psi_t(z)\Psi_t^\dagger(z)dz}{\int_0^L \bar{n}(z)\bar{n}_g(z)\Psi_t(z)\Psi_t^\dagger(z)dz}\right\}\right]^{-1} R_{sp} \\ &= -\frac{1}{\mathcal{G}}R_{sp} \end{aligned} \tag{4.116}$$

$$\frac{d\phi}{dt} = -\frac{\omega_r}{2}\mathrm{Re}\left\{\frac{\xi \int_0^L \Psi_t(z)\Psi_t^\dagger(z)dz}{\int_0^L \bar{n}(z)\bar{n}_g(z)\Psi_t(z)\Psi_t^\dagger(z)dz}\right\} = 2\pi\Delta f \tag{4.117}$$

$$\frac{J_o}{ed} - \frac{N_o}{\tau_e} - \frac{a(N_o - N_{tr})}{(1+\epsilon p)} v_g p = 0\,, \tag{4.118}$$

respectively. $\mathcal{G}$ in (4.116) is the steady-state net longitudinal modal gain and Δf is the steady-state net frequency shift. Therefore, to calculate S_o, Δf, and N_o, one needs to consider the eigenvalue problem in (4.77) with appropriate boundary conditions simultaneously with (4.116)-(4.118) at a given bias current density.

The eigenvalue problem in (4.77) may be solved by taking into account the longitudinal variations of the photon and carrier densities and effective index distributions. To this end, the laser cavity is divided into a number of segments such that for the k-th segment of length l_k, we have $\Lambda \ll l_k \ll L$. Within each segment, the above parameters are assumed to be constant. However, they are allowed to vary from segment to segment. Each segment can be described by the so called transfer matrix in the longitudinal direction as described in Chapter 3. That is,

$$\begin{bmatrix} A_f(z_{k+1}) \\ A_b(z_{k+1}) \end{bmatrix} = \mathbf{T}_k \begin{bmatrix} A_f(z_k) \\ A_b(z_k) \end{bmatrix} \tag{4.119}$$

where for gratings of either symmetric or asymmetric

$$\mathbf{T}_k = \begin{bmatrix} ch(\gamma_k l_k) + \zeta_k \frac{sh(\gamma_k l_k)}{\gamma_k} & (\kappa^r_{fb} + \kappa_2)\frac{sh(\gamma_k l_k)}{\gamma_k} \\ -(\kappa^r_{bf} + \kappa_{-2})\frac{sh(\gamma_k l_k)}{\gamma_k} & ch(\gamma_k l_k) - \zeta_k \frac{sh(\gamma_k l_k)}{\gamma_k} \end{bmatrix} \tag{4.120}$$

where

$$\zeta_k = -\alpha - j\delta + (1 - j\alpha_H) g_k + \xi' + k^r_{ff}$$

Note that for gratings of either symmetric or asymmetric type, we have

$$\kappa^r_{ff} = \kappa^r_{bb} \tag{4.121a}$$

$$\kappa^r_{fb} = \kappa^r_{bf} \tag{4.121b}$$

The overall transfer matrix relating $A_f(z)$ and $A_b(z)$ at two ends can be obtained by cascading the transfer matrices corresponding to each segment. Therefore,

$$\begin{bmatrix} A_f(L)) \\ A_b(L) \end{bmatrix} = \mathbf{T} \begin{bmatrix} A_f(0) \\ A_b(0)) \end{bmatrix} \tag{4.122}$$

where

$$\mathbf{T} = \prod_{k=M}^{1} \mathbf{T}_k \tag{4.123}$$

Applying the boundary conditions at $z = 0$ and $z = L$ leads to the lasing oscillation condition. More precisely, at $z = 0$, we have

$$\begin{bmatrix} A_f(0) \\ A_b(0) \end{bmatrix} = \begin{bmatrix} R(0) \\ 1 \end{bmatrix} A_b(0) \tag{4.124}$$

At $z = L$, one may write

$$\begin{bmatrix} R(L) & -1 \end{bmatrix} \begin{bmatrix} A_f(L) \\ A_b(L) \end{bmatrix} = 0 \tag{4.125}$$

Using (4.124) and (4.125) in (4.122) yields the characteristic equation for the lasing condition

$$\begin{bmatrix} R(L) & -1 \end{bmatrix} \prod_{k=M}^{1} \mathbf{T}_k \begin{bmatrix} R(0) \\ 1 \end{bmatrix} = 0 \tag{4.126}$$

The laser eigenvalue ξ is the solution of the above equation.

In a similar fashion, the carrier rate equation may also be discretized by assuming that the carrier density N_o is constant within each segment. That is,

$$\frac{J_o}{ed} - \frac{N_k}{\tau_e} - \frac{a(N_k - N_{tr})}{(1 + \epsilon p_k)} v_g p_k = 0 \tag{4.127}$$

where $N_k = N_o(z_k)$, $k = 1, 2, \ldots M$ and

$$p_k = S(t) \frac{\bar{n}(z_k)\bar{n}_g(z_k)|\Psi_t(z_k)|^2}{\mathrm{w} d_{eff} \int_0^L \bar{n}(z)\bar{n}_g(z)|\Psi_t(z)|^2 dz} \tag{4.128}$$

In order to obtain a self-consistent solution we use an iterative approach. First, we assume uniform gain throughout the laser cavity. The eigenvalue ξ and eigenvector $\Psi(z)$ obtained from this assumption is used to obtain R_{sp} and S_o in (4.116). Substituting these values into (4.127) leads to M simultaneous equations for the unknowns N_k. Using the solutions for N_k in the gain model of each segment leads to the modification of (4.126). We use the new value of ξ and $\Psi(z)$ to improve the carrier density. After reaching convergence, the steady state photon number S_o, the frequency shift Δf, as well as the carrier and photon densities along the laser cavity can be obtained as a function of the injection current density J_o. This completes the static analysis of second-order DFB lasers. It should be emphasized that the same ideas can be used in the case of circular gratings. In the next section we present the expressions for the far-field patterns.

4.5.1 Far-Field Pattern

To calculate the far-field pattern, we need to calculate the Fourier transform of the near-field pattern of the radiation field on the aperture. For symmetric and asymmetric gratings, we have

$$E_y^{rad}(z \in \text{aperture}) \sim A_f(z) \pm A_b(z) \tag{4.129}$$

Thus using the relation for the far-field pattern in (2.67) with suitable coordinate transformation one may easily obtain the far-field pattern. More precisely, if we consider the x axis as the polar axis, and the azimuthal angle is measured from the y axis, we have

$$\begin{aligned} \mathbf{E}(\theta,\phi) \;\sim\; & \hat{\theta}\left[\tilde{A}_f(k\,sin\theta\,cos\phi) \pm \tilde{A}_b(k\,sin\theta\,cos\phi)\right] cos\phi - \\ & \hat{\phi}\left[\tilde{A}_f(k\,sin\theta\,cos\phi) \pm \tilde{A}_b(k\,sin\theta\,cos\phi)\right] sin\phi\,cos\theta \end{aligned} \tag{4.130}$$

where $\tilde{A}_f(\alpha)$ and $\tilde{A}_b(\alpha)$ are the Fourier transforms of $A_f(z)$ and $A_b(z)$, respectively.

Finally, in order to obtain the far-field pattern of circular-grating laser, we use the aperture field due to the radiation component. As illustrated in Chapter 3, within the limits of the validity of large argument approximation for the Hankel functions, using (3.22) one may write

$$E_\phi^{rad}(\rho \in \text{aperture}) \sim A_f(\rho)e^{j\beta_o\rho}H_1^{(2)}(\beta_o\rho) \mp jA_b(\rho)e^{-j\beta_o\rho}H_1^{(1)}(\beta_o\rho) \quad (\rho > 0.5\ \mu\text{m}) \tag{4.131}$$

Moreover, since the laser field is azimuthally invariant, it vanishes at the center of the laser. Consequently, it is reasonable to ignore the the radiation part of the aperture field around the center of the laser. Having determined the aperture field, one may construct the auxiliary functions $E^{\pm}(\rho)$, as described in Chapter 2, on the aperture. For circularly symmetric beam, we have $E^{+}(\rho) = -E^{-}(\rho)$. Now using

$$\hat{E}^{\pm}(\alpha) = \int_0^\infty E^{\pm}(\rho)J_{\pm 1}(\alpha\rho)\rho d\rho \tag{4.132}$$

we have

$$\hat{E}^{+}(\alpha) = \hat{E}^{-}(\alpha) \tag{4.133}$$

Now using (2.80), we have

$$\mathbf{E}(\theta,\phi) \sim \hat{\phi}\, cos\theta \hat{E}^{+}(k\, sin\theta) \tag{4.134}$$

In the next section, we consider a typical circular-grating DFB laser and present some numerical results.

4.6 Numerical Results

This section is devoted to an illustrative example. We consider a typical circular-grating bulk DFB laser with second-order grating as depicted in Fig. 4.2. The

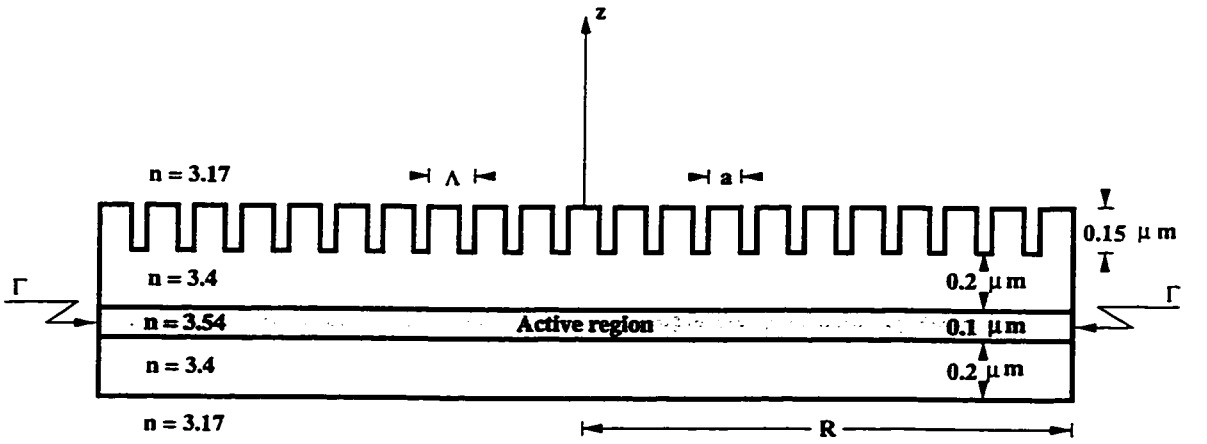

Figure 4.2: The cross sectional view of a typical circular-grating bulk DFB laser

fixed parameters used in the numerical calculations are listed in Table 4.1. In all calculations, we have ignored the spatial hole burning. In the first example, we assume that the radius of the laser is 100 μm and the facet reflectivity at the laser edge Γ is equal to 0.3. In addition, let the the duty cycle of the grating $\frac{a}{\Lambda}$ be 0.6. With these parameters, the calculated surface-emission power of the first mode versus injected current is shown in Fig. 4.3. The side mode suppression ratio of the surface emission as a function of the injected current is shown in Fig. 4.4. As illustrated, the second mode is effectively suppressed above the threshold.

This fact is verified by referring to Fig. 4.5 where the total number of photons of the first and the second mode are plotted. It can be easily seen that above the threshold, the number of photons of the first mode is three orders of magnitude larger than that of the second mode. Hence, the large side mode suppression ratio. It should be noted that since the number of photons are proportional to the energy and power, we have

$$\text{Number of photons in dB} = 10\, log_{10}(\text{Number of photons})$$

Non-radiative recombination coefficient (A)	2.5×10^{8} s^{-1}
Bimolecular Carrier recombination coefficient (B)	1.0×10^{-10} cm^{3} s^{-1}
Auger carrier recombination coefficient (C)	3.0×10^{-29} cm^{6} s^{-1}
Nonlinear gain coefficient (ϵ)	2.0×10^{-17} cm^{3}
Differential gain (a)	3.0×10^{-16} cm^{2}
Transparency carrier density (N_{tr})	1.0×10^{18} cm^{-3}
Absorption and scattering loss of the central region (α)	25 cm^{-1}
Linewidth enhancement factor (α_{H})	3.5
Reference wavelength (λ)	1.55 μm

Table 4.1: Parameters used in the analysis of the circular-grating bulk DFB laser

The lasing wavelengths of the first and the second mode are plotted in Fig. 4.6. As illustrated, the lasing wavelength is very stable in the above-threshold region. Moreover, the first or dominant lasing mode is on the shorter wavelength of the stop band. In Fig. 4.7, the normalized intensity of the first modes inside the laser cavity is illustrated. The sampling current is 25 mA. We have considered the value of $|A_f(\rho)|^2 + |A_b(\rho)|^2$ as the normalized intensity. For sufficiently large distances from the laser center, this value is proportional to the number of photons inside an annular region. Therefore, most of the photons are accumulated near the edge of the laser.

The near-field intensity pattern which is proportional to $|A_f(\rho) + A_b(\rho)|^2$ is illustrated in Fig. 4.8. The near-field profile shows the destructive interference around $\rho = 40$ μm. This is the characteristic feature of the first mode in a second-order DFB laser [60], [104]. In fact, since the first mode has smaller radiation loss, it is favored.

The normalized far-field pattern of the first mode is illustrated in Fig. 4.9.

It can be seen that the laser beamwidth is less than 0.5° and the laser is highly directional. However, as anticipated before, there is a dark spot at the center of the far-field pattern. Moreover, the far-field patterns at different bias currents; e.g., I= 30, 35 mA are the same as that shown in Fig. 4.9. Moreover, the far-field patterns at different bias currents, e.g., I= 30, 35 mA, are the same as that shown in Fig. 4.9.

For the purpose of comparison, the surface-emitted power and the total output power from the laser facet of the first mode as a function of injected current are plotted in Fig. 4.10. Because of the split near-field distribution, the power from the surface is about one-third of that from the facet. The surface-emitted power versus injected current of the first mode for four different reflection coefficients are plotted in Fig. 4.11. For this range of reflection coefficient the threshold current decreases with increasing reflection coefficient. However, for the same bias current the output power increases with increasing reflection coefficient.

The normalized far-field intensity pattern as a function of the facet reflectivity is shown in Fig. 4.12. The surface-emitted power from two lasers with different radii are plotted in Fig. 4.13. As one might expect, the laser beam emitted from the larger aperture is narrower. This fact is clearly shown in Fig. 4.14. In Fig. 4.15, the relative intensity spectra of the power from the facet are plotted for two different radii.

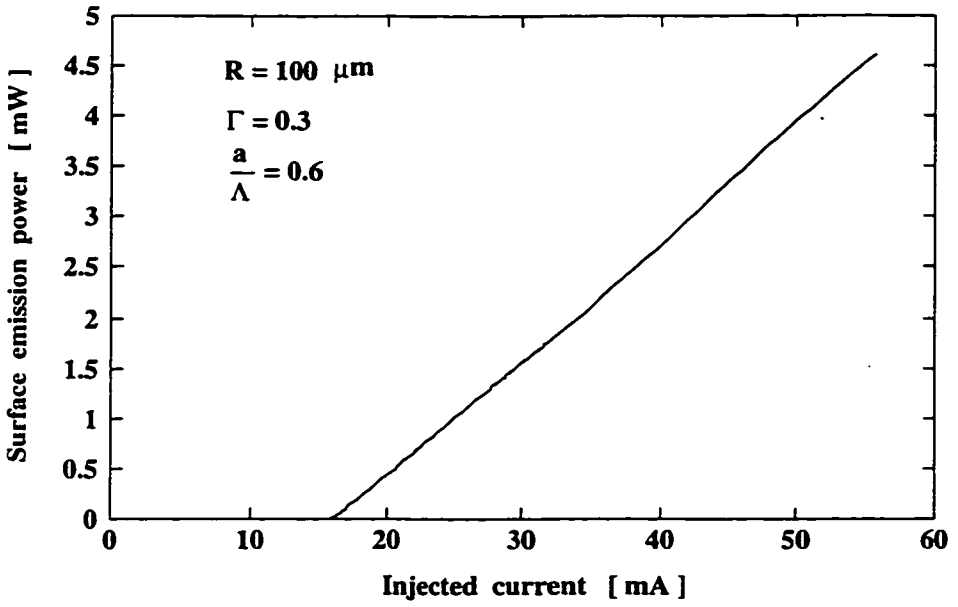

Figure 4.3: Power-current characteristic of the surface emission

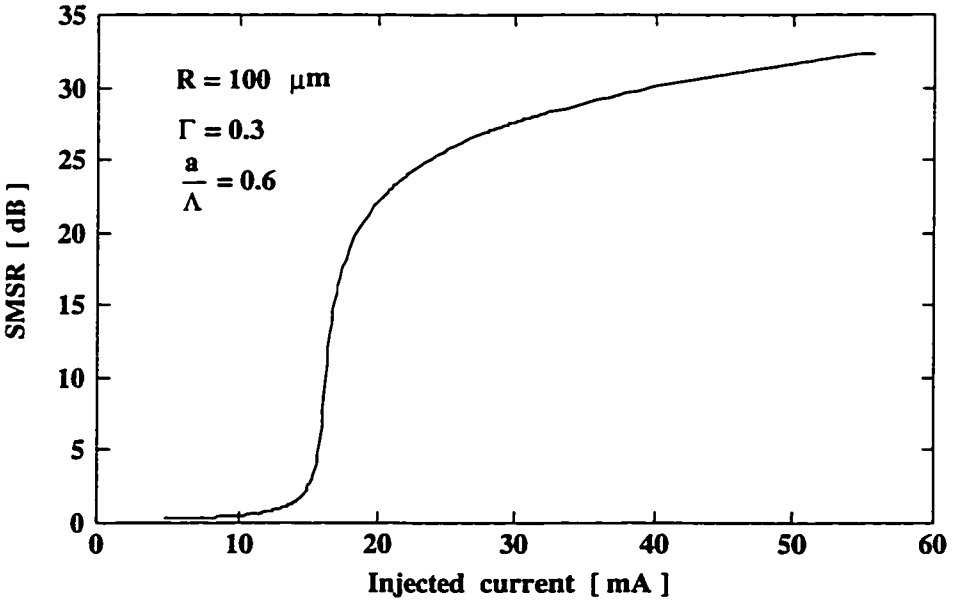

Figure 4.4: Side mode suppression ratio of surface emission power

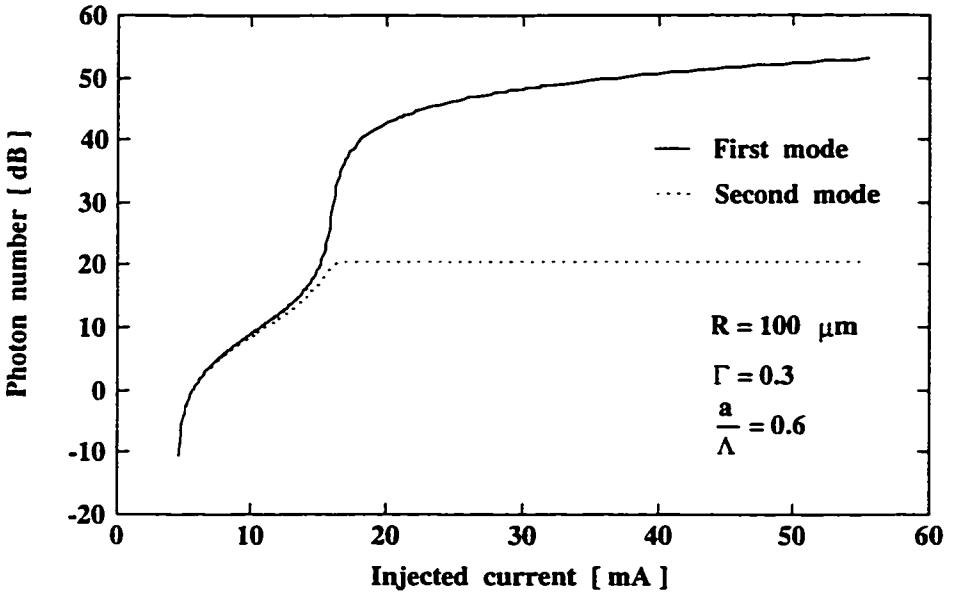

Figure 4.5: Photon numbers of the first and second mode.

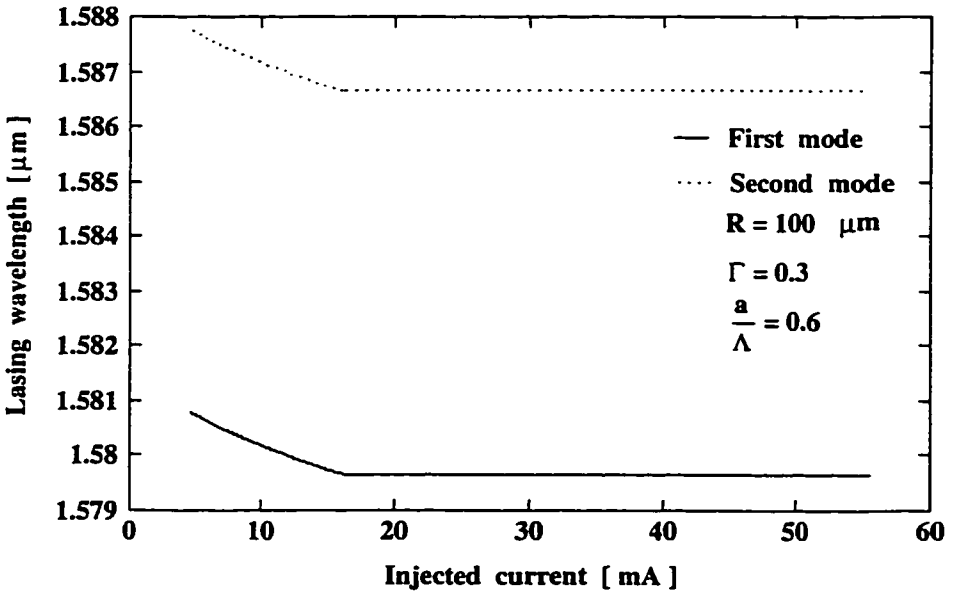

Figure 4.6: Lasing wavelengths of the first and second mode

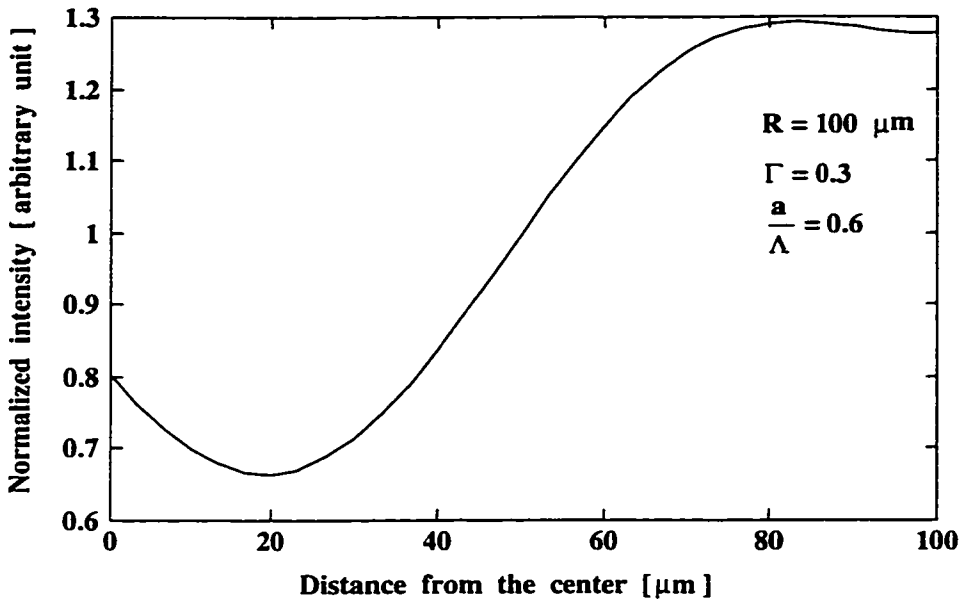

Figure 4.7: Normalized intensity of the first mode inside the laser cavity

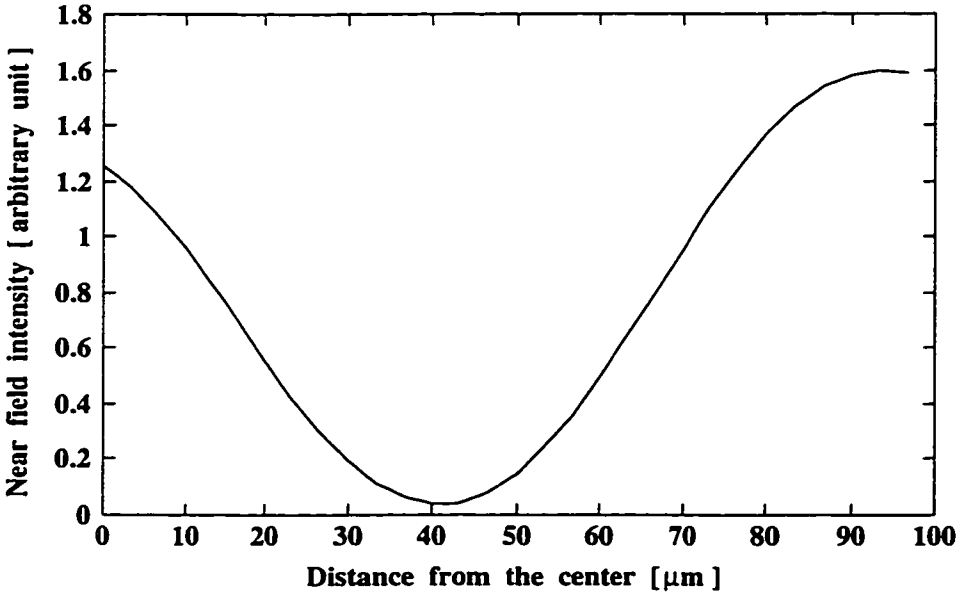

Figure 4.8: Near-field intensity pattern of the first mode inside the laser cavity

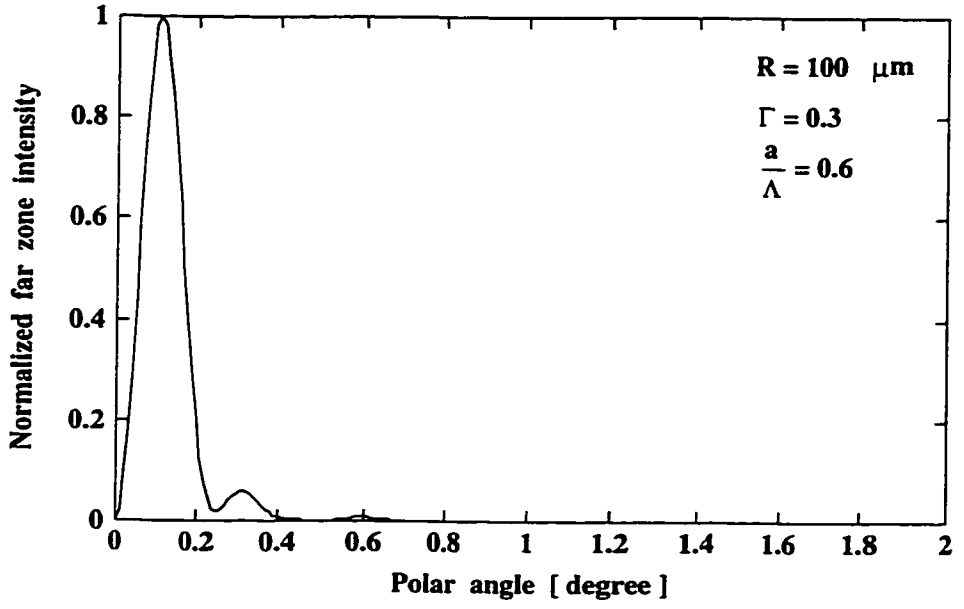

Figure 4.9: Normalized far-field intensity pattern of the first mode

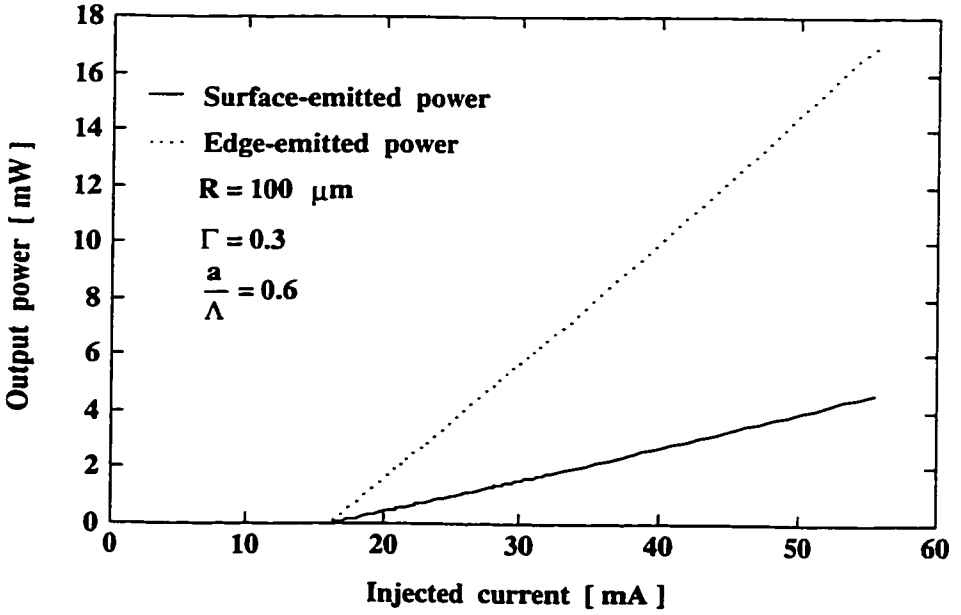

Figure 4.10: Surface- and edge-emitted power versus injected current

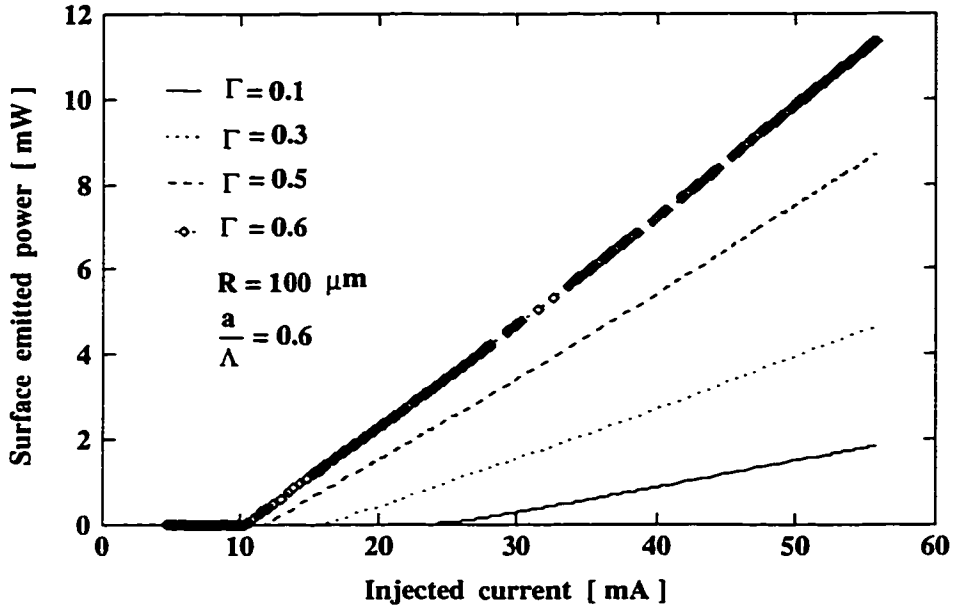

Figure 4.11: Surface-emitted power versus the current and the facet reflectivity

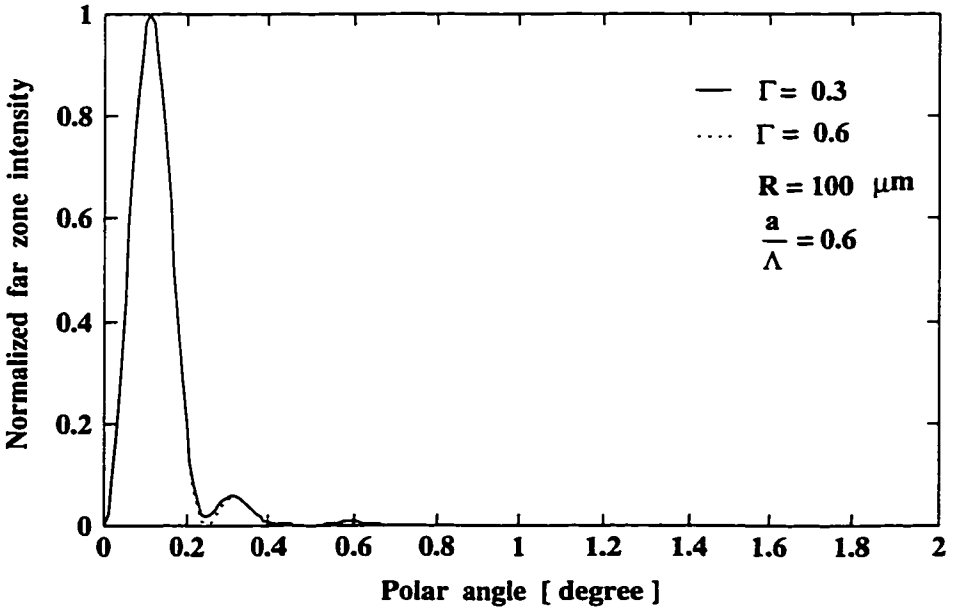

Figure 4.12: Normalized far-field intensity pattern of the first mode for two different facet reflectivities

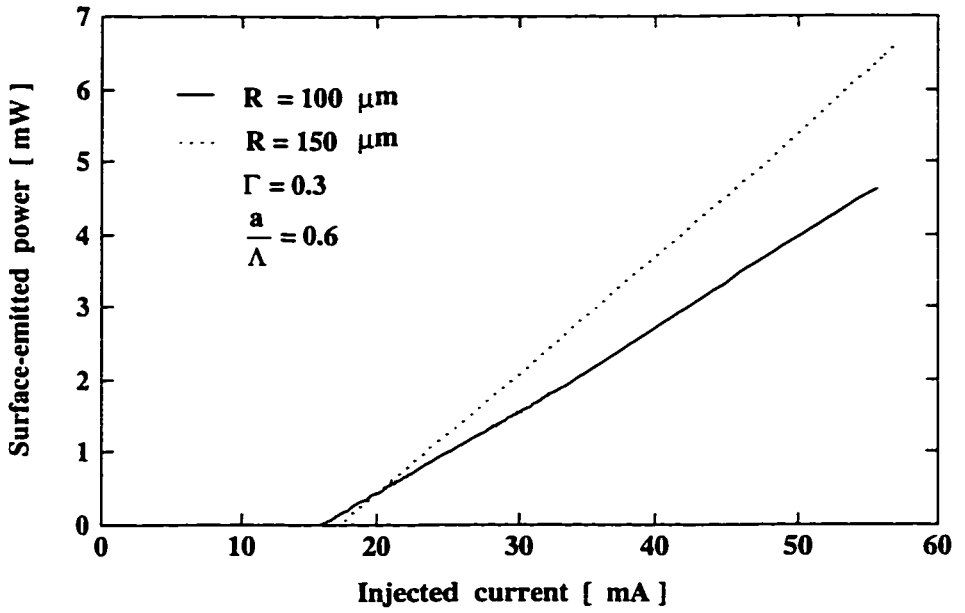

Figure 4.13: Surface-emitted power from two lasers with different radii

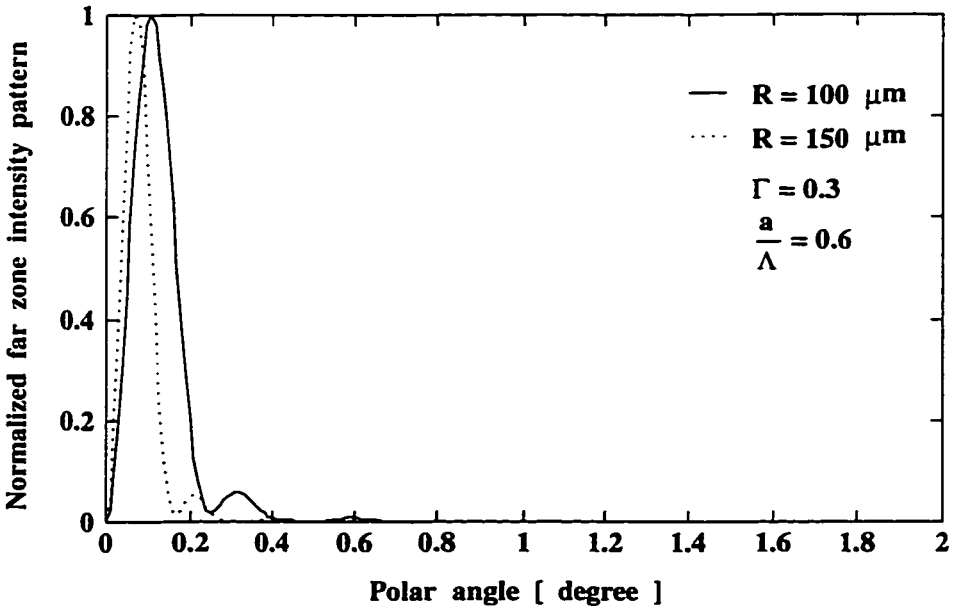

Figure 4.14: Normalized far-field intensity pattern of two lasers with different radii

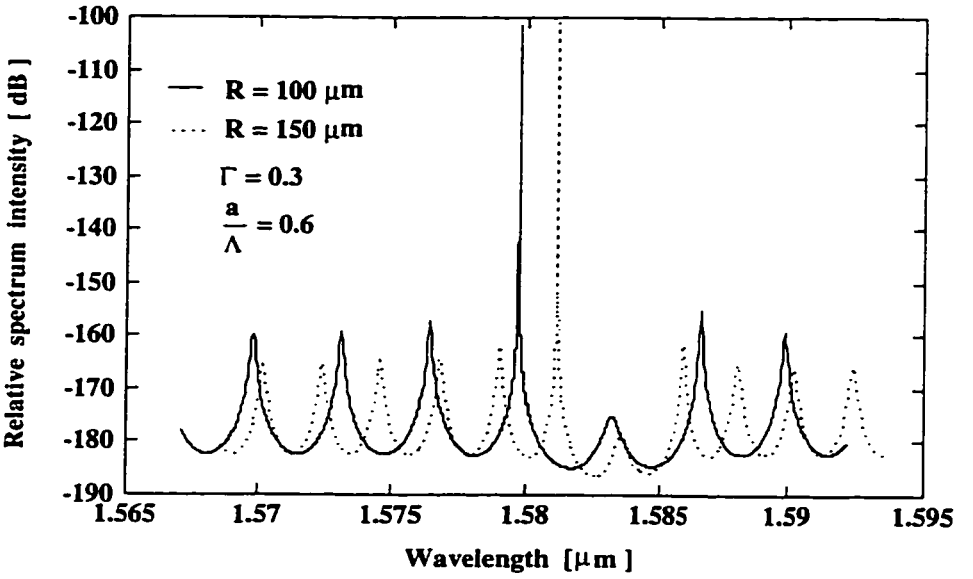

Figure 4.15: Relative intensity spectrum of the power from the facet for two lasers with different radii

4.7 Summary

In this chapter, we have developed a method for treating second-order DFB lasers in the above-threshold region. The rate equations for the total number of photons and the phase of the optical amplitude inside the laser cavity are derived from Maxwell's equations. Our approach is an alternative one to the existing models which are based on the traveling wave formulation. This approach is based on the generalization of the time domain standing-wave method used for treating first-order DFB lasers. This formulation is basically two-dimensional in nature, that is, the lateral or azimuthal variations are ignored. As an illustrative example, the rate equations for a typical circular grating surface have been solved in the above-threshold region under static condition.

Chapter 5

Generalized Coupled-Mode Equations for Planar Dielectric Waveguides with Circular Grating

5.1 Introduction

So far, in the study of circular-grating surface-emitting lasers, we have assumed that the laser beam is circularly symmetric. This assumption extremely simplifies the exact mathematical formulation. However, a circularly-symmetric beam causes the laser to suffer from a dark spot at the center of its far-field pattern. On the other hand, only first harmonic azimuthal variation can produce a nonzero far-field pattern on the laser axis. Consequently, depending on the applications, this laser mode may be the mostly desirable one and must be favored. Although the general methods of treating first-order circular gratings reported in the literature [30], [32] combined with the Green's function approach described in Chapter 2 can be used in

a perturbational fashion to obtain the radiation field, this method is a noncoherent approach in nature. That is, the direct influence of the radiation field on the laser performance is neglected. It should be noted that including azimuthal variation increases the complexity of the problem and the ρ component of the electric field comes into the picture. Therefore, more general formulation is needed to model circular-grating lasers.

The coupling between the guided modes of corrugated optical disk waveguides was first investigated by Kerner *et al.* [16]. Zheng and Lacroix [17] considered the coupling between the guided modes in the analysis of finger print (circular-grating) resonators. As one step toward more general formulation, Wu *et al.* considered TE-TM coupling. In all other coupled-mode equations formulated for circular gratings [23], [24], [30], and [19] coupling to the radiation modes has been ignored. In this chapter, for the first time, we present a generalized coupled-mode equations for planar dielectric waveguides using circular gratings. The characteristic feature that distinguishes it from other formulations is the inclusion of the radiation modes. In this formulation, the background materials treated in Appendix A are fundamental. Moreover, the method is essentially based on the Erdogan's approach [30] in dealing with first-order circular-grating DFB lasers. However, to generalize this approach, we need some modifications at the very beginning of the formulation. Moreover, we use the ideal mode expansion. The details of this method will be described in the next section.

5.2 Basic Formulation

This section focuses on the derivation of the fundamental equation on which the generalized coupled-mode equations are based. To this end, we start from Maxwell's

equations

$$\begin{cases} \nabla \times \mathbf{E} = -j\omega\mu_o \mathbf{H} \\ \nabla \times \mathbf{H} = j\omega\epsilon_o\epsilon_r(\rho, z)\mathbf{E} \end{cases} \tag{5.1}$$

where we have assumed that $\epsilon_r(\mathbf{r})$ is independent of ϕ. Instead of eliminating $\mathbf{H}$, we eliminate $\mathbf{E}$ from the above equations. This leads to the following equation for the $\mathbf{H}$ field

$$\nabla \times \nabla \times \mathbf{H} - \epsilon_r(\rho, z)k_o^2\mathbf{H} = j\omega_o\epsilon_o\nabla\epsilon_r(\rho, z) \times \mathbf{E} \tag{5.2}$$

where $k_o^2 = \omega^2\mu_o\epsilon_o$. In non-magnetic materials which is of our interest, we have $\nabla \cdot \mathbf{H} = 0$. Consequently,

$$\nabla\nabla \cdot \mathbf{H} = 0 \tag{5.3}$$

Subtracting (5.3) from (5.2) leads to the following equation for the $\mathbf{H}$ field

$$\nabla \times \nabla \times \mathbf{H} - \nabla\nabla \cdot \mathbf{H} - \epsilon_r(\rho, z)k_o^2\mathbf{H} = j\omega_o\epsilon_o\nabla\epsilon_r(\rho, z) \times \mathbf{E} \tag{5.4}$$

Expanding the above equation for TE_z mode in cylindrical coordinate system leads to the following equations

$$\nabla^2 H_\rho - \frac{1}{\rho^2}H_\rho - \frac{2}{\rho^2}\frac{\partial H_\phi}{\partial \phi} + \epsilon_r(\rho, z)k_o^2 H_\rho = j\omega\epsilon_o\frac{\partial \epsilon_r}{\partial z}E_\phi \tag{5.5a}$$

$$\nabla^2 H_\phi - \frac{1}{\rho^2}H_\phi + \frac{2}{\rho^2}\frac{\partial H_\rho}{\partial \phi} + \epsilon_r(\rho, z)k_o^2 H_\phi = -j\omega\epsilon_o\frac{\partial \epsilon_r}{\partial z}E_\rho \tag{5.5b}$$

$$\nabla^2 H_z + \epsilon_r(\rho, z)k_o^2 H_z = -j\omega\epsilon_o\frac{\partial \epsilon_r}{\partial \rho}E_\phi \tag{5.5c}$$

where

$$\nabla^2 \equiv \frac{\partial^2}{\partial \rho^2} + \frac{1}{\rho}\frac{\partial}{\partial \rho} + \frac{1}{\rho^2}\frac{\partial^2}{\partial \phi^2} + \frac{\partial^2}{\partial z^2}$$

and we have assumed that $\frac{\partial \epsilon_r}{\partial \phi} = 0$ and $E_z = 0$.

It is important to note that for TE_z mode, since all field components can be obtained from the axial component of the magnetic field, it is only necessary to

consider (5.5c) as the fundamental equation governing TE_z mode in an azimuthally invariant circular grating. Eq. (5.5c) can be written in a more convenient form, if one substitute $\epsilon_r(\rho, z)$ by

$$\epsilon_r(\rho, z) = \epsilon_r(z) + \Delta\epsilon_r(\rho, z) \tag{5.6}$$

As a result, (5.5c) reduces to the following form

$$\nabla^2 H_z + \epsilon_r(z) k_o^2 H_z = -k_o^2 \Delta\epsilon_r(\rho, z) H_z - j\omega\epsilon_o \frac{\partial \Delta\epsilon_r}{\partial \rho} E_\phi \tag{5.7}$$

Equation (5.7) is the fundamental governing equation for TE_z mode which is exact for the azimuthally invariant circular gratings. At this stage, one may choose two different approaches.

In the first approach, one may ignore $\frac{\partial \epsilon_r}{\partial \rho}$ on the right hand side of (5.7). This assumption leads to

$$\nabla \cdot \mathbf{E} = 0 \tag{5.8}$$

Eq. (5.8) directly follows from

$$\nabla \cdot \mathbf{E} = -\frac{1}{\epsilon_r} \frac{\partial \Delta\epsilon_r}{\partial \rho} E_\rho \tag{5.9}$$

which is valid for TE_z mode and azimuthally invariant perturbation of the dielectric. Since scalar approaches are based on the assumption of solenoidal electric field, the first approach is referred as the scalar approach.

In the second approach, it is assumed that $\frac{\partial \epsilon_r}{\partial \rho}$ is nonzero. Therefore, the exact nature of the vector field is unchanged. We refer to this approach as the vector approach. Due to the presence of the additional term on the right hand side of (5.7), the vector approach is more complicated than the scalar one. Therefore, in order to illustrate the basic ideas, in the next section we start from the scalar approach.

5.3 Scalar Approach

In this approach, to derive the coupled-mode equations describing the interaction between the guided and the radiation modes, we use the following equation

$$\nabla^2_{\rho\phi} + \frac{\partial^2 H_z}{\partial z^2} + \epsilon_r(z) k_o^2 H_z = -k_o^2 \Delta\epsilon_r(\rho, z) H_z \tag{5.10}$$

where we have used

$$\nabla^2 \equiv \nabla_{\rho\phi} + \frac{\partial^2}{\partial z^2}$$

The above equation is similar to Eq. (7) in [24] where the role of Ψ has been changed to H_z. However, Ψ in [24] is the scalar potential from which a TE_z mode can be constructed. Referring to Appendix A, it is obvious that Ψ is proportional to H_z. Let us write

$$H_z = U(\rho, \phi)\hat{F}(z) + \int_{-\infty}^{\infty} \bar{R}(\rho, \phi; \alpha_t)\Re(z; \alpha_t) d\alpha_t \tag{5.11}$$

where $\hat{F}(z)$ is the normalized *form function* of the fundamental guided modes satisfying the eigenvalue equation

$$\frac{d^2\hat{F}}{dz^2} + \epsilon_r(z) k_o^2 \hat{F} = \beta_t^2 \hat{F} \tag{5.12}$$

In our formulation, we only consider the fundamental guided modes. This is the case for circular-grating lasers. The second term on the right hand side of (5.11) represents the radiation component of the magnetic field. This term distinguishes our formulation from that used by Erdogan [24]. Note that as described in Section A.8.4, we have used the generalized Fourier kernel $\Re(z; \alpha)$ which is the combination of the substrate and the cover modes. $\Re(z; \alpha)$ satisfies the following differential equation

$$\frac{\partial^2 \Re}{\partial z^2} + \left[\epsilon_r(z) k_o^2 - \beta^2(\alpha)\right] \Re = 0 \tag{5.13}$$

where

$$\beta^2(\alpha) = \begin{cases} \epsilon_{r_c} k_o^2 - \alpha^2 & \alpha > 0 \\ \epsilon_{r_s} k_o^2 - \alpha^2 & \alpha < 0 \end{cases} \tag{5.14}$$

and ϵ_{r_s} and ϵ_{r_c} are the dielectric constants of the substrate and the cover, respectively. It should be emphasized that (5.14) implies that $\Re(z;\alpha)$ for negative values of α corresponds to the substrate radiation modes. In addition, we assume that $\Re(z;\alpha)$ is normalized. That is,

$$\int_{-\infty}^{\infty} \Re(z;\alpha)\Re^*(z;\alpha_1)dz = \delta(\alpha - \alpha_1) \tag{5.15}$$

Substituting (5.11) into (5.10) and using (5.12) and (5.13), we get

$$(\nabla^2_{\rho\phi} + \beta_1^2)\, U(\rho,\phi)\widehat{F}(z) + \int_{-\infty}^{\infty} [\nabla^2_{\rho\phi} + \beta^2(\alpha_1)]\tilde{R}(\rho,\phi;\alpha_1)\Re(z;\alpha_1)d\alpha_1 =$$
$$-k_o^2 \Delta\epsilon_r(\rho,z)\, U(\rho,\phi)\widehat{F}(z) - k_o^2 \int_{-\infty}^{\infty} \Delta\epsilon_r(\rho,z)\tilde{R}(\rho,\phi;\alpha_1)\Re(z;\alpha_1)d\alpha_1 \tag{5.16}$$

In order to obtain the equations for $U(\rho,\phi)$ and $\tilde{R}(\rho,\phi,\alpha)$, one may take advantage of the orthogonality of the *form functions* appearing in (5.16). More precisely, multiplying both sides of (5.16) by $\widehat{F}(z)$ and integrating from $-\infty$ to ∞, we obtain

$$(\nabla^2_{\rho\phi} + \beta_1^2)\, U(\rho,\phi) = K(\rho)U(\rho,\phi) + \int_{-\infty}^{\infty} K_{\mathrm{U}}(\rho;\alpha_1)\tilde{R}(\rho,\phi;\alpha_1)d\alpha_1 \tag{5.17}$$

where

$$K(\rho) = -k_o^2 \int_{-\infty}^{\infty} \Delta\epsilon_r(\rho,z)\widehat{F}^2(z)dz \tag{5.18a}$$

$$K_{\mathrm{U}}(\rho;\alpha_1) = -k_o^2 \int_{-\infty}^{\infty} \Delta\epsilon_r(\rho,z)\Re(z;\alpha_1)\widehat{F}(z)dz \tag{5.18b}$$

In a similar fashion, by multiplying both sides of (5.16) by $\Re^*(z;\alpha)$ and integrating from $-\infty$ to ∞, one may write

$$\left[\nabla^2_{\rho\phi} + \beta^2(\alpha)\right] \Re(z;\alpha) = K_{\mathrm{UR}}(\rho;\alpha)U(\rho,\phi) + \int_{-\infty}^{\infty} K_{\mathrm{RR}}(\rho;\alpha,\alpha_1)\tilde{R}(\rho,\phi;\alpha_1)d\alpha_1 \tag{5.19}$$

where

$$K_{UR}(\rho;\alpha) = -k_o^2 \int_{-\infty}^{\infty} \Delta\epsilon_r(\rho,z)\hat{F}(z)\Re^*(z;\alpha)dz \tag{5.20a}$$

$$K_{RR}(\rho;\alpha,\alpha_1) = -k_o^2 \int_{-\infty}^{\infty} \Delta\epsilon_r(\rho,z)\Re(z;\alpha_1)\Re^*(z;\alpha)dz \tag{5.20b}$$

On the other hand, we know that $U(\rho,\phi)$ and $\tilde{R}(\rho,\phi;\alpha)$ are periodic functions of ϕ. Consequently, one may express them by the following Fourier series

$$U(\rho,\phi) = \sum_{n=-\infty}^{\infty} U_n(\rho)e^{jn\phi} \tag{5.21a}$$

$$\tilde{R}(\rho,\phi;\alpha) = \sum_{n=-\infty}^{\infty} \tilde{R}_n(\rho;\alpha)e^{jn\phi} \tag{5.21b}$$

Substituting (5.21a) into (5.16) and (5.21b) into (5.19) and using orthogonality of $e^{jn\phi}$, we have

$$(\mathcal{B}_n + \beta_1^2)U_n(\rho) = Q_n(\rho) \tag{5.22a}$$

$$\left[\mathcal{B}_n + \beta^2(\alpha)\right]\tilde{R}_n(\rho;\alpha) = P_n(\rho;\alpha) \tag{5.22b}$$

where

$$\mathcal{B}_n \equiv \frac{\partial^2}{\partial\rho^2} + \frac{1}{\rho}\frac{\partial}{\partial\rho} - \frac{n^2}{\rho^2} \tag{5.23}$$

$$Q_n(\rho) = K(\rho)U_n(\rho) + \int_{-\infty}^{\infty} K_U(\rho;\alpha_1)\tilde{R}_n(\rho;\alpha_1)d\alpha_1 \tag{5.24}$$

$$P_n(\rho;\alpha) = K_{UR}(\rho;\alpha)U_n(\rho) + \int_{-\infty}^{\infty} K_{RR}(\rho;\alpha,\alpha_1)\tilde{R}_n(\rho;\alpha_1)d\alpha_1 \tag{5.25}$$

Equations (5.22)-(5.25) show the mutual interactions of the guided and radiation modes with nth harmonic of azimuthal variation. In order to obtain the explicit form of these interactions (5.22a) and (5.22b) must be solved. To this end, we use the Green's function approach. Therefore, first, we obtain the Green's function $G_n(\rho,\rho';\alpha)$ satisfying the following differential equation

$$\left[\mathcal{B}_n + \beta^2(\alpha)\right]G_n(\rho,\rho';\alpha) = \frac{1}{\rho}\delta(\rho-\rho') \tag{5.26}$$

The differential operator acting on $G(\rho,\rho';\alpha)$ is the Bessel differential operator. Therefore, one may expect the Green's function can be expressed in terms of the Bessel functions. Depending on the values of $\beta^2(\alpha)$ three different cases may happen. That is, $\beta^2(\alpha) > 0$, $\beta^2(\alpha) = 0$ and $\beta^2(\alpha) < 0$. However, the case $\beta^2(\alpha) < 0$ need not be treated separately. It can be directly obtained from the Green's function obtained for $\beta^2(\alpha) > 0$ simply by changing $\beta(\alpha)$ to $-j\sqrt{-\beta^2(\alpha)}$. In Appendix F.1 the outlines of the derivation of the Green's function are described. Accordingly, we have

$$G_o(\rho,\rho') = ln(\rho^>)\,; \qquad \beta(\alpha) = 0 \tag{5.27a}$$

$$G_n(\rho,\rho') = \frac{1}{2n}\left(\frac{\rho^<}{\rho^>}\right)^n\,; \qquad \beta(\alpha) = 0 \tag{5.27b}$$

$$G_n(\rho,\rho';\alpha) = J_n[\beta(\alpha)\rho^<]\, H_n^{(2)}[\beta(\alpha)\rho^>]\,; \qquad \beta(\alpha) > 0 \tag{5.27c}$$

where $\rho^<$ and $\rho^>$ denote smaller and the larger values of ρ and ρ', respectively. Having obtained the Green's function, one may solve (5.22a) and (5.22b) for $U_n(\rho)$ and $\tilde{R}_n(\rho)$, respectively. Solution for $U_n(\rho)$ is as follows

$$\begin{aligned} U_n(\rho) \;=\; & \left[\frac{j\pi}{2}\int_a^\rho J_n(\beta_1\rho')Q_n(\rho')\,\rho'd\rho'\right] H_n^{(2)}(\beta_1\rho) + \\ & \left[\frac{j\pi}{2}\int_\rho^L H_n^{(2)}(\beta_1\rho')Q_n(\rho')\,\rho'd\rho'\right] J_n(\beta_1\rho) \end{aligned} \tag{5.28}$$

where we have assumed that the grating extends from $\rho = a$ to $\rho = L$. Eq. (5.28) can be written in a more convenient form, if one uses the following identity

$$J_n(\beta_1\rho) = \frac{1}{2}\left[H_n^{(1)}(\beta_1\rho) + H_n^{(2)}(\beta_1\rho)\right] \tag{5.29}$$

More precisely, substituting (5.29) into (5.28), we obtain

$$U_n(\rho) = A_n(\rho)H_n^{(2)}(\beta_1\rho) + B_n(\rho)H_n^{(1)}(\beta_1\rho) \tag{5.30}$$

where

$$A_n(\rho) = \frac{j\pi}{4}\left[\int_a^\rho 2J_n(\beta_1\rho')Q_n(\rho')\,\rho'd\rho' + \int_\rho^L H_n^{(2)}(\beta_1\rho')Q_n(\rho')\,\rho'd\rho'\right] \quad (5.31a)$$

$$B_n(\rho) = \frac{j\pi}{4}\int_\rho^L H_n^{(2)}(\beta_1\rho')Q_n(\rho')\,\rho'd\rho' \quad (5.31b)$$

From (5.31a) and (5.31b), we obtain

$$\frac{dA_n}{d\rho} = \frac{j\pi\rho}{4}Q_n(\rho)H_n^{(1)}(\beta_1\rho') \quad (5.32a)$$

$$\frac{dB_n}{d\rho} = -\frac{j\pi\rho}{4}Q_n(\rho)H_n^{(2)}(\beta_1\rho') \quad (5.32b)$$

where we have used (5.29).

In order to obtain the solution for $\tilde{R}_n(\rho;\alpha)$, we consider those spectra of the radiation modes such that $\beta^2(\alpha) > 0$. The other cases can be treated in the same way. Following the same procedure as we have used for $U_n(\rho)$, we have

$$\tilde{R}_n(\rho;\alpha) = M_n(\rho;\alpha)H_n^{(2)}[\beta(\alpha)\rho] + N_n(\rho;\alpha)H_n^{(1)}[\beta(\alpha)\rho] \quad (5.33)$$

where

$$M_n(\rho;\alpha) = \frac{j\pi}{4}\left[\int_a^\rho 2J_n[\beta(\alpha)\rho']P_n(\rho')\,\rho'd\rho' + \int_\rho^L H_n^{(2)}[\beta(\alpha)\rho']P_n(\rho')\,\rho'd\rho'\right] \quad (5.34a)$$

$$N_n(\rho;\alpha) = \frac{j\pi}{4}\int_\rho^L H_n^{(2)}[\beta(\alpha)\rho']P_n(\rho')\,\rho'd\rho' \quad (5.34b)$$

Therefore,

$$\frac{\partial M_n}{\partial\rho} = \frac{j\pi\rho}{4}P_n(\rho)H_n^{(1)}[\beta(\alpha)\rho] \quad (5.35a)$$

$$\frac{\partial N_n}{\partial\rho} = -\frac{j\pi\rho}{4}P_n(\rho)H_n^{(2)}[\beta(\alpha)\rho] \quad (5.35b)$$

Eqs. (5.32) and (5.35) are the desired coupled-mode equations. This fact can be seen by substituting (5.30) and (5.33) into (5.24) and (5.25). That is,

$$Q_n(\rho) = K(\rho)\left[A_n(\rho)H_n^{(2)}(\beta_1\rho) + B_n(\rho)H_n^{(1)}(\beta_1\rho)\right] +$$

$$\int_{-\infty}^{\infty} K_U(\rho;\alpha_1)\left(M_n(\rho;\alpha_1)H_n^{(2)}[\beta(\alpha_1)\rho] + N_n(\rho;\alpha_1)H_n^{(1)}[\beta(\alpha_1)\rho]\right) d\alpha_1 \tag{5.36}$$

$$\begin{aligned} P_n(\rho;\alpha) &= K_{UR}(\rho;\alpha)\left[A_n(\rho)H_n^{(2)}(\beta_1\rho) + B_n(\rho)H_n^{(1)}(\beta_1\rho)\right] + \\ &\int_{-\infty}^{\infty} K_{RR}(\rho;\alpha,\alpha_1)\left(M_n(\rho;\alpha_1)H_n^{(2)}[\beta(\alpha_1)\rho] + N_n(\rho;\alpha_1)H_n^{(1)}[\beta(\alpha_1)\rho]\right) d\alpha_1 \end{aligned} \tag{5.37}$$

In the next section we use the similar procedure to obtain the coupled-mode equations from (5.7) in the presence of the second term on its right hand side.

5.4 Vector Approach

To derive the coupled-mode equations from (5.7), it is necessary to substitute for E_ϕ on the right hand side. To this end, we use the ideal mode expansion approach. According to (A.20), for TE_z mode, we have

$$H_z = \frac{1}{\mu_r(z)}\beta^2\Psi^h \tag{5.38}$$

where Ψ^h is the Hertzian scalar potential function. On the other hand, (A.19) states that

$$E_\phi = j\omega\mu_o\frac{\partial\Psi^h}{\partial\rho} \tag{5.39}$$

Comparing (5.38) with (5.39) leads to

$$E_\phi = \frac{j\omega\mu_o}{\beta^2}\frac{\partial H_z}{\partial\rho} \tag{5.40}$$

where we have assumed that $\mu_r(z) = 1$. By ideal mode expansion, we mean that if one assumes the expression in (5.11) for H_z, the corresponding electric field is

$$E_\phi = \frac{j\omega\mu_o}{\beta_1^2}\frac{\partial U}{\partial\rho}\widehat{F}(z) + \int_{-\infty}^{\infty}\frac{j\omega\mu_o}{\beta^2(\alpha_1)}\frac{\partial\tilde{R}}{\partial\rho}\Re(z;\alpha_1)\,d\alpha_1 \tag{5.41}$$

This assumption is the main difference between our approach and that was used by Erdogan [30]. However, the approximation used by Erdogan reduces his formulation to ours when it is used only for the guided modes.

Let us substitute (5.11) and (5.41) into (5.7) and follow the same procedure described in the preceding section. That is, using the Fourier series in (5.21) and taking advantage of the orthogonality of the *form functions*. With this procedure, we end up with (5.22a) and (5.22b). However, the main difference in the vector approach is the modification of $Q_n(\rho)$ and $P_n(\rho;\alpha)$. In fact, $Q_n(\rho)$ and $P_n(\rho;\alpha)$ reduce to

$$\begin{aligned} Q_n(\rho) &= K(\rho)U_n(\rho) - \frac{1}{\beta_1^2}\frac{dK}{d\rho}\frac{dU_n}{d\rho} + \\ &\int_{-\infty}^{\infty} K_U(\rho;\alpha_1)\tilde{R}_n(\rho;\alpha_1)d\alpha_1 - \int_{-\infty}^{\infty}\frac{1}{\beta^2(\alpha_1)}\frac{\partial K_U}{\partial\rho}\frac{\partial\tilde{R}_n}{\partial\rho}d\alpha_1 \end{aligned} \tag{5.42}$$

$$\begin{aligned} P_n(\rho;\alpha) &= K_{UR}(\rho;\alpha)U_n(\rho) - \frac{1}{\beta_1^2}\frac{\partial K_{UR}}{\partial\rho}\frac{dU}{d\rho} + \\ &\int_{-\infty}^{\infty} K_{RR}(\rho;\alpha,\alpha_1)\tilde{R}_n(\rho;\alpha_1)d\alpha_1 - \int_{-\infty}^{\infty}\frac{1}{\beta^2(\alpha_1)}\frac{\partial K_{RR}}{\partial\rho}\frac{\partial\tilde{R}_n}{\partial\rho}d\alpha_1 \end{aligned} \tag{5.43}$$

After solving (5.22a) and (5.22b) by Green's function method, it can be seen that the expressions for $U_n(\rho)$ and $R_n(\rho;\alpha)$ in (5.30) and (5.33) are still valid. Specifically, the coupled-mode equations in (5.32) and (5.35) are applicable in the vector approach. However, it should be noted that $O_n(\rho)$ and $P_n(\rho)$ are modified according to (5.42) and (5.43), respectively. This means that the derivatives of the amplitude functions; i.e., $\frac{dA_n}{d\rho}$, $\frac{dB_n}{d\rho}$, $\frac{\partial M_n}{\partial\rho}$, and $\frac{\partial N_n}{\partial\rho}$ appear on the right hand sides of the corresponding equations. For example, by considering (5.33), we have

$$\frac{dU_n}{d\rho} = \frac{dA_n}{d\rho}H_n^{(2)}(\beta_1\rho) + \frac{dB_n}{d\rho}H_n^{(1)}(\beta_1\rho) + A_n(\rho)\frac{dH_n^{(2)}}{d\rho} + B_n(\rho)\frac{dH_n^{(1)}}{d\rho} \tag{5.44}$$

When only the guided modes are concerned, Erdogan [30] simply by solving a system of two linear equations showed that the derivatives of the amplitude functions on the right hand side can be ignored. In this case we have a system of an infinite number of linear equations. However, as far as numerical considerations are concerned, one may ignore the derivatives of the amplitude functions on the right hand sides of the associated equations. In practice, by discretizing the integrals, one ends up with a system of finite number of equations. By transferring the derivative of the amplitude functions to the left hand side of the equations, the coefficient matrix is not the identity matrix anymore. However, it can be seen that the coefficient matrix is of the form

$$\mathbf{C} = \mathbf{I} + \mathbf{B} \tag{5.45}$$

where $\mathbf{I}$ is an $2n \times 2n$ identity matrix. The general form of $\mathbf{B}$ is given by

$$\mathbf{B} = \begin{bmatrix} -a_2 a_1 b_{12}^{12} & -a_2^2 b_{12}^{12} & -a_2 a_3 b_{34}^{12} & \cdots & -a_2 a_{2n} b_{2n-1,2n}^{12} \\ a_1^2 b_{12}^{12} & a_1 a_2 b_{12}^{12} & a_1 a_3 b_{34}^{12} & \cdots & a_1 a_{2n} b_{2n-1,2n}^{12} \\ -a_4 a_1 b_{12}^{34} & -a_4 a_2 b_{12}^{34} & -a_4 a_3 b_{34}^{34} & \cdots & -a_4 a_{2n} b_{2n-1,2n}^{34} \\ a_3 a_1 b_{12}^{34} & a_3 a_2 b_{12}^{34} & a_3^2 b_{34}^{34} & \cdots & a_3 a_{2n} b_{2n-1,2n}^{34} \\ \vdots & \vdots & \vdots & \cdots & \vdots \\ \vdots & \vdots & \vdots & \cdots & \vdots \\ -a_{2n} a_1 b_{12}^{2n-1,2n} & -a_{2n} a_2 b_{12}^{2n-1,2n} & -a_{2n} a_3 b_{34}^{2n-1,2n} & \cdots & -a_{2n}^2 b_{2n-1,2n}^{2n-1,2n} \\ a_{2n-1} a_1 b_{12}^{2n-1,2n} & a_{2n-1} a_2 b_{12}^{2n-1,2n} & a_{2n-1} a_3 b_{34}^{2n-1,2n} & \cdots & a_{2n-1} a_{2n} b_{2n-1,2n}^{2n-1,2n} \end{bmatrix} \tag{5.46}$$

A careful look at $\mathbf{B}$ reveals that if one starts from the first row or the first column, one realizes that its two consecutive rows and columns are dependent. This special feature can be used to obtain the determinant of the coefficient matrix $\mathbf{C}$. To see this fact, suppose that we do an elementary row operation such that the

first row of **B** vanishes. This operation reduces the matrix **C** to

$$\mathbf{C}_1 = \mathbf{A}_1 + \mathbf{B}_1 \tag{5.47}$$

The elements of $\mathbf{B}_1$ are exactly the same as the elements of **B** except for the first row which is identically zero. Note that the determinant of $\mathbf{C}_1$ is equal to the determinant of **C**. In the next step, we do an elementary column operation such that the second column of $\mathbf{B}_1$ vanishes. As a result, $\mathbf{C}_1$ reduces to

$$\mathbf{C}_2 = \mathbf{I} + \mathbf{B}_2 \tag{5.48}$$

The elements of $\mathbf{B}_2$ are exactly the same as those of **B**, except for its first row and second column which are identically zero. Now the whole idea is clear. One needs to continue the elementary row and column operation to eliminate the successive odd rows and even columns of $\mathbf{B}_2$. It should be emphasized that after each step, the determinant of $\mathbf{C}_i$ remains unchanged. After $2n$ step, one ends up with

$$\mathbf{C}_{2n} = \mathbf{I} + \mathbf{B}_{2n} \tag{5.49}$$

where **I** is the identity matrix and $\mathbf{B}_{2n}$ is a matrix such that its odd rows and even columns are identically zero. All its nonzero elements are the corresponding elements of **B**. From the above considerations, $\mathbf{C}_{2n}$ can be written as

$$\mathbf{C}_{2n} = \begin{bmatrix} 1 & 0 & 0 & 0 \ldots 0 \\ a_1^2 b_{12}^{12} & 1 & a_1 a_3 b_{34}^{12} & 0 \ldots 0 \\ 0 & 0 & 1 & 0 \ldots 0 \\ \cdot & \cdot & \cdot & \cdot \ldots \\ \cdot & \cdot & \cdot & \cdot \ldots \\ a_{2n-1} a_1 b_{12}^{2n-1,2n} & 0 & a_{2n-1} a_3 b_{12}^{2n-1,2n} & 0 \ldots 1 \end{bmatrix} \tag{5.50}$$

It is a trivial matter to show that the determinant of $\mathbf{C}_{2n}$ is equal to 1. Consequently, the determinant of **C** is also equal to 1.

On the other hand, the right hand side of the system of equations is of the form

$$\mathbf{D} = \begin{bmatrix} a_2 L_{12} \\ -a_1 L_{12} \\ a_4 L_{34} \\ -a_3 L_{34} \\ \cdot \\ \cdot \\ a_{2n} L_{2n-1,2n} \\ -a_{2n-1} L_{2n-1,2n} \end{bmatrix} \tag{5.51}$$

Now if we use Cramer's rule to obtain the ith unknown; that is, the derivative of the ith amplitude, the numerator is the determinant of the matrix

$$\mathbf{C}' = \mathbf{I}_i' + \mathbf{B}' \tag{5.52}$$

where the elements of $\mathbf{I}_i'$ are the elements of the identity matrix, except for the iith element which is identically zero. Moreover, $\mathbf{B}'$ can be obtained from $\mathbf{B}$ by replacing its ith column by the column vector $\mathbf{D}$ in (5.51). Matrix $\mathbf{B}'$ has almost the same property as $\mathbf{B}$; that is, starting from the first row every two consecutive rows are dependent. Similarly, starting from the first column every two consecutive columns are dependent except for the ith column and one of its neighbors. In this case by the elementary row and column operation it is possible to show that the determinant of $\mathbf{C}'$ is equal to the ith element of the column vector $\mathbf{D}$.

We have already shown that the determinant in the denominator is equal to 1. This means that the derivative of the ith amplitude in the system of coupled-mode equations is simply equal to the right hand side of the ith equation without the derivative of the corresponding amplitude. In other words, in vector approach, one may use the coupled-mode equations in (5.32) and (5.35) with $Q_n(\rho)$ and $P_n(\rho, \alpha)$

given by (5.42) and (5.43), respectively. However, one may ignore the derivatives of the amplitudes appear on the right hand sides. This completes the derivation of coupled-mode equation using vector approach.

In the next section, we briefly describe how to use the coupled-mode equations that we have derived in the threshold analysis of circular-grating lasers.

5.5 Application to Circular-Grating Lasers

The coupled-mode equations derived in Sections 5.3 and 5.4 can be used for a DFB laser near the threshold. However, due to the complexity of the equations, especially the presence of the radiation modes these equations must be solved by a perturbational approach. First, we expand the dielectric perturbation in a Fourier series and discard improper terms due to the phase mismatch. For example, first-order interaction of the guided modes with the grating results in the whole spectrum of the radiation modes. For the sake of simplicity, we ignore the mutual interactions of the radiation modes with each other. Moreover, as far as the laser operation is concerned, one needs to consider radiation modes in the visible range only. That is, those radiation modes with positive value of $\beta^2(\alpha)$.

With the above considerations, by ignoring the radiation modes, one may obtain an initial guess for the guided modes. We can obtain the amplitudes of the radiation modes using the amplitudes of the guided modes in the coupled-mode equations. Substituting the amplitudes of the radiation modes in the coupled-mode equations describing the guided modes, results in the modified coupled-mode equations such that the radiation coupling factor comes into the picture.

As suggested by [59] in treating DFB lasers with straight gratings, more accurate

calculation of the radiation modes is possible, if one solves the modified coupled-mode equations to obtain a better approximation of the amplitude of the guided modes. These amplitudes in turn can be used to obtain a better approximation for the radiation modes. This procedure can be continued until it converges to a self-consistent solution. From the final coupled-mode equation, one may obtain the radiation coupling factor.

5.6 Summary

In this chapter we have developed a generalized coupled-mode equation for planar dielectric waveguides with circularly-symmetric gratings. The special feature in our formulation is the inclusion of the radiation modes. This feature distinguishes it from the previous works reported in the literature. We have considered two different approaches. The scalar approach is based on the ignorance of $\frac{\partial \Delta\epsilon}{\partial \rho}$ in the fundamental governing equation. However, in the vector approach, the coupled-mode equations are derived by considering $\frac{\partial \Delta\epsilon}{\partial \rho}$.

Chapter 6

Conclusions and Direction for Future Research

This concluding chapter provides a survey of the materials covered in the entire thesis and the scientific contributions resulting from this Ph.D. research work. Moreover, some guidelines for conducting the future research are presented.

In this thesis, the emphasis has been to consider the radiation field in the modeling of CGSELs. This special feature distinguishes it from previous works. Moreover, including the radiation field in the model enables one to obtain better criteria for the design of these lasers. With this aim in mind, the following original contributions have been achieved.

- *Developing the mathematical theory of radiation modes in a multilayer planar structure*

  For the first time, a systematic and mathematically rigorous approach has been used in the study of lossless multilayer planar structures. The central focus in this study are the radiation modes. This formulation makes it easy

to treat the radiation modes in a multilayer planar structure. By introducing the *form functions* and considering their inner products as distribution, the orthogonality of the radiation modes has been placed in a proper structural form. This is the most important contribution of this study. We have also proved the orthogonality of the degenerate radiation modes. As a consequence of this theorem, we have introduced another theorem called the Brewster theorem in honor of Brewster and the famous angle he introduced. For the first time, we have presented the mathematical proof of the simple analytical formulas for the normalization of the radiation modes. In addition, we have shown that the *form functions* of the radiation modes can be considered as a kernel of a generalized Fourier transform. Finally, we have presented a systematic approach for constructing real-valued *form functions*. All of these materials are covered in Appendix A.

- *Deriving closed-form spectral dyadic Green's function of multilayer planar structures*

  Using the transfer matrix technique, we have derived a closed-form spectral domain dyadic Green's function of a multilayer planar structure. Therefore, it is very well suited for numerical implementation. The importance of this work stems from the fact that both rectangular and cylindrical coordinate systems are treated in the same mathematical framework. Introducing auxiliary functions in the cylindrical coordinate system brings about such a possibility. The formulation explicitly shows that the Green's function is independent of the branch cut of the dispersion parameter of each layer having finite thickness. This formulation has been used in the investigation of the far-field pattern of a novel circular-grating laser at threshold. Chapter 2 is devoted to considering these materials.

- *Including the radiation effects in the threshold analysis of second-order CGSELs*

  Inclusion of the radiation field in the threshold analysis of circular-grating lasers is another original contribution of this dissertation. The formulation is based on the azimuthally invariant electric field. Based on this assumption, for the first time, we have obtained the coupling factor to the radiation field in describing the mutual interaction of two guided modes in a cylindrical laser. The derivation of the radiation coupling factor has been done by using the Green's function method. Moreover, by using the TMM we have obtained the exact Green's function.

- *Developing the rate equations of second-order CGSELs*

  The above-threshold analysis of circular-grating lasers is the heart of this thesis. For the first time, we have developed a model based on the time domain standing wave approach for treating second-order DFB lasers. This formulation is an alternative approach to the existing ones using the traveling wave method. In this model, starting from Maxwell's equations, we have derived the rate equations for the total number of photons inside the laser cavity and the phase of the optical amplitude. The effect of the radiation field has been properly and accurately included in the model. Although small signal and large signal analysis can be done from the rate equations, we have only considered the above-threshold static analysis of CGSELs. As a result, we have succeeded in obtaining the relationship between the injected current and the radiated output power. It is interesting to note that from this relationship it is possible to obtain some guidelines for the design of these kinds of lasers. Again, an azimuthally invariant electric field is the basic assumption in our formulation.

- *Developing generalized coupled-mode equations of planar waveguides with circular grating*

  As far as the effect of the radiation field in circular-grating lasers is concerned, our modeling is mostly based on the circularly symmetric beam assumption. On the other hand, the electric fields that have the first harmonic of azimuthal variation are the only aperture fields that can produce a nonzero far-field pattern on the laser axis. Therefore, the next step in the modeling of circular-grating lasers is to consider this type of variation. To this end, we have developed generalized coupled-mode equations in planar waveguides with circular gratings. The original contribution to this development is the inclusion of the radiation modes in the derivation of the coupled-mode equations. Our theoretical study of radiation modes is the core of this generalized formulation. We have derived the coupled-mode equations based on the scalar and vector approaches.

The above is the scope of the main contributions of this research work in the study of circular-grating lasers. However, to make such lasers commercially available, there is still a long way to go. There are important theoretical and technological difficulties that must be faced in order to use these lasers in optical communication systems. We address some of these challenges in the next section.

6.1 Suggestions for Future Research

- *Discriminating of different azimuthal modes*

  One of the most important issues in the study and fabrication of circular-grating lasers is the mode control mechanism. The theoretical formulation of

first-order circular-gratings reveals that the modes with different azimuthal orders are in competition. At least, within the limits of the validity of the large argument approximation of the Hankel functions, all even order azimuthal modes lase simultaneously and the same is true for azimuthal modes of odd order. The discrimination between even and odd orders can be done through phase control of the grating. Even if different orders of the Hankel functions do not behave in the same fashion, however, the mode competition in first-order circular-grating lasers is very high. In second-order circular-grating lasers, due to the presence of the complex coupling factor, it is not clear whether the mode competition is as high as in the case of first-order grating. To investigate this problem, it is necessary to obtain an accurate model to predict the behavior of the laser modes with different azimuthal orders. Although we have developed generalized coupled-mode equations for different azimuthal modes in the presence of the radiation modes, however, we do not recommend using this approach as a first attempt towards this end.

An immediate next step in the study of circular-grating lasers is to consider the laser mode with the first-order azimuthal variation. Since this type of field is almost linearly polarized, the easiest way to analyze this mode may be by the modification of the LP mode technique in the study of optical fibers. Armed with the analysis of this type of mode, one may assess different ways of discriminating between the circularly symmetric beam and the beam with the first-order azimuthal variation. In fact, the suppression of unwanted azimuthal modes is the most challenging issue in the study of circular-grating lasers.

- *Suppressing the radiation field in the substrate*

  In general, the radiation field propagates both in the substrate and the cover

regions. This feature may be undesirable in many applications. Therefore, another challenging issue for future research is the suppression of the radiation field in the substrate.

- *Considering small signal and large signal analysis*
  Needless to say, using these architectures in optical communication systems necessitate considering their modulation responses. Therefore, small signal and large signal analysis is another approach for future work.

- *Considering different architectures*
  There are still other possibilities for designing circular-grating lasers. For example, one may design a laser with a passive second-order grating at the center enclosed by a first-order DFB laser, or, the other way around. That is, a first-order DFB laser at the center enclosed by a passive second-order grating. It is also possible to apply some other existing techniques used for improving the performance of surface-emitting lasers with straight gratings. For example, using a two-section DFB/DBR with a continuous second-order grating and central pumped region [105], [106]. Finally, first-order circular-grating DFB lasers can be used in folded cavity lasers. That is, by using an integrated mirror suited internally or externally to the laser cavity, the edge-emitting power is redirected in the normal direction.

In summary, surface-emitting lasers using circular gratings are in the early stages of development. There are many opportunities for research. Much more theoretical and experimental work is required to make them commercially available. Many problems are still open and can be the subject of other Ph.D. theses. However, those who are interested in entering into this area should be aware of many difficulties

in their way and the number of challenges ahead. Working in this area requires persistence. Insight and inspiration will follow.

Appendix A

Mathematical Theory of Multilayer Planar Structures

A.1 Introduction

The study of integrated optics starts with the stack theory of planar structures. Moreover, many important properties of most of the state-of-the art semiconductor lasers are based on the engineering of multilayer planar structures (MPSs). For this reason, we have devoted an appendix on the theoretical study of these geometries. In fact, this appendix provides the necessary background material upon which the entire thesis is based.

Although the core of the subject matter treated in this appendix is normally covered in the literature, however, we treat MPSs in a systematic and self-contained fashion. We use the potential approach in the study of MPSs which is a departure from customary practice of dealing with the components of the vector fields. We tackle a full vectorial problem by defining two suitable scalar potential functions.

These scalar generating functions enjoy interesting properties among which the characteristic behavior of the electromagnetic fields in MPSs can be obtained.

One of the main purposes of this appendix is to introduce suitable basis functions for treating radiation modes. We believe that the analytical method employed in the literature to prove the orthogonality relation of the radiation modes only satisfies credulous readers and can not be accepted by more scrupulous readers. In this appendix an attempt has been made to achieve mathematical rigor of this issue using the distribution theory. In this study some simplifying assumptions in treating of MPSs, e.g. symmetric geometries or limited number of layers have been relaxed. Especially, by using the transfer matrix method we treat arbitrary number of layers and prove the orthogonality of degenerate radiation modes. More importantly, simple analytical formulas have been derived for the normalization of radiation modes. This is the central focus of this appendix.

A.2 Basic Formulation

Let us consider the geometry shown in Fig. A.1. By a multilayer planar structure, we mean a stack of N homogeneous dielectric films which make a stratified medium sandwiched between two semi-infinite homogeneous dielectric mediums. The upper and lower semi-infinite mediums are called the *cover* and *substrate*, respectively. To make the formulation completely general, we also assume different homogeneous linear magnetic properties for each film or medium. For the sake of simplicity and for the purposes of this thesis, we assume no gain or loss in our model, i.e., we consider only lossless MPSs.

The above description of the structure permits us to write Maxwell's equation

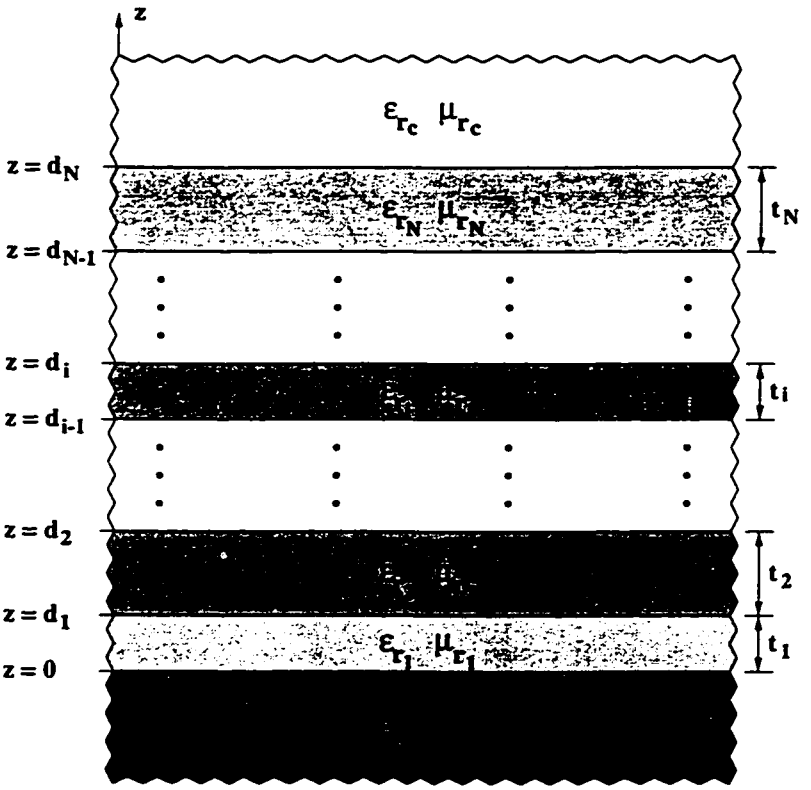

Figure A.1: The cross section of a multilayer medium consisting of N dielectric planar films

in the ith *source-free* region as

$$\nabla \times \mathbf{E}_i = -j\omega\mu_o\mu_{r_i}\mathbf{H}_i \tag{A.1}$$

$$\nabla \times \mathbf{H}_i = j\omega\epsilon_o\epsilon_{r_i}\mathbf{E}_i \tag{A.2}$$

where $e^{j\omega t}$ time variation has been assumed. ϵ_o and μ_o are permittivity and permeability of vacuum, respectively. The subscript i denotes the associated layer number which can also be c or s standing for the cover and substrate, respectively. By an arbitrary electromagnetic field we mean any electromagnetic field satisfies Maxwell's equation in each region subject to the boundary conditions at the interface and the radiation conditions at infinity.

In view of the solenoidal character of $\mathbf{E}_i$ in the ith region, we can express the electric field in terms of the curl of the so-called magnetic type of Hertzian vector potential $\mathbf{\Pi}_i^h$ [107] (pp. 30-34) as

$$\mathbf{E}_i = -j\omega\mu_o \nabla \times \mathbf{\Pi}_i^h \tag{A.3}$$

Substituting (A.3) into (A.1) leads to

$$\mathbf{H}_i = \frac{1}{\mu_{r_i}} \nabla \times \nabla \times \mathbf{\Pi}_i^h. \tag{A.4}$$

where $\nabla \cdot \mathbf{\Pi}_i^h$ is as yet arbitrary. By imposing the Lorentz condition on $\mathbf{\Pi}_i^h$ [107] (pp. 30-34), the equation for $\mathbf{\Pi}_i^h$ becomes the vector Helmholtz equation

$$\nabla^2 \mathbf{\Pi}_i^h + \epsilon_{r_i}\mu_{r_i} k_o^2 \mathbf{\Pi}_i^h = 0 \tag{A.5}$$

where $k_o = \omega\sqrt{\mu_o\epsilon_o}$ is the free space wave number. Note that the Hertzian vector potential defined in (A.3) is slightly different than that defined in [107] (pp. 30-34). In fact, the Hertzian vector potential in (A.3) is the multiple of the corresponding potential function defined in [107] (pp. 30-34). The reason of this fact will be explained later.

In a dual manner, we let

$$\mathbf{H}_i = j\omega\epsilon_o \nabla \times \mathbf{\Pi}_i^e \tag{A.6}$$

where $\mathbf{\Pi}_i^e$ is the electric Hertzian vector potential. Following the same line as before, we find that $\mathbf{\Pi}_i^e$ satisfies the following equation

$$\nabla^2 \mathbf{\Pi}_i^e + \epsilon_{r_i}\mu_{r_i} k_o^2 \mathbf{\Pi}_i^e = 0, \tag{A.7}$$

and the electric field is given by

$$\mathbf{E}_i = \frac{1}{\epsilon_{r_i}} \nabla \times \nabla \times \mathbf{\Pi}_i^e \tag{A.8}$$

In principle, an arbitrary electromagnetic field in each *homogeneous source-free* region can be expressed in terms of either Π_i^h or Π_i^e, i.e., a single vector potential function. For example, one may start from the general form of the solution of the vector wave equation (A.5) in each region and match the boundary conditions by using (A.3) and (A.4). However, this is a difficult task in practice. This problem can be solved by taking advantage of the special form of the field description in terms of vector potential functions in (A.3) and (A.6). More precisely, let us assume that $\hat{\mathbf{u}}$ is an arbitrary fixed unit vector. By choosing the particular form of Π_i^h as

$$\Pi_i^h = \hat{\mathbf{u}}\Psi_i^h \tag{A.9}$$

and using (A.3), one obtains

$$\mathbf{E}_i = j\omega\mu_o\hat{\mathbf{u}} \times \nabla\Psi_i^h \tag{A.10}$$

As can be seen the corresponding electric field is perpendicular to the unit vector $\hat{\mathbf{u}}$. Thus, the associated electric field due to the particular choice of Π_i^h in (A.9) is *transverse* to $\hat{\mathbf{u}}$; the so-called $\mathrm{TE}_\mathbf{u}$ field. In a similar fashion, the particular choice of Π_i^e as

$$\Pi_i^e = \hat{\mathbf{u}}\Psi_i^e \tag{A.11}$$

results in a *transverse magnetic field* with respect to the direction of $\hat{\mathbf{u}}$.

In general the associated fields due to the above choices of Π_i^h or Π_i^e only satisfy Maxwell's equations in the ith region and do not satisfy the boundary conditions at the interfaces. Moreover, an arbitrary electromagnetic field is neither $\mathrm{TE}_\mathbf{u}$ nor $\mathrm{TM}_\mathbf{u}$. Thus, these particular choices of Π_i^h and Π_i^e are only useful if one employ the principle of superposition and express part of the field in terms of Π_i^h defined in (A.9). Therefore, the remaining part of the field which is of $\mathrm{TM}_\mathbf{u}$ type can be expressed by Π_i^e in (A.11). In fact, an arbitrary electromagnetic field in each layer

can be decomposed into $\mathrm{TE_u}$ and $\mathrm{TM_u}$ parts. Now we express the electromagnetic field in each layer as

$$\mathbf{E}_i = -j\omega\mu_o\nabla \times \mathbf{\Pi}_i^h + \frac{1}{\mu_{r_i}}\nabla \times \nabla \times \mathbf{\Pi}_i^e, \tag{A.12}$$

$$\mathbf{H}_i = j\omega\epsilon_o\nabla \times \mathbf{\Pi}_i^e + \frac{1}{\epsilon_{r_i}}\nabla \times \nabla \times \mathbf{\Pi}^h \tag{A.13}$$

where $\mathbf{\Pi}_i^h$ and $\mathbf{\Pi}_i^e$ are directed in the $\hat{\mathbf{u}}$ direction as expressed by (A.9) and (A.11), respectively. Thus the $\mathrm{TE_u}$ part of the field can be derived from Ψ_i^h and Ψ_i^e generates the $\mathrm{TM_u}$ part. Using the identity

$$\nabla \times \nabla \times \mathbf{\Pi}_i^{(e,h)} = \nabla\nabla \cdot \mathbf{\Pi}_i^{(e,h)} - \nabla^2\mathbf{\Pi}_i^{(e,h)}$$

and noting that $\mathbf{\Pi}_i^e$ and $\mathbf{\Pi}_i^h$ are the solutions of (A.5) and (A.7), we obtain

$$\mathbf{E}_i = j\omega\mu_o\hat{\mathbf{u}} \times \nabla\Psi_i^h + \frac{1}{\mu_{r_i}}\nabla\left(\frac{\partial\Psi_i^e}{\partial u}\right) + \epsilon_{r_i}k_o^2\Psi_i^e\hat{\mathbf{u}} \tag{A.14}$$

$$\mathbf{H}_i = -j\omega\epsilon_o\hat{\mathbf{u}} \times \nabla\Psi_i^e + \frac{1}{\epsilon_{r_i}}\nabla\left(\frac{\partial\Psi_i^h}{\partial u}\right) + \mu_{r_i}k_o^2\Psi_i^h\hat{\mathbf{u}} \tag{A.15}$$

where u is the variable along the $\hat{\mathbf{u}}$ direction and Ψ_i^h and Ψ_i^e are the solutions of *scalar* Helmholtz equation

$$\nabla^2\Psi_i^{(e,h)} + \epsilon_{r_i}\mu_{r_i}k_o^2\Psi_i^{(e,h)} = 0 \tag{A.16}$$

We shall find it possible to choose Ψ_i^e and Ψ_i^h sufficiently general to express an arbitrary electromagnetic field by (A.14) and (A.15). Thus, *an arbitrary electromagnetic field in each source-free homogeneous layer can be expressed by the two types of scalar potential functions* Ψ_i^h *and* Ψ_i^e.

A.3 LSM and LSE Fields

In the preceding section a general method for constructing an arbitrary electromagnetic field in a source-free MPS has been described. This method is completely

general and can be applied to an arbitrary *piecewise homogeneous and source-free region*. It has been shown that in general two types of scalar potential functions completely determine an arbitrary electromagnetic field in a source-free MPS. In Chapter 2, we have used Green's function approach to study MPSs in the presence of the source. In that case, by using the principle of superposition, we have shown that the *source-free* constraint can be relaxed and even in the presence of the source the electromagnetic fields can be obtained from the two types of scalar potential functions. In this appendix we stick on the *source-free* constraint.

As far as engineering is concerned, we are interested in constructing of electromagnetic field in their simplest form. More importantly, these simplest forms of solutions can be considered as the building blocks of more general solutions. Therefore, the question may be raised at this point is that
How to construct the simple forms of the solutions of the Maxwell's equations in a MPS ?

To answer the above question we have to specify what we mean by *the simple form of the solutions*. Let us consider the *simple forms* of the solutions as those kinds of solutions that can be obtained from one type of scalar potential function. In this context, the above question can be answered by a careful study of (A.14) and (A.15). It should be mentioned that the direction of $\hat{\mathbf{u}}$ in (A.14) and (A.15) is completely arbitrary. For planar structures it is natural to choose $\hat{\mathbf{u}}$ either parallel or perpendicular to the planar interfaces. We now consider each case separately.

Case A: $\hat{\mathbf{u}}$ is parallel to the planar interfaces

In this case any attempt to construct an electromagnetic field from one type of the potential functions without any restriction on the potential function leads to a complete failure. For example, suppose that we want to construct an electromagnetic field from Ψ_i^h's. With this goal in mind, from (A.14) and (A.15) we

get

$$\mathbf{E}_i = j\omega\mu_o\hat{\mathbf{u}} \times \nabla\Psi_i^h \tag{A.17}$$

$$\mathbf{H}_i = \frac{1}{\mu_{r_i}}\nabla\left(\frac{\partial\Psi_i^h}{\partial u}\right) + \epsilon_{r_i}k_o^2\Psi_i^h\,\hat{\mathbf{u}} \tag{A.18}$$

Now (A.17) requires that $\epsilon_{r_i}\Psi_i^h$'s be continuous at each interface whereas (A.18) results in the continuity of $\frac{1}{\mu_{r_i}}\Psi_i^h$'s. A dual reasoning can also be applied to show that in general a potential function of the electric type only is not sufficient to support an electromagnetic field. However, a suitable condition on the potential functions makes it possible to construct an electromagnetic field from one type of the potential function only.

Let us assume that Ψ_i^h's are independent of the coordinate normal to $\hat{\mathbf{u}}$ in the planar interfaces. In this case, the electromagnetic fields constructed from (A.17) and (A.18) have only three components and completely fulfill the boundary conditions at all interfaces. The only requirements are the continuity of $\frac{\partial\Psi_i^h}{\partial n}$ and $\frac{1}{\mu_{r_i}}\frac{\partial}{\partial n}\left(\frac{\partial\Psi_i^h}{\partial n}\right)$ at all interfaces. By $\frac{\partial}{\partial n}$, we mean the directional derivative with respect to the normal to the interfaces. Moreover, it can be shown that $\frac{\partial\Psi_i^h}{\partial n}$ is the solution of the following partial differential equation

$$\frac{\partial^2}{\partial n^2}\left(\frac{\partial\Psi_i^h}{\partial n}\right) + \frac{\partial^2}{\partial u^2}\left(\frac{\partial\Psi_i^h}{\partial n}\right) + \epsilon_{r_i}\mu_{r_i}k_o^2\frac{\partial\Psi_i^h}{\partial n} = 0.$$

As will be shown later, the above conditions are completely self-consistent. Imposing similar conditions on Ψ_i^e's bring the possibility of constructing an electromagnetic field from Ψ_i^e's only.

It is always possible to rotate the coordinate axes parallel to the planar interfaces in such away that the dependence of the potential function on one variable vanishes. Therefore, in principle, choosing a suitable direction parallel to the interfaces of a MPS makes it possible to generate an electromagnetic field from only one type of

the potential function. However, each *simple form* is associated with a different direction. This is the main drawback of choosing $\hat{\mathbf{u}}$ parallel to the interfaces.

Case B: $\hat{\mathbf{u}}$ is perpendicular to the planar interfaces

With this choice of $\hat{\mathbf{u}}$, (A.14) and (A.15) reveal the possibility of single-potential construction without any restrictive condition on the potential functions. In this case, the boundary conditions require that

$$\nabla_t \Psi^h_{i+1}|_{z=d_i} = \nabla_t \Psi^h_i|_{z=d_i} \quad i = 0, 1, 2, \ldots N$$

$$\frac{1}{\mu_{r_{i+1}}} \nabla_t \left(\frac{\partial \Psi^h_{i+1}}{\partial u}\right)|_{z=d_i} = \frac{1}{\mu_{r_i}} \nabla_t \left(\frac{\partial \Psi^h_i}{\partial u}\right)|_{z=d_i} \quad i = 0, 1, 2, \ldots N$$

where the indices 0 and N+1 correspond to the substrate and cover layers, respectively. Therefore, continuity of Ψ^h_i's and the normal derivatives of $\frac{1}{\mu_{r_i}}\Psi^h_i$'s at each interface are sufficient to meet the above requirements in constructing TE_u field. Whereas construction of TM_u requires that Ψ^e_i's and the normal derivatives of $\frac{1}{\epsilon_{r_i}}\Psi^e_i$'s be continuous. Furthermore, this choice of $\hat{\mathbf{u}}$ direction is useful not only in the rectangular coordinate system. It is also advantageous to choose $\hat{\mathbf{u}}$ in the axial direction of the cylindrical coordinate system which is usually set up in the direction perpendicular to the planar interfaces.

In this case, since the electric field of the so-called TE_u field does not have any component transverse to the interfaces and completely lies in the planar interfaces, the field is also called the longitudinal-section electric (LSE) field. These types of fields first were introduced in the investigation of closed-boundary waveguides [107] (Chap. 6.). Therefore, the word '*longitudinal*' is more appropriate for closed-boundary waveguides rather than MPSs. However, we use the same terminology in the investigation of MPSs. By the same token, the TM_u field generated by the electric Hertzian potential function is referred to as the longitudinal-section magnetic (LSM) field.

As illustrated in Fig. A.1, the coordinate axes are set up in such a way that the z axis is normal to the interfaces. As will be shown later, this choice of the z axis makes it possible to use the same footing in the investigation of MPSs in the rectangular and cylindrical coordinate systems. Now the LSE and LSM modes in a coordinate-free system can be described as

LSE mode:

$$\mathbf{E}_i^h = j\omega\mu_o\hat{\mathbf{z}} \times \nabla\Psi_i^h \tag{A.19}$$

$$\mathbf{H}_i^h = \frac{1}{\mu_{r_i}}\nabla(\frac{\partial\Psi_i^h}{\partial z}) + \epsilon_{r_i}k_o^2\Psi_i^h\hat{\mathbf{z}} \tag{A.20}$$

subject to the continuity of Ψ_i^h and $\frac{1}{\mu_{r_i}}\frac{\partial\Psi_i^h}{\partial z}$ at all interfaces.

LSM mode:

$$\mathbf{H}_i^e = -j\omega\epsilon_o\hat{\mathbf{z}} \times \nabla\Psi_i^e \tag{A.21}$$

$$\mathbf{E}_i^e = \frac{1}{\epsilon_{r_i}}\nabla(\frac{\partial\Psi_i^e}{\partial z}) + \mu_{r_i}k_o^2\Psi_i^e\hat{\mathbf{z}} \tag{A.22}$$

subject to the continuity of Ψ_i^e and $\frac{1}{\epsilon_{r_i}}\frac{\partial\Psi_i^e}{\partial z}$ at all interfaces. $\Psi_i^{(e,h)}$ are the solutions of the (A.16).

The special forms of the Hertzian potential functions defined in (A.3) and (A.6) result in the continuity of the potential functions and the discontinuity of their normal derivatives at all interfaces. However, those defined in [107] (pp. 30-34) require that the normal derivatives be continuous and the potentials themselves be discontinuous at each interface. This behavior is the result of the continuity of appropriate field components at the interfaces. Since all the normal derivatives must be considered as one-sided derivatives, it is not a problem at all. However, we are interested in the continuity of the potential functions rather than their derivatives. For this reason, we use (A.3) and (A.6) as the definition of the Hertzian potential functions.

Equations (A.19)-(A.22) are the starting point in the study of MPSs in a coordinate-free system. In the absence of the current source, the LSE and LSM fields are decoupled and can exist independently. Since the fields are obtained from the scalar potential functions, one might expect these generating scalar fields completely reflect the properties of the electromagnetic fields in MPS. Therefore, it is natural to focus on the potential functions rather that the vector fields. This is the topic of the following section.

A.4 Characterization of the Potential Functions

So far, we have shown that how a vector field problem in a MPS can be reduced to a scalar one. This problem can be further simplified if one tries to find the simplest form of the potential functions. We turn now to a systematic treatment of this matter. To this end, we return to (A.16), the basis for constructing the potential functions. According to (A.16), $\Psi_i^{(e,h)}$ are the solutions of the scalar Helmholtz equation

$$(\nabla_t^2 + \frac{\partial^2}{\partial z^2} + \epsilon_{r_i}\mu_{r_i}k_o^2)\Psi_i^{(e,h)} = 0 \tag{A.23}$$

where ∇_t^2 is the Laplacian operator in the *transverse* plane to the z axis. Since the Helmholtz equation is separable, it is possible to find the solutions of the form

$$\Psi_i^{(e,h)} = A^{(e,h)}(u_1, u_2)F_i^{(e,h)}(z) \tag{A.24}$$

where (u_1, u_2) are suitable transverse coordinates to the z axis, i.e., (x, y) and (ρ, ϕ) in the rectangular and cylindrical coordinate systems, respectively.

The special factorization form in (A.24) follows from Marcuvitz [109] in the treatment of the closed-boundary waveguides. To explain the basic idea, let us

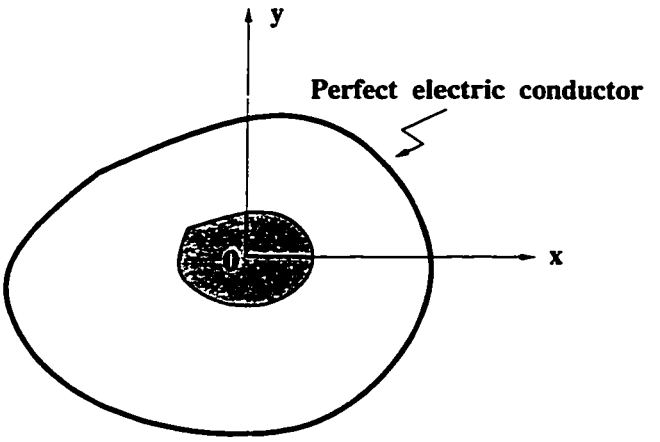

Figure A.2: The cross section of a closed-boundary waveguide

consider a general closed-boundary waveguide with an arbitrary cross section transverse to the propagation direction as illustrated in Fig. A.2. According to Marcuvitz [109], the electric and magnetic field components of each mode of the *closed-boundary* waveguide are factorable into the *form functions*, depending only on the cross-sectional coordinates transverse to the propagation direction, and into the *amplitude functions*, depending only on the coordinate in the propagation direction. That is,

$$\mathbf{E}^{(e,h)}(u,v,z) = a^{(e,h)}(z)\,\mathbf{e}^{(e,h)}(u_1,u_2) \tag{A.25}$$

$$\mathbf{H}^{(e,h)}(u,v,z) = a^{(e,h)}(z)\,\mathbf{h}^{(e,h)}(u_1,u_2) \tag{A.26}$$

where (u_1, u_2) are suitable coordinates transverse to the propagation direction. The characteristic equation of the waveguide can be obtained by applying the boundary conditions on the waveguide cross section.

Using the Marcuvitz terminology in the factorization of the potential functions in (A.24), the *form functions* of a MPS depend only on the z variable (cross-sectional coordinate) and the amplitude functions are dependent on u and v coordinates (direction of propagation) transverse to the z axis. The mathematical representations

of the amplitude functions defined by Marcuvitz for *closed-boundary* waveguides are the same for waveguides with different cross sections and the *form functions* depend on the geometry of the cross section of the waveguide. However, in the case of MPSs, the *form functions* have the same mathematical representation and the amplitude functions are geometry-dependent. In both cases by applying suitable boundary conditions on the *form function*, the characteristic equations of the waveguide can be obtained. In order to satisfy the boundary conditions at all interfaces, the dependence of the potential functions on u and v in each layer must be the same. For this reason, the amplitude functions in (A.24) do not depend on the layer index.

Using the method of separation of variables, the amplitude functions in the rectangular coordinate system can be written as

$$A^{(e,h)}(x,y) = e^{-j[k_x^{(e,h)}x + k_y^{(e,h)}y]} \tag{A.27}$$

With a suitable coordinate transformation, that is, by rotating the planar coordinates in the x-y plane, the amplitude functions can be rewritten as

$$A^{(e,h)}(\eta,\xi) = e^{-j\beta^{(e,h)}\xi}$$

where

$$\left[\beta^{(e,h)}\right]^2 = \left[k_x^{(e,h)}\right]^2 + \left[k_y^{(e,h)}\right]^2$$

Consequently, if one substitutes (A.24) and (A.27) into (A.16), one finds that $F_i^{(e,h)}(z)$ are the solutions of the following differential equation

$$\frac{d^2F_i^{(e,h)}}{dz^2} + \left(\epsilon_{r_i}\mu_{r_i}k_o^2 - [\beta^{(e,h)}]^2\right)F_i^{(e,h)} = 0 \tag{A.28}$$

Now the boundary conditions for the the LSE field require that

$$F_{i+1}^h(d_i) = F_i^h(d_i) \qquad i = 0,1,2,\ldots N \tag{A.29}$$

$$\frac{1}{\mu_{r_{i+1}}}\frac{dF_{i+1}^{h}}{dz}|_{d_i} = \frac{1}{\mu_{r_i}}\frac{dF_i^{h}}{dz}|_{d_i} \qquad i = 0, 1, 2, \ldots N \tag{A.30}$$

The *form functions* $F_i^e(z)$ of the LSM field satisfy the following boundary conditions

$$F_{i+1}^{e}(d_i) = F_i^{e}(d_i) \qquad i = 0, 1, 2, \ldots N \tag{A.31}$$

$$\frac{1}{\epsilon_{r_{i+1}}}\frac{dF_{i+1}^{e}}{dz}|_{d_i} = \frac{1}{\epsilon_{r_i}}\frac{dF_i^{e}}{dz}|_{d_i} \qquad i = 0, 1, 2, \ldots N \tag{A.32}$$

Note that the continuity of the *form functions* is the direct consequence of choosing the Hertzian potential function as defined in (A.3) and (A.6).

Using the same technique in the cylindrical coordinate system, the amplitude functions can be written as

$$A^{(e,h)}(\rho, \phi) = e^{jn\phi} B_n[\beta^{(e,h)}\rho] \tag{A.33}$$

where $B_n[\beta^{(e,h)}\rho]$ are suitable Bessel functions satisfying

$$\frac{d^2 B_n}{d\rho^2} + \frac{1}{\rho}\frac{dB_n}{d\rho} + \left([\beta^{(e,h)}]^2 - \frac{n^2}{\rho^2}\right) B_n = 0 \tag{A.34}$$

On substitution of (A.24) and (A.33) into (A.16) and using (A.34), it can be easily seen that $F_i^{(e,h)}(z)$ satisfy the same differential equation in (A.28) with the same boundary conditions.

The important implication of the above considerations is that the investigation of MPSs in the rectangular and cylindrical coordinate systems leads to the same characteristic behavior of the *form functions*. This makes it possible to treat these structures on the same footing. Since the *form functions* completely determine the nature of the electromagnetic field supported by the MPS, we entirely focus on these functions.

As will be shown later, the solutions of (A.28) fall into two basic categories. The first type of the solutions for the *form functions* leads to those kinds of electromagnetic fields that are tightly bound to the stack and can not reach very far inside

the cover or the substrate. These types of fields are called *surface waves* or *guided modes*. The surface waves are peculiar to MPSs and in order to be supported at least two barriers are needed to trap the wave. Solutions of these types lead to an eigenvalue problem with a discrete set of eigenvalues.

There are still other types of the *form functions* that lead to the so-called radiation fields. These types of *form functions* have an oscillatory behavior in the substrate and cover or in the substrate only. Since the resulting electromagnetic field is no longer tightly bound to the stack, it is sometimes referred to as an unbound state in analogy with the hydrogen atom. These states are necessary to describe the scattering phenomena in MPSs. More detailed study of the radiation modes will be done later in this appendix.

From the above considerations, the *form functions* are central to the investigation of MPSs. Since these functions satisfy the differential equation (A.28) subject to the boundary conditions (A.29) and (A.30) or (A.31) and (A.32), it is worth seeking a systematic approach to tackle (A.28) in MPSs. To this end, we have shown that (A.28) and the corresponding boundary conditions can be replaced with suitable *matrix equations*. Since this thesis heavily relies on this method, in Appendix B.1 this technique is described in more details.

A.5 Surface Waves

Multilayer planar structures have the potential of guiding electromagnetic waves. This characteristic feature enables MPSs to support an electromagnetic field that is tightly bound to the stack with an exponential amplitude decay both in the substrate and cover regions. Therefore, MPSs are sometimes referred to as open-boundary or surface waveguides. The mechanism of guidance in a MPS is based

on the trapping of the wave between at least two barriers. This phenomena is only possible if there exist at least one layer with index l such that its refractive index $\sqrt{\mu_{r_l}\epsilon_{r_l}}\,k_o$ is larger than $\max(\sqrt{\mu_{r_c}\epsilon_{r_c}}\,k_o, \sqrt{\mu_{r_s}\epsilon_{r_s}}\,k_o)$.

The study of surface waves or the so-called guided waves in MPSs is very similar to the study of an electron trapped in multiple quantum wells. Each eigenvalue of Schrödinger equation correspond to an allowed energy state of the electron. In a similar fashion, surface waves are the eigenvalue solutions of the characteristic equation of a MPS.

Since *form functions* reflect the characteristic behavior of the electromagnetic wave in a MPS, it can be easily seen that a MPS can support a surface wave with a *form function* defined in the entire space as

$$F^{(e,h)}(z) = \begin{cases} a_c^{(e,h)} e^{-\gamma_c^{(e,h)}(z-d_N)} & z > d_N \\ A_i^{(e,h)} ch[\gamma_i^{(e,h)}(z-d_{i-1})] + B_i^{(e,h)} sh[\gamma_i^{(e,h)}(z-d_{i-1})] & d_{i-1} < z < d_i \\ b_s^{(e,h)} e^{\gamma_s z} & z < 0 \end{cases} \tag{A.35}$$

where $ch(\cdot)$ and $sh(\cdot)$ stand for $cosh(\cdot)$ and $sinh(\cdot)$, respectively. Moreover,

$$\gamma_c^{(e,h)} = \sqrt{[\beta^{(e,h)}]^2 - \epsilon_{r_c}\mu_{r_c}k_o^2}\,, \tag{A.36a}$$

$$\gamma_i^{(e,h)} = \sqrt{[\beta^{(e,h)}]^2 - \epsilon_{r_i}\mu_{r_i}k_o^2}\,, \tag{A.36b}$$

$$\gamma_s^{(e,h)} = \sqrt{[\beta^{(e,h)}]^2 - \epsilon_{r_s}\mu_{r_s}k_o^2}\,. \tag{A.36c}$$

$\beta^{(e,h)}$ is as yet unknown and to be determined in such a way that $F^{(e,h)}(z)$ meet all required boundary conditions.

In Appendix B.1 we have discussed how the boundary conditions can be reduced to a matrix equation. More precisely, the boundary conditions at each interface

$z = d_i$, $i = 1 \ldots N-1$, leads to a matrix equation

$$\begin{bmatrix} A_{i+1}^{(e,h)} \\ \gamma_{i+1}^{(e,h)} B_{i+1}^{(e,h)} \end{bmatrix} = \mathbf{T}_{i+1,i}^{(e,h)} \begin{bmatrix} A_i^{(e,h)} \\ \gamma_i^{(e,h)} B_i^{(e,h)} \end{bmatrix} \tag{A.37}$$

where $\mathbf{T}_{i+1,i}^{(e,h)}$ is a transfer matrix between two adjacent layers i and $i+1$. Its elements are derived in Appendix B.1. In a similar fashion, the boundary conditions at $z = 0$ requires that

$$\begin{bmatrix} A_1^{(e,h)} \\ \gamma_1^{(e,h)} B_1^{(e,h)} \end{bmatrix} = \mathbf{T}_{1,0}^{(e,h)} \begin{bmatrix} 1 \\ \gamma_s^{(e,h)} \end{bmatrix} b_s^{(e,h)} \tag{A.38}$$

where

$$\mathbf{T}_{1,0}^{(e,h)} = \begin{bmatrix} 1 & 0 \\ 0 & p^{(e,h)} \end{bmatrix} \tag{A.39}$$

with $p^e = \frac{\epsilon_{r_1}}{\epsilon_{r_s}}$, $p^h = \frac{\mu_{r_1}}{\mu_{r_s}}$. Finally, applying the boundary conditions at $z = d_N$ leads to

$$\begin{bmatrix} 1 \\ -\gamma_c^{(e,h)} \end{bmatrix} a_c^{(e,h)} = \mathbf{T}_{N+1,N}^{(e,h)} \begin{bmatrix} A_N^{(e,h)} \\ \gamma_N^{(e,h)} B_N^{(e,h)} \end{bmatrix} \tag{A.40}$$

Different approaches use the so-called matrix formalism for obtaining the characteristic equations of a multilayer stack [110]-[112]. The essence of this method is based on the three matrix equations in (A.37)-(A.40). By successive elimination of the amplitude coefficients of the *form functions* in each region, we end up with a system of two homogeneous linear equations in two unknowns

$$\begin{bmatrix} 1 \\ -\gamma_c^{(e,h)} \end{bmatrix} a_c^{(e,h)} - \mathbf{T}^{(e,h)} \begin{bmatrix} 1 \\ \gamma_s^{(e,h)} \end{bmatrix} b_s^{(e,h)} = 0 \tag{A.41}$$

where

$$\mathbf{T}^{(e,h)} = \prod_{i=N}^{0} \mathbf{T}_{i+1,i}^{(e,h)}. \tag{A.42}$$

Note that from (B.14), we have

$$\begin{aligned} \det\left(\mathbf{T}^{(e,h)}\right) &= \prod_{i=N}^{0} \det\left(\mathbf{T}_{i+1,i}^{(e,h)}\right) \\ &= \prod_{i=N}^{0} \frac{c_{i+1}^{(e,h)}}{c_i^{(e,h)}} \\ &= \frac{c_c^{(e,h)}}{c_s^{(e,h)}} \end{aligned} \tag{A.43}$$

where $c_i^h = \mu_{r_i}$ and $c_i^e = \epsilon_{r_i}$. Multiplying both sides of the matrix equation (A.41) by the row matrix $[\gamma_c^{(e,h)} \quad 1]$ leads to the cancelation of $a_c^{(e,h)}$. Nontrivial solution requires that the resulting coefficient of $b_s^{(e,h)}$ be equal to 0. That is,

$$-[\gamma_c^{(e,h)} \quad 1]\mathbf{T}^{(e,h)} \begin{bmatrix} 1 \\ \gamma_s^{(e,h)} \end{bmatrix} = 0. \tag{A.44}$$

The two different equations in (A.44) are the characteristic equations of the normal LSE and LSM fields of the MPS shown in Fig.A.1. The roots of these equations are the eigenvalues of the surface waves, the so-called normal mode propagation constants. A careful look at (A.44) reveals that the characteristic equations are the determinants of coefficient matrices in (A.41). As shown in Appendix B.1, for a lossless MPS the elements of the transfer matrices are real. Therefore, from (A.36a), (A.36c), and (A.44) the characteristic equation of a lossless MPS is a real function of $\beta^{(e,h)}$, if

$$\beta^{(e,h)} > \max(\sqrt{\mu_{r_c}\epsilon_{r_c}}k_o, \sqrt{\mu_{r_s}\epsilon_{r_s}}k_o)$$

In fact, the real roots of the characteristic equations (A.44) in the range of

$$\max(\sqrt{\mu_{r_c}\epsilon_{r_c}}k_o, \sqrt{\mu_{r_s}\epsilon_{r_s}}k_o) < \beta^{(e,h)} < \max(\sqrt{\mu_{r_i}\epsilon_{r_i}}k_o) \qquad i = 1, 2, \ldots N \tag{A.45}$$

correspond to the eigenvalues of the surface waves that can be supported by the MPS. The largest root gives the fundamental mode.

Multiplying both sides of (A.41) by $\left(\mathbf{T}^{(e,h)}\right)^{-1}$ leads to

$$\left(\mathbf{T}^{(e,h)}\right)^{-1}\begin{bmatrix} 1 \\ -\gamma_c^{(e,h)} \end{bmatrix} a_c^{(e,h)} - \begin{bmatrix} 1 \\ \gamma_s^{(e,h)} \end{bmatrix} b_s^{(e,h)} = 0 \tag{A.46}$$

If one multiplies both sides of the above equation by the row matrix $[-\gamma_s^{(e,h)} \quad 1]$ and uses the same arguments, one obtains the characteristic equations of LSM and LSE modes in the form

$$[-\gamma_s^{(e,h)} \quad 1]\left(\mathbf{T}^{(e,h)}\right)^{-1}\begin{bmatrix} 1 \\ -\gamma_c^{(e,h)} \end{bmatrix} = 0 \tag{A.47}$$

At first glance, the two types of the characteristic equations in (A.44) and (A.47) seems to be different. However, except within a multiplicative factor, these two equations have the same mathematical representations. More precisely, we have

$$[-\gamma_s^{(e,h)} \quad 1]\left(\mathbf{T}^{(e,h)}\right)^{-1}\begin{bmatrix} 1 \\ -\gamma_c^{(e,h)} \end{bmatrix} = \frac{c_s^{(e,h)}}{c_c^{(e,h)}} \times \left(-[\gamma_c^{(e,h)} \quad 1]\mathbf{T}^{(e,h)}\begin{bmatrix} 1 \\ \gamma_s^{(e,h)} \end{bmatrix}\right) \tag{A.48}$$

Therefore, (A.44) and (A.47) have the same roots.

The characteristic equations of the MPS can still be written in a different form. For example, by changing the variable z to $u = d_N - z$, the characteristic equations reduce to either

$$-[\gamma_s^{(e,h)} \quad 1]\hat{\mathbf{T}}^{(e,h)}\begin{bmatrix} 1 \\ \gamma_c^{(e,h)} \end{bmatrix} = 0. \tag{A.49}$$

or

$$[-\gamma_c^{(e,h)} \quad 1]\left(\hat{\mathbf{T}}^{(e,h)}\right)^{-1}\begin{bmatrix} 1 \\ -\gamma_s^{(e,h)} \end{bmatrix} = 0 \tag{A.50}$$

where

$$\hat{\mathbf{T}}^{(e,h)} = \prod_{i=0}^{N} \hat{\mathbf{T}}_{i,i+1}^{(e,h)}\,, \tag{A.51}$$

$$\hat{\mathbf{T}}_{0,1} = \begin{bmatrix} 1 & 0 \\ 0 & q^{(e,h)} \end{bmatrix} \tag{A.52}$$

$$\hat{\mathbf{T}}_{i,i+1}^{(e,h)} = \begin{bmatrix} ch(\gamma_{i+1}^{(e,h)} t_{i+1}) & \frac{sh(\gamma_{i+1}^{(e,h)} t_{i+1})}{\gamma_{i+1}^{(e,h)}} \\ \frac{c_i^{(e,h)}}{c_{i+1}^{(e,h)}} \gamma_{i+1}^{(e,h)} sh(\gamma_{i+1}^{(e,h)} t_{i+1}) & \frac{c_i^{(e,h)}}{c_{i+1}^{(e,h)}} ch(\gamma_{i+1}^{(e,h)} t_{i+1}) \end{bmatrix}, \tag{A.53}$$

$q^e = \frac{\epsilon_{rN}}{\epsilon_{rc}}$, and $q^h = \frac{\mu_{rN}}{\mu_{rc}}$. In this case even if the mathematical forms of (A.44) and (A.49) are totally different, however, physical considerations require that these two different characteristic equations have the same set of solutions. The same is true for (A.47) and (A.50).

Since the *form functions* are the solutions of a homogeneous differential equation with homogeneous boundary conditions, they can be obtained within a multiplicative constant. Therefore, one of the coefficients can be chosen arbitrarily. If, for example, $b_s^{(e,h)}$ is chosen as a real number, from matrix equations in (A.37)-(A.40) and noting that the eigenvalues of the surface waves are within the range specified in (A.45), it can be shown that the *form functions* are real valued.

Further interesting properties of the *form functions* associated with the surface waves may be obtained by using the following definition.

DEFINITION A.1 *Let $F_a^{(e,h)}(z)$ and $F_b^{(e,h)}(z)$ be two entire form functions corresponding to two surface waves supported by a lossless MPS. The notation*

$$< F_a^{(e,h)}, F_b^{(e,h)} >$$

denotes the symmetric inner product of $F_a^{(e,h)}(z)$ and $F_b^{(e,h)}(z)$ and is defined by

$$< F_a^{(e,h)}, F_b^{(e,h)} >= \int_{-\infty}^{\infty} w^{(e,h)}(z) F_a^{(e,h)}(z) F_b^{(e,h)}(z) dz \tag{A.54}$$

where $w^e(z) = \frac{1}{\epsilon_r(z)}$ and $w^h(z) = \frac{1}{\mu_r(z)}$. The notation

$$\ll F_a^{(e,h)}, F_b^{(e,h)} \gg$$

denotes the Hermitian inner product of $F_a^{(e,h)}(z)$ *and* $F_b^{(e,h)}(z)$ *which is defined as*

$$\ll F_a^{(e,h)}, F_b^{(e,h)} \gg = \int_{-\infty}^{\infty} w^{(e,h)}(z) F_a^{(e,h)}(z) [F_b^{(e,h)}(z)]^* dz \qquad \text{(A.55)}$$

where * *means complex conjugate.*

An important property of the *form functions* is the orthogonality relation which is stated in the following theorem.

THEOREM A.1 *Let* $F_a^{(e,h)}(z)$ *and* $F_b^{(e,h)}(z)$ *be two different form functions of a lossless MPS corresponding to two different eigenvalues* $\beta_a^{(e,h)}$ *and* $\beta_b^{(e,h)}$*, respectively. Then*

$$< F_a^{(e,h)}, F_b^{(e,h)} >= 0 \qquad \text{(A.56)}$$

and

$$\ll F_a^{(e,h)}, F_b^{(e,h)} \gg = 0 \qquad \text{(A.57)}$$

The proof of the above theorem is given in Appendix B.2. Note that (A.57) is not valid for a lossy MPS. Moreover, there is no cross orthogonality between F^e and F^h.

By a symmetric MPS, we mean a MPS such that

$$\epsilon_{r_i} = \epsilon_{r_{N+1-i}}$$

$$\mu_{r_i} = \mu_{r_{N+1-i}}$$

The *form functions* of surface waves in a symmetric MPS enjoy an interesting property. They are either symmetric or asymmetric. More precisely, a MPS can not support a surface wave with a *form function* which is neither symmetric nor asymmetric. This important property is stated as follows.

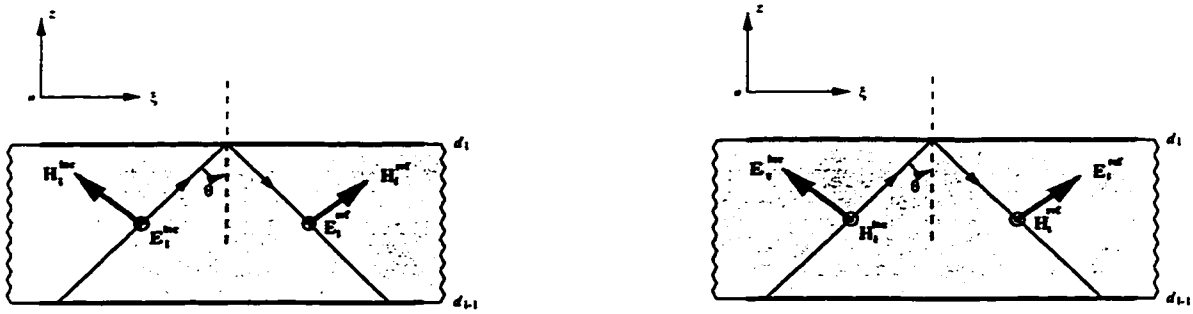

Perpendicular Polarization

Parallel Polarization

Figure A.3: Two different polarization states

THEOREM A.2 *The form functions of surface waves supported by a symmetric MPS are either symmetric or asymmetric about the plane of the symmetry of the MPS.*

We have proved Theorem A.2 in Appendix B.3. When we introduce radiation modes of MPS, it will be seen that the above theorem is *not necessarily* valid for the radiation modes.

In the next section the other possible solutions for the *form functions*, the so-called radiation modes, will be discussed. Since our approach is based on the plane wave concepts, it is also insightful to relate the wave guiding mechanism of MPSs to plane waves . As noted earlier, the solutions of the characteristic equations of a MPS are within the range specified by (A.45). Therefore, at least in the *l-th* layer with the highest value of the refractive index $\sqrt{\mu_{r_l}\epsilon_{r_l}}$, we have

$$\sqrt{\mu_{r_l}\epsilon_{r_l}}\,k_o > \beta^{(e,h)}$$

Using (A.35) and (A.36b), the above condition means that the electromagnetic field within the *l-th* layer can be considered as a superposition of an upward and downward propagating plane wave. With the plane wave concepts, as illustrated in

Fig. A.3, the LSE and LSM modes correspond to *perpendicular* and *parallel* polarization [113], respectively. Moreover, no matter whether or not the electromagnetic field within other layers can be expressed as a superposition of plane waves, there is no possibility of the waves escaping from the boundaries at $z = 0$ and $z = d_N$. Therefore, in the z direction, the MPS can be considered as a one-dimensional transmission line resonator.

The resonance condition, referred to as *transverse resonance condition* [114], leads to the characteristic equations in (A.44) or (A.47). Such a behavior is the physical basis of wave guiding property of MPSs. Moreover, with this physical picture in mind, we see that why there is no possibility to have surface waves with eigenvalues larger than $\max(\sqrt{\mu_{r_i}\epsilon_{r_i}}\,k_0)$.

A.6 Radiation Modes

As mentioned earlier, there is still other possibility to construct an electromagnetic field in a MPS such that the field reaches undiminished to infinite distances in the substrate or cover regions. Due to this property, these types of modes are called *radiation modes*. In the literature, it is common practice to study the radiation modes of MPSs after investigating the guided modes. However, in principle, these types of modes are introduced much sooner than that. In fact, radiation modes are considered as the simplest examples of the solutions of Maxwell's equations in the elementary courses of electromagnetics.

The concepts such as *plane waves*, normal and oblique incidence of plane waves on a dielectric or several dielectrics are nothing but the radiation modes. Therefore, one may expect that these modes are not peculiar to MPSs. More precisely, there is no need to have any barriers for supporting the radiation modes. For example,

free space can support its own radiation modes. In fact, all modes of free space are radiation modes. Two semi-infinite dielectric materials separated at a barrier, or even a dielectric film sandwiched between two other dielectric regions of higher refractive indices can support radiation modes. Whereas, it is not possible to have guided modes in these structures. This fact is a distinctive feature of radiation modes in comparison with the guided modes.

The *form functions* of the radiation modes of a MPS and the study of a free electron incident on the several potential barriers are dual problems. It is well-known that there is no restriction on the electron's energy. Therefore, radiation modes can be considered as an eigenvalue problem with a continuous spectrum. Mathematically, radiation modes are not square integrable functions. Therefore, no physical process can excite a single radiation mode. This is another difference between the radiation modes and the guided modes. Superposition of radiation modes, however, within a range of their spectra leads to a physical system. This idea is very similar to the so-called wave packet concept in quantum mechanics. In fact, the wave function of a localized particle can be considered as a superposition of the wave functions of a free particle which is a non-physical system. In the theory of Fourier transforms we have a similar situation. That is, even if the Fourier kernels are not square integrable, however, every square integrable functions can be considered as a superposition of them.

Like guided modes, radiations modes are orthogonal among themselves. However, the orthogonality is not in the ordinary sense. In fact, as will be explained later, radiation modes are orthogonal in the *distribution* sense. Radiation modes are also orthogonal to each guided modes in the ordinary sense. In view of the orthogonality of the radiation modes, constructing an orthonormal set of these modes is highly desirable. However, since these modes are not bound, this task

does not seem to be quite straightforward as in the case of guided modes. Detailed investigation of these important issues are addressed in this section.

After this introduction we turn now to the way of constructing of the basis functions of the radiation field in a MPS. In the preceding section, the mechanism of waveguidance of MPSs has been described in terms of the excitation of plane waves inside the stack which suffer total internal reflection at some boundaries. The question may be raised at this point is that whether it is possible that a traveling wave exists inside the cover or substrate regions with such mechanism. It should be noted that such a behavior necessitate that either $\beta^{(e,h)} < \max(\sqrt{\mu_{r_c}\epsilon_{r_c}}\,k_o, \sqrt{\mu_{r_s}\epsilon_{r_c}}\,k_o)$ or $\beta^{(e,h)}$ be purely imaginary number. A non trivial field of this type results in the determinantal equations of the form (A.44). However, within the range shown above, there is no value of $\beta^{(e,h)}$ such that the resulting field exhibits such a characteristic behavior. Physically, it is impossible to obtain steady power from a finite amount of energy. This is why the determinantal equations do not have any solutions in this range. This fact provides us other possibilities for constructing the solution.

With a proper discontinuity of the appropriate field components in a finite range, it is possible to have a purely traveling wave in the cover or in the substrate. Such fields, however, are not the solutions of *homogeneous* Maxwell's equations. In fact, they are responses to some kinds of excitations. This is the topic Chapter 2 in dealing with the Green's functions in the spectral domain. If this discontinuity recedes to $z = \pm\infty$, the problem reduces to the excitation of the MPS with a plane wave which is still a homogeneous problem. It should be noted that, however, solutions of these types have standing waves nature at least in the cover or in the substrate.

Let us excite the MPS shown in Fig. A.4 with a plane wave incident from the

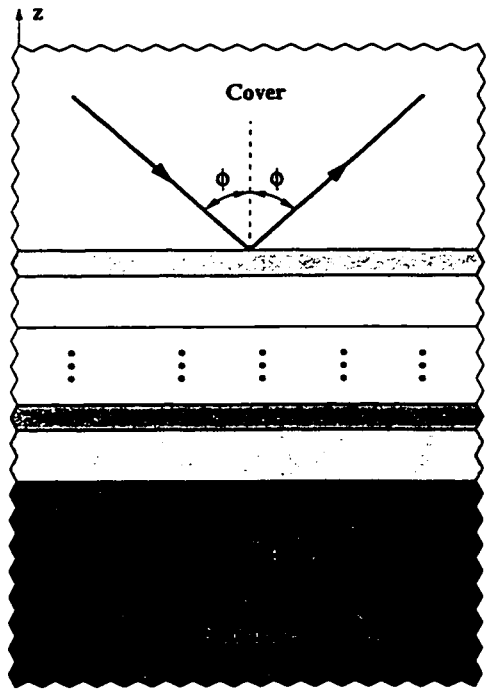

Figure A.4: Cover radiation modes

top in the cover. Moreover, assume that

$$\sqrt{\mu_{r_s}\epsilon_{r_s}} > \sqrt{\mu_{r_c}\epsilon_{r_c}} \tag{A.58}$$

It is not difficult to show that the entire *form functions* $F_c^{(e,h)}(z;s)$ are of the form

$$F_c^{(e,h)}(z;s) = \begin{cases} b_c e^{js(z-d_N)} + a_c^{(e,h)}(s)\, e^{-js(z-d_N)} & z > d_N \\ A_i^{(e,h)}(s)\, ch[\gamma_i(z-d_{i-1})] + B_i^{(e,h)}(s)\, sh[\gamma_i(z-d_{i-1})] & d_{i-1} < z < d_i \\ b_s^{(e,h)}(s)\, e^{j\tau_s z} & z < 0 \end{cases} \tag{A.59}$$

where

$$s = \sqrt{\mu_{r_c}\epsilon_{r_c}\, k_o^2 - \beta^2} > 0 \tag{A.60a}$$

$$\gamma_i = \sqrt{\beta^2 - \mu_{r_i}\epsilon_{r_i}\, k_o^2} \tag{A.60b}$$

$$\tau_s = \sqrt{\mu_{r_s}\epsilon_{r_s}\, k_o^2 - \beta^2} \tag{A.60c}$$

In our terminology, the radiation modes with the above *form functions* are called *cover radiation modes* or *cover modes* for short. As will be explained later, this terminology is slightly different than the conventional one usually used in the literature. For the cover radiation modes it is usually more convenient to consider the real variable s, called *radiation parameter*, as an independent variable and express the dispersion parameters defined in (A.60) in terms of it. Therefore,

$$\beta = \sqrt{\mu_{r_c}\epsilon_{r_c}\, k_o^2 - s^2} \tag{A.61a}$$

$$\gamma_i = \sqrt{(\mu_{r_c}\epsilon_{r_c} - \mu_{r_i}\epsilon_{r_i})k_o^2 - s^2} \tag{A.61b}$$

$$\tau_s = \sqrt{(\mu_{r_s}\epsilon_{r_s} - \mu_{r_c}\epsilon_{r_c})k_o^2 + s^2} \tag{A.61c}$$

Note that the value of s is not restricted to some discrete values. It covers the complete range of positive real numbers. Now some important results can be derived from (A.61). As can be seen from (A.61a) within the range $0 < s < \sqrt{\mu_{r_c}\epsilon_{r_c}}\, k_o$, β is real and $0 < \beta < \sqrt{\mu_{r_c}\epsilon_{r_c}}\, k_o$. All cover modes with radiation parameter in this range are called *visible* or *propagating* cover modes. The term *propagating* means propagation in the direction transverse to the z axis. These modes are associated with real values of β. On the other hand, for $s > \sqrt{\mu_{r_c}\epsilon_{r_c}}\, k_o$, β is purely imaginary. We call these types of radiation modes, with imaginary values of β, *invisible* or *decaying* cover modes. For the sake of mathematical completeness, invisible modes are necessary to describe an arbitrary discontinuity in the *amplitude functions* at the junction of two different waveguides.

From (A.58) and (A.61c), one may find that $\tau_s > s > 0$. Thus, if the refractive index of the substrate is larger than that of the cover, the field of the cover mode in the substrate region is of traveling type irrespective of the radiation parameter. Of course, this field in the cover region is a standing wave. Since the amplitude b_c is related to the incident plane wave, we call it *incident amplitude*. Incident

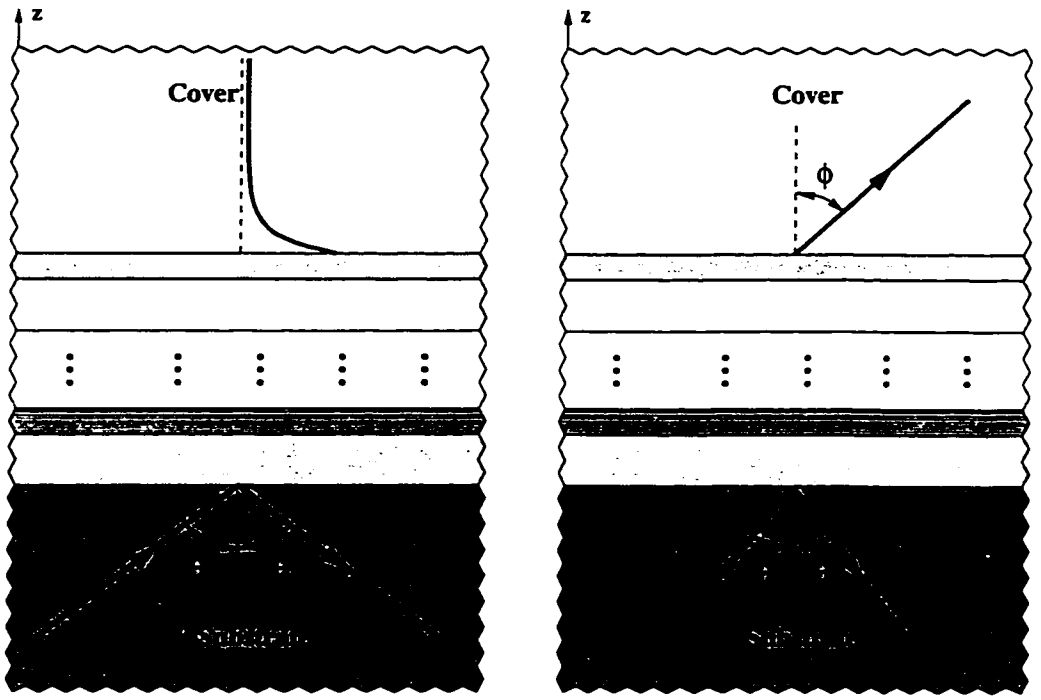

Figure A.5: Substrate radiation modes: (a) Type I. (b) Type II.

amplitude can be chosen arbitrarily. All other amplitudes are called *scattered* amplitudes. Scattered amplitudes can be uniquely determined in terms of the incident amplitude.

There is still other possibility to construct radiation modes. Let the MPS be excited by a plane wave incident from the bottom in the substrate as depicted in Fig. A.5. In this case the entire *form functions* $F_s^{(e,h)}(z;s)$ can be described by the following expression

$$F_s^{(e,h)}(z;s) = \begin{cases} a_c^{(e,h)}(s)\, e^{-\gamma_c(z-d_N)} & z > d_N \\ A_i^{(e,h)}(s)\, ch[\gamma_i(z-d_{i-1})] + B_i^{(e,h)}(s)\, sh[\gamma_i(z-d_{i-1})] & d_{i-1} < z < d_i \\ a_s e^{-jsz} + b_s^{(e,h)}(s)\, e^{jsz} & z < 0 \end{cases} \tag{A.62}$$

where $s > 0$ is the radiation parameter and

$$\beta = \sqrt{\mu_{r_s}\epsilon_{r_s} k_o^2 - s^2}\ , \tag{A.63a}$$

$$\gamma_i = \sqrt{(\mu_{r_s}\epsilon_{r_s} - \mu_{r_i}\epsilon_{r_i})k_o^2 - s^2}\ , \tag{A.63b}$$

$$\gamma_c = \sqrt{(\mu_{r_s}\epsilon_{r_s} - \mu_{r_c}\epsilon_{r_c})k_o^2 - s^2}\ . \tag{A.63c}$$

The radiation fields with the *form functions* in (A.62) are called *substrate radiation modes* or *substrate modes* for short. Again our terminology, using substrate modes as a class of radiation modes, is different than that in the literature. Note also how the role of radiation parameter has been changed. For these modes a_s is called incident amplitude and all other amplitudes are called scattered amplitudes. Radiation parameters in the interval $0 < s < \sqrt{\mu_{r_s}\epsilon_{r_s}}\, k_o$ correspond to the visible or propagating substrate modes and those larger than $\sqrt{\mu_{r_s}\epsilon_{r_s}}\, k_o$ are associated with the invisible or decaying modes.

From (A.58) and those values of s such that $0 < s < \sqrt{\mu_{r_s}\epsilon_{r_s} - \mu_{r_c}\epsilon_{r_c}}\, k_o$, γ_c is real. This means that the wave can only tunnel the barrier at $z = d_N$ and has a decaying character in the cover. These types of radiation modes are called substrate modes of type I. For these modes β is within the range $\sqrt{\mu_{r_c}\epsilon_{r_c}}k_o < \beta < \sqrt{\mu_{r_s}\epsilon_{r_s}}k_o$. Substrate radiation modes of type II are those substrate modes that are obtained for $s > \sqrt{\mu_{r_s}\epsilon_{r_s} - \mu_{r_c}\epsilon_{r_c}}\, k_o$. These modes have traveling wave character in the cover. Therefore, substrate modes are either decaying or traveling wave in the cover. These modes are standing wave in the substrate. It should be noted that β in the above consideration is doubled-valued. We have only considered positive or positive-imaginary values of β.

A.7 LSEM Fields

So far, we have categorized the electromagnetic fields supported by a MPS as LSE and LSM fields. In either type of fields we have one component transverse to the planar interfaces. However, when radiation modes come into the picture there is possible to have an electromagnetic field that completely lies in the transverse plane to the z axis. Therefore, in order to be consistent with our terminology, we call these types of fields *longitudinal section electric and magnetic* (LSEM) fields.

In order to see how these fields can exist in a MPS, let us start from a LSE radiation mode. The field components can be derived from (A.19) and (A.20). Especially, we have

$$H_{z_i}^h = \frac{1}{\mu_{r_i}} \frac{\partial^2 \Psi_i^h}{\partial^2 z} + \epsilon_{r_i} k_o^2 \Psi_i^h \tag{A.64}$$

In order that $H_{z_i}^h$ be zero, it is necessary to have

$$\frac{\partial^2 \Psi_i^h}{\partial^2 z} + \mu_{r_i} \epsilon_{r_i} k_o^2 \Psi_i^h = 0 \tag{A.65}$$

On the other hand Ψ_i^h is the solution of (A.16). Substituting (A.65) into (A.16), we have

$$\nabla_t^2 \Psi_i^{(e,h)} = 0 \tag{A.66}$$

Now, if we write Ψ_i^h as a product of the *form function* and amplitude function as shown in (A.24), the conditions in (A.65) and (A.66) necessitate that

$$\frac{d^2 F_i^h}{dz^2} + \mu_{r_i} \epsilon_{r_i} k_o^2 F_i^h = 0 \tag{A.67}$$

$$\nabla_t^2 A^h(u_1, u_2) = 0 \tag{A.68}$$

The amplitude function of the LSEM field is the solution of Laplace equation. This means that we do not have wave propagation in the plane transverse to the

z axis. This can also be seen from (A.67). Comparing (A.67) with (A.28), we see that $\beta = 0$. This value of β is permissible for the radiation modes. As a matter of fact, visible and invisible radiation modes meet each other at $\beta = 0$. It should be stressed that F_i^h satisfies the same boundary conditions as before. If, instead of LSE field, we start with LSM field, by using the same argument, we have

$$\frac{d^2 F_i^e}{dz^2} + \mu_{r_i} \epsilon_{r_i} k_o^2 F_i^e = 0 \tag{A.69}$$

$$\nabla_t^2 A^e(u_1, u_2) = 0 \tag{A.70}$$

The LSEM field corresponds to normal incidence of plane wave on single or several dielectrics. This type of field plays an important role in the theory of second-order DFB lasers. This matter will be described in Chapter 3.

A.8 Characteristic Features of the Form Functions of the Radiation Modes

As mentioned earlier, like surface waves, the *form functions* of the radiation modes are orthogonal to each other. However, this orthogonality must be considered in the distribution sense. This fact will be explained later. The orthogonality of the *form functions* in turn leads to the question of how to set up an orthonormal set of *form functions*. This is one of the most challenging problems when one deals with the radiation modes. Consulting with some good references [115]-[118], even in the simplest cases, shows that it may be an overwhelming task. Fortunately, this is not the case. Due to some interesting relationship between the amplitudes of the *form functions* normalization of radiation modes is much easier than has been thought before. It is even easier than the normalization of the guided modes.

These relationships are based on the some physical considerations. Based on these considerations and without any explanations, simple expressions for the normalized radiation modes of a lossless MPS are given in [59]. These relations are described in the following theorems.

THEOREM A.3 *Let $F_c^{(e,h)}(z)$ in (A.59) be the form function of the cover mode of a lossless MPS such that (A.58) holds. Then for all values of $s > 0$, we have*

$$|b_c|^2 = |a_c(s)|^2 + \frac{c_c^{(e,h)}}{c_s^{(e,h)}} \frac{\tau_s}{s} |b_s(s)|^2 \tag{A.71}$$

where $c^e_{(c,s)} = \epsilon_{r(c,s)}$ and $c^h_{(c,s)} = \mu_{r(c,s)}$.

In general, the proof of the above theorem is not easy. For example, with the expressions given for the normalized radiation modes in [59], it is difficult to prove the above theorem. However, with the transfer matrix formulation that we have developed, this theorem can be proved very easily. The details of the proof of this theorem are given in Appendix B.4

THEOREM A.4 *Let $F_s^{(e,h)}(z)$ in (A.62) be the form function of the substrate mode of a lossless MPS such that (A.58) holds. Then for the substrate mode of type I, we have*

$$|a_s|^2 = |b_s^{(e,h)}(s)|^2 \tag{A.72}$$

and for the substrate mode of type II, the following relationship between the amplitudes holds.

$$|a_s|^2 = |b_s^{(e,h)}(s)|^2 + \frac{c_s^{(e,h)}}{c_c^{(e,h)}} \frac{\tau_c}{s} |a_c^{(e,h)}(s)|^2 \tag{A.73}$$

We have proved the above theorem in Appendix B.5.

The relationships between the amplitudes of the *form functions* of the radiation modes stated in the Theorems A.3 and A.4 rely on some physical basis. In fact, they are another statement of the power conservation. In Appendix B.6, using the plane wave concepts, the physical interpretation of Theorems A.3 and A.4 is given.

A.8.1 Orthogonality of the Radiation Modes

In Section A.3, we have shown that the *form functions* of the surface modes are orthogonal. This is due to the fact that the entire form functions and their weighted derivatives are continuous at each interface. Moreover, they have decaying character in the substrate and in the cover regions, such that both the *form functions* and their derivatives vanish at $z = \pm\infty$. Radiation modes like surface modes are orthogonal among themselves. However, due to the oscillatory nature of the fields in the substrate and cover, the conventional reasoning in the proof of the orthogonality of bound modes is not valid in this case.

So far, orthogonality of the radiation modes has not been treated carefully in the literature and has been overcome by *ad hoc* construction. This problem can, however, be dealt with in a rigorous manner by using the concept of generalized functions and the distribution theory [119]. More precisely, let us consider the inner products of the *form functions* defined in Section A.5 in the distribution sense. That is, we consider them as linear forms or functionals that are defined on the class of the so-called *test functions* which are continuous and satisfy, at least for our purposes, very mild conditions. Under these conditions all the limits must be considered as the *generalized limits*.

As will be presently shown, the term $e^{\pm j(s\pm s')z}$ appears in the inner products of the *form functions* of the radiation modes. Considering the inner product as a

distribution, orthogonality of the *form functions* requires that

$$\lim_{z\to\pm\infty} e^{j(s\pm s')z} = 0$$

where the limit must be considered as a generalized limit. In fact, this is the case as stated in the following theorem.

THEOREM A.5 *Let us consider $e^{\pm jsz}$ as a distribution which is a process that acts on a test function $\phi(s)$ with bounded derivative through the following integral*

$$e^{\pm jsz} \otimes \phi(s) = \int_{-\infty}^{\infty} e^{\pm jsz}\phi(s)ds \tag{A.74}$$

Then, for $s \neq 0$ and in a generalized sense, we have

$$lim_{z\to\pm\infty} e^{\pm jsz} = 0 \tag{A.75}$$

that is,

$$lim_{z\to\pm\infty} \int_{-\infty}^{\infty} e^{\pm jsz}\phi(s)ds = 0 \tag{A.76}$$

The proof of the above theorem which is based on the Riemann-Lebesgue Lemma is given in [120]. Note that the distribution defined in (A.74) assigns to a test function $\phi(s)$ its Fourier transform $\tilde{\phi}_{\pm}(z)$. One of the important implication of Theorem A.5 is that the Fourier transform of not necessarily square integrable functions approach zero for large values of the Fourier argument. Note that from the above theorem, for $s \neq 0$, we also have

$$lim_{z\to\pm\infty} cos\, sz = lim_{z\to\pm\infty} sin\, sz = 0 \tag{A.77}$$

One of the applications of Theorem A.5 is in the calculation of the distribution which is defined by the following integral

$$\tilde{U}_{\pm}(s) = \int_{0}^{\infty} e^{\pm jsz}dz \tag{A.78}$$

Integrals of the above type are very useful for normalization of the radiation modes. In Appendix B.7, using the residue calculus, it is shown that

$$\int_0^\infty e^{\pm jsz}dz = \begin{cases} \pm\frac{j}{s} & s \neq 0 \\ \pi\delta(s) & 0^- < s < 0^+ \end{cases} \tag{A.79}$$

where $\delta(\cdot)$ is the Dirac delta function.

Once we have established Theorem A.5, we may prove the orthogonality relation between the *form functions* of the radiation modes which is stated in the following theorems.

THEOREM A.6 *Consider a lossless MPS. Let* $F_c^{(e,h)}(z;s_1)$ *and* $F_c^{(e,h)}(z;s_2)$ *be the form functions of the cover modes associated with two different radiation parameters* s_1 *and* s_2*, respectively. Then, in the distribution sense, we have*

$$< F_c^{(e,h)}(z;s_1), F_c^{(e,h)}(z;s_2) >= 0 \tag{A.80}$$

$$\ll F_c^{(e,h)}(z;s_1), F_c^{(e,h)}(z;s_2) \gg= 0 \tag{A.81}$$

where $< \cdot,\cdot >$ *and* $\ll \cdot,\cdot \gg$ *are defined in (A.54) and (A.55), respectively.*

THEOREM A.7 *Consider a lossless MPS. Let* $F_s^{(e,h)}(z;s_1)$ *and* $F_s^{(e,h)}(z;s_2)$ *be the form functions of the substrate modes associated with two different radiation parameters* s_1 *and* s_2*, respectively. Then, in the distribution sense, we have*

$$< F_s^{(e,h)}(z;s_1), F_s^{(e,h)}(z;s_2) >= 0 \tag{A.82}$$

$$\ll F_s^{(e,h)}(z;s_1), F_s^{(e,h)}(z;s_2) \gg= 0 \tag{A.83}$$

Note that according to the Theorem A.7 substrate modes of the same or different types are orthogonal to each other.

THEOREM A.8 *Let $F_s^{(e,h)}(z;s_1)$ and $F_c^{(e,h)}(z;s_2)$ be the form functions of the substrate and cover modes of a lossless MPS, respectively. Moreover, assume that the two modes are nondegenerate, that is, each mode corresponds to different values of β. This condition is equivalent to*

$$s_1 \neq \sqrt{(\epsilon_{r_s} - \epsilon_{r_c})k_o^2 + s_2^2} \tag{A.84}$$

Then, in the distribution sense, we have

$$< F_s^{(e,h)}(z;s_1), F_c^{(e,h)}(z;s_2) >= 0 \tag{A.85}$$

$$\ll F_s^{(e,h)}(z;s_1), F_c^{(e,h)}(z;s_2) \gg= 0 \tag{A.86}$$

The above theorems are based on the nondegenerate mode assumption. Their proof are similar to each other. Therefore, only the proof of Theorem A.8 is given in Appendix B.8.

A.8.2 Degenerate Radiation Modes

By definition, two modes with the same value of β are called *degenerate modes*. Degeneracy for surface waves may happen only within a multiplicative constant. This property has been exploited in the proof of Theorem A.1. However, this is not the case for the radiation modes. For example, two plane waves travel in opposite directions with the same propagation constants are degenerate modes of free space whereas they are mathematically independent. In the case of a MPS, two cover and substrate modes with the following *form functions* are degenerate modes.

$$F_c^{(e,h)}(z;s) = \begin{cases} b_c e^{js(z-d_N)} + a_c^{(e,h)}(s)\, e^{-js(z-d_N)} & z > d_N \\ A_i^{(e,h)}(s)\, ch[\gamma_i(z-d_{i-1})] + B_i^{(e,h)}(s)\, sh[\gamma_i(z-d_{i-1})] & d_{i-1} < z < d_i \\ b_s^{(e,h)}(s)\, e^{j\tau_s z} & z < 0 \end{cases} \tag{A.87}$$

$$F_s^{(e,h)}(z;\tau_s) = \begin{cases} a_c^{(e,h)}(\tau_s)\, e^{-js(z-d_N)} & z > d_N \\ A_i^{(e,h)}(\tau_s)\, ch[\gamma_i(z-d_{i-1})] + B_i^{(e,h)}(\tau_s)\, sh[\gamma_i(z-d_{i-1})] & d_{i-1} < z < d_i \\ a_s e^{-j\tau_s z} + b_s^{(e,h)}(\tau_s)\, e^{j\tau_s z} & z < 0 \end{cases} \tag{A.88}$$

with

$$\tau_s = \sqrt{(\epsilon_{r_s} - \epsilon_{r_c})k_o^2 + s^2}$$

In the functional space of the *form functions* of either surface or radiating wave type, we have defined symmetric and Hermitian inner products as appeared in (A.54) and (A.55), respectively. In a real space there is no differences between these two types of inner products. As stated before, for a lossless MPS, it is always possible to construct a real-valued *form function* for surface waves. Therefore, there is no superiority between the inner products for the surface waves. However, this is not the case for the radiation modes.

The cover and substrate modes defined according to our terminology are complex-valued functions. Mathematically, it is more convenient to define Hermitian inner product (HIP) in a complex linear space. HIP brings the possibility to define *norm* of a complex vector. That is why linear spaces with HIP are called *normed linear spaces*. In an electromagnetic system the concept of norm can be related to the power which is the fundamental physical quantity. Furthermore, in comparison with the HIP, symmetric inner product (SIP) has two disadvantages. In some complex linear spaces such that the SIP defined as a generalized function, a vector may happen to be orthogonal to itself! For example, consider a plane wave in free space with the *form function*

$$F^{(e,h)}(z;s) = e^{-jsz}$$

We now may write

$$\begin{aligned} < F^{(e,h)}(z;s), F^{(e,h)}(z;s) > &= \int_{-\infty}^{\infty} \frac{1}{c^{(e,h)}} e^{-j2sz} dz \\ &= \frac{1}{c^{(e,h)}} \left[\frac{e^{-j2sz}}{-j2s} \right]_{z=-\infty}^{z=\infty} \\ &= 0 \end{aligned}$$

where we have used Theorem A.5.

As will be explained later, for the purposes of normalization and continuous spectrum representation of radiation modes, it is desirable that the degenerate radiation modes defined in (A.87) and (A.88) be orthogonal. This property avoids the Gram-Schmidt process in constructing an orthogonal set which is not an easy task if the inner products are defined in a generalized sense. In the SIP sense, the form functions of two degenerate radiation modes are not orthogonal. This can be seen in the plane wave example stated above. In this case, the two plane waves with the *form functions*

$$F_s^{(e,h)}(z;s) = e^{-jsz}$$

and

$$F_c^{(e,h)}(z;s) = e^{jsz}$$

are degenerate modes. Whereas,

$$< F_s^{(e,h)}(z;s), F_c^{(e,h)}(z;s) >= \frac{2\pi}{c^{(e,h)}} \delta(s) \neq 0$$

However, the HIP of the *form functions* of this two degenerate radiation modes is zero. Therefore, if we only consider the HIP, the non-degenerate condition in the Theorem A.8 can be relaxed and we have the following theorem. theorem is stated as

THEOREM A.9 *Let $F_c^{(e,h)}(z;s_1)$ and $F_s^{(e,h)}(z;s)$ be the form functions of the cover and substrate modes of a lossless MPS, respectively. Then, in the generalized sense, we have*

$$\ll F_c^{(e,h)}(z;s_1), F_s^{(e,h)}(z;s) \gg = 0 \tag{A.89}$$

The above theorem in the case of two degenerate modes is called *Reciprocity Theorem*. The general method used in the proof of Theorem A.6—A.8 is not applicable for this theorem. To prove it, we need to calculate the HIP directly. The proof of the above theorem which in turn necessitates the use of the following lemma is given in Appendix B.10.

LEMMA A.1 *Let f(x) be a monotonic function of x. Then*

$$\delta[f(x) - f(a)] = \frac{1}{|f'(a)|}\delta(x-a) \tag{A.90}$$

We prove this lemma in Appendix B.9

An immediate consequence of the reciprocity theorem is the Brewster theorem which is stated as follows.

THEOREM A.10 BREWSTER THEOREM. *Let a MPS be transparent to a substrate mode, then it is also transparent to the corresponding degenerate cover mode and vice versa.*

The proof of this theorem which is based on the Theorem A.9 is given in Appendix B.11.

Finally, as will be discussed in the next section, the HIP of the *form function* of radiation modes allows us to obtain simple analytical formulas for the normalization of the *form functions*. This is another advantage of HIP in comparison with SIP.

A.8.3 Normalization of the Radiation Modes

So far, we have shown that the introduced set of radiation modes are orthogonal. An interesting problem is how to construct an orthonormal set of radiation modes. That is, how to normalize the radiation modes. This task looks a challenging issue in the literature for many reasons. The most important one is that the norm of the *form function* of a radiation mode is not finite. In fact, due to the oscillatory nature of the radiation field in the substrate or the cover region, a delta function appears in the norm of the *form function*. Therefore, the first important challenge in this issue is the recognition of the delta function. This is the main source of the difficulty in the process of the normalization of the radiation modes. Due to this reason, normalization of the radiation modes seems an overwhelming task in the literature.

As we have mentioned before, the type of the radiation modes we have introduced enjoy interesting properties. This makes their normalization problem much simpler than has been thought before. Moreover, as will be explained later, the type of radiation modes introduced in the literature are linear combination of these fundamental basis functions. According to the Theorem A.9, since there is no cross-coupling between these modes, the principle of superposition of the square of the norms can be used in the normalization of those radiation modes in the literature. However, before that, in the following two theorems we investigate the interesting problem of the normalization of the cover and substrate modes.

THEOREM A.11 *Let* $F_c^{(e,h)}(z;s_1)$ *and* $F_c^{(e,h)}(z;s)$ *be the form functions of two cover modes with radiation parameters* s_1 *and* s*, respectively. Then*

$$\ll F_c^{(e,h)}(z;s_1), F_c^{(e,h)}(z;s) \gg = \frac{2\pi}{c_c^{(e,h)}} |b_c|^2 \delta(s-s_1) \qquad \text{(A.91)}$$

where b_c is the incident amplitude of each cover mode.

THEOREM A.12 *Let $F_s^{(e,h)}(z;s_1)$ and $F_s^{(e,h)}(z;s)$ be the form functions of two substrate modes with radiation parameters s_1 and s, respectively. Then*

$$\ll F_s^{(e,h)}(z;s_1), F_s^{(e,h)}(z;s) \gg = \frac{2\pi}{c_s^{(e,h)}} |a_s|^2 \delta(s - s_1) \tag{A.92}$$

where a_s is the incident amplitude of each substrate mode.

According to the Theorems A.11 and A.12, we have

$$\ll F_c^{(e,h)}(z;s_1), F_c^{(e,h)}(z;s) \gg = \int_{-\infty}^{\infty} \frac{1}{c_c^{(e,h)}} |b_c|^2 e^{-j(s_1 - s)z} dz \tag{A.93}$$

$$\ll F_s^{(e,h)}(z;s_1), F_s^{(e,h)}(z;s) \gg = \int_{-\infty}^{\infty} \frac{1}{c_s^{(e,h)}} |a_s|^2 e^{-j(s_1 - s)z} dz \tag{A.94}$$

Eq. (A.93) implies that the HIP of the *form functions* of the cover modes of a MPS is exactly the same as the HIP of the *form functions* of uniform plane waves propagate in a homogeneous medium with exactly the same properties as the cover region. Eq. (A.94) shows that the same argument may be applied for the substrate modes.

With the necessary background we have provided in the preceding section, the proofs of the above theorems are very straightforward. In Appendix B.12, we prove Theorem A.12 which is more general than Theorem A.11.

At this point the study of radiation modes is completed. Radiation modes have been systematically treated in our approach. For lossless MPSs, this study is completely general and no further development is required. In the rest of this appendix we will only discuss about some applications of our formulation for the radiation modes.

A.8.4 Form Functions of Radiation Modes as a Kernel of an Integral Transform

The purpose of this section is to link the radiation modes with the idea of *integral transform*. More precisely, let us assume that the space of the functions $\Psi^{(e,h)}(u,v,z)$, excluding bound functions in the z direction, satisfy the scalar Helmholtz equation in a MPS. Moreover, assume that all the functions in this space satisfy LSE or LSM type boundary conditions. That is,

$$\nabla_t \Psi^{(e,h)}|_{z=d_i^-} = \nabla_t \Psi^{(e,h)}|_{z=d_i^+} \quad i = 0,1,2,\ldots N$$

$$\frac{1}{c_i^{(e,h)}} \nabla_t \left(\frac{\partial \Psi^{(e,h)}}{\partial z}\right)|_{z=d_i^-} = \frac{1}{c_{i+1}^{(e,h)}} \nabla_t \left(\frac{\partial \Psi^{(e,h)}}{\partial z}\right)|_{z=d_i^+} \quad i = 0,1,2,\ldots N$$

We will show that in this functional space it is possible to define an integral transform by the kernel which is the *form functions* of either substrate or cover modes.

To illustrate the basic idea, we will first show that how the ordinary Fourier transform can be connected to the modal analysis in a homogeneous space. Let $\Psi^{(e,h)}(u,v,z)$ be the Hertzian scalar potential functions in a homogeneous space. These functions can be related to their Fourier transforms as follows

$$\begin{aligned} \Psi^{(e,h)}(u,v,z) &= \sqrt{\frac{c^{(e,h)}}{2\pi}} \int_{-\infty}^{\infty} \tilde{\Psi}^{(e,h)}(u,v,\alpha) e^{-j\alpha z} d\alpha \\ &= \int_{-\infty}^{\infty} \tilde{\Psi}^{(e,h)}(u,v,\alpha) \left(\sqrt{\frac{c^{(e,h)}}{2\pi}} e^{-j\alpha z}\right) d\alpha \end{aligned} \tag{A.95}$$

where $c^e = \epsilon_r$ and $c^h = \mu_r$ are introduced for the purpose of normalization as will be described shortly. If we define the HIP in the space of the kernel of the above transform, we have

$$\begin{aligned} \ll \sqrt{\frac{c^{(e,h)}}{2\pi}} e^{-j\alpha z}, \sqrt{\frac{c^{(e,h)}}{2\pi}} e^{-j\alpha_1 z} \gg &= \int_{-\infty}^{\infty} \frac{1}{c^{(e,h)}} \left(\sqrt{\frac{c^{(e,h)}}{2\pi}} e^{-j\alpha z}\right) \left(\sqrt{\frac{c^{(e,h)}}{2\pi}} e^{-j\alpha_1 z}\right)^* dz \\ &= \delta(\alpha - \alpha_1) \end{aligned} \tag{A.96}$$

Thus, taking the HIP of both sides of (A.95) with $\sqrt{\frac{c^{(e,h)}}{2\pi}}e^{-j\alpha_1 z}$ leads to

$$\ll \Psi^{(e,h)}(u,v,z), \sqrt{\frac{c^{(e,h)}}{2\pi}}e^{-j\alpha_1 z} \gg = \int_{-\infty}^{\infty} \tilde{\Psi}^{(e,h)}(u,v,\alpha) \left(\ll \sqrt{\frac{c^{(e,h)}}{2\pi}}e^{-j\alpha z}, \sqrt{\frac{c^{(e,h)}}{2\pi}}e^{-j\alpha_1 z} \gg \right) d\alpha \tag{A.97}$$

Using (A.96) in (A.97), we obtain

$$\tilde{\Psi}^{(e,h)}(u,v,\alpha_1) = \int_{-\infty}^{\infty} \frac{1}{c^{(e,h)}} \Psi^{(e,h)}(u,v,z) \left(\sqrt{\frac{c^{(e,h)}}{2\pi}}e^{j\alpha_1 z} \right) dz \tag{A.98}$$

The above relation is the inverse Fourier transform of (A.95).

Let us look at (A.95) from another point of view. By a simple change of variable, (A.95) can be rewritten as

$$\begin{aligned} \Psi^{(e,h)}(u,v,z) &= \int_0^{\infty} \tilde{\Psi}^{(e,h)}(u,v,-s) \left(\sqrt{\frac{c^{(e,h)}}{2\pi}}e^{jsz} \right) ds \\ &+ \int_0^{\infty} \tilde{\Psi}^{(e,h)}(u,v,s) \left(\sqrt{\frac{c^{(e,h)}}{2\pi}}e^{-jsz} \right) ds \end{aligned} \tag{A.99}$$

Now in this homogeneous space, we define the cover modes with the normalized *form functions* as

$$\tilde{F}_c^{(e,h)}(z;s) = \sqrt{\frac{c^{(e,h)}}{2\pi}}e^{jsz} \tag{A.100}$$

By a cover mode, we mean a plane wave incident from $z = \infty$. We note that since the medium is homogeneous there is no reflected wave in the cover mode. Similarly, it is possible to define the substrate modes with the normalized *form functions* as

$$\tilde{F}_s^{(e,h)}(z;s) = \sqrt{\frac{c^{(e,h)}}{2\pi}}e^{-jsz} \tag{A.101}$$

By a substrate mode, we mean a plane wave incident from $z = -\infty$. Eq. (A.99) can be interpreted as expressing $\Psi^{(e,h)}(u,v,z)$ in terms of a continuous spectrum of

the cover and substrate modes. Therefore,

$$\Psi^{(e,h)}(u,v,z) = \int_0^\infty A_c^{(e,h)}(u,v,s)\check{F}_c^{(e,h)}(z;s)ds + \int_0^\infty A_s^{(e,h)}(u,v,s)\check{F}_s^{(e,h)}(z;s)ds \tag{A.102}$$

where

$$A_c^{(e,h)}(u,v,s) = \bar{\Psi}^{(e,h)}(u,v,-s) \qquad (s>0) \tag{A.103}$$

$$A_s^{(e,h)}(u,v,s) = \bar{\Psi}^{(e,h)}(u,v,s) \qquad (s>0) \tag{A.104}$$

According to our theory, substrate and cover modes are orthogonal. That is,

$$\begin{aligned} \ll \check{F}_c^{(e,h)}(z;s), \check{F}_s^{(e,h)}(z;s_1) \gg &= \int_{-\infty}^{\infty} \frac{1}{c^{(e,h)}} \left(\sqrt{\frac{c^{(e,h)}}{2\pi}} e^{jsz}\right) \left(\sqrt{\frac{c^{(e,h)}}{2\pi}} e^{-js_1 z}\right)^* dz \\ &= \frac{1}{2\pi}\int_{-\infty}^{\infty} e^{j(s+s_1)z}dz \\ &= 0 \end{aligned} \tag{A.105}$$

Moreover, we have

$$\ll \check{F}_c^{(e,h)}(z;s), \check{F}_c^{(e,h)}(z;s_1) \gg = \ll \check{F}_s^{(e,h)}(z;s), \check{F}_s^{(e,h)}(z;s_1) \gg = \delta(s-s_1) \tag{A.106}$$

Therefore, using (A.105) and (A.106), from (A.102), one may obtain

$$A_c^{(e,h)}(u,v,s_1) = \ll \Psi^{(e,h)}(u,v,z), \check{F}_c^{(e,h)}(z;s_1) \gg \tag{A.107}$$

$$A_s^{(e,h)}(u,v,s_1) = \ll \Psi^{(e,h)}(u,v,z), \check{F}_s^{(e,h)}(z;s_1) \gg \tag{A.108}$$

Now let us consider a MPS. An arbitrary scalar Hertzian potential in this structure can be represented by a continuous spectrum of the cover and substrate modes as in (A.102). In this case $\check{F}_c^{(e,h)}(z;s)$ and $\check{F}_s^{(e,h)}(z;s)$ must be interpreted as the *form functions* of the cover and substrate modes, respectively. Eq. (A.102) can be rewritten as

$$\Psi^{(e,h)}(u,v,z) = \int_{-\infty}^0 A_c^{(e,h)}(u,v,-\alpha)\check{F}_c^{(e,h)}(z;-\alpha)d\alpha + \int_0^\infty A_s^{(e,h)}(u,v,\alpha)\check{F}_s^{(e,h)}(z;\alpha)d\alpha \tag{A.109}$$

Let us define an integral transform defined by the equation

$$\Psi^{(e,h)}(u,v,z) = \int_{-\infty}^{\infty} \widehat{\Psi}^{(e,h)}(u,v,\alpha)\Re^{(e,h)}(z;\alpha)d\alpha \tag{A.110}$$

where

$$\Re^{(e,h)}(z;\alpha) = \begin{cases} \tilde{F}_s^{(e,h)}(z;\alpha) & \alpha > 0 \\ \tilde{F}_c^{(e,h)}(z;-\alpha) & \alpha < 0 \end{cases} \tag{A.111}$$

With the above choice of the kernel, the inverse transform is

$$\widehat{\Psi}^{(e,h)}(u,v,\alpha_1) = \begin{cases} A_s^{(e,h)}(u,v,\alpha_1) & \alpha_1 > 0 \\ A_c^{(e,h)}(u,v,-\alpha_1) & \alpha_1 < 0 \end{cases} \tag{A.112}$$

It is also possible to choose the kernel as

$$\Re^{(e,h)}(z;\alpha) = \begin{cases} \tilde{F}_c^{(e,h)}(z;\alpha) & \alpha > 0 \\ \tilde{F}_s^{(e,h)}(z;-\alpha) & \alpha < 0 \end{cases} \tag{A.113}$$

For this choice, we have

$$\widehat{\Psi}^{(e,h)}(u,v,\alpha_1) = \begin{cases} A_c^{(e,h)}(u,v,\alpha_1) & \alpha_1 > 0 \\ A_s^{(e,h)}(u,v,-\alpha_1) & \alpha_1 < 0 \end{cases} \tag{A.114}$$

In either case, the inverse transform is

$$\widehat{\Psi}^{(e,h)}(u,v,\alpha_1) = \ll \Psi^{(e,h)}(u,v,z), \Re^{(e,h)}(u,v,\alpha_1) \gg \tag{A.115}$$

A.8.5 Radiation Modes With Real-Valued Form Functions

The *form functions* of the radiation modes defined in the preceding sections are the simplest and the most appropriate basis functions that span the z-dependent part of the radiation field. As illustrated before, these basis functions are orthogonal and enjoy interesting properties which make their normalization a trivial matter.

Therefore, constructing an orthonormal set of basis functions for a typical lossless MPS is not a big deal. In the preceding section, we have shown that how to construct more general solutions from these building blocks.

We have introduced these basis functions from the complex-valued solutions of the differential equation in (A.28). It is also possible to start from the real-valued solutions. This approach is used in the literature. If we consider it as the starting point, we encounter some difficulty in constructing orthonormal complete basis functions. This makes their study a challenging issue. However, an attempt to construct these real-valued solutions by superposing the complex-valued degenerate solutions leads to very interesting results and more insight in their development.

For substrate modes of type I, degeneracy happens only within a multiplicative constant. On the other hand, there must be real-valued solutions for this type of modes. Therefore, one might expect the possibility of obtaining real-valued solutions from complex exponential solutions. In fact, this is the case. To show this matter, let us consider a substrate mode of type I with the *form function* of unit incident amplitude as follows

$$\bar{F}_{s_I}^{(e,h)}(z;s) = \begin{cases} T_{s_I}(s)^{(e,h)}(s)\, e^{-\gamma_c(z-d_N)} & z > d_N \\ A_i^{(e,h)}(s)\, ch[\gamma_i(z-d_{i-1})] + B_i^{(e,h)}(s)\, sh[\gamma_i(z-d_{i-1})] & d_{i-1} < z < d_i \\ e^{-jsz} + R_{s_I}^{(e,h)}(s)\, e^{jsz} & z < 0 \end{cases} \tag{A.116}$$

where $R_{s_I}^{(e,h)}(s)$ and $T_{s_I}(s)^{(e,h)}(s)$ are called the *reflection* and *transmission* functions of the substrate mode of type I. $R_{s_I}^{(e,h)}(s)$ can be obtained from (B.47) in Appendix B.5. It can be seen that for the substrate mode of type I, we have

$$R_{s_I}^{(e,h)}(s) = -\frac{\left[D^{(e,h)}(s)\right]^*}{D^{(e,h)}(s)} \tag{A.117}$$

Let

$$F_{s_I}^{(e,h)}(z;s) = -ja_s\bar{F}_{s_I}^{(e,h)}(z;s) \tag{A.118}$$

If one chooses

$$a_s = D^{(e,h)}(s) \tag{A.119}$$

one obtains

$$b_s^{(e,h)}(s) = R_{s_I}^{(e,h)}(s)a_s = -a_s^* \tag{A.120}$$

where $b_s^{(e,h)}(s)$ is the coefficient of e^{jsz} in the substrate. With this choice, it can be easily seen that

$$\begin{aligned} a_s e^{-jsz} + b_s^{(e,h)}(s)\, e^{jsz} &= [a_s + b_s^{(e,h)}(s)]cos(sz) + j[-a_s + b_s^{(e,h)}(s)]sin(sz) \\ &= j2\,\mathrm{Im}\{a_s\}cos(sz) - j2\,\mathrm{Re}\{a_s\}sin(sz) \end{aligned} \tag{A.121}$$

where $\mathrm{Re}\{\cdot\}$ and $\mathrm{Im}\{\cdot\}$ stand for the real and imaginary parts of a complex number, respectively. Therefore, according to (A.118) the *form function* in the substrate is real. Since this is the case, by using the transfer matrix method it can be shown that the *form function* in the cover and in the other layers is also real. Now if one starts from the real solution, one obtains

$$\mathcal{F}_s^{(e,h)}(z;s) = \begin{cases} a_c^{(e,h)}(s)\, e^{-\gamma_c(z-d_N)} & z > d_N \\ A_i^{(e,h)}(s)\, ch[\gamma_i(z-d_{i-1})] + B_i^{(e,h)}(s)\, sh[\gamma_i(z-d_{i-1})] & d_{i-1} < z < d_i \\ A_s^{(e,h)}(s)cos(sz) + B_s^{(e,h)}(s)sin(sz) & z < 0 \end{cases} \tag{A.122}$$

In the literature, radiation modes with the *form functions* in (A.122) are called substrate radiation modes. The reason for this terminology is the oscillatory behavior of the electromagnetic fields in the substrate as illustrated in Fig. A.6. Comparing (A.122) with (A.121) leads to

$$A_s^{(e,h)} = a_s\left[1 + R_s^{(e,h)}(s)\right] \tag{A.123a}$$

$$B_s^{(e,h)}(s) = ja_s\left[-1 + R_s^{(e,h)}(s)\right] \tag{A.123b}$$

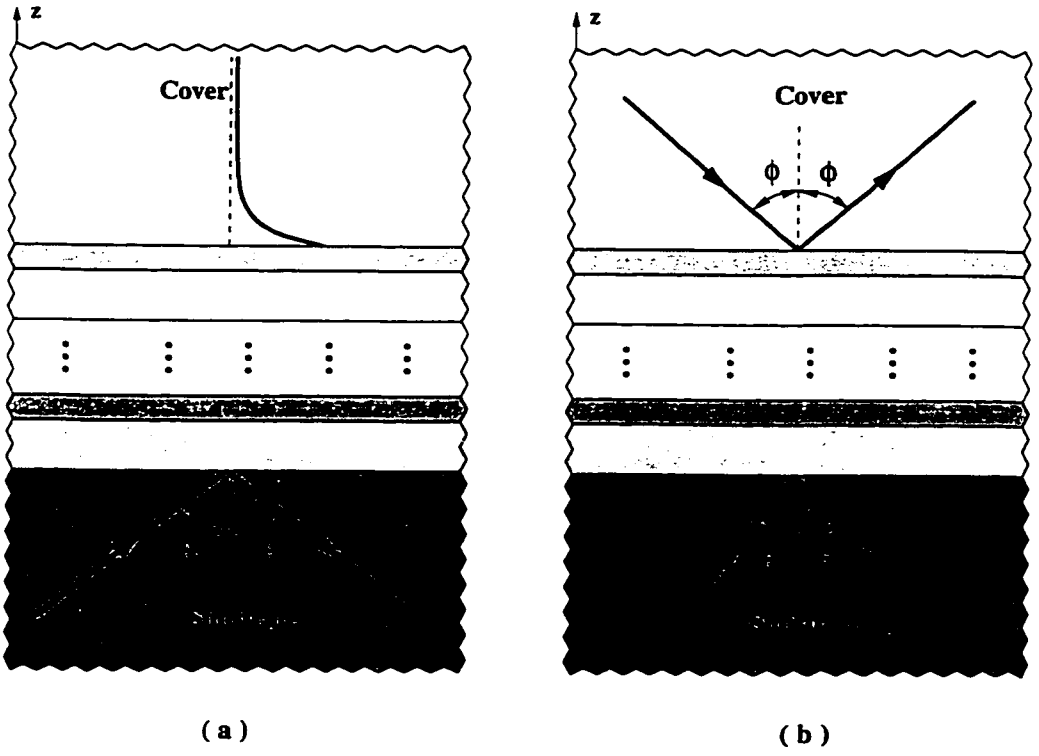

Figure A.6: Radiation modes: (a) Substrate modes. (b) Substrate-cover modes.

Therefore, substrate modes correspond to the substrate modes of the first type according to (A.123). In substrate modes of the first type there is only one degree of freedom, that is, a_s can be chosen arbitrarily. Thus, for substrate modes there is also one degree of freedom.

If we choose $A_s^{(e,h)}$ arbitrarily, $B_s^{(e,h)}(s)$ can be obtained from $A_s^{(e,h)}$ via the following relation

$$B_s^{(e,h)}(s) = j\frac{R_s^{(e,h)}(s)-1}{R_s^{(e,h)}(s)+1}A_s^{(e,h)} \tag{A.124}$$

Note also that $B_s^{(e,h)}(s)$ can be obtained from $A_s^{(e,h)}$ by using the following matrix

equation

$$\mathbf{T}^{(e,h)}(s)\begin{bmatrix}0\\ s\end{bmatrix}B_s^{(e,h)}(s)-\begin{bmatrix}1\\ -\gamma_c\end{bmatrix}a_c^{(e,h)}(s)=-\mathbf{T}^{(e,h)}(s)\begin{bmatrix}1\\ 0\end{bmatrix}A_s^{(e,h)} \qquad \text{(A.125)}$$

Since the coefficient matrix in (A.125) is real $B_s^{(e,h)}(s)$ should be real if $A_s^{(e,h)}$ is chosen real. This consideration leads to the fact that the coefficient of $A_s^{(e,h)}$ in (A.124) must be real for substrate modes of the first type. From (A.123), substrate modes in the literature are substrate modes of the first type, according to our terminology, with

$$a_s=\frac{A_s^{(e,h)}+jB_s^{(e,h)}(s)}{2} \qquad \text{(A.126)}$$

Therefore, these modes are orthogonal.

Orthogonality of the substrate modes can be proved directly, if one uses (A.77). Since substrate modes are real-valued function, we have

$$<\mathcal{F}_s^{(e,h)}(s),\mathcal{F}_s^{(e,h)}(s)>=\ll\mathcal{F}_s^{(e,h)}(s),\mathcal{F}_s^{(e,h)}(s)\gg \qquad \text{(A.127)}$$

Moreover,

$$\begin{aligned}\ll\mathcal{F}_s^{(e,h)}(s),\mathcal{F}_s^{(e,h)}(s)\gg &= \frac{2\pi}{c^{(e,h)}}|a_s|^2\delta(s-s)\\ &= \frac{\pi}{2}\left(|A_s^{(e,h)}(s|^2+|B_s^{(e,h)}(s|^2\right)\delta(s-s) \qquad \text{(A.128)}\end{aligned}$$

Note that (A.128) can be obtained from the integral formulas given in Appendix B.15.

It is also possible to combine two degenerate cover and substrate modes such that the *form function* of the resulting mode be real. This leads to the concept of *conjugate modes* which is defined as follows.

DEFINITION A.2 *Two degenerate cover and substrate modes are called conjugate modes, if the form function of their superposition is real.*

As we have seen before, in a symmetric MPS the cover and substrate modes that have been introduced according to our terminology are not symmetric. This is due to the fact that the degeneracy of the radiation modes does not happen within a multiplicative factor. However, by proper linear combinations of the cover and substrate modes, it is possible to make symmetric or asymmetric modes in a symmetric MPS. Now let us see how to construct *conjugate modes*. To this end, consider two degenerate cover and substrate modes with the *form functions* of unit incident amplitudes as follows

$$\bar{F}_c^{(e,h)}(z;s) = \begin{cases} e^{js(z-d_N)} + R_c^{(e,h)}(s)\, e^{-js(z-d_N)} & z > d_N \\ A_i^{(e,h)}(s)\, ch[\gamma_i(z-d_{i-1})] + B_i^{(e,h)}(s)\, sh[\gamma_i(z-d_{i-1})] & d_{i-1} < z < d_i \\ T_c^{(e,h)}(s)\, e^{js_2 z} & z < 0 \end{cases} \tag{A.129}$$

$$\bar{F}_s^{(e,h)}(z;s_2) = \begin{cases} T_s^{(e,h)}(s_2)\, e^{-js(z-d_N)} & z > d_N \\ A_i^{(e,h)}(s_2)\, ch[\gamma_i(z-d_{i-1})] + B_i^{(e,h)}(s_2)\, sh[\gamma_i(z-d_{i-1})] & d_{i-1} < z < d_i \\ e^{-js_2 z} + R_s^{(e,h)}(s_2)\, e^{js_2 z} & z < 0 \end{cases} \tag{A.130}$$

$R_c^{(e,h)}(s)$ and $R_s^{(e,h)}(s_2)$ are called the *reflection functions* of the cover and substrate modes, respectively. $T_c^{(e,h)}(s)$ and $T_s^{(e,h)}(s_2)$ are called the *transmission functions* of the cover and substrate modes, respectively. Let $\mathcal{F}_{s-c}^{(e,h)}(z;s)$ be the *form function* a linear combination of these two modes. That is,

$$\mathcal{F}_{s-c}^{(e,h)}(z;s) = a_s \bar{F}_s^{(e,h)}(z;s_2) + b_c \bar{F}_c^{(e,h)}(z;s) \tag{A.131}$$

Therefore,

$$\mathcal{F}_{s-c}^{(e,h)}(z;s) = \begin{cases} A_c^{(e,h)}(s) cos\,[s(z-d_N)] + B_c^{(e,h)}(s)\, sin\,[s(z-d_N)] & z > d_N \\ U_i^{(e,h)}(s)\, ch[\gamma_i(z-d_{i-1})] + V_i^{(e,h)}(s)\, sh[\gamma_i(z-d_{i-1})] & d_{i-1} < z < d_i \\ A_s^{(e,h)}(s) cos\,(s_2 z) + B_s^{(e,h)}(s)\, sin\,(s_2 z) & z < 0 \end{cases} \tag{A.132}$$

where

$$A_c^{(e,h)}(s) = T_s^{(e,h)}(s_2)a_s + \left[1 + R_c^{(e,h)}(s)\right] b_c \tag{A.133a}$$

$$B_c^{(e,h)}(s) = -jT_s^{(e,h)}(s_2)a_s + j\left[1 - R_c^{(e,h)}(s)\right] b_c \tag{A.133b}$$

$$A_s^{(e,h)}(s) = \left[R_s{}^{(e,h)}(s_2) + 1\right] a_s + T_c^{(e,h)}(s)b_c \tag{A.133c}$$

$$B_s^{(e,h)}(s) = j\left[R_s{}^{(e,h)}(s_2) - 1\right] a_s + jT_c^{(e,h)}(s)b_c \tag{A.133d}$$

Moreover,

$$U_i^{(e,h)}(s) = a_s\, A_i^{(e,h)}(s_2) + b_c\, A_i^{(e,h)}(s) \tag{A.134a}$$

$$V_i^{(e,h)}(s) = a_s\, B_i^{(e,h)}(s_2) + b_c\, B_i^{(e,h)}(s) \tag{A.134b}$$

Note that s and s_2 are not independent. They are related to each other through

$$s_2 = \sqrt{(\epsilon_{r_s}\mu_{r_s} - \epsilon_{r_c}\mu_{r_c})k_o^2 + s^2} \tag{A.135}$$

Radiation modes with the *form functions* as expressed in (A.132) are called substrate-cover modes. As shown in Fig. A.6(b), the oscillatory nature of the field in the substrate and the cover calls for this terminology which is adopted in the literature. The fields both in the substrate and in the cover are of the standing wave type. Note that we consider s, the corresponding radiation parameter of the cover mode, as the radiation parameter of substrate-cove mode. In constructing of substrate-cover modes there are two degrees of freedom, that is, a_s and b_c can be chosen arbitrarily. Each pair of a_s and b_c uniquely determines a substrate-cover mode. Therefore, in order to catch this pair, one might expect that in constructing these modes by using (A.132), any two coefficient can be chosen arbitrarily. In fact, this is the case as can be seen from (A.133). a_s and b_s are uniquely defined in terms of any pairs of coefficients on the left hand sides of (A.133). It is also possible to choose any pair of coefficients defined in (A.134) as an independent variables. However, it is useful to choose a pair of coefficients in (A.133) arbitrarily.

Let $A_s^{(e,h)}$ and $B_s^{(e,h)}$ be chosen arbitrarily. Thus from (A.133c) and (A.133d), we have

$$a_s = \frac{1}{2}A_s^{(e,h)} + \frac{j}{2}B_s^{(e,h)} \tag{A.136a}$$

$$b_c = \frac{1 - R_s^{(e,h)}(s_2)}{2T_c^{(e,h)}(s)}A_s^{(e,h)} - j\frac{1 + R_s^{(e,h)}(s_2)}{2T_c^{(e,h)}(s)}B_s^{(e,h)} \tag{A.136b}$$

If one uses (A.136a) and (A.136b) to substitute for a_s and b_c in (A.133a) and (A.133b), one may write

$$\begin{aligned} A_c^{(e,h)}(s) = &\frac{T_c^{(e,h)}(s)T_s^{(e,h)}(s_2) + \left[1 + R_c^{(e,h)}(s)\right]\left[1 - R_s^{(e,h)}(s_2)\right]}{2T_c^{(e,h)}(s)}A_s^{(e,h)} \\ &+j\frac{T_c^{(e,h)}(s)T_s^{(e,h)}(s_2) - \left[1 + R_c^{(e,h)}(s)\right]\left[1 + R_s^{(e,h)}(s_2)\right]}{2T_c^{(e,h)}(s)}B_s^{(e,h)} \end{aligned} \tag{A.137a}$$

$$\begin{aligned} B_c^{(e,h)}(s) = &j\frac{\left[1 - R_c^{(e,h)}(s)\right]\left[1 - R_s^{(e,h)}(s_2)\right] - T_c^{(e,h)}(s)T_s^{(e,h)}(s_2)}{2T_c^{(e,h)}(s)}A_s^{(e,h)} \\ &+\frac{\left[1 - R_c^{(e,h)}(s)\right]\left[1 + R_s^{(e,h)}(s_2)\right] + T_c^{(e,h)}(s)T_s^{(e,h)}(s_2)}{2T_c^{(e,h)}(s)}B_s^{(e,h)} \end{aligned} \tag{A.137b}$$

Note also that $A_c^{(e,h)}(s)$ and $B_c^{(e,h)}(s)$ can be obtained from $A_s^{(e,h)}$ and $B_s^{(e,h)}(s)$ by using the following matrix equation

$$\begin{bmatrix} 1 \\ 0 \end{bmatrix} A_c^{(e,h)}(s) + \begin{bmatrix} 0 \\ s \end{bmatrix} B_c^{(e,h)}(s) = \mathbf{T}^{(e,h)}(s)\left(\begin{bmatrix} 1 \\ 0 \end{bmatrix} A_s^{(e,h)} + \begin{bmatrix} 0 \\ s_2 \end{bmatrix} B_s^{(e,h)}\right) \tag{A.138}$$

If real values are chosen for $A_s^{(e,h)}$ and $B_s^{(e,h)}$, $A_c^{(e,h)}(s)$ and $B_c^{(e,h)}(s)$ should be real. This is due to the fact that the coefficient matrices in (A.138) are real-valued matrices. Therefore, the coefficient of $A_s^{(e,h)}$ and $B_s^{(e,h)}$ in (A.137a) and (A.137b) must be real.

For conjugate modes the amplitudes on the left hand sides of equations in (A.133) are real. This means that the amplitudes of the total response in cover or substrate region are complex conjugates of the amplitudes of excitation in the

respective regions. That is why we use the conjugate mode terminology. For example, from (A.133a) and (A.133b) one may argue that $T_s^{(\epsilon,h)}(s_2)a_s + R_c^{(\epsilon,h)}(s)b_c$ is the complex conjugate of b_c.

Orthogonality of substrate-cover modes can be proved directly by using (A.77). This result can also be obtained from the fact that they are superposition of two degenerate cover and substrate modes. Moreover, since the *form functions* of substrate-cover modes are real-valued functions, we have

$$< \mathcal{F}_{s-c}^{(\epsilon,h)}(z;s_a), \mathcal{F}_{s-c}^{(\epsilon,h)}(z;s_b) >=\ll \mathcal{F}_{s-c}^{(\epsilon,h)}(z;s_a), \mathcal{F}_{s-c}^{(\epsilon,h)}(z;s_b) \gg \tag{A.139}$$

Let

$$\mathcal{F}_{(s-c)1}^{(\epsilon,h)}(z;s) = b_{c_1}\bar{F}_c^{(\epsilon,h)}(z;s) + a_{s_1}\bar{F}_s^{(\epsilon,h)}(z;s_2) \tag{A.140a}$$

$$\mathcal{F}_{(s-c)2}^{(\epsilon,h)}(z;s) = b_{c_2}\bar{F}_c^{(\epsilon,h)}(z;s) + a_{s_2}\bar{F}_s^{(\epsilon,h)}(z;s_2) \tag{A.140b}$$

then, we have

$$\begin{aligned} \ll \mathcal{F}_{(s-c)1}^{(\epsilon,h)}(z;s), \mathcal{F}_{(s-c)2}^{(\epsilon,h)}(z;s_a) \gg &= \ll b_{c_1}\bar{F}_c^{(\epsilon,h)}(z;s), b_{c_2}\bar{F}_c^{(\epsilon,h)}(z;s_a) \gg + \\ &\quad \ll a_{s_1}\bar{F}_s^{(\epsilon,h)}(z;s_2), a_{s_2}\bar{F}_s^{(\epsilon,h)}(z;s_{2_a}) \gg \\ &= \frac{2\pi b_{c_1}b_{c_2}^*}{c^{(\epsilon,h)}}\delta(s-s_a) + \frac{2\pi a_{s_1}a_{s_2}^*}{c^{(\epsilon,h)}}\delta(s_2-s_{2_a}) \\ &= \frac{2\pi}{c^{(\epsilon,h)}}(b_{c_1}b_{c_2}^* + \frac{s_{2_a}}{s_a}a_{s_1}a_{s_2}^*)\delta(s-s_a) \end{aligned} \tag{A.141}$$

where we have used Lemma A.1. From (A.133a) and (A.133b), we obtain

$$b_c = \frac{1}{2}A_c^{(\epsilon,h)} - j\frac{1}{2}B_c^{(\epsilon,h)} \tag{A.142}$$

Therefore, using (A.136a) and (A.142) in (A.141), we have

$$\ll \mathcal{F}_{(s-c)1}^{(\epsilon,h)}(z;s), \mathcal{F}_{(s-c)2}^{(\epsilon,h)}(z;s_a) \gg = P_{12}^{(\epsilon,h)}\delta(s-s_a) \tag{A.143}$$

where

$$P_{12}^{(e,h)} = \frac{\pi}{2c^{(e,h)}}\left[\frac{s_{1a}}{s_a}(A_{c_1}^{(e,h)}A_{c_2}^{(e,h)} + B_{c_1}^{(e,h)}B_{c_2}^{(e,h)}) + A_{s_1}^{(e,h)}A_{s_2}^{(e,h)} + B_{s_1}^{(e,h)}B_{s_2}^{(e,h)}\right] \quad \text{(A.144)}$$

Note that since the LHS of (A.143) is real, the coefficient of the delta function in (A.143) must also be real. Therefore, when this coefficient is expressed in terms of A's and B's the imaginary parts must vanish. It should be emphasized that (A.143) and (A.144) can also be derived from the integral formulas in Appendix B.15.

Let us see how to construct an arbitrary Hertzian scalar potential function of the radiation field in terms of the substrate and substrate-cover modes. To this end, (A.102) can be rewritten as

$$\Psi^{(e,h)}(u,v,z) = \int_0^\infty A_c^{(e,h)}(u,v,s)\check{F}_c^{(e,h)}(z;s)ds + \int_0^\infty A_s^{(e,h)}(u,v,s_2)\check{F}_s^{(e,h)}(z;s_2)ds_2 \quad \text{(A.145)}$$

where $\check{F}_c^{(e,h)}(z;s)$ and $\check{F}_s^{(e,h)}(z;s_2)$ are the normalized *form functions* of the cover and substrate modes, respectively. Let

$$s_2 = \sqrt{a^2 + s^2} \quad \text{(A.146)}$$

where

$$a^2 = (\mu_{r_s}\epsilon_{r_s} - \mu_{r_c}\epsilon_{r_c})k_o^2$$

Using (A.146) in (A.145), we obtain

$$\begin{aligned}\Psi^{(e,h)}(u,v,z) &= \int_0^\infty \left[A_c^{(e,h)}(u,v,s)\check{F}_c^{(e,h)}(z;s) + \frac{s}{s_2}A_s^{(e,h)}(u,v,s_2)\check{F}_s^{(e,h)}(z;s_2)\right]ds \\ &+ \int_0^a A_s^{(e,h)}(u,v,s)\check{F}_{s_I}^{(e,h)}(z;s_2)ds_2 \quad \text{(A.147)}\end{aligned}$$

Now

$$\check{F}_{s_I}^{(e,h)}(z;s_2) = \sqrt{\frac{c_s^{(e,h)}}{2\pi}}\bar{F}_{s_I}^{(e,h)}(z;s_2) = j\frac{1}{D^{(e,h)}(s_2)}\sqrt{\frac{c_s^{(e,h)}}{2\pi}}\mathcal{F}_s^{(e,h)}(z;s_2) \quad \text{(A.148)}$$

Thus, $\check{F}_{s_I}^{(e,h)}(z;s_2)$ can be expressed in terms of the substrate modes.

For each value of s, it is also possible to express $\check{F}_c^{(e,h)}(z;s)$ and $\check{F}_s^{(e,h)}(z;s_2)$ in terms of the substrate-cover modes. More precisely, it is possible to extract $\check{F}_c^{(e,h)}(z;s)$ and $\check{F}_s^{(e,h)}(z;s_2)$ from two independent substrate-cover modes. By independent, we mean that two modes do not differ within a multiplicative constant. Let

$$\begin{bmatrix} a_{s_1} & b_{c_1} \\ a_{s_2} & b_{c_2} \end{bmatrix} \begin{bmatrix} \bar{F}_s^{(e,h)}(z;s_2) \\ \bar{F}_c^{(e,h)}(z;s) \end{bmatrix} = \begin{bmatrix} \mathcal{F}_{(s-c)1}^{(e,h)}(z;s) \\ \mathcal{F}_{(s-c)2}^{(e,h)}(z;s) \end{bmatrix} \tag{A.149}$$

In order to obtain $\bar{F}_c^{(e,h)}(z;s)$ and $\bar{F}_s^{(e,h)}(z;s_2)$ in terms of $\mathcal{F}_{(s-c)1}^{(e,h)}(z;s)$ and $\mathcal{F}_{(s-c)2}^{(e,h)}(z;s)$ the determinant of the coefficient matrix in (A.149) must be nonzero. This in turn means that

$$\mathcal{F}_{(s-c)1}^{(e,h)}(z;s) \neq K\mathcal{F}_{(s-c)2}^{(e,h)}(z;s) \tag{A.150}$$

Eq. (A.150) implies that

$$\frac{A_{s_1}^{(e,h)}}{A_{s_2}^{(e,h)}} \neq \frac{B_{s_1}^{(e,h)}}{B_{s_2}^{(e,h)}} \tag{A.151}$$

Therefore, if (A.151) holds, from (A.149), we have

$$\begin{bmatrix} \bar{F}_s^{(e,h)}(z;s_2) \\ \bar{F}_c^{(e,h)}(z;s) \end{bmatrix} = \frac{1}{a_{s_1}b_{c_2} - a_{s_2}b_{c_1}} \begin{bmatrix} b_{c_2} & -b_{c_1} \\ -a_{s_2} & a_{s_1} \end{bmatrix} \begin{bmatrix} \mathcal{F}_{(s-c)1}^{(e,h)}(z;s) \\ \mathcal{F}_{(s-c)2}^{(e,h)}(z;s) \end{bmatrix} \tag{A.152}$$

where

$$a_{s_i} = \frac{1}{2}A_{s_i}^{(e,h)} + j\frac{1}{2}B_{s_i}^{(e,h)} \qquad (i=1,2) \tag{A.153a}$$

$$b_{c_i} = \frac{1}{2}A_{c_i}^{(e,h)} - j\frac{1}{2}B_{c_i}^{(e,h)} \qquad (i=1,2) \tag{A.153b}$$

Thus, for each value of s, we may obtain $\bar{F}_s^{(e,h)}(z;s_2)$ and $\bar{F}_c^{(e,h)}(z;s)$ from two independent substrate-cover modes through (A.152) and (A.153).

In constructing substrate-cover modes there are two degrees of freedom, e.g., $A_s^{(e,h)}$ and $B_s^{(e,h)}$. If condition (A.151) holds, the two substrate-cover modes are

independent. However, we can put additional constraint on A_s's and B_s's. These constraints are just only a matter of convenience. It is highly desirable that the two substrate-cover modes be orthogonal. To this end, referring to (A.141) or (A.143) and (A.144), the condition for orthogonality is

$$b_{c_1} b^*_{c_2} + \frac{s_2}{s} a_{s_1} a^*_{s_2} = 0 \tag{A.154}$$

or equivalently,

$$A^{(e,h)}_{c_1} A^{(e,h)}_{c_2} + B^{(e,h)}_{c_1} B^{(e,h)}_{c_2} + \frac{s_2}{s}(A^{(e,h)}_{s_1} A^{(e,h)}_{s_2} + B^{(e,h)}_{s_1} B^{(e,h)}_{s_2}) = 0 \tag{A.155}$$

Consequently, orthogonal substrate-cover modes can be constructed by imposing (A.155).

After choosing $A^{(e,h)}_{s_1}$, $B^{(e,h)}_{s_1}$, $A^{(e,h)}_{s_2}$, ans $B^{(e,h)}_{s_2}$ these modes can be normalized according to (A.143) and (A.144). Assume that $\check{\mathcal{F}}^{(e,h)}_{(s-c)1}(z;s)$ and $\check{\mathcal{F}}^{(e,h)}_{(s-c)2}(z;s)$ be two normalized orthogonal substrate-cover modes. Substituting back into (A.152), let

$$\begin{bmatrix} \bar{F}^{(e,h)}_s(z;s_2) \\ \bar{F}^{(e,h)}_c(z;s) \end{bmatrix} = \begin{bmatrix} K^{(e,h)}_{s1}(s) & K^{(e,h)}_{s2}(s) \\ K^{(e,h)}_{c1}(s) & K^{(e,h)}_{c2}(s) \end{bmatrix} \begin{bmatrix} \check{\mathcal{F}}^{(e,h)}_{(s-c)1}(z;s) \\ \check{\mathcal{F}}^{(e,h)}_{(s-c)2}(z;s) \end{bmatrix} \tag{A.156}$$

Now if we use

$$\check{F}^{(e,h)}_s(z;s_2) = \sqrt{\frac{c^{(e,h)}_s}{2\pi}} \bar{F}^{(e,h)}_s(z;s_2) \tag{A.157a}$$

$$\check{F}^{(e,h)}_c(z;s) = \sqrt{\frac{c^{(e,h)}_c}{2\pi}} \bar{F}^{(e,h)}_c(z;s) \tag{A.157b}$$

then substituting (A.148) into (A.147) leads to the construction of an arbitrary Hertzian scalar potential function of the radiation field with substrate and substrate-cover modes. Note how this idea is closely related to the Fourier transform of sine and cosine type.

In a symmetric MPS, as one might expect that there is no substrate mode. However, we may think of the possibility of symmetric and asymmetric substrate-cover modes as two orthogonal modes. As we will show shortly, there is such a possibility. However, before that we define a class of MPSs more general than symmetric ones, the so-called *quasi-symmetric* MPSs.

DEFINITION A.3 *A MPS is called quasi-symmetric if the cover and substrate are identical. That is,*

$$c_c^{(\epsilon,h)} = c_s^{(\epsilon,h)} \tag{A.158}$$

THEOREM A.13 *In a lossless quasi-symmetric MPS we have*

$$T_s^{(\epsilon,h)}(s) = T_c^{(\epsilon,h)}(s) \tag{A.159a}$$

$$|R_s^{(\epsilon,h)}(s)| = |R_c^{(\epsilon,h)}(s)| \tag{A.159b}$$

(A.159c)

Note that the above theorem does not require the layers in the stack be symmetric. The details of the proof are given in Appendix B.13.

THEOREM A.14 *Let the* $\mathbf{T}^{(\epsilon,h)}(s)$ *be the transfer matrix of a lossless symmetric MPS such that*

$$\mathbf{T}^{(\epsilon,h)}(s) = \begin{bmatrix} t_{11}^{(\epsilon,h)}(s) & t_{12}^{(\epsilon,h)}(s) \\ t_{21}^{(\epsilon,h)}(s) & t_{22}^{(\epsilon,h)}(s) \end{bmatrix} \tag{A.160}$$

Then we have

$$t_{11}^{(\epsilon,h)}(s) = t_{22}^{(\epsilon,h)}(s) \tag{A.161}$$

To prove the above theorem, we take advantage of an interesting property of symmetric MPSs. For complete proof of this theorem see Appendix B.14.

After stating the above theorems we explain how to construct symmetric and asymmetric substrate-cover modes in a symmetric MPS. First, we note that for a symmetric MPS, we have

$$T_s^{(e,h)}(s) = T_c^{(e,h)}(s) = \hat{T}^{(e,h)}(s) \tag{A.162a}$$

$$R_s^{(e,h)}(s) = R_c^{(e,h)}(s) = \hat{R}^{(e,h)}(s) \tag{A.162b}$$

Now a symmetric *form function* results if the MPS is excited symmetrically, that is, if

$$a_s = b_c \tag{A.163}$$

Now under symmetric excitation, the equations (A.133) reduce to

$$A_c^{(e,h)}(s) = \left[1 + \hat{T}^{(e,h)}(s) + \hat{R}^{(e,h)}(s)\right] a_s \tag{A.164a}$$

$$B_c^{(e,h)}(s) = j\left[1 - \hat{T}^{(e,h)}(s) - \hat{R}^{(e,h)}(s)\right] a_s \tag{A.164b}$$

$$A_s^{(e,h)}(s) = \left[1 + \hat{T}^{(e,h)}(s) + \hat{R}^{(e,h)}(s)\right] a_s \tag{A.164c}$$

$$B_s^{(e,h)}(s) = -j\left[1 - \hat{T}^{(e,h)}(s) - \hat{R}^{(e,h)}(s)\right] a_s \tag{A.164d}$$

As can be seen from the above set of equations in constructing of symmetric modes there is only one degree of freedom, that is, the choice of a_s. Equivalently, $A_s^{(e,h)}(s)$ can be chosen arbitrarily. Moreover, for a symmetric mode we have

$$A_c^{(e,h)}(s) = A_s^{(e,h)}(s) \tag{A.165a}$$

$$B_c^{(e,h)}(s) = -B_s^{(e,h)}(s) \tag{A.165b}$$

In order to obtain all other amplitudes it is also necessary to obtain $B_s^{(e,h)}(s)$. However, in this case $B_s^{(e,h)}(s)$ linearly depends on $A_s^{(e,h)}(s)$. To obtain the constant of proportionality, we use (A.165) in the matrix equation given by (A.138). Therefore, after rearrangement, for a symmetric mode, we have

$$\begin{bmatrix} 1 - t_{11}^{(e,h)}(s) & s t_{12}^{(e,h)}(s) \\ -t_{21}^{(e,h)}(s) & s\left[1 + t_{22}^{(e,h)}(s)\right] \end{bmatrix} \begin{bmatrix} A_s^{(e,h)}(s) \\ B_s^{(e,h)}(s) \end{bmatrix} = 0 \tag{A.166}$$

Since the above matrix equation has a non-trivial solution, the determinants of the coefficient matrix must be zero. In fact, this is the case. If one expands the determinant of the coefficient matrix in (A.166), uses Theorem A.14 and the fact that $c_c^{(e,h)} = c_s^{(e,h)}$ and $t_{11}^{(e,h)}(s)t_{22}^{(e,h)}(s) - t_{12}^{(e,h)}(s)t_{21}^{(e,h)}(s) = \frac{c_c^{(e,h)}}{c_s^{(e,h)}} = 1$, one can easily show that the determinant of the coefficient matrix in (A.166) is zero. Therefore,

$$\frac{B_s^{(e,h)}(s)}{A_s^{(e,h)}(s)} = \frac{t_{11}^{(e,h)}(s) - 1}{st_{12}^{(e,h)}(s)} = \frac{t_{21}^{(e,h)}(s)}{s\left[1 + t_{22}^{(e,h)}(s)\right]} \tag{A.167}$$

Note also that from (A.164c) and (A.164d), one may write

$$\frac{B_s^{(e,h)}(s)}{A_s^{(e,h)}(s)} = -j\frac{1 - \hat{T}^{(e,h)}(s) - \hat{R}^{(e,h)}(s)}{1 + \hat{T}^{(e,h)}(s) + \hat{R}^{(e,h)}(s)} \tag{A.168}$$

Therefore, in a symmetric MPS the RHS of (A.168) must be real.

To construct an asymmetric mode, we need

$$b_c = -a_s \tag{A.169}$$

In this case, from (A.133), we have

$$A_c^{(e,h)}(s) = -\left[1 + \hat{R}^{(e,h)}(s) - \hat{T}^{(e,h)}(s)\right] a_s \tag{A.170a}$$

$$B_c^{(e,h)}(s) = -j\left[1 - \hat{R}^{(e,h)}(s) + \hat{T}^{(e,h)}(s)\right] a_s \tag{A.170b}$$

$$A_s^{(e,h)}(s) = \left[1 + \hat{R}^{(e,h)}(s) - \hat{T}^{(e,h)}(s)\right] a_s \tag{A.170c}$$

$$B_s^{(e,h)}(s) = -j\left[1 - \hat{R}^{(e,h)}(s) + \hat{T}^{(e,h)}(s)\right] a_s \tag{A.170d}$$

Consequently,

$$A_c^{(e,h)}(s) = -A_s^{(e,h)}(s) \tag{A.171a}$$

$$B_c^{(e,h)}(s) = B_s^{(e,h)}(s) \tag{A.171b}$$

For an asymmetric mode, $A_s^{(e,h)}(s)$ and $B_s^{(e,h)}(s)$ satisfy the following matrix equation

$$\begin{bmatrix} 1 + t_{11}^{(e,h)}(s) & -st_{12}^{(e,h)}(s) \\ t_{21}^{(e,h)}(s) & s\left[1 - t_{22}^{(e,h)}(s)\right] \end{bmatrix} \begin{bmatrix} A_s^{(e,h)}(s) \\ B_s^{(e,h)}(s) \end{bmatrix} = 0 \tag{A.172}$$

Thus

$$\frac{B_s^{(e,h)}(s)}{A_s^{(e,h)}(s)} = \frac{1 + t_{11}^{(e,h)}(s)}{s t_{12}^{(e,h)}(s)} = \frac{t_{21}^{(e,h)}(s)}{s\left[t_{22}^{(e,h)}(s) - 1\right]} \tag{A.173}$$

Note also that from (A.164c) and (A.164d), one may write

$$\frac{B_s^{(e,h)}(s)}{A_s^{(e,h)}(s)} = -j\frac{1 - \hat{R}^{(e,h)}(s) + \hat{T}^{(e,h)}(s)}{1 + \hat{R}^{(e,h)}(s) - \hat{T}^{(e,h)}(s)} \tag{A.174}$$

Therefore, in a symmetric MPS the RHS of (A.174) must be real. It should be noted that the symmetric and asymmetric radiation modes in a symmetric MPS are orthogonal. In fact, (A.155) is valid, if (A.165) and (A.171) hold.

A.9 General Hertzian Potential Functions and Vector Fields

So far, we have entirely focused on the *form functions*. We have obtained interesting properties of these functions as a part of the potential functions in a MPS. The modal electromagnetic fields and the potential functions themselves satisfy some useful orthogonality properties, the so-called modal orthogonality. We have used the *form function* orthogonality and the modal orthogonality interchangeably. Although in many cases the modal orthogonality can be obtained from the orthogonality of the *form functions*. However, the concept of modal orthogonality is more general than the orthogonality of the *form functions*.

As a matter of fact, in constructing the potential functions, in addition to the *form functions*, we have one more choice. That is, the amplitude functions. Amplitude functions are not unique to the form functions. Many different amplitude functions can be associated with a fixed *form function* such that the resulting

potential function is still a valid one. In the rectangular coordinate system any double-exponent function

$$A(x,y) = e^{-j(k_x x + k_y y)} \tag{A.175}$$

such that $k_x^2 + k_y^2 = \beta^2$ can be considered as an amplitude function associated with the *form function* with eigenvalue β. Moreover, on a line $y = y_1$ in the x-y plane, we have

$$\int_{-\infty}^{\infty} e^{-j(k_x x + k_y y_1)} e^{j(k_x' x + k_y' y_1)} dx = 2\pi e^{-j(k_y - k_y')y_1} \delta(k_x - k_x') \tag{A.176}$$

In the cylindrical coordinate system any function of the form

$$A(\rho,\phi) = e^{jn\phi} B_n(\beta\rho) \qquad (n = \ldots, -1, 0, 1, \ldots) \tag{A.177}$$

where $B_n(\beta\rho)$ is an arbitrary Bessel function and is a valid amplitude function for a *form function* with eigenvalue β. Furthermore, on a circle of radius ρ_1 centered at the origin in the x-y plane, we have

$$\int_0^{2\pi} e^{jm\phi} B_m(\beta\rho_1) \left[e^{jn\phi} B_n(\beta\rho_1)\right]^* \rho_1 d\phi = 2\pi\delta_{mn} B_m(\beta\rho_1) B_n^*(\beta\rho_1) \tag{A.178}$$

where δ_{mn} is the Kronecker delta symbol, which is nonzero only if $m = n$. The orthogonality relations of the *form functions* in the z direction and the amplitude functions on a line parallel to, say, the y-axis or on a circle in the x-y plane suggest to define some general inner products. These general inner products are defined in the literature, e.g, [121],[19]. We review some of them and show that how they can be easily derived from the formulation developed without resorting to any complicated mathematical procedure.

Consider a lossless MPS and let S be the x-z plane in the rectangular coordinate system or a cylindrical surface of a fixed but arbitrary radius ρ_1 extending from $z = -\infty$ to $z = \infty$. Of course, the axis of this cylindrical surface coincides with the

z axis. Moreover, assume that $\Psi_a^{(e,h)}$ and $\Psi_b^{(e,h)}$ be different Hertzian scalar potential functions in this structure. By different, we mean that the potential functions differ at least by the *form functions* or the amplitude functions. It is also possible the potential functions differ by both the *form functions* and the amplitude functions. With the above assumptions, we have

$$\iint_S \frac{1}{c^{(e,h)}} \Psi_a^{(e,h)} \left[\Psi_b^{(e,h)}\right]^* dS = 0 \tag{A.179}$$

The above orthogonality relation is proved in [122] by using the *coupled-power theorem*. The relation in (A.179) can be easily verified, if we substitute for the potential functions in terms of the *form functions* and the amplitude functions. In fact,

$$\iint_S \frac{1}{c^{(e,h)}} \Psi_a^{(e,h)} \left[\Psi_b^{(e,h)}\right]^* dS = \int_{-\infty}^{\infty} F_a^{(e,h)} \left[F_b^{(e,h)}\right]^* dz \int_0^{2\pi} A_a^{(e,h)} \left[A_b^{(e,h)}\right]^* \rho_1 d\phi \tag{A.180}$$

For two different modes, at least one of the integrals on the RHS of (A.180) vanishes. Therefore, (A.179) is valid. Note also that by using the normalization relations for the *form functions* and the amplitude functions, the integrals on the LHS of (A.180) can be easily evaluated.

We can also derive some useful orthogonality relations between the vector fields. Let us consider the vector space of paired 3-D complex vectors $(\mathbf{A}, \mathbf{B})$ in the rectangular coordinate system. In this space, we may define two different inner products as follows

Inner product of the first type

$$(\mathbf{A}_1, \mathbf{B}_1) \wedge (\mathbf{A}_2, \mathbf{B}_2) = \iint_S [\mathbf{A}_1 \times \mathbf{B}_2^* + \mathbf{A}_2^* \times \mathbf{B}_1] \cdot \hat{\mathbf{y}} dS \tag{A.181}$$

Inner product of the second type

$$(\mathbf{A}_1, \mathbf{B}_1) \vee (\mathbf{A}_2, \mathbf{B}_2) = \iint_S [\mathbf{A}_1 \times \mathbf{B}_2^* - \mathbf{A}_2^* \times \mathbf{B}_1] \cdot \hat{\mathbf{y}} dS \tag{A.182}$$

Let $(\mathbf{E}_a, \mathbf{H}_a)$ and $(\mathbf{E}_b, \mathbf{H}_b)$ be two independent modal solutions of Maxwell's equation in a lossless MPS. Then, from Maxwell's equations, it can be shown that [121]

$$(\mathbf{E}_a, \mathbf{H}_a) \wedge (\mathbf{E}_b, \mathbf{H}_b) = (\mathbf{E}_a, \mathbf{H}_a) \vee (\mathbf{E}_b, \mathbf{H}_b) = 0 \tag{A.183}$$

Therefore,

$$\iint_S \mathbf{E}_a \times \mathbf{H}_b^* \cdot \hat{\mathbf{y}} dS = 0 \tag{A.184}$$

Now consider the vector space of paired 3-D complex vectors $(\mathbf{A}, \mathbf{B})$ in the cylindrical coordinate system. Let us define an inner product in this linear space as follows

$$(\mathbf{A}_1, \mathbf{B}_1) \circ (\mathbf{A}_2, \mathbf{B}_2) = \iint_S [\mathbf{A}_1 \times \mathbf{B}_2^* + \mathbf{A}_2^* \times \mathbf{B}_1] \cdot \hat{\rho} dS \tag{A.185}$$

In this case, it can be argued that [122], [19]

$$(\mathbf{E}_a, \mathbf{H}_a) \circ (\mathbf{E}_b, \mathbf{H}_b) = \mathrm{C} \tag{A.186}$$

where C is a constant number independent of the radius of the cylindrical surface. The relation in (A.186) is called the *coupled- power theorem*. Using the fact that C is constant, it can be shown that

$$\iint_S \mathbf{E}_a \times \mathbf{H}_b^* \cdot \hat{\rho} dS = 0 \tag{A.187}$$

We may combine the orthogonality relations in (A.184) and (A.187) together and write

$$\iint_S \mathbf{E}_a \times \mathbf{H}_b^* \cdot \hat{\mathbf{n}} dS = 0 \tag{A.188}$$

Note that the only requirement for satisfaction of (A.188) is that the corresponding fields be the modal solutions of MPS. Therefore, as one might expect,

there is no restriction on the type of the fields. More precisely, we have the following orthogonality relations

$$\iint_S \mathbf{E}_a^h \times \left[\mathbf{H}_b^h\right]^* \cdot \hat{\mathbf{n}} dS = 0 \tag{A.189a}$$

$$\iint_S \mathbf{E}_a^h \times [\mathbf{H}_b^e]^* \cdot \hat{\mathbf{n}} dS = 0 \tag{A.189b}$$

$$\iint_S \mathbf{E}_a^e \times \left[\mathbf{H}_b^h\right]^* \cdot \hat{\mathbf{n}} dS = 0 \tag{A.189c}$$

$$\iint_S \mathbf{E}_a^e \times [\mathbf{H}_b^e]^* \cdot \hat{\mathbf{n}} dS = 0 \tag{A.189d}$$

To show (A.189a), according to (A.19) and (A.20), we substitute for $\mathbf{E}_a^h$ and $\mathbf{H}_b^h$ in terms of the Ψ_a^h and Ψ_b^h, respectively. Therefore,

$$\iint_S \mathbf{E}_a^h \times \left[\mathbf{H}_b^h\right]^* \cdot \hat{\mathbf{n}} dS = \iint_S \left[j\omega\mu_o \hat{\mathbf{z}} \times \boldsymbol{\nabla}_t \Psi_a^h\right] \times \frac{1}{\mu_r(z)} \left[\boldsymbol{\nabla}_t \left(\frac{\partial \Psi_a^h}{\partial z}\right) + \beta_b^2 \Psi_b^h \hat{\mathbf{z}}\right]^* \cdot \hat{\mathbf{n}} dS \tag{A.190}$$

where the subscript t means transverse to the z axis. Moreover, we have used

$$\frac{\partial^2 \Psi_b^h}{\partial z^2} + \mu_r(z)\epsilon_r(z)\, k_o^2 \Psi_b^h = \beta_b^2 \Psi_b^h \tag{A.191}$$

Using the vector identity

$$\mathbf{A} \times (\mathbf{B} \times \mathbf{C}) = (\mathbf{A} \cdot \mathbf{C})\mathbf{B} - (\mathbf{A} \cdot \mathbf{B})\mathbf{C} \tag{A.192}$$

it can be easily seen that

$$\begin{aligned} \iint_S \mathbf{E}_a^h \times \left[\mathbf{H}_b^h\right]^* \cdot \hat{\mathbf{n}} dS &= j\omega\mu_o\beta_b^2 \iint_S \frac{1}{\mu_r(z)} \nabla_t \Psi_a^h \nabla_t \left[\Psi_b^h\right]^* \cdot \hat{\mathbf{n}} dS \\ &= j\omega\mu_o\beta_b^2 \int_{-\infty}^{\infty} \frac{1}{\mu_r(z)} F_a^h(z) \left[F_b^h\right]^* dz \times \\ &\quad \int_l A_a^h(u_1, u_2) \nabla_t \left[A_b^h(u_1, u_2)\right]^* \cdot \hat{\mathbf{n}} dl \end{aligned} \tag{A.193}$$

For two different modes at least one of the integrals on the RHS of (A.193) vanishes. This shows the validity of (A.189a). Note how the integral in (A.189a) can be

evaluated with the formulas developed so far. The same argument can be used for the proof of (A.189d). To prove (A.189b), we write

$$\iint_S \mathbf{E}_a^h \times [\mathbf{H}_b^e]^* \cdot \hat{\mathbf{n}} dS = \iint_S \left[j\omega\mu_o \hat{\mathbf{z}} \times \nabla_t \Psi_a^h\right] \times j\omega\epsilon_o \hat{\mathbf{z}} \times \nabla_t \left[\Psi_b^h\right]^* \hat{\mathbf{n}} dS \qquad \text{(A.194)}$$

successive application of (A.192) and noting that $z \cdot \hat{\mathbf{n}} = 0$ leads to the conclusion that (A.189b) is identically zero. The proof of (A.189c) using the potential approach is not straightforward.

A.10 Summary

Throughout this appendix, the theory of surface waves and radiation modes of a lossless MPS has been treated rigorously. For the first time, the radiation modes have been investigated in a complete and self-contained rigorous fashion. Many interesting properties of the radiation modes have been stated in terms of theorems. The transfer matrix method is fundamental in the proof of all these theorems. Without using this techniques it is almost impossible to show the validity of the theorems. This fact shows the beauty and importance of this method.

As we have seen before, the complete set of solutions for the physical field consists of one or more surface waves and a continuous spectrum of the radiation fields. The surface waves correspond to $\max(\sqrt{\mu_{r_c}\epsilon_{r_c}}\, k_o, \sqrt{\mu_{r_s}\epsilon_{r_s}}\, k_o) < \beta < \max(\sqrt{\mu_{r_i}\epsilon_{r_i}}\, k_o)$ and the spectrum of the radiation fields is divided into two parts. The spectrum of visible or propagating radiation field is in the range of $0 < \beta < \max(\sqrt{\mu_{r_c}\epsilon_{r_c}}\, k_o, \sqrt{\mu_{r_s}\epsilon_{r_s}}\, k_o)$. The invisible or evanescent radiation fields with $\beta = j\alpha$ and $0 < \alpha < \infty$ is the second part of the radiation spectrum. In general, the field radiated by an arbitrary source can be expressed in terms of the above types of fields.

The characteristic equations of MPS in (A.44) leading to the eigenvalues of the surface waves have an infinite number of solutions with complex roots. One may also correspond modes to these complex roots. However, these modes do not satisfy the radiation conditions at infinity and have a growing character deep into the substrate or the cover. Since these types of solutions correspond to the power leakage from the MPS surface, they are referred as *leaky modes*. Due to the non physical character of these types of the solutions, they do not belong to the proper eigenvalue spectrum. Despite this fact, in many cases it is possible to deform the contour integral representing the radiation field of a source into the *steepest descent path* such that some of these non physical poles be captured. Therefore, it is possible to utilize these modes to *partially* represent the radiated fields. As one might expect, the leaky modes like surface waves contribute to the near field pattern. They are not significant in the far-zone field. The mathematical theory of MPS will be complete if one adds the concept of *leaky modes*. However, since these modes are only a mathematical tool, the meaningful discussion of them is difficult without considering the excitation of MPS. Therefore, we do not follow this concept here.

Appendix B

B.1 Transfer Matrix Method

In this appendix, a systematic method for replacing (A.28) and the corresponding boundary conditions in (A.29)–(A.32) with suitable matrix equations will be discussed. In each layer one may write

$$F_i^{(e,h)}(z) = A_i^{(e,h)}\, U_i^{(e,h)}(z) + B_i^{(e,h)}\, V_i^{(e,h)}(z) \tag{B.1}$$

where $U_i^{(e,h)}(z)$ and $V_i^{(e,h)}(z)$ are any two independent solutions of

$$\frac{d^2 F_i^{(e,h)}}{dz^2} - \gamma_i^{(e,h)} F_i^{(e,h)} = 0 \tag{B.2}$$

with $\gamma_i^{(e,h)} = [\beta^{(e,h)}]^2 - \epsilon_{r_i}\mu_{r_i}k_o^2$. Now applying the boundary conditions in (A.29)–(A.32) leads to

$$\mathbf{C}_{i+1}^{(e,h)} \begin{bmatrix} U_{i+1}^{(e,h)}(d_i) & V_{i+1}^{(e,h)}(d_i) \\ \frac{dU_{i+1}^{(e,h)}(d_i)}{dz} & \frac{dV_{i+1}^{(e,h)}(d_i)}{dz} \end{bmatrix} \begin{bmatrix} A_{i+1}^{(e,h)} \\ B_{i+1}^{(e,h)} \end{bmatrix} = \mathbf{C}_i^{(e,h)} \begin{bmatrix} U_i^{(e,h)}(d_i) & V_i^{(e,h)}(d_i) \\ \frac{dU_i^{(e,h)}(d_i)}{dz} & \frac{dV_i^{(e,h)}(d_i)}{dz} \end{bmatrix} \begin{bmatrix} A_i^{(e,h)} \\ B_i^{(e,h)} \end{bmatrix} \tag{B.3}$$

where

$$\mathbf{C}_i^e = \begin{bmatrix} 1 & 0 \\ 0 & \frac{1}{\epsilon_{r_i}} \end{bmatrix} \tag{B.4}$$

and

$$\mathbf{C}_i^h = \begin{bmatrix} 1 & 0 \\ 0 & \frac{1}{\mu_{r_i}} \end{bmatrix} \tag{B.5}$$

From (B.3), one may write

$$\begin{bmatrix} A_{i+1}^{(e,h)} \\ B_{i+1}^{(e,h)} \end{bmatrix} = \mathbf{Q}_{i+1,i}^{(e,h)} \begin{bmatrix} A_i^{(e,h)} \\ B_i^{(e,h)} \end{bmatrix} \tag{B.6}$$

where

$$\mathbf{Q}_{i+1,i}^{(e,h)} = \begin{bmatrix} U_{i+1}^{(e,h)} & V_{i+1}^{(e,h)} \\ \frac{dU_{i+1}^{(e,h)}}{dz} & \frac{dV_{i+1}^{(e,h)}}{dz} \end{bmatrix}^{-1} \left(\mathbf{C}_{i+1}^{(e,h)}\right)^{-1} \left(\mathbf{C}_i^{(e,h)}\right) \begin{bmatrix} U_i^{(e,h)} & V_i^{(e,h)} \\ \frac{dU_i^{(e,h)}}{dz} & \frac{dV_i^{(e,h)}}{dz} \end{bmatrix} \tag{B.7}$$

The matrix equation in (B.6) shows that the amplitudes in each layer can be expressed in terms of the amplitudes of the layer immediately above or below it.

Eq. (B.2) is the simplest form of the Sturm-Liouville equation of the form

$$\frac{d}{d\xi}[p(\xi)\frac{d\psi}{d\xi}] + [q(\xi) + \lambda\sigma(\xi)]\psi(\xi) = 0 \tag{B.8}$$

with

$$p(\xi) = \sigma(\xi) \equiv 1$$

$$q(\xi) \equiv 0$$

$$\lambda = -[\gamma_i^{(e,h)}]^2$$

A useful property of the Sturm-Liouville equation is that the product of $p(\xi)$ and the Wronskian determinant $W(\xi)$ is constant. Using this property, let us assume that

$$U_i^{(e,h)}(z)\frac{dV_i^{(e,h)}(z)}{dz} - V_i^{(e,h)}(z)\frac{dU_i^{(e,h)}(z)}{dz} = \eta_i^{(e,h)} \tag{B.9}$$

Moreover, let

$$C_i^{(e,h)}(z) = U_i^{(e,h)}(z) \tag{B.10}$$

$$S_i^{(e,h)}(z) = \frac{1}{\eta_i^{(e,h)}} V_i^{(e,h)}(z) \tag{B.11}$$

Substituting (B.10) and (B.11) into (B.1) and following the same procedure, one may write

$$\begin{bmatrix} A_{i+1}^{(e,h)} \\ \eta_{i+1}^{(e,h)} B_{i+1}^{(e,h)} \end{bmatrix} = \mathbf{T}_{i+1,i}^{(e,h)} \begin{bmatrix} A_i^{(e,h)} \\ \eta_i^{(e,h)} B_i^{(e,h)} \end{bmatrix} \tag{B.12}$$

where

$$\mathbf{T}_{i+1,i}^{(e,h)} = \begin{bmatrix} C_{i+1}^{(e,h)} & S_{i+1}^{(e,h)} \\ \frac{dC_{i+1}^{(e,h)}}{dz} & \frac{dS_{i+1}^{(e,h)}}{dz} \end{bmatrix}^{-1} \left(\mathbf{C}_{i+1}^{(e,h)}\right)^{-1} \left(\mathbf{C}_i^{(e,h)}\right) \begin{bmatrix} C_i^{(e,h)} & S_i^{(e,h)} \\ \frac{dC_i^{(e,h)}}{dz} & \frac{dS_i^{(e,h)}}{dz} \end{bmatrix} \tag{B.13}$$

From the above considerations it can be easily seen that

$$\det\left(\mathbf{T}_{i+1,i}^{(e,h)}\right) = \frac{c_{i+1}^{(e,h)}}{c_i^{(e,h)}} \tag{B.14}$$

where $c_i^h = \mu_{r_i}$ and $c_i^e = \epsilon_{r_i}$. This means that $\det\left(\mathbf{T}_{i+1,i}^{(e,h)}\right)$ is independent of the Wronskian determinant. This fact greatly simplifies transfer matrix technique. Let

$$U_i^{(e,h)}(z) = ch[\gamma_i^{(e,h)}(z - d_{i-1})] \tag{B.15}$$

$$V_i^{(e,h)}(z) = sh[\gamma_i^{(e,h)}(z - d_{i-1})] \tag{B.16}$$

With the above choice of the solutions, we have

$$\eta_i^{(e,h)} = \gamma_i^{(e,h)}$$

Therefore, (B.12) reduces to

$$\begin{bmatrix} A_{i+1}^{(e,h)} \\ \gamma_{i+1}^{(e,h)} B_{i+1}^{(e,h)} \end{bmatrix} = \mathbf{T}_{i+1,i}^{(e,h)} \begin{bmatrix} A_i^{(e,h)} \\ \gamma_i^{(e,h)} B_i^{(e,h)} \end{bmatrix} \tag{B.17}$$

where from (B.15), we have

$$\mathbf{T}_{i+1,i}^{(e,h)} = \begin{bmatrix} ch(\gamma_i^{(e,h)} t_i) & \frac{sh(\gamma_i^{(e,h)} t_i)}{\gamma_i^{(e,h)}} \\ \frac{c_{i+1}^{(e,h)}}{c_i^{(e,h)}} \gamma_i^{(e,h)} sh(\gamma_i^{(e,h)} t_i) & \frac{c_{i+1}^{(e,h)}}{c_i^{(e,h)}} ch(\gamma_i^{(e,h)} t_i) \end{bmatrix} \tag{B.18}$$

For a lossless MPS, the elements of the above transfer matrices are real and are insensitive to the sign of $\gamma_i^{(e,h)}$. Moreover, these elements are well-behaved as $\gamma_i^{(e,h)} \to 0$. These important properties are very useful in the numerical calculations and are the direct consequences of introducing the transfer matrices as defined in (B.12).

B.2 Proof of Theorem A.1

To prove Theorem A.1, we follow the same approach that is used in the proof of the orthogonality of the Sturm-Liouville eigenfunctions. It is known that $F_a^{(e,h)}(z)$ and $F_b^{(e,h)}(z)$ in the region $d_{i-1} < z < d_i$ are the solutions of (A.28) which can be rewritten as

$$\frac{d^2 F_{ai}^{(e,h)}}{dz^2} + \epsilon_{r_i}\mu_{r_i} k_o^2 F_{ai}^{(e,h)} = [\beta_a^{(e,h)}]^2 F_{ai}^{(e,h)} \tag{B.19}$$

$$\frac{d^2 F_{bi}^{(e,h)}}{dz^2} + \epsilon_{r_i}\mu_{r_i} k_o^2 F_{bi}^{(e,h)} = [\beta_b^{(e,h)}]^2 F_{bi}^{(e,h)} \tag{B.20}$$

Let $c_i^e = \epsilon_{r_i}$ and $c_i^h = \mu_{r_i}$. Multiplying the equation for $F_{ai}^{(e,h)}$ by $\frac{1}{c_i^{(e,h)}} F_{bi}^{(e,h)}$ and (B.20) by $\frac{1}{c_i^{(e,h)}} F_{ai}^{(e,h)}$, subtracting gives

$$\frac{d}{dz}\left[\frac{1}{c_i^{(e,h)}} F_{bi}^{(e,h)} \frac{dF_{ai}^{(e,h)}}{dz} - \frac{1}{c_i^{(e,h)}} F_{ai}^{(e,h)} \frac{dF_{bi}^{(e,h)}}{dz}\right] = \left([\beta_a^{(e,h)}]^2 - [\beta_b^{(e,h)}]^2\right) \frac{1}{c_i^{(e,h)}} F_{ai}^{(e,h)} F_{bi}^{(e,h)} \tag{B.21}$$

Integrating (B.21) from $z = d_{i-1}$ to $z = d_i$ gives

$$[\beta_{dif}^{(e,h)}]^2 \int_{d_{i-1}}^{d_i} \frac{1}{c_i^{(e,h)}} F_{ai}^{(e,h)} F_{bi}^{(e,h)} dz = \left[\frac{1}{c_i^{(e,h)}} F_{bi}^{(e,h)} \frac{dF_{ai}^{(e,h)}}{dz} - \frac{1}{c_i^{(e,h)}} F_{ai}^{(e,h)} \frac{dF_{bi}^{(e,h)}}{dz}\right]_{d_{i-1}}^{d_i} \tag{B.22}$$

where

$$[\beta_{dif}^{(e,h)}]^2 = [\beta_a^{(e,h)}]^2 - [\beta_b^{(e,h)}]^2$$

Let

$$\int_{-\infty}^{\infty} w^{(\epsilon,h)}(z)F_a^{(\epsilon,h)}(z)F_b^{(\epsilon,h)}(z)dz = I_{-\infty} + I_N + I_{\infty} \tag{B.23}$$

where

$$I_{-\infty} = \int_{-\infty}^{0} \frac{1}{c_s^{(\epsilon,h)}} F_a^{(\epsilon,h)}(z)F_b^{(\epsilon,h)}(z)dz$$

$$I_N = \sum_{i=0}^{N} \int_{d_{i-1}}^{d_i} \frac{1}{c_i^{(\epsilon,h)}} F_a^{(\epsilon,h)}(z)F_b^{(\epsilon,h)}(z)dz$$

$$I_{\infty} = \int_{d_N}^{\infty} \frac{1}{c_c^{(\epsilon,h)}} F_a^{(\epsilon,h)}(z)F_b^{(\epsilon,h)}(z)dz$$

Using (B.22) and the fact that $F_{(a,b)}^{(\epsilon,h)}$ and $\frac{1}{c_i^{(\epsilon,h)}} \frac{dF_{(a,b)}^{(\epsilon,h)}}{dz}$ are continuous at $z = d_{i-1}$ and d_i, $i = 0, 1, \ldots N$, from (B.23), we get

$$\begin{aligned}
[\beta_{dif}^{(\epsilon,h)}]^2 \int_{-\infty}^{\infty} w^{(\epsilon,h)}(z)F_a^{(\epsilon,h)}(z)F_b^{(\epsilon,h)}(z)dz &= \frac{1}{c_c^{(\epsilon,h)}} \left[F_b^{(\epsilon,h)} \frac{dF_a^{(\epsilon,h)}}{dz} - F_a^{(\epsilon,h)} \frac{dF_b^{(\epsilon,h)}}{dz} \right]_{z=\infty} - \\
&\quad \frac{1}{c_s^{(\epsilon,h)}} \left[F_b^{(\epsilon,h)} \frac{dF_a^{(\epsilon,h)}}{dz} - F_a^{(\epsilon,h)} \frac{dF_b^{(\epsilon,h)}}{dz} \right]_{z=-\infty} \\
&= 0
\end{aligned} \tag{B.24}$$

The above result is due to the fact that *form functions* and their derivative exponentially decay in the substrate and the cover regions. If $F_a^{(\epsilon,h)}$ and $F_b^{(\epsilon,h)}$ correspond to different eigenvalues, $[\beta_{dif}^{(\epsilon,h)}]^2 \neq 0$. Therefore, (A.56) follows from (B.24).

To prove (A.57), we only need to multiply (B.19) by $\frac{1}{c_i^{(\epsilon,h)}}[F_b^{(\epsilon,h)}]^*$ and the complex conjugate of (B.20) by $\frac{1}{c_i^{(\epsilon,h)}} F_a^{(\epsilon,h)}$. The remaining steps are the same. Moreover, we use the fact that $c_i^{(\epsilon,h)}$ are real which means that $[F_b^{(\epsilon,h)}]^*$ in addition to $\frac{1}{c_i^{(\epsilon,h)}} \frac{d[F_b^{(\epsilon,h)}]^*}{dz}$ are continuous at $z = d_{i-1}$ and $z = d_i$. □

B.3 Proof of Theorem A.2

To prove Theorem A.2, all we need is to show that

$$F^{(e,h)}(z_o) = \pm F^{(e,h)}(d_N - z_o) \tag{B.25}$$

where z_o is an arbitrary number. To this end, we know that $F^{(e,h)}(z)$ is the solution of

$$\frac{d^2 F^{(e,h)}}{dz^2} + \epsilon_r(z)\mu_r(z)k_o^2 F^{(e,h)} = [\beta^{(e,h)}]^2 F^{(e,h)} \tag{B.26}$$

The above differential equation is valid for each value of z. Especially if we apply (B.26) at $z = d_N - z_o$, we have

$$\frac{d^2 F^{(e,h)}}{dz^2}|_{z=d_N-z_o} + \epsilon_r(d_N - z_o)\mu_r(d_N - z_o)k_o^2 F^{(e,h)}(d_N - z_o) = [\beta^{(e,h)}]^2 F^{(e,h)}(d_N - z_o) \tag{B.27}$$

Let us define a new variable u such that

$$u = d_N - z \tag{B.28}$$

Then, we have

$$\frac{d^2}{dz^2} \equiv \frac{d^2}{du^2} \tag{B.29}$$

Using (B.29) in (B.27) leads to

$$\frac{d^2 F^{(e,h)}}{du^2}|_{u=u_o} + \epsilon_r(u_o)\mu_r(u_o)k_o^2 F^{(e,h)}(u_o) = [\beta^{(e,h)}]^2 F^{(e,h)}(u_o) \tag{B.30}$$

where $u_o = d_N - z_o$. The above differential equation is valid for an arbitrary value of u_o. Therefore, $F^{(e,h)}$ as a function of u satisfies the following differential equation

$$\frac{d^2 F^{(e,h)}}{du^2} + \epsilon_r(u)\mu_r(u)k_o^2 F^{(e,h)} = [\beta^{(e,h)}]^2 F^{(e,h)} \tag{B.31}$$

Since the MPS is symmetric, we have

$$\epsilon_r(z = a) = \epsilon_r(u = a)$$

$$\mu_r(z = a) = \mu_r(u = a)$$

Thus, (B.26) and (B.31) are identical differential equations. Moreover, the boundary conditions are the same. Therefore, (B.26) and (B.31) are identical eigenvalue problems. That is, $F^{(e,h)}(z)$ and $F^{(e,h)}(u)$ are two eigenfunctions corresponding to the same eigenvalues $\beta^{(e,h)}$. However, for surface waves, since the *form functions* in the substrate and cover regions are described by one amplitude, the eigenfunction degeneracy happens within a multiplicative constant. This is so because we have only one degree of freedom. This is not necessarily the case for the radiation modes. Therefore,

$$\begin{aligned} F^{(e,h)}(z) &= KF^{(e,h)}(u) \\ &= KF^{(e,h)}(d_N - z) \end{aligned} \tag{B.32}$$

The above equation is valid for each z. At $z = z_o$, we have

$$F^{(e,h)}(z_o) = KF^{(e,h)}(d_N - z_o) \tag{B.33}$$

If we use (B.32) at $z = d_N - z_o$, we get

$$F^{(e,h)}(d_N - z_o) = KF^{(e,h)}(z_o) \tag{B.34}$$

Using (B.34) in (B.33), we get

$$F^{(e,h)}(z_o) = K^2 F^{(e,h)}(z_o)$$

which requires that

$$K^2 = 1$$

or

$$K = \pm 1$$

Substituting the value of K into (B.32) leads to (B.25) which in turn completes the proof. □

B.4 Proof of Theorem A.3

To prove this theorem, we need to find the relationship between b_c, a_c and b_s. To this end, by applying the boundary condition on $F_c^{(e,h)}(z)$ at each interface and successive elimination of the coefficients, we end up with the following matrix equation

$$\begin{bmatrix} 1 \\ js \end{bmatrix} b_c + \begin{bmatrix} 1 \\ -js \end{bmatrix} a_c^{(e,h)}(s) = \mathbf{T}^{(e,h)}(s) \begin{bmatrix} 1 \\ j\tau_s \end{bmatrix} b_s^{(e,h)}(s) \tag{B.35}$$

where

$$\mathbf{T}^{(e,h)}(s) = \prod_{i=N}^{0} \mathbf{T}_{i+1,i}^{(e,h)}(s),$$

Note that

$$\det\left[\mathbf{T}^{(e,h)}(s)\right] = \frac{c_c^{(e,h)}}{c_s^{(e,h)}} \tag{B.36}$$

where $c_{(c,s)}^{e} = \epsilon_{r_{(c,s)}}$ and $c_{(c,s)}^{h} = \mu_{r_{(c,s)}}$.

Eq. (B.35) can be rewritten as

$$\mathbf{T}^{(e,h)}(s) \begin{bmatrix} 1 \\ j\tau_s \end{bmatrix} b_s^{(e,h)}(s) - \begin{bmatrix} 1 \\ -js \end{bmatrix} a_c^{(e,h)}(s) = \begin{bmatrix} 1 \\ js \end{bmatrix} b_c \tag{B.37}$$

Solving for $b_s^{(e,h)}(s)$ and $a_c^{(e,h)}(s)$ in terms of the incident amplitude b_c, leads to

$$b_s^{(e,h)}(s) = \frac{\begin{bmatrix} js & 1 \end{bmatrix} \begin{bmatrix} 1 \\ js \end{bmatrix}}{D^{(e,h)}(s)} b_c \tag{B.38}$$

$$a_c^{(e,h)}(s) = \frac{\begin{bmatrix} -j\tau_s & 1 \end{bmatrix} \left[\mathbf{T}^{(e,h)}(s)\right]^{-1} \begin{bmatrix} 1 \\ js \end{bmatrix}}{\hat{D}^{(e,h)}(s)} b_c \tag{B.39}$$

where

$$D^{(e,h)}(s) = \begin{bmatrix} js & 1 \end{bmatrix} \mathbf{T}^{(e,h)}(s) \begin{bmatrix} 1 \\ j\tau_s \end{bmatrix} \tag{B.40}$$

$$\hat{D}^{(e,h)}(s) = -\begin{bmatrix} -j\tau_s & 1 \end{bmatrix} \left[\mathbf{T}^{(e,h)}(s)\right]^{-1} \begin{bmatrix} 1 \\ -js \end{bmatrix} \tag{B.41a}$$

$$= \frac{c_s^{(e,h)}}{c_c^{(e,h)}} D^{(e,h)}(s) \tag{B.41b}$$

We also have

$$\begin{bmatrix} -j\tau_s & 1 \end{bmatrix} \left[\mathbf{T}^{(e,h)}(s)\right]^{-1} \begin{bmatrix} 1 \\ js \end{bmatrix} = -\frac{c_s^{(e,h)}}{c_c^{(e,h)}} \begin{bmatrix} -js & 1 \end{bmatrix} \mathbf{T}^{(e,h)}(s) \begin{bmatrix} 1 \\ j\tau_s \end{bmatrix} \tag{B.42}$$

Using (B.41a) and (B.42) in (B.39), we have

$$a_c^{(e,h)}(s) = \frac{-\begin{bmatrix} -js & 1 \end{bmatrix} \mathbf{T}^{(e,h)}(s) \begin{bmatrix} 1 \\ j\tau_s \end{bmatrix}}{D(s)} \tag{B.43}$$

Let

$$\mathbf{T}^{(e,h)}(s) = \begin{bmatrix} t_{11}^{(e,h)}(s) & t_{12}^{(e,h)}(s) \\ t_{21}^{(e,h)}(s) & t_{22}^{(e,h)}(s) \end{bmatrix} \tag{B.44}$$

Now, the rest of the steps is just a trivial matter. We need only to expand the numerators and denominators in (B.38) and (B.43). To simplify the resulting expression, it should be noted that for a lossless MPS the transfer matrix elements are real valued, therefore, all parameters in (B.44) are real. Moreover, we have

$$\det\left[\mathbf{T}^{(e,h)}(s)\right] = t_{11}^{(e,h)}(s)t_{22}^{(e,h)}(s) - t_{12}^{(e,h)}(st_{21}^{(e,h)}(s) \tag{B.45a}$$

$$= \frac{c_c^{(e,h)}}{c_s^{(e,h)}} \tag{B.45b}$$

Following the above considerations leads to (A.71). This completes the proof of Theorem A.3. □

B.5 Proof of Theorem A.4

To prove this theorem, we follow the same line as we have used in the proof of Theorem A.3. In this case, the scattered amplitudes in the cover and the substrate are related to the incident amplitude through the following matrix equation

$$\mathbf{T}^{(e,h)}(s)\begin{bmatrix}1\\ js\end{bmatrix}b_s^{(e,h)}(s)-\begin{bmatrix}1\\ -\gamma_c\end{bmatrix}a_c^{(e,h)}(s)=-\mathbf{T}^{(e,h)}(s)\begin{bmatrix}1\\ -js\end{bmatrix}a_s \tag{B.46}$$

Solving the above equation for $b_s^{(e,h)}(s)$ and $a_c^{(e,h)}(s)$, leads to

$$b_s^{(e,h)}(s)=\frac{-\begin{bmatrix}\gamma_c & 1\end{bmatrix}\mathbf{T}^{(e,h)}(s)\begin{bmatrix}1\\ -js\end{bmatrix}}{\begin{bmatrix}\gamma_c & 1\end{bmatrix}\mathbf{T}^{(e,h)}(s)\begin{bmatrix}1\\ js\end{bmatrix}}a_s \tag{B.47}$$

$$a_c^{(e,h)}(s)=\frac{-\frac{c_c^{(e,h)}}{c_s^{(e,h)}}\begin{bmatrix}-js & 1\end{bmatrix}\begin{bmatrix}1\\ -js\end{bmatrix}}{\begin{bmatrix}\gamma_c & 1\end{bmatrix}\mathbf{T}^{(e,h)}(s)\begin{bmatrix}1\\ js\end{bmatrix}}a_s \tag{B.48}$$

where we have used

$$-\begin{bmatrix}-js & 1\end{bmatrix}\left[\mathbf{T}^{(e,h)}(s)\right]^{-1}\begin{bmatrix}1\\ -\gamma_c\end{bmatrix}=\frac{c_s^{(e,h)}}{c_c^{(e,h)}}\begin{bmatrix}\gamma_c & 1\end{bmatrix}\mathbf{T}^{(e,h)}(s)\begin{bmatrix}1\\ js\end{bmatrix}$$

For substrate mode of type I, γ_c is a real number. Thus, as can be seen from (B.47), since all other parameters are real, the numerator is the negative of the complex conjugate of the denominator. This means that

$$|b_s^{(e,h)}(s)|=|a_s|$$

which proves the first part of Theorem A.4.

The second part of the theorem can be proved by noting that γ_c is a purely imaginary number, that is,

$$\gamma_c = j\tau_c.$$

Next, we need to follow the same reasoning to as we have used in Theorem A.3 which is not repeated here. □

B.6 Physical Interpretation of Theorems A.3 and A.4

In this appendix we use the plane wave concepts to prove Theorems 2.3 and 2.4. To this end, suppose that we have a substrate radiation mode of LSE type. As mentioned earlier, it is always possible to rotate the x-y axis such that the dependence of the fields on η in (η, ξ) coordinates system vanishes. Note that this coordinate transformation does not affect the *form function*. Thus, let the Hertzian scalar potential function of magnetic type in (η, ξ, z) coordinate system be

$$\Psi^h(\eta, \xi, z) = e^{-j\beta\xi} F_s(z) \tag{B.49}$$

where we have assumed that the *amplitude function* is

$$A^h(\eta, \xi) = e^{-j\beta\xi}$$

In the substrate region, we have

$$\Psi_s^h(\eta, \xi, z) = e^{-j\beta\xi}[a_s e^{-jsz} + b_s(s)e^{jsz}] \tag{B.50}$$

This potential function can be considered as a superposition of

$$\Psi_{si}^h(\eta, \xi, z) = a_s e^{-j(\beta\xi + sz)} \tag{B.51}$$

which generates an incident plane wave with perpendicular polarization, and

$$\Psi^h_{sr}(\eta,\xi,z) = b^h_s(s)e^{-j(\beta\xi - sz)} \tag{B.52}$$

the potential function due to the reflected plane wave as shown in Fig. A.5. The incident plane wave propagates in the direction ν_i which is specified by the unit vector

$$\begin{aligned}\hat{\nu}_i &= \frac{\beta}{\sqrt{s^2+\beta^2}}\hat{\xi} + \frac{s}{\sqrt{s^2+\beta^2}}\hat{z} \\ &= \frac{\beta}{\sqrt{\mu_{r_s}\epsilon_{r_s}}\,k_o}\hat{\xi} + \frac{s}{\sqrt{\mu_{r_s}\epsilon_{r_s}}\,k_o}\hat{z}\end{aligned} \tag{B.53}$$

The propagation direction of the reflected wave is ν_r which is specified by the unit vector $\hat{\nu}_r$ such that

$$\hat{\nu}_r = \frac{\beta}{\sqrt{\mu_{r_s}\epsilon_{r_s}}\,k_o}\hat{\xi} + \frac{-s}{\sqrt{\mu_{r_s}\epsilon_{r_s}}\,k_o}\hat{z} \tag{B.54}$$

For substrate mode of type II, there is a transmitted plane wave in the cover region with the potential function

$$\Psi^h_{st}(\eta,\xi,z) = a^h_c(s)e^{-j(\beta\xi + \tau_c z)} \tag{B.55}$$

The transmitted plane wave propagates in the direction ν_t with the unit vector

$$\hat{\nu}_t = \frac{\beta}{\sqrt{\mu_{r_c}\epsilon_{r_c}}\,k_o}\hat{\xi} + \frac{\tau_c}{\sqrt{\mu_{r_c}\epsilon_{r_c}}\,k_o}\hat{z} \tag{B.56}$$

From (A.19), the incident electric field in the substrate is

$$\mathbf{E}^h_{si} = -j\omega\mu_o\beta a_s e^{-j(\beta\xi + sz)}\hat{\eta} \tag{B.57}$$

Thus

$$\|\mathbf{E}^h_{si}\| = \omega\mu_o\beta|a_s| \tag{B.58}$$

Using the plane wave concepts, the Poynting vector of the incident wave is

$$\begin{aligned}\mathbf{P}_i^h &= \frac{\|\mathbf{E}_{si}^h\|^2}{\eta_o}\sqrt{\frac{\epsilon_{r_s}}{\mu_{r_s}}}\hat{\nu}_i \\ &= \frac{(\omega\mu_o\beta)^2|a_s|^2}{\eta_o\mu_{r_s}k_o}(\beta\hat{\boldsymbol{\xi}} + s\hat{\mathbf{z}}) \qquad \text{(B.59)}\end{aligned}$$

where we have used (B.53). Furthermore, $\eta_o = \sqrt{\frac{\mu_o}{\epsilon_o}}$ is the free space wave impedance. Let $\mathbf{P}_r^h$ and $\mathbf{P}_t^h$ be the Poynting vectors of the reflected wave in the substrate and transmitted wave in the cover, respectively. In a similar fashion, one may argue that

$$\mathbf{P}_r^h = \frac{(\omega\mu_o\beta)^2|b_s^h(s)|^2}{\eta_o\mu_{r_s}k_o}(\beta\hat{\boldsymbol{\xi}} - s\hat{\mathbf{z}}) \qquad \text{(B.60)}$$

$$\mathbf{P}_t^h = \frac{(\omega\mu_o\beta)^2|a_c^h(s)|^2}{\eta_o\mu_{r_c}k_o}(\beta\hat{\boldsymbol{\xi}} + \tau_c\hat{\mathbf{z}}) \qquad \text{(B.61)}$$

It can be easily shown that the total power carried in the z direction is the sum of the powers carried by the incident and reflected waves in that direction. Note that this statement is not true for the power carried in the ξ direction. In view of lossless character of the MPS is, this means that transferred power in the z direction must be equal to the differences of the incident and reflected powers in that direction. Therefore, in terms of the Poynting vectors in (B.59), (B.60), and (B.61), we have

$$\hat{\mathbf{z}}\cdot\mathbf{P}_t^h = \hat{\mathbf{z}}\cdot(\mathbf{P}_i^h + \mathbf{P}_r^h)$$

from which one may obtain

$$\frac{(\omega\mu_o\beta)^2|a_c^h(s)|^2}{\eta_o\mu_{r_c}k_o}\tau_c = \frac{(\omega\mu_o\beta)^2|a_s|^2}{\eta_o\mu_{r_s}k_o}s - \frac{(\omega\mu_o\beta)^2|b_s^h(s)|^2}{\eta_o\mu_{r_s}k_o}s$$

Consequently,

$$|a_s|^2 = |b_s^h(s)| + \frac{\mu_{r_s}}{\mu_{r_c}}\frac{\tau_c}{s}|a_c^h(s)|^2$$

For substrate mode of type I, since there is no power transfer in the z direction the incident and reflected power in that direction must be equal. That is,

$$|a_s|^2 = |b_s^h(s)|^2$$

In the case of LSM mode, we may follow the same reasoning in a dual manner. In this case, from (A.20), the incident magnetic field in the substrate is

$$\mathbf{H}_{si}^e = -j\omega\epsilon_o\beta a_s e^{-j(\beta\xi+sz)}\hat{\boldsymbol{\eta}} \tag{B.62}$$

Thus

$$\|\mathbf{H}_{si}^e\| = \omega\epsilon_o\beta|a_s| \tag{B.63}$$

The Poynting vector of the incident wave is

$$\begin{aligned}\mathbf{P}_i^e &= \|\mathbf{H}_{si}^e\|^2\eta_o\sqrt{\frac{\mu_{r_s}}{\epsilon_{r_s}}}\hat{\boldsymbol{\nu}}_i \\ &= \frac{\eta_o(\omega\epsilon_o\beta)^2|a_s|^2}{\epsilon_{r_s}k_o}(\beta\hat{\boldsymbol{\xi}} + s\hat{\mathbf{z}})\end{aligned} \tag{B.64}$$

Similarly, $\mathbf{P}_r^e$ and $\mathbf{P}_t^e$ can be obtained from the following relations

$$\mathbf{P}_r^e = \frac{\eta_o(\omega\epsilon_o\beta)^2|b_s^e(s)|^2}{\epsilon_{r_s}k_o}(\beta\hat{\boldsymbol{\xi}} - s\hat{\mathbf{z}})$$

$$\mathbf{P}_t^e = \frac{\eta_o(\omega\epsilon_o\beta)^2|a_c^e(s)|^2}{\epsilon_{r_c}k_o}(\beta\hat{\boldsymbol{\xi}} + \tau_c\hat{\mathbf{z}})$$

Using the conservation of power in the z direction, we have

$$|a_s|^2 = |b_s^e(s)|^2 + \frac{\epsilon_{r_s}}{\epsilon_{r_c}}\frac{\tau_c}{s}|a_c^e(s)|^2$$

The same argument can be used for the cover modes.

B.7 Derivation of Equation (A.79)

For $s \neq 0$, we have

$$\begin{aligned} \tilde{U}_+(s) &= \int_0^\infty e^{jsz} dz \\ &= \left[\frac{e^{jsz}}{js}\right]_{z=0}^{z=\infty} \\ &= \frac{j}{s} \qquad s \neq 0 \end{aligned} \tag{B.65}$$

where we have used (A.75). The integral in (A.78) can be considered as the Fourier transform of the unit step function. Therefore, using the inverse Fourier transform, we have

$$\frac{1}{2\pi}\int_{-\infty}^{\infty} \tilde{U}_+(s)e^{-jsz}ds = \begin{cases} 1 & z > 0 \\ \frac{1}{2} & z = 0 \\ 0 & z < 0 \end{cases} \tag{B.66}$$

Eq. (B.66) can be rewritten as

$$\frac{1}{2\pi}\left(\int_{-\infty}^{0-} \tilde{U}_+(s)e^{-jsz}ds + \int_{0-}^{0+} \tilde{U}_+(s)e^{-jsz}ds + \int_{0+}^{\infty} \tilde{U}_+(s)e^{-jsz}ds\right) = \begin{cases} 1 & z > 0 \\ \frac{1}{2} & z = 0 \\ 0 & z < 0 \end{cases} \tag{B.67}$$

On the other hand, using the residue theory, it can be shown that

$$\frac{1}{2\pi}\left(\int_{-\infty}^{0^-} \tilde{U}_+(s)e^{-jsz}ds + \int_{0+}^{\infty} \tilde{U}(s)e^{-jsz}ds\right) = \begin{cases} \frac{1}{2} & z > 0 \\ 0 & z = 0 \\ -\frac{1}{2} & z < 0 \end{cases} \tag{B.68}$$

More precisely, let us calculate the contour integral

$$\frac{1}{2\pi}\int_C \frac{j}{s}e^{-jsz}ds \tag{B.69}$$

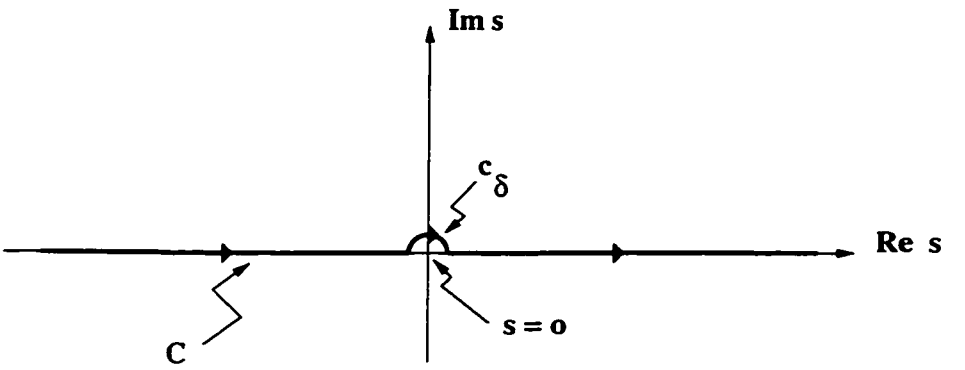

Figure B.1: Contour for the complex integral in (A.55)

on the contour C in the s plane as illustrated in Fig B.1. If $z > 0$, we may close the contour by a semicircle of large (eventually infinite) radius in the lower half plane. Since in the lower half plane Im $s < 0$, the contribution along the large semicircle vanishes. Therefore, according to the theory of Cauchy integral, we have

$$\begin{aligned}\frac{1}{2\pi}\int_C \frac{j}{s}e^{-jsz}ds &= \frac{1}{2\pi}\left(\int_{-\infty}^{0^-}\frac{j}{s}e^{-jsz}ds + \int_{C_\epsilon}\frac{j}{s}e^{-jsz}ds + \int_{0^+}^{\infty}\frac{j}{s}e^{-jsz}ds\right)\\ &= \frac{1}{2\pi}\left[-\text{Res}(\frac{je^{-jsz}}{s})\right]\\ &= 1\end{aligned} \tag{B.70}$$

The minus sign in front of Res(.) accounts for the clockwise direction of the contour. Again, using the residue theory, the contribution of the semicircle c_δ of infinitesimal radius to the contour integral is

$$\begin{aligned}\frac{1}{2\pi}\int_{C_\epsilon}\frac{j}{s}e^{-jsz}ds &= \frac{1}{2\pi}\left[-\frac{1}{2}\text{Res}(\frac{je^{-jsz}}{s})\right]\\ &= \frac{1}{2}\end{aligned} \tag{B.71}$$

Using (B.70) and (B.71), leads to (B.68) for $z > 0$.

For $z < 0$, we may close the contour by a semicircle of large (eventually infinite) radius in the upper half plane. In the upper half plane Im $s > 0$, therefore, the

contribution along the large semicircle vanishes. However, in this case the contour does not capture any poles. This means that for $z < 0$, we have

$$\begin{aligned} \frac{1}{2\pi}\int_C \frac{j}{s}e^{-jsz}ds &= \frac{1}{2\pi}\left(\int_{-\infty}^{0^-}\frac{j}{s}e^{-jsz}ds + \int_{C_\epsilon}\frac{j}{s}e^{-jsz}ds + \int_{0^+}^{\infty}\frac{j}{s}e^{-jsz}ds\right) \\ &= 0 \end{aligned} \tag{B.72}$$

Thus, (B.68) can be derived for $z < 0$, if one uses (B.71) and (B.72).

For $z = 0$, the contour can be closed by a semicircle of large radius either in the upper or lower half plane. Suppose that we close the contour by a semicircle C_R in the upper half plane. Let us assume that the radius of the large semicircle be R and that of c_δ be δ. If we substitute

$$s = \delta e^{j\theta}$$

on c_δ and

$$s = Re^{j\theta}$$

on C_R, it can be easily seen that their contributions to the contour integral cancel each other. Therefore, since no pole is captured, we obtain (B.68) for $z = 0$.

Having established (B.68), one may derive

$$\frac{1}{2\pi}\int_{0^-}^{0^+}\tilde{U}(s)ds = \frac{1}{2} \tag{B.73}$$

if one uses (B.68) in (B.67). From (B.73), we obtain

$$\tilde{U}_+(s) = \pi\delta(s) \qquad 0^- < s < 0^+ \tag{B.74}$$

This final result proves that

$$\int_0^\infty e^{jsz}dz = \begin{cases} \frac{j}{s} & s \neq 0 \\ \pi\delta(s) & 0^- < s < 0^+ \end{cases} \tag{B.75}$$

We follow the same reasoning to prove (A.79) with minus sign in front of j. In this case we need to show that

$$\frac{1}{2\pi}\left(\int_{-\infty}^{0^-}\frac{-j}{s}e^{jsz}ds+\int_{0^+}^{\infty}\frac{-j}{s}e^{jsz}ds\right)=\begin{cases}\frac{1}{2} & z>0\\ 0 & z=0\\ -\frac{1}{2} & z<0\end{cases} \tag{B.76}$$

This can be done by calculating the contour integral

$$\frac{1}{2\pi}\int_C\frac{-j}{s}e^{jsz}ds \tag{B.77}$$

on the contour C shown in Fig. B.1. In this case, for $z>0$, we may close the contour by a semicircle of large (eventually infinite) radius in the upper half plane and vice versa for $z<0$.

B.8 Proof of Theorem A.8

To prove this theorem we follow the same line in the proof of Theorem A.1. All steps in the proof of Theorem A.1 up to (B.24) can be used in the process of proving Theorem A.8. Therefore, we may write

$$\begin{aligned}\beta_{dif}^2<F_s^{(e,h)}(z;s_1),F_c^{(e,h)}(z;s_2)> &= \beta_{dif}^2\int_{-\infty}^{\infty}w^{(e,h)}(z)F_s^{(e,h)}(z;s_1)F_c^{(e,h)}(z;s_2)dz\\ &= \frac{1}{c_c^{(e,h)}}\left[F_c^{(e,h)}\frac{dF_s^{(e,h)}}{dz}-F_s^{(e,h)}\frac{F_c^{(e,h)}}{dz}\right]_{z=\infty}\\ &- \frac{1}{c_s^{(e,h)}}\left[F_c^{(e,h)}\frac{dF_s^{(e,h)}}{dz}-F_s^{(e,h)}\frac{dF_c^{(e,h)}}{dz}\right]_{z=-\infty}\end{aligned} \tag{B.78}$$

where

$$\beta_{dif}^2=\beta^2(s_1)-\beta^2(s_2)\neq 0 \tag{B.79}$$

However,

$$\left[F_c^{(e,h)}\frac{dF_s^{(e,h)}}{dz} - F_s^{(e,h)}\frac{F_c^{(e,h)}}{dz}\right]_{z=\infty} = -A_+\left[b_c a_c^{(e,h)}(s_1)e^{(-\gamma_c+js_2)(z-d_N)}\right]_{z=\infty} - A_-\left[a_c^{(e,h)}(s_1)a_s^{(e,h)}(s_2)e^{(-\gamma_c-js_2)(z-d_N)}\right]_{z=\infty} \tag{B.80}$$

where

$$A_\pm = \gamma_c \pm js_2$$

$$\gamma_c = \sqrt{(\mu_{r_s}\epsilon_{r_s} - \mu_{r_c}\epsilon_{r_c})k_o^2 - s^2}$$

For substrate modes of type I, γ_c is real. Therefore, the above expression is zero in the ordinary sense. Substrate radiation modes of type II result in imaginary values for γ_c. Since it has been assumed that the two modes are not degenerate, according to the Theorem A.5, (B.80) is zero as a generalized limit. The same argument can be used to show that

$$\left[F_c^{(e,h)}\frac{dF_s^{(e,h)}}{dz} - F_s^{(e,h)}\frac{F_c^{(e,h)}}{dz}\right]_{z=-\infty} = 0 \tag{B.81}$$

if we consider the limit as a generalized limit. Using (B.80) and (B.81) in (B.78), in the distribution sense, we have

$$\beta_{dif}^2 < F_s^{(e,h)}(z;s_1), F_c^{(e,h)}(z;s_2) >= 0 \tag{B.82}$$

Since $\beta_{dif}^2 \neq 0$, (A.85) can be derived from (B.82).

We may use the same argument to prove (A.86). □

B.9 Proof of Lemma A.1

To prove this lemma, we need to show that for each test function $\psi(x)$, we have

$$\int_{-\infty}^{\infty} \delta[f(x) - f(a)]\psi(x)dx = \frac{1}{|f'(a)|}\psi(a). \tag{B.83}$$

To this end, let

$$y = f(x) \tag{B.84a}$$

$$y_o = f(a) \tag{B.84b}$$

$$x = f^{-1}(y) \tag{B.84c}$$

Note that since it has been assumed that $f(x)$ is monotonic, it is possible to define its inverse function. Furthermore, $f'(x) \neq 0$. We now consider two cases separately.

First we assume that $f(x)$ is monotically increasing. Then, substituting (B.84) into (B.83), we obtain

$$\begin{aligned}\int_{-\infty}^{\infty} \delta[f(x) - f(a)]\psi(x)dx &= \int_{-\infty}^{\infty} \delta(y - y_o)\psi[f^{-1}(y)](\frac{df^{-1}}{dy})dy \\ &= \psi[f^{-1}(y_o)]\left[\frac{df^{-1}}{dy}\right]_{y=y_o}\end{aligned} \tag{B.85}$$

On the other hand,

$$\begin{aligned}\left[\frac{df^{-1}}{dy}\right]_{y=y_o} &= \left[\frac{df}{dx}\right]^{-1}_{x=f^{-1}(y_o)} \\ &= \frac{1}{f'(a)}\end{aligned} \tag{B.86}$$

Therefore,

$$\int_{-\infty}^{\infty} \delta[f(x) - f(a)]\psi(x)dx = \frac{1}{|f'(a)|}\psi(a) \tag{B.87}$$

where we have used the fact that $f'(a) = |f'(a)|$. This proves the lemma for monotically increasing function.

For monotically decreasing function, we have

$$\begin{aligned}\int_{-\infty}^{\infty}\delta[f(x)-f(a)]\psi(x)dx &= \int_{\infty}^{-\infty}\delta(y-y_o)\psi[f^{-1}(y)](\frac{df^{-1}}{dy})dy \\ &= -\frac{1}{f'(a)}\psi(a) \end{aligned} \tag{B.88}$$

In this case, we have

$$f'(a) = -|f'(a)| \tag{B.89}$$

Using (B.89) in (B.88) completes the proof of the lemma for monotically decreasing function. □

B.10 Proof of Theorem A.9

Let us consider the *form function* of a cover mode with a fixed radiation parameter s_1 as

$$F_c^{(e,h)}(z;s_1) = \begin{cases} b_c e^{js_1(z-d_N)} + a_c^{(e,h)}(s_1)\, e^{-js_1(z-d_N)} & z > d_N \\ A_i^{(e,h)}(s_1)\, ch[\gamma_i(z-d_{i-1})] + B_i^{(e,h)}(s_1)\, sh[\gamma_i(z-d_{i-1})] & d_{i-1} < z < d_i \\ b_s^{(e,h)}(s_1)\, e^{js_2 z} & z < 0 \end{cases} \tag{B.90}$$

where

$$s_2 = \sqrt{(\mu_{r_s}\epsilon_{r_s} - \mu_{r_c}\epsilon_{r_c})k_o^2 + s_1^2} \tag{B.91}$$

The scattered amplitudes in the cover and substrate are related to the incident amplitude via the following matrix equation

$$\mathbf{T}^{(e,h)}(s_1)\begin{bmatrix} 1 \\ js_2 \end{bmatrix} b_s^{(e,h)}(s_1) - \begin{bmatrix} 1 \\ -js_1 \end{bmatrix} a_c^{(e,h)}(s_1) = \begin{bmatrix} 1 \\ js_1 \end{bmatrix} b_c \tag{B.92}$$

where

$$\mathbf{T}^{(e,h)}(s_1) = \prod_{i=N}^{0} \mathbf{T}_{i+1,i}^{(e,h)}(s_1).$$

Moreover, consider the substrate modes with variable radiation parameter s and the *form functions* as

$$F_s^{(e,h)}(z;s) = \begin{cases} a_c^{(e,h)}(s)\, e^{-js_1'(z-d_N)} & z > d_N \\ A_i^{(e,h)}(s)\, ch[\gamma_i(z-d_{i-1})] + B_i^{(e,h)}(s)\, sh[\gamma_i(z-d_{i-1})] & d_{i-1} < z < d_i \\ a_s e^{-jsz} + b_s^{(e,h)}(s)\, e^{jsz} & z < 0 \end{cases} \tag{B.93}$$

where

$$s_1' = \sqrt{s^2 - (\mu_{r_s}\epsilon_{r_s} - \mu_{r_c}\epsilon_{r_c})k_o^2} \tag{B.94}$$

Note that the coefficients in the cover and substrate modes are distinguished by their arguments. For the substrate modes the scattered amplitudes in the cover and substrate regions are related to the incident amplitude via

$$-\mathbf{T}^{(e,h)}(s)\begin{bmatrix} 1 \\ js \end{bmatrix} b_s^{(e,h)}(s) + \begin{bmatrix} 1 \\ -js_1' \end{bmatrix} a_c^{(e,h)}(s) = \mathbf{T}^{(e,h)}(s)\begin{bmatrix} 1 \\ -js \end{bmatrix} a_s \tag{B.95}$$

Now, let

$$H_{s_1}(s) = \ll F_c^{(e,h)}(z;s_1), F_s^{(e,h)}(z;s) \gg \tag{B.96a}$$

$$I_{-\infty}(s_1,s) = \int_{-\infty}^{0} \frac{1}{c^{(e,h)}(z)} F_c^{(e,h)}(z;s_1)\left[F_s^{(e,h)}(z;s)\right]^* dz \tag{B.96b}$$

$$I_N(s_1,s) = \int_{0}^{d_N} \frac{1}{c^{(e,h)}(z)} F_c^{(e,h)}(z;s_1)\left[F_s^{(e,h)}(z;s)\right]^* dz \tag{B.96c}$$

$$I_{\infty}(s_1,s) = \int_{d_N}^{\infty} \frac{1}{c^{(e,h)}(z)} F_c^{(e,h)}(z;s_1)\left[F_s^{(e,h)}(z;s)\right]^* dz \tag{B.96d}$$

Thus,

$$H_{s_1}(s) = I_{-\infty}(s_1,s) + I_N(s_1,s) + I_{\infty}(s_1,s) \tag{B.97}$$

According to Theorem A.8, we have

$$H_{s_1}(s) = 0 \qquad (s \neq s_2) \tag{B.98}$$

Substituting for $F_c^{(\epsilon,h)}(z;s_1)$ and $F_s^{(\epsilon,h)}(z;s)$, we may write

$$\begin{aligned} I_{-\infty}(s_1,s) &= \int_{-\infty}^{0} \frac{1}{c_s^{(\epsilon,h)}} b_s^{(\epsilon,h)}(s_1)\left[a_s^* e^{j(s+s_2)z} + [b_s^{(\epsilon,h)}(s)]^* e^{-j(s-s_2)z}\right] dz \\ &= \frac{1}{c_s^{(\epsilon,h)}} b_s^{(\epsilon,h)}(s_1)\left[\frac{-j}{2s_2} a_s^* + \pi[b_s^{(\epsilon,h)}(s=s_2)]^* \delta(s-s_2)\right] \qquad (s_2^- < s < s_2^+) \end{aligned} \tag{B.99}$$

where we have used (A.79) and

$$\int_{-\infty}^{0} e^{\pm jsz} dz = \int_{0}^{\infty} e^{\mp jsz} dz$$

In a similar fashion, we have

$$I_{\infty}(s_1,s) = \int_{d_N}^{\infty} \frac{1}{c_c^{(\epsilon,h)}} \left[a_c^{(\epsilon,h)}(s=s_2)\right]^* \left[b_c e^{j(s_1+s_1')(z-d_N)} + a_c^{(\epsilon,h)}(s_1) e^{-j(s_1-s_1')(z-d_N)}\right] dz \tag{B.100}$$

Note that

$$s_1' = s_1 \qquad (s=s_2) \tag{B.101}$$

Therefore, using (A.79), we obtain

$$I_{\infty}(s_1,s) = \frac{1}{c_c^{(\epsilon,h)}} \left[a_c^{(\epsilon,h)}(s=s_2)\right]^* \left[\frac{j}{2s_1} b_c + \pi a_c^{(\epsilon,h)}(s_1)\delta(s_1'-s_1)\right] \qquad (s_2^- < s < s_2^+) \tag{B.102}$$

Let

$$s_1' = f(s) \tag{B.103}$$

where $f(s)$ defined by (B.94). Then,

$$s_1' - s_1 = f(s) - f(s_2) \tag{B.104}$$

According to Lemma A.1, we may write

$$\begin{aligned} \delta(s_1'-s_1) &= \frac{1}{f'(s_2)}\delta(s-s_2) \\ &= \frac{s_1}{s_2}\delta(s-s_2) \end{aligned} \tag{B.105}$$

Eq. (B.105) can be easily memorized if we write it in a more convenient form as follows

$$\frac{1}{s_1}\delta(s_1' - s_1) = \frac{1}{s_2}\delta(s - s_2) \tag{B.106}$$

From (B.97)–(B.99), (B.102), and (B.105), we may write

$$H_{s_1}(s) = \begin{cases} 0 & s \neq s_2 \\ A^{(e,h)}(s_1, s_2)\delta(s - s_2) + K^{(e,h)}(s_1, s_2) & s_2^- < s < s_2^+ \end{cases} \tag{B.107}$$

where

$$A^{(e,h)}(s_1, s_2) = \pi\left(\frac{1}{c_s^{(e,h)}} b_s^{(e,h)}(s_1)\left[b_s^{(e,h)}(s = s_2)\right]^* + \frac{1}{c_c^{(e,h)}}\frac{s_1}{s_2} a_c^{(e,h)}(s_1)\left[a_c^{(e,h)}(s = s_2)\right]^*\right) \tag{B.108}$$

$$K^{(e,h)}(s_1, s_2) = \frac{-j}{2s_2 c_s^{(e,h)}} b_s^{(e,h)}(s_1) a_s^* + I_N(s_1, s_2) + \frac{j}{2s_1 c_s^{(e,h)}} b_c\left[a_c^{(e,h)}(s = s_2)\right]^* \tag{B.109}$$

Since the inner products of the radiation modes must be considered as generalized functions, they are meaningful only if they appear under an integral sign with respect to the radiation parameter. Therefore, as far as the orthogonality of the radiation modes are concerned, the finite value $K^{(e,h)}$ is not important. Only the coefficient of delta function in (B.107) matters. However, as will be presently shown

$$A^{(e,h)}(s_1, s_2) = 0 \tag{B.110}$$

To prove (B.110), we invoke the matrix equations in (B.92) and (B.95). According to the reasoning we have used in the proof of Theorems A.3 and A.4, the solutions of (B.92) are

$$b_s^{(e,h)}(s_1) = \frac{\begin{bmatrix} js_1 & 1 \end{bmatrix}\begin{bmatrix} 1 \\ js_1 \end{bmatrix}}{\begin{bmatrix} js_1 & 1 \end{bmatrix}\mathbf{T}^{(e,h)}(s_1)\begin{bmatrix} 1 \\ js_2 \end{bmatrix}} b_c \tag{B.111}$$

$$a_c^{(e,h)}(s_1) = \frac{\begin{bmatrix} -js_2 & 1 \end{bmatrix} \left[\mathbf{T}^{(e,h)}\right]^{-1}(s_1) \begin{bmatrix} 1 \\ js_1 \end{bmatrix}}{\frac{c_s^{(e,h)}}{c_c^{(e,h)}} \begin{bmatrix} js_1 & 1 \end{bmatrix} \mathbf{T}^{(e,h)}(s_1) \begin{bmatrix} 1 \\ js_2 \end{bmatrix}} b_c \tag{B.112}$$

The complex conjugate of (B.95) at $s = s_2$ can be written as

$$\mathbf{T}^{(e,h)}(s_2) \begin{bmatrix} 1 \\ -js_2 \end{bmatrix} \left[b_s^{(e,h)}(s_2)\right]^* - \begin{bmatrix} 1 \\ js_1 \end{bmatrix} \left[a_c^{(e,h)}(s_2)\right]^* = -\mathbf{T}^{(e,h)}(s_2) \begin{bmatrix} 1 \\ js_2 \end{bmatrix} a_s^* \tag{B.113}$$

where we have used the fact that the transfer matrices of a lossless MPS are real-valued. It should also be emphasized that since two degenerate modes correspond to the same value of β, we have

$$\mathbf{T}^{(e,h)}(s = s_2) = \mathbf{T}^{(e,h)}(s_1) \tag{B.114}$$

Solving (B.113) for $\left[b_s^{(e,h)}(s_2)\right]^*$ and $\left[a_c^{(e,h)}(s_2)\right]^*$, yields

$$\left[b_s^{(e,h)}(s_2)\right]^* = \frac{-\begin{bmatrix} -js_1 & 1 \end{bmatrix} \mathbf{T}^{(e,h)}(s_1) \begin{bmatrix} 1 \\ js_2 \end{bmatrix}}{\begin{bmatrix} -js_1 & 1 \end{bmatrix} \mathbf{T}^{(e,h)}(s_1) \begin{bmatrix} 1 \\ -js_2 \end{bmatrix}} a_s^* \tag{B.115}$$

$$\left[a_c^{(e,h)}(s_2)\right]^* = \frac{-\begin{bmatrix} js_2 & 1 \end{bmatrix} \begin{bmatrix} 1 \\ js_2 \end{bmatrix}}{\frac{c_s^{(e,h)}}{c_c^{(e,h)}} \begin{bmatrix} -js_1 & 1 \end{bmatrix} \mathbf{T}^{(e,h)}(s_1) \begin{bmatrix} 1 \\ -js_2 \end{bmatrix}} a_s^* \tag{B.116}$$

where we have used

$$-\begin{bmatrix} js_2 & 1 \end{bmatrix} \left[\mathbf{T}^{(e,h)}(s_1)\right]^{-1} \begin{bmatrix} 1 \\ js_1 \end{bmatrix} = \frac{c_s^{(e,h)}}{c_c^{(e,h)}} \begin{bmatrix} -js_1 & 1 \end{bmatrix} \mathbf{T}^{(e,h)}(s_1) \begin{bmatrix} 1 \\ -js_2 \end{bmatrix} \tag{B.117}$$

Substituting (B.111), (B.112), (B.115), and (B.116) into (B.108), leads to

$$A^{(e,h)}(s_1,s_2) = G^{(e,h)}\left(\begin{bmatrix} -js_1 & 1 \end{bmatrix}\mathbf{T}^{(e,h)}(s_1)\begin{bmatrix} 1 \\ js_2 \end{bmatrix} + \frac{c_c^{(e,h)}}{c_s^{(e,h)}}\begin{bmatrix} -js_2 & 1 \end{bmatrix}\left[\mathbf{T}^{(e,h)}(s_1)\right]^{-1}\begin{bmatrix} 1 \\ js_1 \end{bmatrix}\right) \tag{B.118}$$

where

$$G^{(e,h)} = -\frac{j2s_1}{\pi c_s^{(e,h)} D^{(e,h)}(s_1)\left[D^{(e,h)}(s_1)\right]^*} b_c a_s^*$$

and

$$D^{(e,h)}(s_1) = \begin{bmatrix} js_1 & 1 \end{bmatrix}\mathbf{T}^{(e,h)}(s_1)\begin{bmatrix} 1 \\ js_2 \end{bmatrix}$$

However,

$$\begin{bmatrix} -js_1 & 1 \end{bmatrix}\mathbf{T}^{(e,h)}(s_1)\begin{bmatrix} 1 \\ js_2 \end{bmatrix} = -\frac{c_c^{(e,h)}}{c_s^{(e,h)}}\begin{bmatrix} -js_2 & 1 \end{bmatrix}\left[\mathbf{T}^{(e,h)}(s_1)\right]^{-1}\begin{bmatrix} 1 \\ js_1 \end{bmatrix} \tag{B.119}$$

Using (B.119) in (B.118 leads to (B.110). This completes the proof. □

AN ALTERNATIVE APPROACH

Multiplying (B.92) by the row matrix $\begin{bmatrix} -js_1 & 1 \end{bmatrix}$ leads to

$$b_s^{(e,h)}(s_1) = \frac{-j2s_1}{\begin{bmatrix} -js_1 & 1 \end{bmatrix}\mathbf{T}^{(e,h)}(s_1)\begin{bmatrix} 1 \\ js_2 \end{bmatrix}} a_c^{(e,h)}(s_1) \tag{B.120}$$

In a similar fashion, from (B.113), one may get

$$\left[b_s^{(e,h)}(s_2)\right]^* = \frac{\begin{bmatrix} -js_2 & 1 \end{bmatrix}\left[\mathbf{T}^{(e,h)}(s_2)\right]^{-1}\begin{bmatrix} 1 \\ js_1 \end{bmatrix}}{-j2s_2}\left[a_c^{(e,h)}(s_2)\right]^* \tag{B.121}$$

Multiplying both sides of (B.120) and (B.121), noting that (B.114) holds and

$$\begin{bmatrix} -js_2 & 1 \end{bmatrix} \left[\mathbf{T}^{(e,h)}(s_2)\right]^{-1} \begin{bmatrix} 1 \\ js_1 \end{bmatrix} = -\frac{c_s^{(e,h)}}{c_c^{(e,h)}} \begin{bmatrix} -js_1 & 1 \end{bmatrix} \mathbf{T}^{(e,h)}(s_1) \begin{bmatrix} 1 \\ js_2 \end{bmatrix} \tag{B.122}$$

we obtain

$$b_s^{(e,h)}(s_1)\left[b_s^{(e,h)}(s_2)\right]^* = -\frac{c_s^{(e,h)}}{c_c^{(e,h)}}\frac{s_1}{s_2} a_c^{(e,h)}(s_1)\left[a_c^{(e,h)}(s_2)\right]^* \tag{B.123}$$

Comparing (B.123) with (B.108) leads to (B.110). □

B.11 Proof of the Brewster Theorem

As stated before, this theorem is an immediate consequence of the reciprocity theorem. To prove the theorem, let the MPS be transparent to a substrate mode for some value of $s_2^{(e,h)}$. This means that

$$b_s^{(e,h)}(s_2^{(e,h)}) = 0 \tag{B.124}$$

Since the corresponding degenerate cover mode is orthogonal to the substrate mode, we have

$$A^{(e,h)}(s_1^{(e,h)}, s_2^{(e,h)}) = 0 \tag{B.125}$$

where $A^{(e,h)}(s_1, s_2)$ is defined in (B.108). On substitution of (B.124) into (B.125) and noting that according to (B.116)

$$a_c^{(e,h)}(s_2^{(e,h)}) \neq 0$$

we end up with the following result

$$a_c^{(e,h)}(s_1^{(e,h)}) = 0 \tag{B.126}$$

Eq. (B.126) means that the reflected wave in the cover mode is zero.

It can also be seen that the numerators in (B.112) and (B.115) are proportional. Therefore, vanishing of $b_s^{(e,h)}(s_2)$ results in the vanishing of $a_c^{(e,h)}(s_1)$ and vice versa. This fact can also be seen from another view. If $b_s^{(e,h)}(s_2) = 0$, then the numerator in (B.121) must be zero. According to (B.122), the denominator of (B.120) must also be zero. This is only possible if $a_c^{(e,h)}(s_1) = 0$. Thus, the first part of the proof has been completed. Similar reasoning can be used to prove $b_s^{(e,h)}(s_2) = 0$, if $a_c^{(e,h)}(s_1) = 0$. □

B.12 Proof of Theorem A.12

Let us consider the *form function* of the substrate mode with the radiation parameter s as follows

$$F_s^{(e,h)}(z;s) = \begin{cases} a_c^{(e,h)}(s)\, e^{-\gamma_c(z-d_N)} & z > d_N \\ A_i^{(e,h)}(s)\, ch[\gamma_i(z-d_{i-1})] + B_i^{(e,h)}(s)\, sh[\gamma_i(z-d_{i-1})] & d_{i-1} < z < d_i \\ a_s e^{-jsz} + b_s^{(e,h)}(s)\, e^{jsz} & z < 0 \end{cases} \tag{B.127}$$

where

$$\gamma_c = \sqrt{(\mu_{r_s}\epsilon_{r_s} - \mu_{r_c}\epsilon_{r_c})k_o^2 - s^2} \tag{B.128}$$

Following the proof of Theorem A.9, let

$$H_{s_1}(s) = \ll F_s^{(e,h)}(z;s_1), F_s^{(e,h)}(z;s) \gg \tag{B.129a}$$

$$I_{-\infty}(s_1,s) = \int_{-\infty}^{0} \frac{1}{c^{(e,h)}(z)} F_s^{(e,h)}(z;s_1)\left[F_s^{(e,h)}(z;s)\right]^* dz \tag{B.129b}$$

$$I_N(s_1,s) = \int_{0}^{d_N} \frac{1}{c^{(e,h)}(z)} F_s^{(e,h)}(z;s_1)\left[F_s^{(e,h)}(z;s)\right]^* dz \tag{B.129c}$$

$$I_{\infty}(s_1,s) = \int_{d_N}^{\infty} \frac{1}{c^{(e,h)}(z)} F_s^{(e,h)}(z;s_1)\left[F_s^{(e,h)}(z;s)\right]^* dz \tag{B.129d}$$

Therefore,

$$H_{s_1}(s) = I_{-\infty}(s_1, s) + I_N(s_1, s) + I_\infty(s_1, s) \tag{B.130}$$

According to Theorem A.7, we have

$$H_{s_1}(s) = 0 \qquad (s \neq s_1) \tag{B.131}$$

Moreover,

$$\begin{aligned} I_{-\infty}(s_1, s) &= \int_{-\infty}^{0} \frac{1}{c_s^{(\epsilon,h)}} \left(|a_s|^2 e^{-j(s_1 - s)} + a_s \left[b_s^{(\epsilon,h)}(s) \right]^* e^{-j(s_1 + s)} \right. \\ &+ \left. b_s^{(\epsilon,h)}(s_1) a_s^* e^{j(s_1 + s)} + b_s^{(\epsilon,h)}(s_1) \left[b_s^{(\epsilon,h)}(s) \right]^* e^{j(s_1 - s)} \right) dz \\ &= \frac{\pi}{c_s^{(\epsilon,h)}} |a_s|^2 \delta(s - s_1) + \frac{j}{2 s_1 c_s^{(\epsilon,h)}} \left(a_s \left[b_s^{(\epsilon,h)}(s_1) \right]^* - b_s^{(\epsilon,h)}(s_1) a_s^* \right) \\ &+ \frac{\pi}{c_s^{(\epsilon,h)}} |b_s(s_1)|^2 \delta(s - s_1) \qquad (s_1^- < s < s_1^+) \end{aligned} \tag{B.132}$$

where we have used (A.79) and

$$\int_{-\infty}^{0} e^{\pm jsz} dz = \int_{0}^{\infty} e^{\mp jsz} dz$$

To calculate $I_\infty(s_1, s)$, we consider substrate modes of type I and II separately. More precisely, let us assume that

$$I_\infty(s_1, s) = \begin{cases} I_\infty(s_1, s, I) & \text{if } F_s^{(\epsilon,h)}(s_1) \text{ is of type I} \\ I_\infty(s_1, s, II) & \text{if } F_s^{(\epsilon,h)}(s_1) \text{ is of type II} \end{cases} \tag{B.133}$$

$$\begin{aligned} I_\infty(s_1, s, I) &= \int_{d_N}^{\infty} \frac{1}{c_c^{(\epsilon,h)}} a_c^{(\epsilon,h)}(s_1) \left[a_c^{(\epsilon,h)}(s) \right]^* e^{(-\gamma_{c1} + j\tau_c)(z - d_N)} dz \\ &= \frac{1}{c_c^{(\epsilon,h)}} |a_c^{(\epsilon,h)}(s_1)|^2 \frac{1}{2\gamma_{c1}} \qquad (s_1^- < s < s_1^+) \end{aligned} \tag{B.134}$$

where

$$\begin{aligned} \gamma_{c_1} &= \sqrt{(\mu_{r_s} \epsilon_{r_s} - \mu_{r_c} \epsilon_{r_c}) k_o^2 - s_1^2} \\ \tau_c &= \sqrt{s^2 - (\mu_{r_s} \epsilon_{r_s} - \mu_{r_c} \epsilon_{r_c}) k_o^2} \end{aligned} \tag{B.135}$$

Note that for substrate mode of type I, we have

$$j\tau_c = -\gamma_{c_1} \qquad (s_1^- < s < s_1^+)$$

On the other hand,

$$\begin{aligned} I_\infty(s_1, s, II) &= \int_{d_N}^{\infty} \frac{1}{c_c^{(e,h)}} a_c^{(e,h)}(s_1) \left[a_c^{(e,h)}(s)\right]^* e^{-j(\tau_{c_1}-\tau_c)(z-d_N)} dz \\ &= \frac{\pi}{c_c^{(e,h)}} |a_c^{(e,h)}(s_1)|^2 \delta(\tau_c - \tau_{c_1}) \qquad (s_1^- < s < s_1^+) \\ &= \frac{\pi}{c_c^{(e,h)}} |a_c^{(e,h)}(s_1)|^2 \frac{\tau_{c_1}}{s_1} \delta(s - s_1) \end{aligned} \tag{B.136}$$

where we have used Lemma A.1 and (B.135). Using (B.129)–(B.134), and (B.136), we may write

$$H_{s_1}(s) = \begin{cases} 0 & s \neq s_2 \\ A_{I,II}^{(e,h)}(s_1)\delta(s - s_1) + K_{I,II}^{(e,h)}(s_1) & s_1^- < s < s_1^+ \end{cases} \tag{B.137}$$

where

$$A_I^{(e,h)}(s_1) = \frac{\pi}{c_s^{(e,h)}} |a_s|^2 + \frac{\pi}{c_s^{(e,h)}} |b_s^{(e,h)}(s_1)|^2 \tag{B.138}$$

$$K_I^{(e,h)}(s_1) = \frac{j}{2s_1 c_s^{(e,h)}} \left(a_s \left[b_s^{(e,h)}(s_1)\right]^* - b_s^{(e,h)}(s_1) a_s^*\right) + \frac{1}{c_c^{(e,h)}} |a_c^{(e,h)}(s_1)|^2 \frac{1}{2\gamma_{c1}} \tag{B.139}$$

$$A_{II}^{(e,h)}(s_1) = \frac{\pi}{c_s^{(e,h)}} |a_s|^2 + \frac{\pi}{c_s^{(e,h)}} |b_s^{(e,h)}(s_1)|^2 + \frac{\pi}{c_c^{(e,h)}} \frac{\tau_{c_1}}{s_1} |a_c^{(e,h)}(s_1)|^2 \tag{B.140}$$

$$K_{II}^{(e,h)}(s_1) = \frac{j}{2s_1 c_s^{(e,h)}} \left(a_s \left[b_s^{(e,h)}(s_1)\right]^* - b_s^{(e,h)}(s_1) a_s^*\right) \tag{B.141}$$

However, according to Theorem A.4, if one uses (A.72) and (A.73) in (B.138) and (B.140), one obtains

$$A_I^{(e,h)}(s_1) = A_{II}^{(e,h)}(s_1) = \frac{2\pi}{c_s^{(e,h)}} |a_s|^2 \tag{B.142}$$

On substitution of (B.142) into (B.137), we may write

$$H_{s_1}(s) = \begin{cases} 0 & s \neq s_2 \\ \frac{2\pi}{c_s^{(e,h)}} |a_s|^2 \delta(s - s_1) + K_{I,II}^{(e,h)}(s_1) & s_1^- < s < s_1^+ \end{cases} \tag{B.143}$$

As emphasized before, the inner product of the radiation modes are meaningful only if they appear under the integral sign. Therefore, (B.143) is equivalent to

$$H_{s_1}(s) = \frac{2\pi}{c_s^{(\epsilon,h)}} |a_s|^2 \delta(s - s_1) \tag{B.144}$$

which is the statement of Theorem A.12. □

B.13 Proof of Theorem A.13

For substrate modes we have

$$\mathbf{T}^{(\epsilon,h)}(s) \begin{bmatrix} 1 \\ js \end{bmatrix} b_s^{(\epsilon,h)}(s) - \begin{bmatrix} 1 \\ -js \end{bmatrix} a_c^{(\epsilon,h)}(s) = -\mathbf{T}^{(\epsilon,h)}(s) \begin{bmatrix} 1 \\ -js \end{bmatrix} a_s \tag{B.145}$$

Therefore,

$$\begin{aligned} T_s^{(\epsilon,h)}(s) \stackrel{\text{def}}{=} \frac{a_c^{(\epsilon,h)}(s)}{a_s} &= \frac{j2s}{-\begin{bmatrix} -js & 1 \end{bmatrix} \left[\mathbf{T}^{(\epsilon,h)}(s)\right]^{-1} \begin{bmatrix} 1 \\ -js \end{bmatrix}} \\ &= \frac{c_c^{(\epsilon,h)}}{c_s^{(\epsilon,h)}} \frac{j2s}{\begin{bmatrix} js & 1 \end{bmatrix} \mathbf{T}^{(\epsilon,h)}(s) \begin{bmatrix} 1 \\ js \end{bmatrix}} \\ &= \frac{j2s}{\begin{bmatrix} js & 1 \end{bmatrix} \mathbf{T}^{(\epsilon,h)}(s) \begin{bmatrix} 1 \\ js \end{bmatrix}} \end{aligned} \tag{B.146}$$

where we have used

$$\frac{c_c^{(\epsilon,h)}}{c_s^{(\epsilon,h)}} = 1$$

For cover modes we have

$$\mathbf{T}^{(\epsilon,h)}(s) \begin{bmatrix} 1 \\ js \end{bmatrix} b_s^{(\epsilon,h)}(s) - \begin{bmatrix} 1 \\ -js \end{bmatrix} a_c^{(\epsilon,h)}(s) = \begin{bmatrix} 1 \\ js \end{bmatrix} b_c \tag{B.147}$$

Consequently,

$$T_c^{(\epsilon,h)}(s) \stackrel{\text{def}}{=} \frac{b_s^{(\epsilon,h)}(s)}{b_c} = \frac{j2s}{\begin{bmatrix} js & 1 \end{bmatrix} \mathbf{T}^{(\epsilon,h)}(s) \begin{bmatrix} 1 \\ js \end{bmatrix}} \tag{B.148}$$

Comparing (B.146) with (B.148), we have

$$T_s^{(\epsilon,h)}(s) = T_c^{(\epsilon,h)}(s)$$

To prove (A.159), first from (B.145), we get

$$R_s^{(\epsilon,h)}(s) \stackrel{\text{def}}{=} \frac{b_s^{(\epsilon,h)}(s)}{a_s} = \frac{-\begin{bmatrix} js & 1 \end{bmatrix} \mathbf{T}^{(\epsilon,h)}(s) \begin{bmatrix} 1 \\ -js \end{bmatrix}}{D^{(\epsilon,h)}(s)} \tag{B.149}$$

where $D^{(\epsilon,h)}(s)$ is the denominator in (B.146).

In a similar fashion, if we use (B.147), we obtain

$$\begin{aligned} R_c^{(\epsilon,h)}(s) \stackrel{\text{def}}{=} \frac{a_c^{(\epsilon,h)}(s)}{b_c} &= \frac{\begin{bmatrix} -js & 1 \end{bmatrix} \left[\mathbf{T}^{(\epsilon,h)}(s)\right]^{-1} \begin{bmatrix} 1 \\ js \end{bmatrix}}{-\begin{bmatrix} -js & 1 \end{bmatrix} \left[\mathbf{T}^{(\epsilon,h)}(s)\right]^{-1} \begin{bmatrix} 1 \\ -js \end{bmatrix}} \\ &= \frac{-\begin{bmatrix} -js & 1 \end{bmatrix} \mathbf{T}^{(\epsilon,h)}(s) \begin{bmatrix} 1 \\ js \end{bmatrix}}{D^{(\epsilon,h)}(s)} \end{aligned} \tag{B.150}$$

Comparing (B.149) with (B.150), we see that the denominators are the same. However, the numerators are complex conjugates of each other. Consequently,

$$|R_s^{(\epsilon,h)}(s)| = |R_c^{(\epsilon,h)}(s)|$$

Therefore, the proof of the theorem is completed. □

B.14 Proof of Theorem A.14

To establish the proof of Theorem A.14, we take advantage of an interesting property of a symmetric MPS. Based on the physical considerations or by changing the variable z to $d_N - \eta$, it can be argued that

$$R_s^{(\epsilon,h)}(s) = R_c^{(\epsilon,h)}(s) \tag{B.151}$$

Now comparing (B.149) with (B.150), we have

$$\begin{bmatrix} js & 1 \end{bmatrix} \mathbf{T}^{(\epsilon,h)}(s) \begin{bmatrix} 1 \\ -js \end{bmatrix} = \begin{bmatrix} -js & 1 \end{bmatrix} \mathbf{T}^{(\epsilon,h)}(s) \begin{bmatrix} 1 \\ -js \end{bmatrix} \tag{B.152}$$

Since the LHS of (B.152) is the complex conjugate of its RHS, the imaginary part of each side must vanish. Using this condition and after matrix multiplication in (B.152), we obtain (A.161). □

B.15 Some Useful Integral Formulas

The following useful integral formulas can be easily obtained by substituting trigonometric functions with their complex exponential representations and using (A.79).

$$\int_0^\infty cos(sz)\,cos(s_1 z)\,dz = \frac{1}{2}\int_{-\infty}^\infty cos(sz)\,cos(s_1 z)\,dz = \frac{\pi}{2}\delta(s - s_1) \tag{B.153}$$

$$\int_0^\infty sin(sz)\,sin(s_1 z)\,dz = \frac{1}{2}\int_{-\infty}^\infty sin(sz)\,sin(s_1 z)\,dz = \frac{\pi}{2}\delta(s - s_1) \tag{B.154}$$

$$\int_0^\infty cos(s - s_1)z\,dz = \frac{1}{2}\int_{-\infty}^\infty cos(s - s_1)z\,dz = \pi\delta(s - s_1) \tag{B.155}$$

$$\int_0^\infty sin(sz)\,cos(s_1 z)\,dz = \begin{cases} \frac{1}{2}\left[\frac{1}{s+s_1} + \frac{1}{s-s_1}\right] & s \neq s_1 \\ \frac{1}{4s_1} & s = s_1 \end{cases} \tag{B.156}$$

$$\int_0^\infty cos(sz)\, sin(s_1 z)\, dz = \begin{cases} \frac{1}{2}\left[\frac{1}{s+s_1} - \frac{1}{s-s_1}\right] & s \neq s_1 \\ \frac{1}{4s_1} & s = s_1 \end{cases} \tag{B.157}$$

$$\int_0^\infty sin(s-s_1)z\, dz = \begin{cases} \frac{1}{s-s_1} & s \neq s_1 \\ 0 & s = s_1 \end{cases} \tag{B.158}$$

Of course, as it may be expected, since the integrands in (B.156)– (B.158) are odd functions of z, all the integrals in (B.156)– (B.158) vanish if the lower limit of the integrals change to $-\infty$.

If one directly calculates the integral (B.155), one obtains

$$\begin{aligned} \int_0^\infty cos(s-s_1)z\, dz &= \left[\frac{sin(s-s_1)z}{s-s_1}\right]_{z=0}^{z=\infty} \\ &= \lim_{z\to\infty} \frac{sin(s-s_1)z}{s-s_1} \end{aligned} \tag{B.159}$$

Comparing (B.159) with (B.155) leads to the following familiar formula

$$\lim_{z\to\infty} \frac{sin(s-s_1)z}{\pi(s-s_1)} = \delta(s-s_1) \tag{B.160}$$

The above formula is usually used for the normalization of the radiation modes in the literature.

Appendix C

C.1 Derivation of $\widetilde{\Psi}^{(e,h)}(k_x, k_y, z)$ for $z_o \geq d_N$

Let

$$\tau = z_o - d_N > 0 \tag{C.1}$$

In this case $\tilde{\Psi}_i^{(e,h)}(k_x, k_y, z)$ can be written as

$$\tilde{\Psi}^{(e,h)}(k_x, k_y, z) = \begin{cases} a_c^{(e,h)}(k_x, k_y) e^{-\gamma_c(z-d_N)} & z > z_o \\ A_c^{(e,h)}(k_x, k_y) ch[\gamma_c(z-d_N)] + B_c^{(e,h)}(k_x, k_y) sh[\gamma_c(z-d_N)] & d_N < z < z_o \\ A_i^{(e,h)}(k_x, k_y) ch[\gamma_i(z-d_{i-1})] + B_i^{(e,h)}(k_x, k_y) sh[\gamma_i(z-d_{i-1})] & d_{i-1} < z < d_i \\ b_s^{(e,h)}(k_x, k_y) e^{\gamma_s z} & z < 0 \end{cases} \tag{C.2}$$

where

$$\gamma_c = \sqrt{k_x^2 + k_y^2 - \mu_{r_c}\epsilon_{r_c} k_o^2} = \sqrt{\beta^2 - \mu_{r_c}\epsilon_{r_c} k_o^2} \tag{C.3a}$$

$$\gamma_i = \sqrt{k_x^2 + k_y^2 - \mu_{r_c}\mu_{r_i}\epsilon_{r_i} k_o^2} = \sqrt{\beta^2 - \mu_{r_c}\epsilon_{r_c} k_o^2} \tag{C.3b}$$

$$\gamma_s = \sqrt{k_x^2 + k_y^2 - \mu_{r_s}\epsilon_{r_s} k_o^2} = \sqrt{\beta^2 - \mu_{r_s}\epsilon_{r_s} k_o^2} \tag{C.3c}$$

As will be shown later, the spectral approach requires that each coefficient be a function of (k_x, k_y) which is reflected in (C.2).

LSM excitation

The boundary conditions (2.26) at $z = z_o$ result in

$$\begin{bmatrix} 1 \\ -\gamma_c \end{bmatrix} a_c^e(k_x,k_y)e^{-\gamma_c\tau} - \mathbf{D}(\gamma_c;\tau)\begin{bmatrix} A_c^e(k_x,k_y) \\ \gamma_c B_c^e(k_x,k_y) \end{bmatrix} = \mathbf{A}^e(k_x,k_y)\begin{bmatrix} \tilde{J}_x(k_x,k_y,z_o) \\ \tilde{J}_y(k_x,k_y,z_o) \end{bmatrix} \tag{C.4}$$

where

$$\mathbf{D}(\gamma_c;\tau) = \begin{bmatrix} ch(\gamma_c\tau) & \frac{sh(\gamma_c\tau)}{\gamma_c} \\ \gamma_c sh(\gamma_c\tau) & ch(\gamma_c\tau) \end{bmatrix} \tag{C.5}$$

$$\mathbf{A}^e(k_x,k_y) = \begin{bmatrix} \frac{k_x}{\omega\epsilon_o(k_x^2+k_y^2)} & \frac{k_y}{\omega\epsilon_o(k_x^2+k_y^2)} \\ 0 & 0 \end{bmatrix} \tag{C.6}$$

It can be easily seen that (C.4) can be rewritten as

$$\mathbf{D}(\gamma_c;\tau)\left(\begin{bmatrix} 1 \\ -\gamma_c \end{bmatrix} a_c^e(k_x,k_y) - \begin{bmatrix} A_c^e(k_x,k_y) \\ \gamma_c B_c^e(k_x,k_y) \end{bmatrix}\right) = \mathbf{A}^e(k_x,k_y)\begin{bmatrix} \tilde{J}_x(k_x,k_y,z_o) \\ \tilde{J}_y(k_x,k_y,z_o) \end{bmatrix} \tag{C.7}$$

where we have used

$$\mathbf{D}(\gamma_c;\tau)\begin{bmatrix} 1 \\ -\gamma_c \end{bmatrix} = \begin{bmatrix} 1 \\ -\gamma_c \end{bmatrix} e^{-\gamma_c\tau}$$

Now, since there is no current source at $z = d_i \quad (i = 0, 1, \ldots N)$, the boundary conditions in (2.26) lead to

$$\begin{bmatrix} A_{i+1}^e(k_x,k_y) \\ \gamma_{i+1}^{(e,h)} B_{i+1}^{(e,h)}(k_x,k_y) \end{bmatrix} = \mathbf{T}_{i+1,i}^e(\beta)\begin{bmatrix} A_i^{(e,h)}(k_x,k_y) \\ \gamma_i^{(e,h)} B_i^{(e,h)}(k_x,k_y) \end{bmatrix} \tag{C.8}$$

where $\mathbf{T}_{i+1,i}^e(\beta)$, $(i \neq 0)$ have exactly the same mathematical form as $\mathbf{T}_{i+1,i}^e$ in (B.18). Moreover,

$$\mathbf{T}_{1,0}^e(\beta) = \begin{bmatrix} 1 & 0 \\ 0 & \frac{\epsilon_{r1}}{\epsilon_{r_s}} \end{bmatrix} \tag{C.9}$$

By successive application of the boundary conditions at $z = d_i \quad (i = 0, 1, \ldots N)$, (C.7) can be rewritten as

$$\begin{bmatrix} 1 \\ -\gamma_c \end{bmatrix} a_c^e - \mathbf{T}^e(\beta) \begin{bmatrix} 1 \\ \gamma_s \end{bmatrix} b_s^e = \mathbf{D}^{-1}(\gamma_c;\tau)\mathbf{A}^e(k_x,k_y) \begin{bmatrix} \tilde{J}_x(k_x,k_y,z_o) \\ \tilde{J}_y(k_x,k_y,z_o) \end{bmatrix} \tag{C.10}$$

where

$$\mathbf{T}^e(\beta) = \prod_{i=N}^{0} \mathbf{T}^e_{i+1,i}(\beta) \tag{C.11}$$

Moreover, the dependence of a_c^e and b_s^e on (k_x, k_y) is tacitly assumed to make the expression in (C.10) simple. Eq. (C.10) can be solved for a_c^e and b_s^e. Following the same procedures as in Appendix B we have

$$a_c^e(k_x,k_y) = \frac{-\frac{\epsilon_{r_c}}{\epsilon_{r_s}} \begin{bmatrix} -\gamma_s & 1 \end{bmatrix} [\mathbf{T}^e(\beta)]^{-1} \mathbf{D}^{-1}(\gamma_c;\tau)\mathbf{A}^e(k_x,k_y) \begin{bmatrix} \tilde{J}_x(k_x,k_y,z_o) \\ \tilde{J}_y(k_x,k_y,z_o) \end{bmatrix}}{D^e(\beta)} \tag{C.12}$$

$$b_s^e(k_x,k_y) = \frac{-\begin{bmatrix} \gamma_c & 1 \end{bmatrix} \mathbf{D}^{-1}(\gamma_c;\tau)\mathbf{A}^e(k_x,k_y) \begin{bmatrix} \tilde{J}_x(k_x,k_y,z_o) \\ \tilde{J}_y(k_x,k_y,z_o) \end{bmatrix}}{D^e(\beta)} \tag{C.13}$$

where

$$D^e(\beta) = \begin{bmatrix} \gamma_c & 1 \end{bmatrix} \mathbf{T}^e(\beta) \begin{bmatrix} 1 \\ \gamma_s \end{bmatrix} \tag{C.14}$$

Once $a_c^e(k_x,k_y)$ and $b_s^e(k_x,k_y)$ have been determined all other coefficients in (C.2) can be obtained by successive application of the transfer matrix method. It should be emphasized the above expressions for a_c^e and b_s^e are still valid if $\tau = 0$, that is, $z_o = d_N$. It is also interesting to note that the denominators in (C.12) and (C.13) have the same mathematical form as the characteristic equation of a MPS for a LSM mode has. That is why the poles of the Green's functions are referred to as surface wave poles. This is the natural consequence of using the spectral domain

approach which is closely linked to the method of the separation of variables. The fact that the poles of the spectral Green's functions of a MPS are the surface waves propagating in the corresponding MPS can only be shown explicitly by using the transfer matrix method. This is another reason for the power and beauty of this method in comparison with other ones.

LSE excitation

In this case, starting with the boundary conditions in (2.27) and following the same line as before, one may obtain

$$\begin{bmatrix} 1 \\ -\gamma_c \end{bmatrix} a_c^h - \mathbf{T}^h(\beta) \begin{bmatrix} 1 \\ \gamma_s \end{bmatrix} b_s^h = \mathbf{D}^{-1}(\gamma_c;\tau)\mu_{r_c}\mathbf{A}^h(k_x,k_y) \begin{bmatrix} \tilde{J}_x(k_x,k_y,z_o) \\ \tilde{J}_y(k_x,k_y,z_o) \end{bmatrix} \quad \text{(C.15)}$$

where

$$\mathbf{A}^h(k_x,k_y) = \begin{bmatrix} 0 & 0 \\ \frac{-jk_y}{k_x^2+k_y^2} & \frac{jk_x}{k_x^2+k_y^2} \end{bmatrix} \quad \text{(C.16)}$$

$$\mathbf{T}^h(\beta) = \prod_{i=N}^{0} \mathbf{T}_{i+1,i}^h(\beta) \quad \text{(C.17)}$$

The mathematical representation of $\mathbf{T}_{i+1,i}^h(\beta)$, $(i \neq 0)$ is given in (B.18). For $i = 0$, we have

$$\mathbf{T}_{1,0}^h(\beta) = \begin{bmatrix} 1 & 0 \\ 0 & \frac{\mu_{r_1}}{\mu_{r_s}} \end{bmatrix} \quad \text{(C.18)}$$

$a_c^h(k_x,k_y)$ and $b_s^h(k_x,k_y)$ can be obtained by similar expressions for $a_c^e(k_x,k_y)$ and $b_s^e(k_x,k_y)$ in (C.12) and (C.13), respectively. That is,

$$a_c^h(k_x,k_y) = \frac{-\frac{\mu_{r_c}}{\mu_{r_s}} \begin{bmatrix} -\gamma_s & 1 \end{bmatrix} \left[\mathbf{T}^h(\beta)\right]^{-1} \mathbf{D}^{-1}(\gamma_c;\tau)\mu_{r_c}\mathbf{A}^h(k_x,k_y) \begin{bmatrix} \tilde{J}_x(k_x,k_y,z_o) \\ \tilde{J}_y(k_x,k_y,z_o) \end{bmatrix}}{D^h(\beta)} \quad \text{(C.19)}$$

$$b_s^h(k_x,k_y)=\frac{-\left[\begin{array}{cc}\gamma_c & 1\end{array}\right]\mathbf{D}^{-1}(\gamma_c;\tau)\mu_{r_c}\mathbf{A}^h(k_x,k_y)\left[\begin{array}{c}\tilde{J}_x(k_x,k_y,z_o)\\ \tilde{J}_y(k_x,k_y,z_o)\end{array}\right]}{D^h(\beta)} \tag{C.20}$$

where

$$D^h(\beta)=\left[\begin{array}{cc}\gamma_c & 1\end{array}\right]\mathbf{T}^h(\beta)\left[\begin{array}{c}1\\ \gamma_s\end{array}\right] \tag{C.21}$$

The same comments for LSM excitation can be applied for this case. Especially, the above expressions for $a_c^h(k_x,k_y)$ and $b_s^h(k_x,k_y)$ are valid for $\tau=0$, that is, when $z_o=d_N$.

C.2 Derivation of $\tilde{\Psi}^{(e,h)}(k_x,k_y,z)$ for $d_{k-1}\le z_o<d_k$

Assume that

$$z_o-d_{k-1}=\tau,\quad 0<\tau<t_k \tag{C.22}$$

For this case, one may write the following expressions for $\tilde{\Psi}^{(e,h)}(k_x,k_y,z)$

$$\tilde{\Psi}^{(e,h)}(k_x,k_y,z)=\begin{cases} a_c^{(e,h)}(k_x,k_y)e^{-\gamma_c(z-d_N)} & z>0\\ A_i^{(e,h)}(k_x,k_y)ch[\gamma_i(z-d_{i-1})]+B_i^{(e,h)}(k_x,k_y)sh[\gamma_i(z-d_{i-1})] & d_{i-1}<z<d_i,\ i\neq k\\ U_k^{(e,h)}(k_x,k_y)ch[\gamma_k(z-d_{k-1})]+V_k^{(e,h)}(k_x,k_y)sh[\gamma_k(z-d_{k-1})] & z_o<z<d_k\\ A_k^{(e,h)}(k_x,k_y)ch[\gamma_k(z-d_{k-1})]+B_k^{(e,h)}(k_x,k_y)sh[\gamma_k(z-d_{k-1})] & d_{k-1}<z<z_o\\ b_s^{(e,h)}(k_x,k_y)e^{\gamma_s z} & z<0\end{cases} \tag{C.23}$$

where γ_c, γ_i, and γ_s are given in (C.3).

LSM excitation

Applying the boundary conditions reflected in (2.26), we have

$$\mathbf{D}(\gamma_k,\tau)\left(\begin{bmatrix} U_k^e(k_x,k_y) \\ \gamma_k V_k^e(k_x,k_y) \end{bmatrix} - \begin{bmatrix} A_k^e(k_x,k_y) \\ \gamma_k B_k^e(k_x,k_y) \end{bmatrix}\right) = \mathbf{A}^e(k_x,k_y)\begin{bmatrix} \tilde{J}_x(k_x,k_y,z_o) \\ \tilde{J}_y(k_x,k_y,z_o) \end{bmatrix} \tag{C.24}$$

where $\mathbf{D}(\gamma_k,\tau)$ is given in (C.5) with γ_c substituted by γ_k. $\mathbf{A}^e(k_x,k_y)$ is expressed by (C.6). By successive application of the boundary conditions at $z = d_k, d_{k+1}, \ldots, d_N$, $U_k^e(k_x,k_y)$ and $\gamma_k V_k^e(k_x,k_y)$ can be evaluated in terms of $a_c^e(k_x,k_y)$ as follows

$$\begin{bmatrix} U_k^e(k_x,k_y) \\ \gamma_k V_k^e(k_x,k_y) \end{bmatrix} = \prod_{i=k}^{N}\left[\mathbf{T}_{i+1,i}^e(\beta)\right]^{-1}\begin{bmatrix} 1 \\ -\gamma_c \end{bmatrix} a_c^e(k_x,k_y) \tag{C.25}$$

Similarly, successive application of the boundary conditions at $z = d_{k-1}, \ldots, d_o(=0)$ yields

$$\begin{bmatrix} A_k^e(k_x,k_y) \\ \gamma_k B_k^e(k_x,k_y) \end{bmatrix} = \prod_{i=k-1}^{0}\mathbf{T}_{i+1,i}^e(\beta)\begin{bmatrix} 1 \\ \gamma_s \end{bmatrix} b_s^e(k_x,k_y) \tag{C.26}$$

Substitution of (C.25) and (C.26) into (C.24) leads to the following system of inhomogeneous linear equations in $a_c^e(k_x,k_y)$ and $b_s^e(k_x,k_y)$

$$\begin{bmatrix} 1 \\ -\gamma_c \end{bmatrix} a_c^e - \mathbf{T}^e(\beta)\begin{bmatrix} 1 \\ \gamma_s \end{bmatrix} b_s^e = \left[\prod_{i=N}^{k}\mathbf{T}_{i+1,i}^e(\beta)\right]\mathbf{D}^{-1}(\gamma_k,\tau)\mathbf{A}^e(k_x,k_y)\times \begin{bmatrix} \tilde{J}_x(k_x,k_y,z_o) \\ \tilde{J}_y(k_x,k_y,z_o) \end{bmatrix} \tag{C.27}$$

where $\mathbf{T}^e(\beta)$ is given by (C.11). Solving (C.27) for $a_c^e(k_x,k_y)$ and $b_s^e(k_x,k_y)$, we get

$$a_c^e(k_x,k_y) = \frac{-\frac{\epsilon_{r_c}}{\epsilon_{r_s}}\begin{bmatrix} -\gamma_s & 1 \end{bmatrix}\mathbf{M}_{k-1}^e(\beta)\mathbf{D}^{-1}(\gamma_k,\tau)\mathbf{A}^e(k_x,k_y)\begin{bmatrix} \tilde{J}_x(k_x,k_y,z_o) \\ \tilde{J}_y(k_x,k_y,z_o) \end{bmatrix}}{D^e(\beta)} \tag{C.28}$$

where $D^e(\beta)$ is given by (C.14) and

$$\mathbf{M}^e_{k-1}(\beta) = \prod_{i=0}^{k-1} \left[\mathbf{T}^e_{i+1,i}(\beta)\right]^{-1} \tag{C.29}$$

$$b^e_s(k_x,k_y) = \frac{-\begin{bmatrix} \gamma_c & 1 \end{bmatrix} \mathbf{N}^e_k(\beta)\mathbf{D}^{-1}(\gamma_k,\tau)\mathbf{A}^e(k_x,k_y) \begin{bmatrix} \tilde{J}_x(k_x,k_y,z_o) \\ \tilde{J}_y(k_x,k_y,z_o) \end{bmatrix}}{D^e(\beta)} \tag{C.30}$$

where

$$\mathbf{N}^e_k(\beta) = \prod_{i=N}^{k} \mathbf{T}^e_{i+1,i}(\beta) \tag{C.31}$$

Once $a^e_c(k_x,k_y)$ and $b^e_s(k_x,k_y)$ have been determined, all other coefficients can be obtained by using the transfer matrix method. Therefore, according to (C.22), $\tilde{\Psi}^e(k_x,k_y,z)$ can be obtained. Note that the above derivation of $\tilde{\Psi}^e(k_x,k_y,z)$ is based on the assumption that $0 < \tau < t_k$. It can be shown that the above results are still valid for $\tau = 0$. That is, $z_o = d_{k-1} \quad (k = 1,\ldots,N)$.

LSE excitation

Following the same reasoning for LSE excitation, the boundary conditions in (2.27) require that

$$\begin{bmatrix} 1 \\ -\gamma_c \end{bmatrix} a^h_c - \mathbf{T}^h(\beta) \begin{bmatrix} 1 \\ \gamma_s \end{bmatrix} b^h_s = \left[\prod_{i=N}^{k} \mathbf{T}^h_{i+1,i}(\beta)\right] \mathbf{D}^{-1}(\gamma_k,\tau)\mu_{r_k} bf A^h(k_x,k_y) \times \begin{bmatrix} \tilde{J}_x(k_x,k_y,z_o) \\ \tilde{J}_y(k_x,k_y,z_o) \end{bmatrix} \tag{C.32}$$

where $\mathbf{A}^h(k_x,k_y)$ is given in (C.16). The above system of equations can be easily solved for $a^h_c(k_x,k_y)$ and $b^h_s(k_x,k_y)$ as before. That is, by changing the superscript e to h and ϵ_r to μ_r, the expressions in (C.28) and (C.30) multiplied by μ_{r_k} can be

used to obtain the solutions for for $a_c^h(k_x,k_y)$ and $b_s^h(k_x,k_y)$. Hence

$$a_c^h(k_x,k_y) = \frac{-\frac{\mu_{r_c}}{\mu_{r_s}}\begin{bmatrix} -\gamma_s & 1 \end{bmatrix}\mathbf{M}_{k-1}^h(\beta)\mathbf{D}^{-1}(\gamma_k;\tau)\mu_{r_k}\mathbf{A}^h(k_x,k_y)\begin{bmatrix} \tilde{J}_x(k_x,k_y,z_o) \\ \tilde{J}_y(k_x,k_y,z_o) \end{bmatrix}}{D^h(\beta)} \tag{C.33}$$

where $D^h(\beta)$ is defined by (C.21). The expression for $\mathbf{M}_{k-1}^h(\beta)$ can be obtained from (C.29) by changing the superscript e to h.

$$b_s^h(k_x,k_y) = \frac{-\begin{bmatrix} \gamma_c & 1 \end{bmatrix}\mathbf{N}_k^h(\beta)\mathbf{D}^{-1}(\gamma_k;\tau)\mu_{r_k}\mathbf{A}^h(k_x,k_y)\begin{bmatrix} \tilde{J}_x(k_x,k_y,z_o) \\ \tilde{J}_y(k_x,k_y,z_o) \end{bmatrix}}{D^h(\beta)} \tag{C.34}$$

$\mathbf{N}_k^h(\beta)$ can also be obtained from (C.31) by changing the superscript e to h. It is also possible to apply the above results when $\tau = 0$. That is, the expressions for the solutions are valid when $z_o = d_{k-1} \quad (k = 1,\ldots,N)$.

C.3 Derivation of $\tilde{\Psi}^{(e,h)}(k_x,k_y,z)$ for $z_o < 0$

As can be seen, the present case is very similar to the case when $z_o \geq d_N$. In this case, we start from the expression for $\tilde{\Psi}^{(e,h)}(k_x,k_y,z)$. Due to the present of the source at $z = z_o$, one might expect that

$$\tilde{\Psi}^{(e,h)}(k_x,k_y,z) = \begin{cases} a_c^{(e,h)}(k_x,k_y)e^{-\gamma_c(z-d_N)} & z > d_N \\ A_i^{(e,h)}(k_x,k_y)ch[\gamma_i(z-d_{i-1})] + B_i^{(e,h)}(k_x,k_y)sh[\gamma_i(z-d_{i-1})] & d_{i-1} < z < d_i \\ A_s^{(e,h)}(k_x,k_y)ch(\gamma_s z) + B_s^{(e,h)}(k_x,k_y)sh(\gamma_s z) & z_o < z < 0 \\ b_s^{(e,h)}(k_x,k_y)e^{\gamma_s z} & z < z_o \end{cases} \tag{C.35}$$

where γ_c, γ_i, and γ_s are defined in Appendix C.1 via (C.3). As before, we consider the LSM and LSE excitations separately.

LSM excitation

Application of the boundary conditions (2.26) at $z = z_o$ requires that

$$\mathbf{D}(\gamma_s; z_o)\left(\begin{bmatrix} A_s^e(k_x,k_y) \\ \gamma_s B_s^e(k_x,k_y) \end{bmatrix} - \begin{bmatrix} 1 \\ \gamma_s \end{bmatrix} b_s^e(k_x,k_y)\right) = \mathbf{A}^e(k_x,k_y)\begin{bmatrix} \tilde{J}_x(k_x,k_y,z_o) \\ \tilde{J}_y(k_x,k_y,z_o) \end{bmatrix} \tag{C.36}$$

where

$$\mathbf{D}(\gamma_s; z_o) = \begin{bmatrix} ch(\gamma_s z_o) & \frac{sh(\gamma_s z_o)}{\gamma_s} \\ \gamma_s sh(\gamma_s z_o) & ch(\gamma_s z_o) \end{bmatrix} \tag{C.37}$$

Application of the boundary conditions at $z = 0$ leads to

$$\begin{bmatrix} A_1^e(k_x,k_y) \\ \gamma_1 B_1^e(k_x,k_y) \end{bmatrix} = \mathbf{T}_{1,0}^e(\beta)\begin{bmatrix} A_s^e(k_x,k_y) \\ \gamma_s B_s^e(k_x,k_y) \end{bmatrix} \tag{C.38}$$

with

$$\mathbf{T}_{1,0}^e(\beta) = \begin{bmatrix} 1 & 0 \\ 0 & \frac{\epsilon_{r_1}}{\epsilon_{r_s}} \end{bmatrix} \tag{C.39}$$

Therefore, successive application of the boundary conditions at $z = d_i$ $(i = 1,\ldots,N)$ leads to the following matrix equation

$$\begin{bmatrix} 1 \\ -\gamma_c \end{bmatrix} a_c^e - \mathbf{T}^e(\beta)\begin{bmatrix} 1 \\ \gamma_s \end{bmatrix} b_s^e = \mathbf{T}^e(\beta)\,\mathbf{D}^{-1}(\gamma_s, z_o)\,\mathbf{A}^e(k_x,k_y)\begin{bmatrix} \tilde{J}_x(k_x,k_y,z_o) \\ \tilde{J}_y(k_x,k_y,z_o) \end{bmatrix} \tag{C.40}$$

Solutions for $a_c^e(k_x,k_y)$ and $b_s^e(k_x,k_y)$ are

$$a_c^e(k_x,k_y) = \frac{-\frac{\epsilon_{r_c}}{\epsilon_{r_s}}\begin{bmatrix} -\gamma_s & 1 \end{bmatrix}\mathbf{D}^{-1}(\gamma_s; z_o)\mathbf{A}^e(k_x,k_y)\begin{bmatrix} \tilde{J}_x(k_x,k_y,z_o) \\ \tilde{J}_y(k_x,k_y,z_o) \end{bmatrix}}{D^e(\beta)} \tag{C.41}$$

$$b_s^e(k_x,k_y)=\frac{-\left[\begin{array}{cc}\gamma_c & 1\end{array}\right]\mathbf{T}^e(\beta)\mathbf{D}^{-1}(\gamma_s;z_o)\mathbf{A}^e(k_x,k_y)\left[\begin{array}{c}\tilde{J}_x(k_x,k_y,z_o)\\ \tilde{J}_y(k_x,k_y,z_o)\end{array}\right]}{D^e(\beta)} \tag{C.42}$$

where $D^e(\beta)$ is given by (C.14).

LSE excitation

Following the same argument, we have

$$\left[\begin{array}{c}1\\ -\gamma_c\end{array}\right]a_c^h-\mathbf{T}^e(\beta)\left[\begin{array}{c}1\\ \gamma_s\end{array}\right]b_s^h=\mathbf{T}^h(\beta)\,\mathbf{D}^{-1}(\gamma_s,z_o)\,\mu_{r_s}\mathbf{A}^h(k_x,k_y)\left[\begin{array}{c}\tilde{J}_x(k_x,k_y,z_o)\\ \tilde{J}_y(k_x,k_y,z_o)\end{array}\right] \tag{C.43}$$

The above system of linear equations can be solved for $a_c^h(k_x,k_y)$ and $b_s^h(k_x,k_y)$ as follows

$$a_c^e(k_x,k_y)=\frac{-\frac{\mu_{r_c}}{\mu_{r_s}}\left[\begin{array}{cc}-\gamma_s & 1\end{array}\right]\mathbf{D}^{-1}(\gamma_s;z_o)\mu_{r_s}\mathbf{A}^h(k_x,k_y)\left[\begin{array}{c}\tilde{J}_x(k_x,k_y,z_o)\\ \tilde{J}_y(k_x,k_y,z_o)\end{array}\right]}{D^h(\beta)} \tag{C.44}$$

$$b_s^e(k_x,k_y)=\frac{-\left[\begin{array}{cc}\gamma_c & 1\end{array}\right]\mathbf{T}^h(\beta)\mathbf{D}^{-1}(\gamma_s;z_o)\mu_{r_s}\mathbf{A}^h(k_x,k_y)\left[\begin{array}{c}\tilde{J}_x(k_x,k_y,z_o)\\ \tilde{J}_y(k_x,k_y,z_o)\end{array}\right]}{D^h(\beta)} \tag{C.45}$$

where $\mathbf{A}^h(k_x,k_y)$ and $D^h(\beta)$ are given by (C.16) and (C.21), respectively.

C.4 Proof of Equation (2.39)

In this appendix, we show that $\widehat{\Psi}_n^{(e,h)}(\alpha,z)$ satisfies the second-order homogeneous differential equation (2.39). To this end, substitution of (2.32) into (2.31), leads to the homogeneous differential equation

$$\left[\mathcal{B}_n+\frac{\partial^2}{\partial z^2}+\mu_r(z)\epsilon_r(z)k_o^2\right]\widehat{\Psi}_n^{(e,h)}(\rho,z)=0 \tag{C.46}$$

where $\mathcal{B}_n$ is the Bessel differential operator

$$\mathcal{B}_n \stackrel{\text{def}}{=} \frac{\partial^2}{\partial \rho^2} + \frac{1}{\rho}\frac{\partial}{\partial \rho} - \frac{n^2}{\rho^2} \tag{C.47}$$

It is shown that [53]

$$\mathcal{H}_n\left(\mathcal{B}_n[f(\rho)];\alpha\right) = -\alpha^2 \widehat{f}(\alpha) \tag{C.48}$$

If we apply the Hankel transform on both sides of the differential equation (C.46) and use (C.48), we end up with (2.39).

C.5 Connection Between the Two-Dimensional Fourier Transform and the Hankel Transform

To establish the relationship between the Hankel transform and the two-dimensional Fourier transform, consider the double Fourier transform of the function $f(x,y)$ as follows

$$\widetilde{f}(k_x,k_y) = \int_{-\infty}^{\infty}\int_{-\infty}^{\infty} f(x,y)e^{j(k_x x + k_y y)}dxdy \tag{C.49}$$

According to the inversion theorem, we have

$$f(x,y) = \frac{1}{(2\pi)^2}\int_{-\infty}^{\infty}\int_{-\infty}^{\infty} \widetilde{f}(k_x,k_y)e^{-j(k_x x + k_y y)}dk_x dk_y \tag{C.50}$$

Let us introduce two pairs of variables (ρ,ϕ) and (α,ν) such that

$$\begin{cases} x = \rho\, cos\phi \\ y = \rho\, sin\phi \end{cases} \qquad \begin{cases} k_x = \alpha\, cos\nu \\ k_y = \alpha\, sin\nu \end{cases} \tag{C.51}$$

Note that (α,ν) is the dual pair of (ρ,ϕ) in the spectral domain. Moreover,

$$k_x^2 + k_y^2 = \alpha^2$$

With such variable transformation, one may write

$$f(x,y) = \sum_{n=-\infty}^{\infty} f_n(\rho) e^{jn\phi} \tag{C.52a}$$

$$\tilde{f}(k_x,k_y) = \sum_{n=-\infty}^{\infty} \tilde{f}_n(\alpha) e^{jn\nu} \tag{C.52b}$$

Substituting (C.52a) into (C.49), changing the order of summation and integration, and using the coordinate transformation in (C.51), we get

$$\tilde{f}(k_x,k_y) = \sum_{n=-\infty}^{\infty} \int_0^{2\pi} \int_0^{\infty} f_n(\rho) e^{j[n\phi+\alpha\rho\cos(\phi-\nu)]} \rho d\phi\, d\rho \tag{C.53}$$

The above expression can be rewritten as

$$\tilde{f}(k_x,k_y) = \sum_{n=-\infty}^{\infty} e^{jn\nu} \int_0^{\infty} f_n(\rho)\rho d\rho \int_{-\nu}^{2\pi-\nu} e^{j(nu+\rho\xi\cos u)} du \tag{C.54}$$

Let us consider the generating-function relation for Bessel functions [56]

$$e^{\frac{1}{2}z(t-t^{-1})} = \sum_{n=-\infty}^{\infty} t^n J_n(z) \tag{C.55}$$

Writing $t = e^{j\theta}$ on both sides of (C.55), we obtain

$$e^{jz\sin\theta} = \sum_{m=-\infty}^{\infty} e^{jm\theta} J_m(z) \tag{C.56}$$

If we change the variable θ to $\frac{\pi}{2} + \theta$ in the above identity, we get

$$e^{jz\cos\theta} = \sum_{m=-\infty}^{\infty} j^m e^{jm\theta} J_m(z) \tag{C.57}$$

Using the above identity in (C.54) leads to the following result

$$\tilde{f}(k_x,k_y) = 2\pi \sum_{n=-\infty}^{\infty} e^{jn\nu} j^{-n}(-1)^n \int_0^{\infty} f_n(\rho) J_n(\alpha\rho)\rho d\rho$$

where we have used

$$J_{-n}(z) = (-1)^n J_n(z)$$

Consequently,

$$\tilde{f}(k_x, k_y) = \sum_{n=-\infty}^{\infty} 2\pi j^n \hat{f}_n(\alpha) e^{jn\nu} \tag{C.58}$$

where $\hat{f}_n(\alpha)$ denotes the Hankel transform of $f_n(\rho)$. Comparing (C.58) with (C.52b) yields

$$\tilde{f}_n(\alpha) = 2\pi j^n \hat{f}_n(\alpha) \tag{C.59}$$

Note that one may start with substituting (C.52b) into (C.50). Then, using the identity

$$e^{-jz\cos\theta} = \sum_{m=-\infty}^{\infty} (-j)^m e^{jm\theta} J_m(z)$$

and comparing the final result with (C.52a) leads to

$$f_n(\alpha) = \frac{1}{2\pi j^n} \int_0^{\infty} \tilde{f}_n(\alpha) J_n(\alpha\rho) \alpha d\alpha \tag{C.60}$$

The above relation states that $\tilde{f}_n(\alpha)$ is the Hankel transform of $2\pi j^n f_n(\rho)$. In other words, applying the Hankel transform on both sides of (C.60), we end up with (C.59).

Appendix D

D.1 Green's Function of Multilayer Planar Structures

In this appendix, we obtain the exact Green's function satisfying (3.21) by using the transfer matrix method. We use two seemingly different approaches. However, it can be shown that these two approaches are the same. Let the grating section extend from $z = d_{k-1}$ to $z = d_k$ as shown in Fig. 3.4. Therefore, z' may be anywhere between d_{k-1} and d_k in the unperturbed waveguide, that is, $d_{k-1} \leq z' \leq d_k$. In both approaches, we take advantage of the fact that $G(z;z')$ is the solution of the following differential equation

$$\frac{d^2G(z;z')}{dz^2} + \epsilon_r(z)k_o^2\,G(z;z') = \begin{cases} 0 & z > z' \\ 0 & z < z' \end{cases} \tag{D.1}$$

subject to the continuity of $G(z;z')$ and $\frac{dG(z;z')}{dz}$ for all values of z except $z \neq z'$. At $z = z'$, $G(z;z')$ is continuous. However, $\frac{dG(z;z')}{dz}$ is discontinuous such that

$$\frac{dG(z;z')}{dz}\Big|_{z=z'+} - \frac{dG(z;z')}{dz}\Big|_{z=z'-} = 1 \tag{D.2}$$

First approach

Since $G(z;z')$ satisfies (D.1), one may write

$$G(z;z') = \begin{cases} a_c(z')e^{-j\tau_c(z-d_N)} & z > d_N \\ A_i(z')cos\tau_i(z-d_{i-1}) + B_i(z')sin\tau_i(z-d_{i-1}) & i \neq k \text{ and } d_{i-1} < z < d_i \\ U_k(z')cos\tau_k(z-d_{k-1}) + V_k sin\tau_k(z-d_{k-1}) & z' < z < z_k \\ A_k(z')cos\tau_k(z-d_{k-1}) + B_k sin\tau_k(z-d_{k-1}) & z_{k-1} < z < z' \\ b_s(z')e^{j\tau_s z} & z < 0 \end{cases} \tag{D.3}$$

where

$$\tau_{c,s} = \sqrt{\epsilon_{r_{c,s}}}\, k_o \tag{D.4a}$$

$$\tau_i = \sqrt{\epsilon_{r_i}}\, k_o \tag{D.4b}$$

Continuity of $G(z;z')$ and its first derivative at all interfaces $z_i \geq z_k$ leads to

$$\begin{bmatrix} A_i(z') \\ \tau_i B_i(z') \end{bmatrix} = \mathbf{T}_i^{-1} \ldots \mathbf{T}_N^{-1} \begin{bmatrix} 1 \\ -j\tau_c \end{bmatrix} a_c(z') \quad i \geq k \tag{D.5}$$

where

$$\mathbf{T}_i = \begin{bmatrix} cos\,\tau_i t_i & \frac{sin\,\tau_i t_i}{\tau_i} \\ -\tau_i\, sin\,\tau_i t_i & cos\,\tau_i t_i \end{bmatrix} \tag{D.6}$$

and t_i is the thickness of the ith layer. In a similar fashion, continuity of $G(z;z')$ and its first derivative at all interface $z_i \leq z_{k-1}$ yields

$$\begin{bmatrix} A_i(z') \\ \tau_i B_i(z') \end{bmatrix} = \mathbf{T}_{i-1} \ldots \mathbf{T}_1 \begin{bmatrix} 1 \\ j\tau_s \end{bmatrix} b_s \quad i \leq k-1 \tag{D.7}$$

Applying the boundary conditions at $z = z'$, we get

$$\mathbf{D}(z' - z_{k-1}) \left(\begin{bmatrix} U_k(z') \\ \tau_k V_k(z') \end{bmatrix} - \begin{bmatrix} A_k(z') \\ \tau_k B_k(z') \end{bmatrix} \right) = \begin{bmatrix} 0 \\ 1 \end{bmatrix} \tag{D.8}$$

where

$$\mathbf{D}(z'-z_{k-1}) = \begin{bmatrix} cos\,\tau_k(z'-z_{k-1}) & \frac{sin\,\tau_k(z'-z_{k-1})}{\tau_k} \\ -\tau_k\,sin\,\tau_k(z'-z_{k-1}) & cos\,\tau_k(z'-z_{k-1}) \end{bmatrix} \tag{D.9}$$

Using (D.5) and (D.7) in (D.9), we have

$$\mathbf{T}_k^{-1}\ldots\mathbf{T}_N^{-1}\begin{bmatrix} 1 \\ -j\tau_c \end{bmatrix} a_c(z') - \mathbf{T}_{k-1}\ldots\mathbf{T}_1\begin{bmatrix} 1 \\ j\tau_s \end{bmatrix} b_s(z') = \mathbf{D}^{-1}(z'-z_{k-1})\begin{bmatrix} 0 \\ 1 \end{bmatrix} \tag{D.10}$$

Now it an easy task to obtain $a_c(z')$ and $b_s(z')$ from the above equation. The procedure is very similar to that one given in Appendix C.2. After obtaining $a_c(z')$ and $b_s(z')$ all other coefficients can be obtained by using the transfer matrices.

Second approach

In this approach, we start from a general formula for the Green's function of the second-order differential equation. According to the theory of second-order differential equations [64], the Green's function satisfying (3.21) can be obtained as

$$G(z;z') = \frac{Z_l(z')Z_u(z)U(z-z') + Z_u(z')Z_l(z)U(z'-z)}{Z_u'(z')Z_l(z') - Z_u(z')Z_l'(z')} \tag{D.11}$$

where $U(\cdot)$ is the unit step function. $Z_u(z)$ is any solution of the homogeneous equation in (D.1) for $z > z'$ subject to the continuity of $Z_u(z)$ and its normal derivatives at each interface $d_i > z'$. The same is true for $Z_l(z)$ with respect to the corresponding continuity conditions at the interfaces $d_i < z'$. It should be noted that derivation of (D.11) is based on (D.2). The above considerations allows us to explicitly write $Z_u(z)$ and $Z_l(z)$ as

$$Z_u(z) = \begin{cases} a_c e^{-j\tau_c(z-d_N)} & z \geq d_N \\ A_i^u\,cos\,\tau_i(z-d_{i-1}) + B_i^u\,sin\,\tau_i(z-d_{i-1}) & d_{i-1} \leq z \leq d_i,\ i > k \\ A_k^u\,cos\,\tau_k(z-d_{k-1}) + B_k^u\,sin\,\tau_k(z-d_{k-1}) & z' < z \leq d_k \end{cases} \tag{D.12}$$

$$Z_l(z) = \begin{cases} A_k^l \cos\tau_k(z-d_{k-1}) + B_k^l \sin\tau_k(z-d_{k-1}) & d_{k-1} \le z < z' \\ A_i^l \cos\tau_i(z-d_{i-1}) + B_i^l \sin\tau_i(z-d_{i-1}) & d_{i-1} \le z \le d_i,\ i < k \\ b_s e^{j\tau_s z} & z \le 0 \end{cases} \tag{D.13}$$

where $\tau_{c,s} = \sqrt{\epsilon_{r_{c,s}}}\, k_o$ and $\tau_i = \sqrt{\epsilon_{r_i}}\, k_o$. Since $Z_u(z)$ and $Z_l(z)$ are the solutions of the homogeneous differential equation, a_c and b_s can be considered as arbitrary numbers. However, (A_i^u, B_i^u) and (A_i^l, B_i^l) are uniquely determined in terms of a_c and b_c, respectively. More precisely, successive application of the boundary conditions at $d_i > z'$, requires that

$$\begin{bmatrix} A_i^u \\ \tau_i B_i^u \end{bmatrix} = \mathbf{T}_i^{-1} \ldots \mathbf{T}_N^{-1} \begin{bmatrix} 1 \\ -j\tau_c \end{bmatrix} a_c \quad i \ge k \tag{D.14}$$

where $\mathbf{T}_i$ is given by (3.6). Similarly, we have

$$\begin{bmatrix} A_i^l \\ \tau_i B_i^l \end{bmatrix} = \mathbf{T}_{i-1} \ldots \mathbf{T}_1 \begin{bmatrix} 1 \\ j\tau_s \end{bmatrix} b_s \quad i \le k \tag{D.15}$$

If one calculates the denominator of the Green's function in (D.11), one can easily prove that

$$\begin{aligned} \Delta &\stackrel{\text{def}}{=} Z_u'(z')\, Z_l(z') - Z_u(z')\, Z_l'(z') \\ &= \left(\begin{bmatrix} A_k^l \\ \tau_k B_k^l \end{bmatrix} \rightleftharpoons \begin{bmatrix} A_k^u \\ \tau_k B_k^u \end{bmatrix} \right) \stackrel{\text{def}}{=} \begin{vmatrix} A_k^l & A_k^u \\ \tau_k B_k^l & \tau_k B_k^u \end{vmatrix} \\ &= \left(\mathbf{T}_{k-1} \ldots \mathbf{T}_1 \begin{bmatrix} 1 \\ j\tau_s \end{bmatrix} b_s \rightleftharpoons \mathbf{T}_k^{-1} \ldots \mathbf{T}_N^{-1} \begin{bmatrix} 1 \\ -j\tau_c \end{bmatrix} a_c \right) \\ &= \begin{bmatrix} j\tau_c & 1 \end{bmatrix} \mathbf{T}_N \ldots \mathbf{T}_1 \begin{bmatrix} 1 \\ j\tau_s \end{bmatrix} a_c\, b_s \end{aligned} \tag{D.16}$$

Therefore, (D.11)-(D.16) provide us the closed form solution of the Green's function satisfying (3.21). It can be easily seen that the product of the two arbitrary

constants is common in the numerator and denominator of (D.11) as might be expected. Consequently, one may set them equal to 1.

Appendix E

E.1 Fundamental Governing Equation of Slowly-Varying Optical Fields

In this appendix we derive the governing equation of slowly-varying optical fields from Maxwell's equations in the time domain. These equations are the starting point for both traveling wave and standing wave approaches. The distinctive feature of this derivation is the inclusion of the spontaneous emission noise at the very beginning. This is different from the conventional heuristic approach of considering the spontaneous emission at the very end of the formulation of the rate equations.

We start from Maxwell's equations

$$\nabla \times \mathcal{E} = -\mu_o \frac{\partial \mathcal{H}}{\partial t} \tag{E.1}$$

$$\nabla \times \mathcal{H} = \frac{\partial \mathcal{D}}{\partial t} \tag{E.2}$$

where

$$\mathcal{D} = \mathcal{D}_o + \mathcal{P}^l + \mathcal{P}^s \tag{E.3}$$

$\mathcal{D}_o$ is related to $\mathcal{E}$ by

$$\mathcal{D}_o(\mathbf{r},t) = \int_0^\infty \epsilon_o \epsilon_r(\mathbf{r},t')\,\mathcal{E}(\mathbf{r},t-t')\,dt' \tag{E.4}$$

with

$$\epsilon_r(\mathbf{r},t) = 1 + \chi_c(\mathbf{r},t)$$

$\chi_c(\mathbf{r},t)$ is the susceptibility of the unpumped lasing medium. $\mathcal{P}^l$ and $\mathcal{P}^s$ are the polarization associated with the lasing medium and spontaneous emission source, respectively. $\mathcal{P}^s$ acts as a random source of the optical field in the laser structure. In the presence of this random source the laser field must be considered as a random field. Note that we have assumed *linear polarization* model with memory for the cold cavity, i.e., the laser cavity in the absence of the injection. On substitution of (E.3) into (E.1) and (E.2), we obtain

$$\nabla \times \nabla \times \mathcal{E} + \mu_o \frac{\partial^2 \mathcal{D}_o}{\partial t^2} = -\mu_o \frac{\partial^2 \mathcal{P}^l}{\partial t^2} - \mu_o \frac{\partial^2 \mathcal{P}^s}{\partial t^2} \tag{E.5}$$

Let

$$\mathcal{E}(\mathbf{r},t) = \mathrm{Re}\left\{\mathbf{E}(\mathbf{r},t)\,e^{j\omega_r t}\right\} \tag{E.6a}$$

$$\mathcal{D}_o(\mathbf{r},t) = \mathrm{Re}\left\{\mathbf{D}_0(\mathbf{r},t)\,e^{j\omega_r t}\right\} \tag{E.6b}$$

$$\mathcal{P}^l(\mathbf{r},t) = \mathrm{Re}\left\{\mathbf{P}^l(\mathbf{r},t)\,e^{j\omega_r t}\right\} \tag{E.6c}$$

$$\mathcal{P}^s(\mathbf{r},t) = \mathrm{Re}\left\{\mathbf{P}^s(\mathbf{r},t)\,e^{j\omega_r t}\right\} \tag{E.6d}$$

where ω_r is a reference frequency. $\mathbf{E}(\mathbf{r},t)$, $\mathbf{D}_o(\mathbf{r},t)$, $\mathbf{P}^l(\mathbf{r},t)$, and $\mathbf{P}^s(\mathbf{r},t)$ are slowly varying amplitudes with respect to time. On substitution of (E.6) into (E.5), we get

$$\nabla \times \nabla \times \mathbf{E} + \mu_o \mathcal{T}^2 \mathbf{D}_o = -\mu_o \mathcal{T}^2 \mathbf{P}^l - \mu_o \mathcal{T}^2 \mathbf{P}^s$$

where

$$\mathcal{T} \equiv \frac{\partial}{\partial t} + j\omega_r$$

By neglecting terms that are of second-order derivatives of $\mathbf{D}_o(\mathbf{r},t)$ and of first-order or higher for $\mathbf{P}^l$ and $\mathbf{P}^s$, one derives

$$\nabla\times\nabla\times\mathbf{E}-\omega_r^2\mu_o\mathbf{D}_o+j2\omega_r\mu_0\frac{\partial\mathbf{D}_o}{\partial t}=\mu_o\omega_r^2\mathbf{P}^l+\mu_o\omega_r^2\mathbf{P}^s \tag{E.7}$$

Let us define the Fourier transform by the kernel $e^{-j\zeta t}$. That is,

$$\tilde{f}(\mathbf{r},\zeta)=\int_{-\infty}^{\infty}f(\mathbf{r},t)e^{-j\zeta t}dt$$

With the above definition, if one applies the Fourier transform to both sides of (E.7), one obtains

$$\nabla\times\nabla\times\tilde{\mathbf{E}}-\omega_r^2\mu_o\widetilde{\mathbf{D}}_o-2\omega_r\mu_0\zeta\widetilde{\mathbf{D}}_o=\mu_o\omega_r^2\tilde{\mathbf{P}}^l+\mu_o\omega_r^2\tilde{\mathbf{P}}^s \tag{E.8}$$

On the other hand, using (E.6) in (E.4), one may obtain the relationship between the Fourier transform of $\mathbf{D}_o(\mathbf{r},t)$ and $\mathbf{E}(\mathbf{r},t)$. More precisely, we have

$$\mathbf{D}_o(\mathbf{r},t)e^{j\omega_r t}=\int_0^{\infty}\epsilon_o\epsilon_r(\mathbf{r},t')\,\mathbf{E}(\mathbf{r},t-t')e^{j\omega_r(t-t')}dt' \tag{E.9}$$

Applying the Fourier transform on (E.9), we obtain

$$\widetilde{\mathbf{D}}_o(\mathbf{r},\zeta-\omega_r)=\epsilon_o\tilde{\epsilon}_r(\mathbf{r},\zeta)\,\tilde{\mathbf{E}}(\mathbf{r},\zeta-\omega_r) \tag{E.10}$$

By changing the variable, one may obtain the following relation from (E.10)

$$\widetilde{\mathbf{D}}_o(\mathbf{r},\zeta)=\epsilon_o\tilde{\epsilon}_r(\mathbf{r},\omega_r+\zeta)\,\tilde{\mathbf{E}}(\mathbf{r},\zeta) \tag{E.11}$$

Since $\widetilde{\mathbf{D}}_o(\mathbf{r},\zeta)$ and $\tilde{\mathbf{E}}(\mathbf{r},\zeta)$ are narrowband functions, they vanish for sufficiently small values of ζ. In this range of small values of ζ, $\tilde{\epsilon}_r(\mathbf{r},\omega_r+\zeta)$ can be expressed in terms of a Taylor series expansion

$$\tilde{\epsilon}_r(\mathbf{r},\omega_r+\zeta)=\tilde{\epsilon}_r(\mathbf{r},\omega_r)+\frac{\partial\tilde{\epsilon}_r}{\partial\omega}|_{\omega=\omega_r}\zeta \tag{E.12}$$

Substituting (E.12) into (E.11), the nonzero values of $\widetilde{\mathbf{D}}_o(\mathbf{r},\zeta)$ and $\tilde{\mathbf{E}}(\mathbf{r},\zeta)$ satisfy the following relation

$$\widetilde{\mathbf{D}}_o(\mathbf{r},\zeta) = \epsilon_o \left[\epsilon_{r_\tau}(\mathbf{r}) + \frac{\partial \tilde{\epsilon}_\tau}{\partial \omega}|_{\omega=\omega_\tau \zeta}\right] \tilde{\mathbf{E}}(\mathbf{r},\zeta) \tag{E.13}$$

where $\epsilon_{r_\tau}(\mathbf{r}) = \tilde{\epsilon}_\tau(\mathbf{r},\omega_\tau)$. Substituting (E.13) into (E.8) and utilizing the constitutive relation

$$\mathbf{P}^l(\mathbf{r},t) = \epsilon_o \chi(\mathbf{r},t)\,\mathbf{E}(\mathbf{r},t) \tag{E.14}$$

where $\chi(\mathbf{r},t)$ is the carrier-dependent susceptibility of the lasing medium, one obtains

$$\nabla \times \nabla \times \tilde{\mathbf{E}} - k_o^2(\epsilon_{r_\tau} + \tilde{\chi}*)\tilde{\mathbf{E}} + \frac{j2\omega_\tau}{v_o^2}\left[(\epsilon_{r_\tau} + \frac{1}{2}\frac{\partial \tilde{\epsilon}_\tau}{\partial \omega}\omega_\tau)\, j\zeta \tilde{\mathbf{E}} + j\frac{\partial \tilde{\epsilon}_\tau}{\partial \omega}\zeta^2 \tilde{\mathbf{E}}\right] = \mu_o \omega_\tau^2 \tilde{\mathbf{P}}^s \tag{E.15}$$

where

$$k_o^2 = \frac{\omega_\tau^2}{v_o^2}$$

$$v_o^2 = \frac{1}{\mu_o \epsilon_o}$$

and $*$ means convolution in the Fourier spectral domain.

Applying the inverse Fourier transform on both sides of (E.15) and noting that

$$\mathcal{F}^{-1}[(\zeta)^n \tilde{f}] = (-j)^n \frac{\partial^n f}{\partial t^n},$$

we obtain

$$\nabla \times \nabla \times \mathbf{E} - k_o^2(\epsilon_{r_\tau} + \chi)\mathbf{E} + \frac{j2\omega_\tau}{v_o^2}\left[\epsilon_g \frac{\partial \mathbf{E}}{\partial t} - \frac{\partial \tilde{\epsilon}_\tau}{\partial \omega}\frac{\partial^2 \mathbf{E}}{\partial t^2}\right] = \mu_o \omega_\tau^2 \mathbf{P}^s \tag{E.16}$$

where ϵ_g is the effective group dielectric constant and is given by

$$\epsilon_g = \epsilon_{r_\tau} + \frac{1}{2}\frac{\partial \epsilon_\tau}{\partial \omega}\omega_\tau$$

Based on the slowly-varying amplitude assumption, we neglect second-order derivative with respect to time. Therefore, from (E.16), one may derive

$$\nabla \times \nabla \times \mathbf{E} - k_o^2(\epsilon_{r_r} + \chi)\mathbf{E} + \frac{j2\omega_r}{v_o^2}\epsilon_g \frac{\partial \mathbf{E}}{\partial t} = \mu_o \omega_r^2 \mathbf{P}^s \tag{E.17}$$

Eq. (E.17) is the fundamental governing equation for the envelope of the laser field in its most general form.

Appendix F

F.1 Green's Function Satisfying (5.26)

In this appendix we attempt to find the Green's function satisfying (5.26). Basically, it is possible to find the Green's function by two different approaches. In the first approach, we write the Green's function as a linear combination of the solutions of the homogeneous equation. The unknown coefficients can be obtained by applying the continuity condition on the Green's function and the discontinuity condition on its first derivative.

The second approach is based on the integral transform technique. The kernel of the integral transform satisfies the homogeneous differential equation. The Green's function can be obtained from the inverse transform by using contour integration and the residue theory. In fact, the second approach is based on the eigenfunction expansion of the Green's function. Although the second approach is more elegant than the first one, it is not as simple as the former. Therefore, we focus only on the first approach.

In the first approach, as mentioned above, it is necessary to obtain the suitable condition on the derivative of the Green's function at the source location. To this

end, it is more convenient to write the differential operator acting on $G(\rho,\rho';\alpha)$ as

$$\frac{1}{\rho}\frac{\partial}{\partial\rho}(\rho\frac{\partial}{\partial\rho})G(\rho,\rho';\alpha)+\left[\beta^2(\alpha)-\frac{n^2}{\rho^2}\right]G(\rho,\rho';\alpha)=\frac{1}{\rho}\delta(\rho-\rho') \qquad \text{(F.1)}$$

If one multiplies the above equation by ρ and integrate the resulting equation from $\rho=\rho'^{-}$ to $\rho=\rho'^{+}$, continuity of $G(\rho,\rho';\alpha)$ at $\rho=\rho'$ results in

$$\left[\frac{\partial G}{\partial\rho}\right]_{\rho=\rho'^{-}}^{\rho=\rho'^{+}}=\frac{1}{\rho} \qquad \text{(F.2)}$$

Eq. (F.2) along with the continuity of $G(\rho,\rho';\alpha)$ at $\rho=\rho'$ are the fundamentals in deriving the Green's function. We consider four cases separately.

(1) $n=0$ and $\beta(\alpha)=0$

In this case, the two independent solutions of the homogeneous equation in (F.1) are constant function and $ln(\rho)$, respectively. Thus,

$$G(\rho,\rho';\alpha)=\begin{cases} A & \rho<\rho' \\ B\,ln(\rho) & \rho>\rho' \end{cases} \qquad \text{(F.3)}$$

Continuity of $G(\rho,\rho';\alpha)$ at $\rho=\rho'$ and (F.2) leads to (5.27a).

(2) $n\neq 0$ and $\beta(\alpha)=0$

In this case, the two independent solutions of the homogeneous equation in (F.1) are ρ^n and ρ^{-n}, respectively. Consequently,

$$G(\rho,\rho';\alpha)=\begin{cases} A\,\rho^n & \rho<\rho' \\ B\,\rho^{-n} & \rho>\rho' \end{cases} \qquad \text{(F.4)}$$

Following the same procedure as before, one ends up with (5.27b).

(3) $\beta^2(\alpha)>0$

In this case, one may write

$$G(\rho,\rho';\alpha)=\begin{cases} A\,J_n[\beta(\alpha)\rho] & \rho<\rho' \\ B\,H_n^{(2)}[\beta(\alpha)\rho] & \rho>\rho' \end{cases} \qquad \text{(F.5)}$$

where

$$H_n^{(2)}(\cdot) = J_n(\cdot) - jN_n(\cdot)$$

Following the same line as before, i.e, using the continuity of $G(\rho, \rho'; \alpha)$ at $\rho = \rho'$ and (F.2), one needs the Wronskian of the Bessel's functions [108] (p. 463)

$$J_n(\beta\rho)\frac{dN_n(\beta\rho)}{d(\beta\rho)} - N_n(\beta\rho)\frac{dJ_n(\beta\rho)}{d(\beta\rho)} = \frac{2}{\pi\rho} \tag{F.6}$$

Using (F.6), we have

$$J_n(\beta\rho)\frac{dH_n^{(2)}(\beta\rho)}{d(\beta\rho)} - H_n^{(2)}(\beta\rho)\frac{dJ_n(\beta\rho)}{d(\beta\rho)} = -\frac{j2}{\pi\rho} \tag{F.7}$$

Therefore, after some algebraic manipulations, we obtain (5.27c).

(4) $\beta^2(\alpha) < 0$

Let us assume that $\beta^2 = -u^2$, $u^2 > 0$. In this case, one may write

$$G(\rho, \rho'; \alpha) = \begin{cases} A\, I_n(u\rho) & \rho < \rho' \\ B\, K_n(u\rho) & \rho > \rho' \end{cases} \tag{F.8}$$

where $I_n(\cdot)$ and $K_n(\cdot)$ are the modified Bessel functions of the first and the second kind, respectively. These functions are defined as [108] (p. 463)

$$I_n(u\rho) = j^n J_n(-ju\rho) \tag{F.9a}$$

$$K_n(u\rho) = \frac{\pi}{2}(-j)^{n+1} H_n^{(2)}(-ju\rho) \tag{F.9b}$$

The Wronskian of the modified Bessel functions is

$$I_n(u\rho)\frac{dK_n(u\rho)}{d(u\rho)} - K_n(u\rho)\frac{dI_n(u\rho)}{d(u\rho)} = -\frac{1}{\rho} \tag{F.10}$$

From (F.10) and the procedure described earlier, we have

$$G(\rho, \rho'; \alpha) = \begin{cases} -K_n(u\rho')I_n(u\rho) & \rho < \rho' \\ -I_n(u\rho')K_n(u\rho) & \rho > \rho' \end{cases} \tag{F.11}$$

Using (F.9), (F.11), and $u = \sqrt{-\beta^2(\alpha)}$, one may write

$$G(\rho,\rho';\alpha) = \begin{cases} \frac{j\pi}{2} H_n^{(2)}[-j\sqrt{-\beta^2(\alpha)}\rho'] J_n[-j\sqrt{-\beta^2(\alpha)}\rho] & \rho < \rho' \\ \frac{j\pi}{2} J_n[-j\sqrt{-\beta^2(\alpha)}\rho'] H_n^{(2)}[-j\sqrt{-\beta^2(\alpha)}\rho] & \rho > \rho' \end{cases} \tag{F.12}$$

A careful look at (F.12) reveals that the Green's function $G(\rho,\rho';\alpha)$ for $\beta^2(\alpha) < 0$ can be obtained from those expressions valid for $\beta^2(\alpha) > 0$ simply by substituting $-j\sqrt{-\beta^2(\alpha)}$ for $\beta(\alpha)$.

Bibliography

[1] H. Soda, K. Iga, C. Kitahara, and Y. Suematsu, "GaInAsP/InP surface emitting injection lasers," *Japan. J. Appl. Phys.*, vol. 18, pp. 2329-2330, Dec. 1979.

[2] K. Iga, F. Koyama, and S. Kinoshita, "Surface emitting lasers," *IEEE J. Quantum Electron.*, vol. 24, pp. 1845-1855, Sept. 1988.

[3] R. S. Geels and L. A. Coldren, "Submilliamp threshold vertical-cavity laser diodes," *Appl. Phys. Lett.*, vol. 57, pp. 1605-1607, Oct. 90.

[4] M. Orenstein, E. Kapon, N. G. Stoffel, J. P. Harbisson, L. T. Florez, and J. Wullert, "Two-dimensional phase-locked arrays of vertical cavity semiconductor lasers by mirror reflectivity modulation," *Appl. Phys. Lett.*, vol. 58, pp. 804-806, Feb. 1991.

[5] H. Kogelnik and C. V. Shank, "Stimulated emission in periodic structures," *Appl. Phys. Lett.*, vol. 18, pp. 152-154, Feb. 1971.

[6] H. Kogelnik and C. V. Shank, "Coupled-wave theory of distributed feedback lasers," *J. Appl. Phys.*, vol. 43,pp. 2327-2335, May 1972.

[7] M. Nakamura, A. Yariv, H. W. Yen, and S. Somekh, "Optically pumped GaAs surface lasers with corrugation feedback," *Appl. Phys. Lett.*, vol. 22, pp. 515-516, May 1973.

[8] D. R. Scifres, R. D. Burnham, and W. Streifer, "Highly collimated laser beams from electrically pumped SH GaAs/GaAlAs distributed-feedback lasers," *Appl. Phys. Lett.*, vol. 26, pp. 48-50, Jan. 1975.

[9] R. D. Burnham, D. R. Scifres, and W. Streifer, "Single-heterostructure distributed-feedback GaAs-diode lasers," *IEEE J. Quantum Electron.*, vol. QE-11, pp. 439-449, July 1975.

[10] Zh. Alferov, V. M. Andreyev, S. A. Gurevich, R.F. Kazarinov, V. R. Laronov, M. N. Mizerov, and E. L. Portony, "Semiconductor lasers with the light output through the diffraction grating on the surface of the waveguide layer," *IEEE J. Quantum Electron.* , vol. QE-11, pp. 449-451, July 1975.

[11] P. Zory and L. D. Comerford, "Grating-coupled double-heterostructure AlGaAs diode lasers," *IEEE J. Quantum Electron.*, vol. QE-11, pp. 451-457, July 1975.

[12] W. Streifer, D. R. Scifres, R. D. Durnham, and R. I. MacDonald, "Radiation losses in distributed feedback lasers and longitudinal mode selection," *IEEE J. Quantum Electron.*, vol. QE-12, pp. 737-739, Nov. 1976.

[13] R. C. Tiberio, G. A. Porkolab, M. J. Rooks, E. D. Wolf, R. J. Lang, A. Larsson, S. Forouhar, J. Cody, G. W. Wicks, T. Erdogan, O. King, and D. G. Hall, "Facetless Bragg reflector surface-emitting AlGaAs/GaAs lasers fabricated by electron-beam lithography and chemically assisted ion-beam

etching," *J. Vac. Sci. Technol. B*, vol. 9, no. 6, pp. 2842-2845, Nov/Dec. 1991.

[14] Z. L. Liao and J. N. Walpole, "Surface-emitting GaInAs/InP laser with low threshold current and high efficiency," *Appl. Phys. Lett.*, vol. 46, no.2, pp. 115-117, Jan. 1985.

[15] P. K. Tien, "Method of forming novel curved-line gratings and their use as reflectors in integrated optics," *Opt. Letts.*, vol. 1, no. 2, pp. 64-66, Aug. 1977.

[16] S. R. Kerner, N. G. Alexopolous, and R. F. Cordero-Iannarella, "On the theory of corrugated optical disk waveguides," *IEEE Trans. Microwave Theory Tech.*, vol. MTT-28, pp. 18-24, Jan. 1980.

[17] X. H. Zheng and S. Lacroix, "Mode coupling in circular-cylindrical system and its application to fingerprint resonators," *J. Lightwave Technol.* vol. 8, pp. 1509-1516, Oct. 1990.

[18] H. Kogelnik, "Theory of dielectric waveguides," in *Integrated Optics*, T. Tamir, ed. Springer-Verlag, New York, 1990.

[19] C. Wu, T. Makino, J. Glinski, R. Maciejko, and S. I. Najafi, "Self-consistent coupled-wave theory for circular gratings on planar dielectric waveguides," *J. Lightwave Technol.*, vol. 9, pp. 1264-1277, Oct. 1991.

[20] C. Wu, T. Makino, R. Maciejko, S. I. Najafi, and M. Svilans, "Simplified coupled-wave equations for cylindrical waves in circular grating planar waveguides," *J. Lightwave Technol.*, vol. 10, pp. 1575-1589 Nov. 1992.

[21] V. A. Kiselev and S. N. Shaposhnikov, "Wide-aperture focusing in the case of excitation of an optical waveguide through an annular grating," *Sov. Phys. Tech. Phys.*, vol. 33, pp. 987-989, 1988.

[22] R. Schimpe, "Cylindrical diffraction grating couplers and distributed feedback resonators for guided wave devices," U.S. Patent No. 4 743 083, May 10, 1988.

[23] M. Toda, "Single-mode behavior of a circular grating for potential disk-shaped DFB lasers," *IEEE J. Quantum Electron.*, vol. 26, pp. 473-481, March 1990.

[24] T. Erdogan and D. G. Hall, "Circularly symmetric distributed feedback semiconductor laser: An analysis," *J. appl. Phys.*, vol. 68, pp. 1435-1444, Aug. 1990.

[25] C. Wu, M. Svilans, M. Fallahi, T. Makino, J. Glinski, C. Maritan, and C. Blaauw, "Optically pumped surface-emitting DFB GaInAsP/InP lasers with circular grating," *Electron. Lett.*, vol.27, pp. 1819-1820, Sept. 1991.

[26] T. Erdogan, O. King, G. W. Wicks, D. G. Hall, C. L. Dennis, and M. J. Rooks, "Spatial modes of a concentric-circle-grating surface-emitting, AlGaAs/GaAs quantum well semiconductor laser," *Appl. Phys. Lett.*, vol. 60, no. 15, pp. 1773-1775, 13 April 1992.

[27] T. Erdogan, O. King, G. W. Wicks, D. G. Hall, E. H. Anderson, and M. J. Rooks, "Circularly symmetric operation of a concentric-circle-grating, surface-emitting, AlGaAs/GaAs quantum-well semiconductor laser," *Appl. Phys. Lett.*, vol. 60, no. 16, pp. 1921-1923, 20 April 1992.

[28] C. Wu, M. Svilans, M. Fallahi, I. Templeon, T. Makino, J. Glinski, R. Maciejko, S. I. Najafi, C. Maritan, C. Blaauw, and G. Knight, "Room tempera-

ture operation of electrically pumped surface-emitting circular grating DBR laser," *Electron. Lett.*, vol. 28, no. 11, pp. 1037-1038, 21st May 1992.

[29] C. Wu, M. Svilans, M. Fallahi, I. Templeon, T. Makino, J. Glinski, R. Maciejko, S. I. Najafi, C. Blaauw, C. Maritan, and G. Knight, "Electrically pumped circular-grating distributed-bragg-reflector lasers," *IEEE Photon. Technol. Lett.*, vol. 4, no. 9, pp. 960-963, Sept. 1992.

[30] T. Erdogan and D. G. Hall, "Circularly symmetric distributed feedback lasers: Coupled mode treatment of TE vector fields," *IEEE J. Quantum Electron.*, vol. 28, pp. 612-623, March 1992.

[31] T. Makino and C. Wu "Circular grating DFB and DBR semiconductor lasers: threshold current analysis," *opt. commun.*, vol. 90, pp. 297-300, 1992.

[32] C. Wu, T. Makino, S. I. Najafi, R. Maciejko, M. Svilans, J. Glinski, M. Fallahi, "Threshold gain and threshold current analysis of circular grating DFB and DBR lasers," *IEEE J. Quantum Electron.*, vol. 29, pp. 2596-2606, Oct. 1993.

[33] X. M. Gong, A. K. Chan, and H. F. Taylor, "Lateral mode discrimination in surface emitting DBR lasers with cylindrical symmetry," *SPIE Laser Diode Technology and Applications III*, vol. 1418, pp . 422-433, 1991.

[34] X. M. Gong, A. K. Chan, and H. F. Taylor, "Lateral mode discrimination in surface emitting DBR lasers with cylindrical symmetry," *IEEE J. Quantum Electron.*, vol. 30, pp. 1212-1218, May 1994.

[35] M. Fallahi, M. Dion, F. Chatenoud, I. M. Templeton, K. A. McGreer, G. Champion, and R. Barber, "Low divergence electrically pumped circular-grating surface-emitting DBR laser on an InGaAs/GaAs structure," *Electron. Lett.*, vol. 29, no. 16, pp. 1412-1414, Aug. 1993.

[36] M. Fallahi, F. Chatenoud, M. Dion, I. Templeton, R. Barber, and J. Thompson, "Circular-grating surface-emitting distributed Bragg reflector lasers on an InGaAs-GaAs structure for 0.98-μm applications," *IEEE, J. Selected Topics in Quantum Electron.*, vol. 1, no. 2, pp. 382-386, June 1995.

[37] K. J. Kasunic and M. Fallahi, "Gain and index saturation in circular-grating distributed-feedback semiconductor lasers," presented at SPIE Conf. Physics and Simulation of Optoelectronic Devices, San Jose, CA, Feb. 97, pp. 205-214.

[38] C. Wu, T. Makino, M. Fallahi, R. G. A. Craig, G. Knight, I. Templeon, C. Blaauw, "Novel circular grating surface-emitting lasers with emission from center," *Jpn. J. Appl. Phys.*, vol. 33, part 2, no. 3B, pp. L427-L429, 15 Mar. 1994.

[39] S. Kristjánsson, M. Li, N. Eriksson, M. Hagberg, K. J. Killius, and A. Larsson, "Circular grating coupled DBR laser with integrated focusing outcoupler," *IEEE Photon. Technol. Lett.*, vol. 9. no. 4, 1997.

[40] R. H. Jordan and D. G. Hall, "Radiation from an annular grating on a planar optical waveguide," *Appl. Phys. Lett.* vol. 65, no. 25, 20 December 1993.

[41] R. H. Jordan and D. G. Hall, "Radiation from concentric-circle grating, surface-emitting planar waveguides: The volume current method," *Appl. Phys. Lett.*, vol.64, no. 23, 6 June 1994.

[42] R. H. Jordan and D. G. Hall, "Highly directional surface emission from concentric-circle gratings of planar optical waveguides: the field expansion method," *J. Opt. Soc. Am.*, vol. 12, no. 1, 1995.

[43] A. W. Snyder, "Radiation losses due to variations of radius on dielectric or optical fibers," *IEEE Trans. Microwave Theory Tech.*, vol. MTT-18, pp. 608-615, 1970.

[44] I. A. White, "Radiation from bends in optical waveguides: The volume current method," *Microwaves, Opt. Acoustics,* vol. 3, pp. 186-188, 1979.

[45] M. Kuznetsuv and H. A. Haus, "Radiation loss in dielectric waveguide structures by the volume current method," *IEEE J. Quantum Electron.*, vol. QE-19, pp. 1505-1514, Oct. 1983.

[46] T. Itoh, "Spectral domain immittance approach for dispersion characteristics of generalized printed transmission lines," *IEEE Trans. Microwave Theory Tech.*, vol. MTT-28, pp. 733-736, July 1980.

[47] T. Umano and T. Itoh, "Spectral Domain Approach," In *Numerical Techniques for Microwave and Millimeter-Wave Passive Structures,* T. Itoh ed. Wiley, New York, 1981, Ch. 5.

[48] L. Vegni, R. Cicchetiti, and P. Capece, "Spectral dyadic Green's function formulation for planar integrated structures," *IEEE Trans. Antennas Propagat.*, vol. 36, pp. 1057-1065, August 1988.

[49] A. S. Omar and K. Schunemann, "Space-domain decoupling of LSE and LSM fields in generalized planar guiding structures," *IEEE Trans. Microwave Theory Tech.*, vol. MTT-32, pp. 1626-1632, 1984.

[50] K. Araki and T. Itoh "Hankel transform domain analysis of open circular microstrip radiating structures," *IEEE Trans. Antennas Propagat.*, vol. AP-29, no. 1, pp. 84-89, Jan. 1981.

[51] I. N. Sneddon *The Use of Integral Transforms*, McGraw-Hill, New York, 1972, Ch. 5.

[52] A. M. Shams-Zadeh-Amiri and W. P. Huang, " Spectral Green's function approach in the investigation of radiation pattern of a novel circular grating surface-emitting lasers," presented at IPR Conf., Technical digest series, pp. 190-192, Boston, MA, April-May 1996.

[53] I. N. Sneddon *The Use of Integral Transforms*, McGraw-Hill, New York, 1972, pp. 311-312.

[54] R. E. Collin, "Radiation From Apertures," in *Antenna Theory,* Part 1, R. E. Collin and F. J. Zucker ed., McGraw-Hill, New York, 1969, pp. 65-67.

[55] R. E. Collin, *Antenna Theory and Radio Wave Propagation,* McGraw-Hill, New York, 1989, pp. 164-169.

[56] N. W. McLachlan, *Bessel Functions for Engineers*, Oxford University Press, London, 1955, pp. 55-56.

[57] J. W. Goodman, *Introduction to Fourier Optics,* McGraw-Hill, New York, 1968, pp. 63-65.

[58] W. Streifer, D. R. Scifres, and R. D. Burnham, "Coupled wave analysis of DFB and DBR lasers," *IEEE J. Quantum Electron.,* vol. QE-13, pp. 134-141, April 1977.

[59] Y. Yamamoto, T. Kamiya, and H. Yanai "Improved coupled mode analysis of corrugated waveguides and lasers", *IEEE, J. Quantum Electron.*, vol. QE-14, no. 4, pp. 245-258, 1978.

[60] R. F. Kazarinov and C. H. Henry, "Second-order distributed feedback lasers with mode selection provided by first-order radiation losses," *IEEE J. Quantum Electron.*, vol. QE-21, pp. 144-150, Feb. 1985.

[61] A. M. Shams-Zadeh-Amiri and W. P. Huang, "Radiation effects in the investigation of threshold gain and threshold current of circular-grating surface-emitting lasers," presented at SPIE Conf. Physics and Simulation of Optoelectronic Devices, San Jose, CA, Feb. 97, pp. 215-228.

[62] T. M. Apostol, *Calculus,* Vol. 2, Blaisdell Publishing Co., Massachusetts, 1969, p. 211.

[63] S. Haykin, *Communication Systems,* Wiley, New York, 1978, pp. 594-595.

[64] P. M. Morse and H. Feshbach, *Methods of Theoretical Physics,* Vol. 1, New York: McGraw-Hill, 1953, p. 832.

[65] J. E. A. Whiteaway, G. H. B. Thompson, A. J. Collar, and C. J. Armistead, "The design and assessment of $\frac{\lambda}{4}$ phase-shifted DFB laser structures," *IEEE J. Quantum Electron.*, vol. 25, no. 6, pp. 1261-1279, 1989.

[66] I. Orfanso, T. Sphicopoulos, A. Tsigopoulos, and C. Caroubalos, "A tractable above-threshold model for the design of DFB and phase-shifted DFB lasers," *IEEE J. Quantum Electron.*, vol. 27, no. 4, pp. 946-956, 1991.

[67] S. Hansmann, "Transfer matrix analysis of the spectral properties of complex distributed feedback laser structures," *IEEE J. Quantum Electron.*, vol. 28, no. 11, pp. 2589-2595, 1992.

[68] T. Makino, "Threshold conditions of DFB semiconductor lasers by the local-normal-mode transfer matrix method: correspondence to the coupled-wave method," *J. Lightwave Technol.,* vol. 12, no. 12, pp. 2092-2099, 1994

[69] P. Vankwikelberge, G. Morthier, and R. Baets, "CLADISS- A longitudinal multimode model for the analysis of the static, dynamic, and stochastic behavior of diode lasers with distributed feedback," *IEEE J. Quantum Electron.*, vol. 26, no. 10, pp. 1728-1741, 1990.

[70] L. M. Zhang and J. E. Carroll, "Large-signal dynamic model of DFB lasers," *IEEE J. Quantum Electron.*, vol. 28, no. 3, pp. 604-611, 1992.

[71] L. M. Zhang, S. F. Yu, M. C. Nowell, D. D. Marcenac, J. E. Carrol, and R. G. S. Plumb, "Dynamic analysis of radiation and side-mode suppression in a second-order DFB laser using time-domain large signal traveling wave model," *IEEE J. Quantum Electron.*, vol. 30, no. 6, pp. 1389-1395, 1994.

[72] C. F. Tsang, D. D. Marcenac, J. E. Carrol, and L. M. Zhang, "Comparison between 'power matrix model' and 'time domain model' in modelling large signal response of DFB lasers," *IEE Proc.-Optoelectron.,* vol. 141, no. 2, pp. 89-96, 1994.

[73] A. J. Lowery, A. Keating, and C. N. Murtonen, "Modeling the static and dynamic behavior of quarter-wave-shifted DFB lasers," *IEEE J. Quantum Electron.*, vol. 28, no. 9, pp. 1874-1883, 1992.

[74] A. J. Lowery, "Comparison between two recent large-signal dynamic DFB laser models," *IEE Proc.-Optoelectron.,* vol. 139, no. 6, pp. 402-406, 1992.

[75] COST 240 GROUP, "Comparison of different DFB laser models within the European COST 240 collaboration," *IEE Proc.-Optoelectron.*, vol. 141, no. 2, pp. 82-88, 1994.

[76] K. Y. Lau and A. Yariv, "High-frequency current modulation of semiconductor injection lasers," *Semiconductors and Semimetals*, Vol. 22, Pt. B, Ch. 7, ed. W. T. Tsang, Academic Press, New York, 1985.

[77] K. Petermann, *Laser Diode Modulation and Noise*, Kluwer Academic Publisher-KTK Scientific Publisher, 1991.

[78] G. P. Agrawal and N. K. Dutta, *Long-Wavelength Semiconductor Lasers*, Van Nostran Reinhold, New York, 1986, chap. 6.

[79] K. Vahala and A. Yariv, "Semiclassical theory of noise in semiconductor lasers-Part I," *IEEE J. Quantum Electron.*, vol. 19, no. 6, pp. 1096-1101, 1983.

[80] K. Vahala and A. Yariv, 'Semiclassical theory of noise in semiconductor lasers-Part II," *IEEE J. Quantum Electron.*, vol. 19, no. 6, pp. 1102-1109, 1983.

[81] T. K. Yee and D. Welford, "A multimode rate-equation analysis for semiconductor lasers applied to the direct intensity modulation of individual longitudinal modes," *IEEE J. Quantum Electron.*, vol. 22, no. 11, pp. 2116-2122, 1986.

[82] J. I. Kinoshita and K. Matsumoto, "Transient chirping in distributed feedback lasers: effects of spatial hole-burning along the laser axis," *IEEE J. Quantum Electron.*, vol. 24, no. 11, pp. 2160-2169, 1988.

[83] B. Tromborg, H. Olesen, X. Pan, and S. Satio, "Transmission line description of optical feedback and injection locking for Fabry-Perot and DFB lasers," *IEEE J. Quantum Electron.*, vol. 23, no. 11, pp. 1875-1899, 1987.

[84] B. Tromborg, H. Olesen, and X. Pan, "Theory of linewidth for multielectrode laser diodes with spatially distributed noise sources," *IEEE J. Quantum Electron.*, vol. 27, no. 2, pp. 178-192, 1991.

[85] C. H. Henry, "Theory of spontaneous emission noise in open resonators and its applications to lasers and optical amplifiers," *J. Lightwave Technol.*, vol. LT-4, no. 3, pp. 288-297, 1986.

[86] X. Li and W. P. Huang, "Analysis of frequencey chirp in DFB lasers integrated with external modulators," *IEEE J. Quantum Electron.*, vol. 30, no. 12, pp. 2756-2766, 1994.

[87] W. P. Huang, X. Li, and T. Makino, "Analytical formulas for modulation responses of semiconductor DFB lasers," *IEEE J. Quantum Electron.*, vol. 31, no. 5, pp. 842-851, 1995.

[88] X. Li, W. P. Huang, "Simulation of DFB semiconductor lasers incorporating thermal effects," *IEEE J. Quantum Electron.*, vol. 31, no. 10, pp. 1848-1855, 1995.

[89] A. D. Sadovnikov, X. Li, and W. P. Huang, "A two-dimensional DFB laser model accounting for carrier transport effects," *IEEE J. Quantum Electron.*, vol. 31, no. 10, pp. 1856-1862, 1995.

[90] R. F. Harrington, *Field Computation by Moment Methods*, Macmillan Publishing Company, New York, 1968.

[91] P. Szczepanski and A. Kujawski, "Non-orthogonality of the longitudinal eigenmodes of a distributed feedback laser," *Opt. Commun.*, vol. 87, pp. 259-262, 1992.

[92] A. E. Siegman, "Orthogonality properties of optical resonator eigenmodes," *Opt. Commun.*, vol. 31, pp. 369-373, 1979.

[93] M. Lax, "Fluctuation and coherence phenomena in classical and quantum physics," *Brandeis University Summer Institute in Theoretical Physics 1966,* Vol. 2, M. Chrétien, E. P. Gross, and S. Deser, eds., Gordon and Breach, New York, 1966.

[94] C. H. Henry, "Theory of the linewidth of semiconductor lasers," *IEEE J. Quantum Electron.*, vol. QE-18, no. 2, pp. 259-264, 1982.

[95] C. H. Henry, "Phase noise in semiconductor lasers," *J. Lightwave Technol.*, vol. LT-4, no. 3, pp. 298-311, 1986.

[96] Y. Champagne and N. McCarthy, "Global excess spontaneous emission factor of semiconductor lasers with axially varying characteristics," *IEEE J. Quantum Electron.*, vol. 28, no. 1, pp. 128-135, 1992.

[97] C. H. Henry, "Theory of spontaneous emission noise in open resonators and its application to lasers and optical amplifiers," *J. Lightwave Technol.*, vol. LT-4, no. 3, pp. 288-297, 1986.

[98] L. D. Landau and E. M. Lifshitz, *Electrodynamics of Continuous Media,* Pergamon Press, Oxford, 1984, pp. 272-276.

[99] W. Elsäßer and E. O. Göbel, "Einstein relations for gain-guided semiconductor lasers," *Electron. lett.*, vol. 19, pp. 335-336, Apr. 1983.

[100] R. H. Pantell and H. E. Puthoff, *Fundamentals of Quantum Electronics,* Wiley, New York, 1969, pp. 174-179.

[101] K. Petermann, "Calculated spontaneous emission factor for double-heterostructure injection lasers with gain-induced waveguiding," *IEEE J. Quantum Electron.,* vol. QE-15, no. 1, pp. 566-570, 1979.

[102] M. W. Fleming and A. Mooradian, "Fundamental line broadening of single-mode (GaAl)As diode lasers," *Appl. Phys. Lett.,* vol. 38, pp. 511-513, Apr. 1981.

[103] C. H. Henry, "Theory of the linewidth of semiconductor lasers," *IEEE J. Quantum Electron.,* vol. QE-18, no. 2, pp. 259-264, 1982.

[104] C. H. Henry. R. F. Kazarinov, R. A. Logan, and R. Yen, "Observation of destructive interference in the radiation loss of second-order distributed feedback lasers," *IEEE J. Quantum Electron.,* vol. QE-21, no.2, 1985.

[105] S. K. Liew, N. W. Carlson, D. P. Bour, G. A. Evans, and E. Van Gieson, "Demonstration of InGaAs/AlGaAs strained-layer distributed-feedback grating-surface-emitting lasers with a buried second order grating structure," *Appl. Phys. Lett.,* vol. 58, no. 3, pp. 228-230, 1991.

[106] S. K. Liew, "Above-threshold analysis of three-section DFB/DBR lasers with second-order gratings," *IEEE J. Selected Topics in Quantum Electron.,* vol. 1, no.2, pp. 363-370, 1995.

[107] R. E. Collin, *Field Theory of Guided Waves* , IEEE Press, New York, 1991.

[108] R. F. Harrington, *Time Harmonic Electromagnetic Fields*, McGraw-Hill, New York, 1961.

[109] N. Marcuvitz, *Waveguide Handbook*, McGraw-Hill Book Company, New York, 1951, p. 2.

[110] M. Born and E. Wolf, *Principles of Optics*, Pergamon Press, New York, 1980, pp. 55-57.

[111] J. Chilwell and I. Hodgkinson "Thin-film field-transfer matrix theory of planar multilayer waveguides and reflection from prism-loaded waveguides," *J. Opt. Soc. Amer. A*, vol. 1, no. 7, pp. 742-753, 1984.

[112] A. K. Ghatak, K. Thyagarajan, and M. R. Shoenoy "Numerical analysis of planar optical waveguides using matrix approach," *J. of Lightwave Technol.*, vol. LT-5, no.5, pp. 660-667, 1987.

[113] S. Ramo, J. R. Whinnery, and T. V. Duzer, *Fields and Waves in Communication Electronics*, John Wiley & Sons, New York, 1994, p. 300.

[114] A. Hessel, "General Characteristics of traveling-wave antennas", in *Antenna Theory*, R. E. Collin and F. J. Zucker, ed. McGraw-Hill, New York, 1969, pp. 156-159.

[115] D. Marcuse, *Theory of Dielectric Optical Waveguides*, Academic Press, Boston, 1991, pp. 19-30.

[116] D. Marcuse, *Light Transmission Optics*, Van Nostrand Reinhold Co., New York, 1982, pp. 313-319.

[117] G. H. Owyang, *Foundations of Optical Waveguides,* Elsevier, New York, 1981, pp. 45-68.

[118] C. Vassallo, *Optical Waveguide Concepts*, Elsevier, New York, 1991.

[119] F. G. Friedlander, *Introduction to the Theory of Distributions*, Cambridge University Press, Cambridge, 1982.

[120] A. Papoulis, *The Fourier Integral and its Applications*, McGraw-Hill, New York, 1962, pp. 277-278.

[121] D. Marcuse, *Light Transmission Optics*, Van Nostrand Reinhold Co., New York, 1982, pp. 322-326.

[122] N. G. Alexopoulos and S. R. Kerner " Coupled power theorem and orthogonality relations for optical disk waveguides", *J. Opt. Soc. Am.*, vol. 67, no. 12, pp. 1634-1638, 1977.

IMAGE EVALUATION TEST TARGET (QA-3)

150mm

6″

APPLIED IMAGE . Inc
1653 East Main Street
Rochester, NY 14609 USA
Phone: 716/482-0300
Fax: 716/288-5989